UNIVERSITY OF LEEDS

DOCTORAL THESIS

Development of decellularised porcine osteochondral scaffolds as matrices for cell implantation

Author:
Patrick STATHAM

Supervisor:
Dr. Hazel FERMOR, Prof. Louise JENNINGS, Dr. Elena JONES and Dr. James WARREN

A thesis submitted in fulfillment of the requirements for the degree of Doctor of Philosophy

in the

School of Biomedical Sciences
Institute of Medical and Biological Engineering

February 22, 2023

UNIVERSITY OF LEEDS

Abstract

Faculty of Biological Sciences

Institute of Medical and Biological Engineering

Doctor of Philosophy

Development of decellularised porcine osteochondral scaffolds as matrices for cell implantation

by Patrick STATHAM

Osteoarthritis currently affects 8.75 million people in the UK alone. This can cause major issues for those living with the disease, such as immobility and pain, which are often accompanied with psychological distress due to a loss in quality of life. One cause of osteoarthritis is damage to the articular cartilage which triggers inflammation and progressive degeneration. Early intervention strategies are employed to prevent disease progression such as microfracture, mosaicplasty and more recently autologous chondrocyte implantation. However, these all have their limitations in either, insufficient quality of repair material, donor site morbidity or limited biomechanical function prior to tissue regeneration.

This study first aimed to investigate the applicability of decellularised porcine osteochondral scaffolds in the treatment of large shallow cartilage lesions. This project built upon previous work, with an aim of enhancing these scaffolds through application with chondrocytes and self-assembling peptide hydrogel with chondroitin sulphate (P_{11}-8/CS) incorporated. The hypothesis was that the resultant scaffold would be an ideal tissue replacement due to the retained native extracellular matrix structure, the increased regenerative potential offered by the cells and the enhanced

biomechanical function from the addition of SAP-CS. These benefits, would ideally allow faster restoration of the healthy biomechanical function of the joint.

Potential for cost-effectiveness versus matrix assisted chondrocyte implantation was observed. The dimensions of the decellularised scaffolds were adapted to dimensions which are clinically appropriate for the treatment of large shallow lesions. The resultant decellularisation quality, cytocompatibility and mechanical properties were all conserved, despite larger dimensions. Following this, a recellularisation process was established for these decellularised scaffolds based using lyophilisation to increase cell penetration. These scaffolds were evaluated in a natural knee joint simulation model, which indicated viability of recellularised chondrocytes at Day 7.

Following this, the ability of the P_{11}-8/CS hydrogel alone to support chondrocyte cell proliferation and survival over a 14-day timecourse was demonstrated, whilst chondrogenic gene expression of encapsulated primary porcine chondrocytes was shown. The lyophilisation method was then developed to deliver SAP-GAG to the osteochondral scaffolds, which showed a trend for improved biomechanical properties.

Overall, this work has shown the potential for both recellularised decellularised scaffolds and self-assembling peptides, as devices to support chondrocyte implantation to aid the regeneration of large shallow cartilage lesions and early stage lesions respectively.

Acknowledgements

First of all, I'd like to thank my supervisor Dr Hazel Fermor for your guidance throughout this process. Your infectious enthusiasm for research and support to try something new is really reflected in the work presented in this thesis. As well as this, I was lucky to have a great multidisciplinary team of supervisors in Dr James Warren, Dr Elena Jones and Professor Louise Jennings, especially for your help for getting our literature review published. I have learnt a lot from all of you, so thank you. I would also like to acknowledge the rest of the key members of the iMBE laboratories that made the experience a pleasure. There are too many names to mention but as there is no word count I will do it anyway: Dr Daniel Thomas, Mrs Nicola Conway, Mrs Natalie Fox, Dr Raelene Cowie, Dr Halina Norbertczak, Dr Kern Cowell and Dr Sahirah Aslam, I appreciate all the time you gave me. In particular I'd like to highlight the last two names, Kern and Sahirah, you both contributed to a lot of laughs and I wish you all the best going forward.

Outside of work, I would like to briefly mention my friends James, Danny, Kern, Simon and Matt for 4 years of 90's R&B and endless football, I would not swap it for anything else, thank you.

To my amazing girlfriend Bethany, thank you for all your patience over these years and support to chase this, I dedicate every pointless "furthermore" to you.

I'd like to acknowledge those close to me. My Mum Kate, who motivated me all these years, I would not be in this position without your guidance. To my Dad, Dr Lawson-Statham, let's be honest I just copied you. To my siblings Christian and Eve, thank you for all your support in decision making, can't wait to see what is next for you both. I would also like to thank my Granny Diana and Gran Margaret, for always being excited to hear updates about the PhD and for vaguely remembering what I am up to all these years.

Finally, I would like to acknowledge my Grandad Geoff and Grandad Peter who instilled in me a lot of what made me capable of doing this, you are both sorely missed.

Contents

1 Introduction **1**

1.1 General Introduction 1

1.2 Knee Joint Anatomy 2

1.3 Knee Joint Biomechanics and Kinematics 2

1.4 Articular cartilage: Structure, Function and Damage 4

1.4.1 Cartilage 4

1.4.2 Articular Cartilage 4

1.4.3 Biomechanical Function of Articular Cartilage 7

1.4.3.1 Multiphasic theory of articular cartilage 8

1.4.3.2 Fixed charge density 8

1.4.3.3 Biphasic lubrication 9

1.4.3.4 Biphasic theory and mechanical testing 9

1.4.4 Chondrocytes and Cartilage Homeostasis 11

1.4.4.1 Articular Chondrocytes 12

1.4.5 Influence of Biomolecules on Chondrocytes and Cartilage Homeostasis 13

1.4.5.1 Transforming Growth Factor and SOX-9 13

1.4.5.2 Bone Morphogenetic Protein 15

1.4.5.3 Insulin Growth Factor 15

1.4.5.4 Molecules Responsible for Cartilage Catabolism . . . 16

1.5 Mechanobiology of articular cartilage 17
1.5.1 The Chondron and the Pericellular Matrix 17
1.5.2 Response of Articular Cartilage to Mechanical Loads 19
1.5.3 Mechanisms of Mechanotransduction 20
1.6 Cartilage Damage 22
1.6.1 Mechanical Injury of Articular Cartilage 22
1.6.2 Response to Mechanical Injury 25
1.7 Osteoarthritis of the knee 26
1.7.1 Inflammation and OA 27
1.7.2 Chondrocyte Hypertrophy and OA 29
1.7.3 Mechanical Stress and OA 31
1.7.4 Symptoms of Osteoarthritis 33
1.8 Treatment of OA and Articular Cartilage Damage 34
1.8.1 Microfracture 35
1.8.2 Osteochondral Autografting (Mosaicplasty) and Allografting . 36
1.8.3 Autologous Chondrocyte Implantation 37
1.8.3.1 Generations of ACI 39
1.8.3.2 Rehabilitation post-ACI 40
1.9 Osteochondral Tissue Engineering 42
1.9.1 Key concepts in Tissue Engineering 43
1.9.2 Cells for cartilage tissue engineering 43
1.9.3 Role of mechanical stimuli in cartilage tissue engineering 45
1.9.4 Scaffolds for cartilage tissue engineering 47
1.9.4.1 Synthetic polymer scaffolds 47
1.9.4.2 Natural biomaterials for cartilage tissue engineering . 50

1.9.4.3 Hydrogels for cell encapsulation and delivery 52

1.9.4.4 Development of self-assembling peptide technology for cartilage tissue engineering 54

1.10 Decellularisation of xenogeneic tissues 56

1.10.1 Decellularised osteochondral scaffolds 57

1.10.2 Recellularisation of decellularised grafts 60

1.11 Rationale for Decellularised Matrix Assisted Cell Implantation 61

2 Materials and Methods **65**

2.1 Materials 65

2.1.1 Equipment 65

2.1.2 Consumables 65

2.1.3 Cell lines 65

2.1.4 Chemicals and reagents 65

2.1.5 Software 66

2.1.6 Glassware 66

2.2 Methods 66

2.2.1 General methods 67

2.2.1.1 Measurement of pH 67

2.2.1.2 Sterilisation 67

2.2.1.3 Microscopy 67

2.2.1.4 Confocal microscopy 68

2.2.2 Acquisition and dissection of porcine legs to obtain femoral condyles 68

2.2.3 Decellularisation solution preparation 69

2.2.3.1 Phosphate Buffered Saline 69

2.2.3.2 PBS with aprotinin (10 KIU.mL^{-1} aprotinin) 69

2.2.3.3 Hypotonic buffer (10 mM Tris, 10 KIU.mL^{-1} aprotinin) 70

2.2.3.4 Antibiotic solution (100 U.mL^{-1} Penicillin and Streptomycin, 5µg.mL^{-1} Amphotericin B 70

2.2.3.5 SDS in hypotonic buffer (0.1 % w/v SDS, 10 mM Tris, 10 KIU.mL^{-1} aprotinin 70

2.2.3.6 Nuclease solution (50 mM Tris, 10 mM $MgCl_2$, 10 U.mL^{-1} Benzonase 70

2.2.3.7 Peracetic acid solution (0.1 % v/v) 70

2.2.4 Decellularisation 71

2.2.5 Fixation, Processing and Paraffin wax embedding of native and decellularised osteochondral tissue 72

2.2.5.1 Sectioning of paraffin embedded blocks 73

2.2.5.2 Dewaxing and rehydration of tissue samples 74

2.2.5.3 Dehydration and mounting of stained tissue sections . 74

2.2.6 Histological staining of paraffin embedded osteochondral tissue 74

2.2.6.1 Haematoxylin & eosin staining of paraffin wax embedded osteochondral tissue 74

2.2.6.2 Safranin O & Fast Green staining of paraffin wax embedded osteochondral tissue 75

2.2.6.3 Sirius red/Miller's elastin staining of paraffin wax embedded osteochondral tissue 75

2.2.6.4 DAPI staining 75

2.2.7 Biochemical quantification of decellularised tissues 76

2.2.7.1 Quantification of DNA content 76

2.2.7.2 Determining the glycosaminoglycan composition of decellularised scaffolds 77

2.2.8 Cell culture techniques 78
2.2.8.1 Cell culture media preparation 79
2.2.8.2 Cell line resurrection 79
2.2.8.3 Cell passaging 79
2.2.8.4 Cell count 80
2.2.8.5 Cell cryopreservation 80
2.2.9 Sterility testing 80
2.2.9.1 Preparation of thioglycollate broth 80
2.2.9.2 Testing the sterility of the decellularised scaffolds . . . 81
2.2.10 Contact Cytotoxicity 81
2.2.11 Extract Cytotoxicity 83
2.2.11.1 ATP Lite Assay 83
2.2.12 Statistical analysis 83
2.2.12.1 Confidence limits 83
2.2.12.2 Comparison of means 84
2.2.12.3 Linear regression analysis 85

3 Cost-effectiveness analysis of decellularised osteochondral scaffolds for cartilage repair 87

3.1 Glossary 87
3.2 Introduction 88
3.3 Aims and Objectives 89
3.4 Model structure 90
3.4.1 Patients Aged 33-55 90
3.5 Model Inputs 91
3.5.1 Costs 91

3.5.1.1 Recurring costs . . . 91
3.5.1.2 Investment costs . . . 93
3.5.1.3 Determining selling price . . . 95
3.5.1.4 Treatment costs . . . 96
3.5.2 Utility . . . 99
3.5.3 Transition probabilities . . . 100
3.5.4 Mortality . . . 103
3.6 Results . . . 103
3.6.1 Base-case cost-effectiveness . . . 103
3.6.2 Sensitivity analysis . . . 104
3.6.3 Probabilistic Markov Model . . . 106
3.7 Discussion . . . 108
3.8 Conclusion . . . 113

4 Optimisation and characterisation of decellularised osteochondral sheets for use in the treatment of large (>2cm^2) cartilage lesions 115

4.1 Introduction . . . 115
4.2 Aims and Objectives . . . 118
4.2.1 Aims . . . 118
4.2.2 Objectives . . . 118
4.3 Materials and Methods . . . 120
4.3.1 Tissue shaping . . . 120
4.3.2 Quality assessment . . . 120
4.3.2.1 Biochemical Quantification . . . 120
4.3.2.2 Histological assessment . . . 121
4.3.2.3 Biocompatibility . . . 121

4.3.3 Immunofluorescence staining of decellularised scaffolds 122
4.3.4 Immunohistochemical staining of decellularised scaffolds . . . 123
4.3.5 Indentation Studies 124
4.3.5.1 Creep Indentation 124
4.3.5.2 Calibration 125
4.3.5.3 Cartilage indentation testing 126
4.3.5.4 Cartilage thickness measurements 126
4.3.6 Finite element determination of biomechanical properties . . . 126
4.4 Results 129
4.4.1 Producing scaffold of appropriate clinical dimensions 129
4.4.2 Removal of cells and DNA 129
4.4.3 Retention of extracellular matrix components in porcine decellularised scaffolds 131
4.4.3.1 Effect of decellularisation on the GAG content of the scaffold 131
4.4.3.2 Collagen II 133
4.4.3.3 Collagen VI 135
4.4.3.4 Fibronectin 136
4.4.4 Biocompatibility testing of decellularised osteochondral sheets 137
4.4.4.1 Sterility testing 137
4.4.4.2 Contact cytotoxicity assay 139
4.4.4.3 Extract cytotoxicity assay 140
4.4.5 Mechanical characterisation of decellularised cartilage 141
4.4.5.1 Calibration 141
4.4.5.2 Determining percentage deformation 142
4.4.5.3 Computational determination of material properties . 144

4.5 Discussion . . . 145

4.5.1 Decellularised sheet production and assessment . . . 145

4.5.2 Extracellular matrix retention . . . 146

4.5.3 Sterility and cytocompatibility . . . 148

4.5.4 Material property determination . . . 149

4.5.5 Conclusions . . . 151

5 Self-assembling peptides for cell delivery **153**

5.1 Introduction . . . 153

5.2 Aims and Objectives . . . 154

5.2.1 Aims . . . 154

5.2.2 Objectives . . . 155

5.3 Materials and Methods . . . 155

5.3.1 Encapsulation of cells within the P_{11}-8/CS system . . . 155

5.3.1.1 Iteration 1 . . . 155

5.3.1.2 Iteration 2 . . . 156

5.3.1.3 Previous P_{11}-8/CS preparation process: Lyophilised method . . . 157

5.3.1.4 Preparation of fully hydrated, cell seeded collagen hydrogels for use as 3D controls . . . 158

5.3.2 Cell Viability Assessment . . . 158

5.3.2.1 Optimisation of Alamar Blue Incubation Times . . . 158

5.3.2.2 alamarBlue Timecourse of encapsulated L929s and C20A4 cells . . . 159

5.3.2.3 Live/Dead Assay of encapsulated L929s and C20A4 cells . . . 160

5.3.3 Gene expression analysis . . . 160

5.3.3.1 Extraction of chondrocytes from viable porcine cartilage . . . 160
5.3.3.2 Culture set up . . . 161
5.3.3.3 RNA extraction . . . 162
5.3.3.4 Reverse transcription . . . 163
5.3.3.5 Quantitative PCR . . . 164
5.3.3.6 Quantitative PCR Analysis - delta delta CT method . . 167
5.3.4 Rheology . . . 167
5.3.4.1 Sample preparation . . . 167
5.3.4.2 Rheometer set up . . . 168
5.3.4.3 Amplitude sweep . . . 169
5.3.4.4 Frequency sweep . . . 170
5.3.5 Transmission electron microscopy . . . 171
5.4 Results . . . 171
5.4.1 P_{11}-8/CS gel preparation methods . . . 171
5.4.1.1 Gelation . . . 171
5.4.2 Rheology . . . 172
5.4.3 TEM . . . 174
5.4.4 Cell Viability within P_{11}-8/CS . . . 176
5.4.4.1 alamarBlue optimisation . . . 176
5.4.4.2 Preparation Method . . . 177
5.4.4.3 L929 fibroblast cell line . . . 178
5.4.4.4 C20A4 chondrocyte cell line . . . 180
5.4.5 Gene expression of encapsulated chondrocytes . . . 183
5.4.5.1 Suitability of cell types for gene expression studies . . 183

5.4.5.2 Gene expression profile of porcine chondrocytes encapsulated in P_{11}-8/CS hydrogels 184

5.5 Discussion 186

5.5.1 Development of P_{11}-8/CS as cytocompatible matrices 186

5.5.2 Encapsulation of cells within P_{11}-8/CS 186

5.5.3 Chondrogenic gene expression of P_{11}-8/CS encapsulated cells . 190

5.5.4 Effect of preparation method on P_{11}-8/CS behaviour and microstructure 193

5.6 Conclusion 195

6 Enhanced Decellularised Matrices **197**

6.1 Introduction 197

6.2 Aims and Objectives 201

6.2.1 Aims 201

6.2.2 Objectives 201

6.3 Materials and Methods 202

6.3.1 Recellularisation of decellularised scaffolds 202

6.3.1.1 Processing of decellularised sheets 202

6.3.2 Seeding chondrocytes onto decellularised plugs using active seeding methods 203

6.3.2.1 Static seeding 204

6.3.2.2 Injection seeding 204

6.3.2.3 Vacuum seeding 204

6.3.3 Active seeding methods with decellularised scaffolds with channels 205

6.3.3.1 Vacuum and channels 205

6.3.3.2 Centrifugation and channels 206

6.3.4 Matrix Disruption methods 206
6.3.4.1 Collagenase digestion 206
6.3.4.2 Lyophilisation 207
6.3.5 Live/Dead Viability Assessment of C20A4 cells seeded onto decellularised plugs 208
6.3.6 Assessment of cell penetration 209
6.3.7 AlamarBlue viability assessment of seeded decellularised matrices 209
6.3.8 GAG delivery to osteochondral matrices 210
6.3.8.1 Indentation testing 210
6.3.8.2 Fixation in EDC 210
6.3.8.3 Cryosectioning 211
6.3.8.4 Safranin O staining of cryoembedded samples 211
6.3.8.5 Fluorescent peptide solution formulation 211
6.3.8.6 Fluorescent microscopy 211
6.4 Results 212
6.4.1 Initial cell seeding optimisation 212
6.4.2 Active cell seeding methods 213
6.4.2.1 Vacuum 214
6.4.2.2 Centrifugation 216
6.4.3 Matrix disruption 219
6.4.3.1 Low concentration collagenase treatment 219
6.4.3.2 Higher concentration collagenase treatment 221
6.4.3.3 Lyophilisation 226
6.4.3.4 Initial optimisation 226

6.4.3.5 Histological examination of lyophilised decellularised cartilage compared with native and decellularised tissues . . . 227
6.4.3.6 Initial seeding of variably lyophilised scaffolds 228
6.4.3.7 Higher media volume with 100% lyophilised scaffolds 230
6.4.3.8 Lyophilised with labelled chondrocytes 231
6.4.4 Restoring the GAG content and biomechanical properties of decellularised cartilage 234
6.4.4.1 Fixation of P_{11}-8 with NBF or EDC fixative 234
6.4.4.2 Restoration of GAG content 235
6.4.4.3 Fluorescent peptide 236
6.4.4.4 Restoration of percentage deformation 238
6.5 Discussion 239
6.5.1 Recellularising decellularised osteochondral scaffolds 239
6.5.1.1 Channels with active seeding methods 239
6.5.1.2 Collagenase digestion 241
6.5.1.3 Lyophilised scaffolds 243
6.5.2 P_{11}-8/CS delivery to decellularised cartilage 245
6.6 Conclusions 248

7 Assessment of recellularised osteochondral matrices under loading in a viable knee joint simulation model 249

7.1 Introduction 249
7.2 Aims and Objectives 250
7.2.1 Aims 250
7.2.2 Objectives 251
7.3 Materials and Methods 251

7.3.1 Tissue procurement . . . 251
7.3.2 Seeded plug preparation . . . 252
7.3.3 Plug implantation and rig set up . . . 252
7.3.4 Single station whole joint loading rig parameters . . . 254
7.3.5 Downstream analysis . . . 255
7.4 Results . . . 255
7.4.1 Implantation . . . 255
7.4.2 Live/Dead Viability Assessment . . . 256
7.5 Discussion . . . 260
7.6 Conclusion . . . 264

8 General Discussion **267**

8.1 Summary of thesis aims and key findings . . . 267
8.2 Decellularised cartilage scaffolds as matrices for cell implantation . . . 269
8.2.1 Clinical need for Decellularised cartilage . . . 269
8.2.2 Decellularised cartilage development . . . 270
8.3 Recellularisation of decellularised matrices . . . 274
8.3.1 Assessment of recellularised scaffolds in a viable porcine knee joint simulation model . . . 281
8.4 Development of self-assembling peptides as matrices for GAG and cell delivery . . . 283
8.4.1 P_{11}-8/CS process adaptation and resultant material properties . 284
8.4.2 Ability of the hydrogels to support viability and phenotypic stability of primary chondrocytes . . . 286
8.4.3 P_{11}-8/CS delivery to decellularised scaffolds . . . 289
8.5 Future work . . . 290
8.5.1 Continued *In-vitro* characterisation . . . 291

8.5.2 Industrialisation 295

8.5.3 Conclusion 296

9 Appendix **299**

9.1 Equipment 300

9.2 Consumables 302

9.3 Chemicals and Reagents 303

Bibliography **307**

List of Figures

1.1 **Anatomy of the knee joint** 2

1.2 **Knee Flexion during a healthy gait cycle** 3

1.3 **Development of articular cartilage and the synovial joint** 5

1.4 **Arrangement of key ECM components and chondrocyte distribution** 6

1.5 **Schematic of an indentation test on an osteochondral construct (articular cartilage attached to subchondral bone)** 11

1.6 **Electron Micrograph of an articular chondrocyte** 12

1.7 **Three key signalling cascades within chondrocytes responsible for the healthy homeostasis of articular cartilage** 14

1.8 **Pericellular matrix structure within the context of cartilage structure** 18

1.9 **Effects of mechanical loading on cartilage matrix and pericellular matrix** 21

1.10 **ICRS Grading System** 25

1.11 **Osteoarthritic Cartilage** 27

1.12 **Inflammatory cytokines in OA** 28

1.13 **Model of hypertrophic like changes and the development of OA** . . 30

1.14 **Effect of different loading regimes on the anabolic and catabolic function of chondrocytes** 32

1.15 **Graphical representation of the microfracture process** 35

1.16 **Surgical procedure of mosaicplasty** 36

1.17 **Overview of the procedure of 1st Generation ACI** 38

1.18 **Second Generation ACI or Matrix Assisted Chondrocyte Implantation** 39

1.19 **The basic paradigm for cartilage tissue engineering** 42

1.20 **Key considerations in scaffold manufacture for tissue engineering** . 47

1.21 **Electrospun PCL scaffold to recapitulate native bioarchitecture** . . . 49

1.22 **Schematic demonstrating the process of delivery an injectable, cell seeded hydrogel** 53

1.23 **Graphic depicting the three interacting elements investigated in this thesis** 63

2.1 **Dissection process for obtaining porcine femoral condyles** 69

2.2 **Decellularisation protocol** 72

2.3 **Histology for decellularised scaffolds** 72

2.4 **Thioglycollate broth** 81

2.5 **Contact Cytotoxicity** 82

3.1 **Markov Model** 90

3.2 **Sensitivity analysis results plotted on a cost-effectiveness plane** . . . 106

3.3 **Stochastic cost-effectiveness plane** 107

3.4 **Cost-effectiveness acceptability curve** 108

3.5 **Transition probabilities comparison** 111

3.6 **Health state distribution comparison between DC-ACI and ACI at 35-55 and 55+ years** 112

4.1 **Shaping, waterpicking and decellularisation of porcine native osteochondral scaffolds** 120

4.2 **Indentation rig set up** 125

4.3 **Schematic of the indentation set up** 127

4.4 **Axisymmetric indentation modelling geometries meshed in ABAQUS** 127

4.5 **Boundary conditions assigned to FE model** 128

4.6 **Comparison of osteochondral scaffold dimensions** 129

4.7 **Assessment of decellularisation** 130

4.8 **DAPI staining** 131

4.9 **Assessment of GAG content of decellularised osteochondral sheets post-decellularisation** 132

4.10 **Chondroitin sulphate staining of decellularised osteochondral tissue** 133

4.11 **Collagen II staining of decellularised osteochondral tissue** 134

4.12 **Sirius red staining of decellularised osteochondral tissue** 135

4.13 **Collagen VI staining of decellularised osteochondral tissue** 136

4.14 **Fibronectin staining of decellularised osteochondral scaffolds** 137

4.15 **Assessment of sterility of decellularised scaffolds using thioglycolatebroths** 138

4.16 **Cytotoxicity of decellularised cartilage and bone in contact with BHK cell line** 139

4.17 **Cytotoxicity of decellularised cartilage and bone in contact with L929 cell line** 140

4.18 **Extract cytotoxicity of decellularised scaffolds with BHK cells and L929 cells** 141

4.19 **LVDT calibration** 141

4.20 **Percentage deformation profiles of native versus decellularised samples** 142

4.21 **Maximum percentage deformation of native and decellularised porcine osteochondral pins** 143

4.22 **GAG content of native and decellularised porcine osteochondral scaffolds following indentation testing** 144

4.23 **Derived material properties of decellularised osteochondral scaffolds** 144

5.1 **P_{11}-8 self-assembling peptide structure** . . . 154

5.2 **Development of the cell encapsulation technique** . . . 156

5.3 **Rheometer set up** . . . 169

5.4 **Rheology test set-up** . . . 169

5.5 **G′ data from a strain amplitude sweep** . . . 170

5.6 **G″ data from a strain amplitude sweep** . . . 170

5.7 **Gelation of the P_{11}-8/CS cell encapsulation device with the improved preparation iteration** . . . 172

5.8 **Shear properties of P_{11}-8/CS hydrogels prepared using cytocompatible preparation methods** . . . 174

5.9 **Effect of equilibration time on P_{11}-8/CS hydrogels, reconstituted in DMEM** . . . 175

5.10 **Comparison of P_{11}-8/CS hydrogel preparation at 12,000x** . . . 176

5.11 **alamarBlue incubation time optimisation** . . . 177

5.12 **Metabolic activity comparison of newly developed P_{11}-8/CS preparation method (Iteration 2) compared with previous method (lyophilised)** 178

5.13 **Cell viability within the P_{11}-8/CS hydrogel** . . . 180

5.14 **Metabolic activity of C20A4 chondrocytes encapsulated within the P_{11}-8/CS hydrogel** . . . 181

5.15 **Cell viability of C20A4 cells encapsulated within the P_{11}-8/CS hydrogel** . . . 182

5.16 **Effect of culture method on gene expression in chondrocytes** . . . 183

5.17 **Gene expression profile of porcine chondrocytes cultured encapsulated in P_{11}-8/CS hydrogels compared with monolayer culture over 21 days** . . . 185

5.18 **CollagenII:I expression ratio in porcine chondrocytes cultured encapsulated in P_{11}-8/CS hydrogels compared with monolayer culture over 21 days** 185

5.19 **Proof of concept experiment comparing metabolic activity in P_{11}-8 with and without CS** 192

6.1 **Interpretation of vacuum cell seeding method** 200

6.2 **Processing of decellularised sheets to generate plugs for culture** . . . 203

6.3 **Vacuum seeding set up** 205

6.4 **Illustration demonstrating method of bisecting scaffold, and removal of a section for LIVE/DEAD staining** 208

6.5 **Decellularised osteochondral scaffolds seeded with C20A4 cells** . . . 213

6.6 **Decellularised cartilage seeded with chondrocytes, with channels and a combination of channels and vacuum** 215

6.7 **DNA content in decellularised cartilage seeded with chondrocytes, with channels and a combination of channels and vacuum** 216

6.8 **Decellularised cartilage seeded with chondrocytes, with channels and a combination of channels and centrifugation** 217

6.9 **DNA content of decellularised cartilage seeded with chondrocytes, with channels and a combination of channels and centrifugation** . . 218

6.10 **Metabolic activity of chondrocytes seeded onto decellularised cartilage with channels and a combination of channels and centrifugation** 218

6.11 **DNA content in decellularised cartilage seeded with chondrocytes, with channels and a combination of channels and centrifugation** . . 219

6.12 **Decellularised osteochondral scaffolds seeded with C20A4 cells** . . . 220

6.13 **Histological assessment of decellularised osteochondral scaffolds treated with 1 mg.mL^{-1} collagenase** 222

6.14 **Distribution of chondrocytes within decellularised matrices with and without collagenase treatment at Day 1 and Day 7** 224

6.15 **Total DNA content of decellularised (n =3), statically seeded (n = 3) and collagenase treated + seeded (n = 3) at Day 1 and Day 7** 225

6.16 **Metabolic activity of chondrocytes seeded on decellularised matrices with and without collagenase treatment** 226

6.17 **Macroscopic comparison of untreated and lyophilised decellularised scaffolds.** 227

6.18 **Histological comparison of native, decellularised and lyophilised decellularised cartilage** 228

6.19 **Effect of the degree of lyophilisation on seeding of decellularised osteochondral scaffolds** 229

6.20 **Viability of chondrocytes seeded onto 100% lyophilised scaffolds in a larger initial seeding volume** 231

6.21 **Dil+ labelled chondrocytes seeded onto decellularised matrices** . . . 232

6.22 **H & E staining of chondrocytes seeded onto decellularised matrices** 233

6.23 **Total DNA content of decellularised , statically seeded and lyophilised + seeded at Day 1 and Day 7** 234

6.24 **Fixation of P_{11}-8/CS hydrogels** 235

6.25 **P_{11}-8/CS delivery to decellularised matrices** 236

6.26 **FITC tagged P_{11}-8/CS delivery to decellularised cartilage** 237

6.27 **GAG concentration in decellularised scaffolds alone (n = 3) versus GAG-'restored' samples (n = 3)** 238

6.28 **Percentage deformation of decellularised (Lyo-DC) and GAG delivery samples** 239

7.1 **Natural knee loading rig set up** 253

7.2 **Condyles aligned on the simulator loading plates** 254

7.3 **Simulator loading profile** 254

7.4 **Decellularised scaffold implantation into porcine femoral condyle post-culture** 255

7.5 **Live/Dead viability assessment of recellularised scaffolds implanted into the whole joint rig at Day 7** 256

7.6 **Enlarged section of seeded scaffold from whole joint rig at Day 7** . . 257

7.7 **Live/Dead assessment of recellularised culture plate controls** 258

7.8 **Presence of chondrocytes on decellularised scaffolds after 7-days in culture** 259

7.9 **DAPI and Cell tracker staining of recellularised scaffolds implanted in the *ex-vivo* living knee joint model** 260

7.10 **Excitation and emission spectra for Dil+ and Ethidium homodime** . 263

8.1 **Graphic depicting the three interacting elements investigated in this thesis** 269

8.2 **Previous and updated osteochondral scaffold dimensions** 271

8.3 **Graphical representation of the proposed clinical usage strategy for repopulated lyophilised decellularised scaffolds** 279

List of Tables

1.1 **Matrix metalloproteinases found in articular cartilage** 16

1.2 **Synthetic Scaffold material applications in cartilage tissue engineering** 48

1.3 **Summary of decellularisation techniques and the effects on tissue** . 57

1.4 **Summary of decellularisation strategies for osteochondral/cartilage tissue** 58

2.1 **Details of Software used in this project** 66

2.2 **Summary of the effect of sample number (n) on the multiplier (t) for calculating 95% confidence limits.** 84

3.1 **Solution costs** 92

3.2 **Recurring costs** 93

3.3 **Investment costs** 94

3.4 **Selling price** 96

3.5 **NHS Cost** 98

3.6 **Procedural Costs** 98

3.7 **Utility Inputs** 100

3.8 **Health state transition probabilities and assumptions** 101

3.9 **Transition probabilities (33-55 years)** 102

3.10 **Transition probabilities (55-100 years)** 102

3.11 **Base-case cost-effectiveness** 104

3.12 **Sensitivity Analysis** 105

4.1 **Details of primary and secondary antibodies, antigen retrieval methods and blocking steps used for immunofluorescent labelling** 123

5.1 **Mastermix formulation for cDNA synthesis** 164

5.2 **Primer sequences and concentrations** 165

5.3 **Primer concentration specific mastermix formulation for 90x reactions.** 166

9.1 **Equipment** 300

9.2 **Consumables** 302

9.3 **Chemical and Reagents** 303

List of Abbreviations

ACAN	Aggrecan
ACI	Autologous chondrocyte implantation
ACTB	β-actin
ALK	Activin receptor-like kinase
ANOVA	analysis of variance
ATP	Adenosine triphosphate
BHK	Baby hamster kidney
BMP	Bone morphogenetic protein
CEAC	Cost-effectiveness acceptability curve
ChABC	Chondroitinase ABC
C.I.	Confidence intervals
COL1A2	Collagen I alpha 2 chain (gene)
COL2A2	Collagen I alpha 2 chain (gene)
COMP	Cartilage oligomeric protein
CS	Chondroitin sulphate
DAMP	Damage associated molecular pattern
DAPI	4',6-diamidino-2-phenylindole
DC-ACI	Decellularised assisted chondrocyte implantation
DMEM	Dulbecco's modified Eagle's medium
DMSO	Dimethylsulfoxide
dsDNA	Double stranded DNA
ECM	Extracellular matrix
EDC	1-ethyl-3-(3-dimethylaminopropyl)carbodiimide hydrochloride
FCD	Fixed charge density
FGF	Fibroblast growth factor

FITC	Fluorescein isothiocyanate
FTE	Functional tissue engineering
G′	Storage modulus
G″	Loss modulus
GAG	Glycosaminoglycan
GMP	Good manufacturing process
HA	Hyaluronic acid
H&E	Haematoxylin and eosin
HTA	Health technology assessment
ICER	Incremental cost-effectiveness ratio
IGF	Insulin growth factor
IHC	Immunohistochemistry
IL	Interleukin
JNK	c-Jun N-terminal kinases
IHH	Indian hedgehog
LVDT	Linear variable differential transformer
L-G	L-glutamine
MACI	Matrix assisted chondrocyte implantation
MATN	Matrilin
MES	2-(N-morpholino)ethanesulfonic acid
MSC	Mesenchymal stem cell
NBF	Neutral buffered formalin
NCAM	Neural cell adhesion molecule
NHS	National health service
NICE	National Institute for Health and Care Excellence
NF-$\kappa\beta$	Nuclear factor kappa B
OA	Osteoarthritis
OC	Osteochondral
OCA	Osteochondral allograft
PAA	Peracetic acid
PBS	Phosphate buffered saline

PCM	Pericellular Matrix
PCR	Polymerase chain reaction
PPIA	Peptidylprolyl Isomerase A
P/S	Penicillin and streptomycin
QALY	Quality adjusted life year
QC	Quality control
RT-PCR	Reverse transcription PCR
SAF O & FG	Safranin O and Fast Green
SAP	Self-assembling peptide
SDS	Sodium dodecyl sulphate
TEM	Transmission electron microscopy
TGF-β	Transforming growth factor-beta
TIMP	Tissue inhibitor of metalloproteinase
TKA/R	Total knee arthroplasty/replacement
TF	Tibiofemoral
TKR	Total knee replacement
TNF-α	Tumour necrosis factor-alpha
TRPV4	Transient receptor potential vanilloid-type 4
VEGF	Vascular endothelial growth factor
WB	Weight bearing
WTP	Willingness to pay

Outputs

Publications

Statham, P., Jones, E., Jennings, L.M. and Fermor, H.L., 2022. "Reproducing the biomechanical environment of the chondrocyte for cartilage tissue engineering". Tissue Engineering Part B: Reviews, 28(2), pp.405-420.

Conferences

Statham, P., Jones, E., Jennings, L., Warren, J. and Fermor, H., 2021. "Recellularising decellularised osteochondral scaffolds for cartilage tissue engineering" (p. 1923).

Statham, P., Jones, E., Jennings, L., Warren, J. and Fermor, H., 2020. "Permeabilising decellularised osteochondral scaffolds for improved chondrocyte penetration". In 22nd Annual White Rose Work in Progress Meeting.

Statham, P., Jones, E., Jennings, L., Warren, J. and Fermor, H., 2020. "Development Of A Composite Decellularised Osteochondral Scaffold For The Treatment Of Articular Cartilage Lesions". In Future Leaders Joint CDT-UKSB Conference.

Statham, P., Jones, E., Jennings, L., Warren, J. and Fermor, H. 2019. "Development of a composite hydrogel-decellularised scaffold intervention for chondrocyte implantation". In TCES-UKSB Conference.

Statham, P., Jones, E., Jennings, L., Warren, J. and Fermor, H. 2019. "Recellularisation of decellularised osteochondral matrices". At Biomaterials and Tissue Engineering Group (BITEG).

Dedicated to Peter and Geoff

Chapter 1

Introduction

1.1 General Introduction

Articular cartilage is a highly specialised tissue, with a structure and extracellular matrix composition which facilitate an ability to support load transmission and smooth joint articulation for millions of cycles over a lifetime.

As a result of injury or age-related changes, cartilage structural integrity can become compromised, resulting in complications including pain, loss of joint function and a reduction in the quality of life for the affected patient. Furthermore, inflammation as a result of the injury can foster an environment primed for the progression of further cartilage degeneration in the form of osteoarthritis (OA).

Due to the avascular nature of cartilage, it has a low regenerative capacity, meaning such lesions commonly are not capable of self-resolution. The progressive nature of OA, often results in the requirement for prosthetic intervention in the form of a total knee replacement (TKR). TKR's in younger patients with more active lifestyles are associated with higher failure rates, therefore restorative techniques such as mosaicplasty, osteochondral allo/autograft transfer, microfracture, and autologous chondrocyte implantation (ACI) are more commonly used in first-line treatment.

Despite pioneering the use of cell therapies for cartilage regeneration, ACI is associated with complications such as low cell retention in the site of repair, a reliance on regeneration for restoration of function and inferior biomechanical properties of the repair tissue.

This thesis will investigate the potential of two medical devices (Self-assembling peptide hydrogels and decellularised osteochondral scaffolds) as scaffolds to assist the implantation of chondrocytes into cartilage defects, to delay the requirement for prosthetic intervention and prolong the lifetime of the natural knee.

1.2 Knee Joint Anatomy

The knee joint (Figure 1.1) is the largest synovial joint in the body, and occurs where the femur and tibia meet to form a hinge-like joint. It serves two principal functions in permitting gait and to transmit, absorb and redistribute applied loads (Masouros *et al.*, 2010).

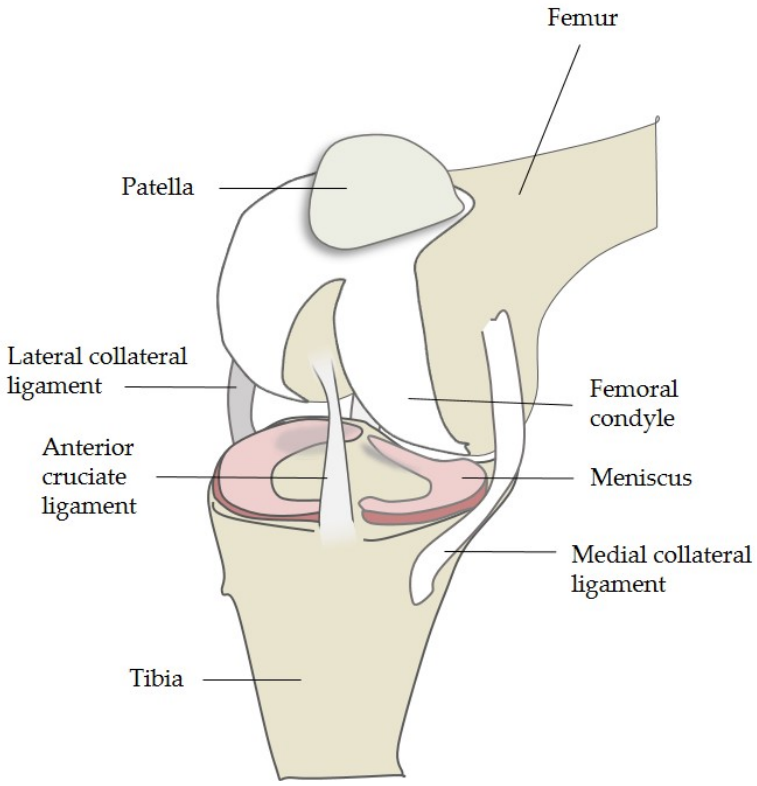

Figure 1.1: Anatomy of the knee joint.

1.3 Knee Joint Biomechanics and Kinematics

Two joints exist within the knee joint. The largest is the tibiofemoral (TF) joint between the articular cartilage on the femoral condyle and the tibial platform. The

other is between the patella and the femoral condyle (patellofemoral joint). The TF joint is categorised as a hinge-like joint, which means that the largest movements occur in the sagittal plane through flexion and extension. However, movement is much more complex than a simple hinge as there is internal rotation and sliding of the articular surfaces. Full extension is defined at the point of 0° rotation in the sagittal plane. In this scenario, both axes of the long bones are aligned. Flexion usually reaches 130-160° depending on whether this is active or passive flexion. In full extension, the joint is optimally aligned for weight support and stability. This places the line of action of the vertical ground reaction force through the joint rather than posterior to the joint, requiring energy expenditure through engaging the quadriceps (Masouros *et al.*, 2010). The most common knee movement occurs during the gait cycle (Figure 1.2) where the knee flexes 70° during the swing phase in order to allow the trailing foot sufficient clearance from the ground. Following this, the quadriceps muscle contracts in order to fully extend the knee. However, shortly after heel strike the knee flexes roughly 15°. This prevents the knee absorbing all of the impact load, as the flexion in the mid-stance stretches the quadriceps muscle allowing it to absorb some impact energy (Masouros *et al.*, 2010).

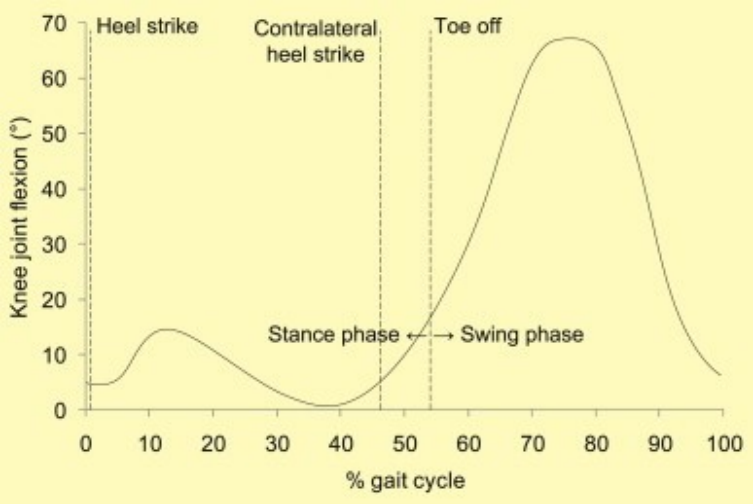

Figure 1.2: Knee Flexion during a healthy gait cycle. Reproduced from (Masouros *et al.*, 2010) under licence number 5160120471664 obtained from Elsevier.

During daily activities, such as walking the knee joint articular surfaces experiences load from external forces such as the ground reaction force as well as internal muscle forces. It is estimated that during walking the joint experiences loads of up to 3.4X

body weight of the individual (Morrison, 1968)

1.4 Articular cartilage: Structure, Function and Damage

1.4.1 Cartilage

Cartilage is a highly specialised musculoskeletal tissue, found in three main forms within the body; elastic, fibrocartilage and hyaline cartilage. Elastic cartilage is found in the ear and larynx, and contains a high amount of elastin derived fibres giving the tissue relative flexibility compared with the other cartilage types (Montes, 1996). Fibrocartilage is a fibrous tissue found in the menisci as well as at synovial joints, and has a high concentration of collagen fibrils allowing the tissue to withstand high compressive loads (Ghosh and Taylor, 1987). Hyaline cartilage is found in articular cartilage, and is principally made up of highly aligned collagen II fibres, as well as proteoglycans, which give the tissue strength in tension as well as compression (Sophia Fox *et al.*, 2009).

1.4.2 Articular Cartilage

Hyaline cartilage can be found at synovial joints, where it is given the denomination of articular cartilage and can be found covering the articulating surfaces at the end of the bone. The synovial joint is comprised of a synovial cavity filled with synovial fluid and a joint capsule which consists of a fibrous outer membrane and an inner synovial membrane responsible for secreting synovial fluid and permitting nutrient exchange (Pacifici *et al.*, 2005). Key synovial joints within the body can be found at the knee, hip, elbow and at vertebrae in the spine (Navarro *et al.*, 2017).

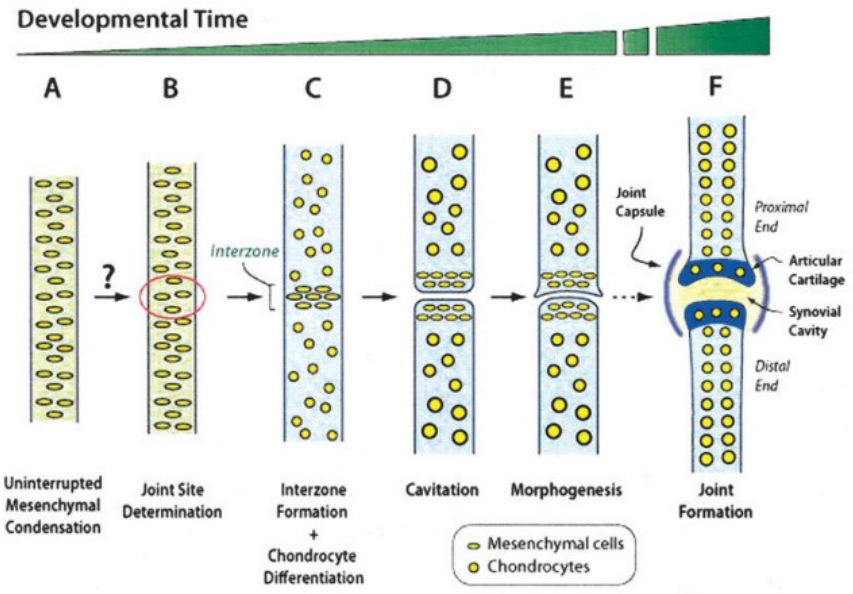

Figure 1.3: Development of articular cartilage and the synovial joint. Reproduced from (Pacifici *et al.*, 2005) with permission from John Wiley and Sons under licence 5160130197654.

In the formation of the synovial joint during the developmental process, articular cartilage is formed through a condensation of mesenchymal stem cells (MSCs) at a site described as the 'interzone' (Figure 1.3). Research indicates that cells found in this interzone have an increased chondrogenic capacity (Pacifici *et al.*, 2005). At this zone MSCs form chondroblasts which are responsible for the production of the cartilage extracellular matrix (ECM), in which they become encapsulated within individual lacunae (Navarro *et al.*, 2017).

The ECM of articular cartilage is composed primarily of collagen, proteoglycans, resident chondrocytes and water. In fact, in normal articular cartilage the fluid phase represents 65-80% of the overall mass (Mow *et al.*, 1992), and of the total dry weight collagen makes up roughly 60% (Sophia Fox *et al.*, 2009). The matrix is organised into several zones within the overall cartilage microstructure displayed in Figure 1.4.

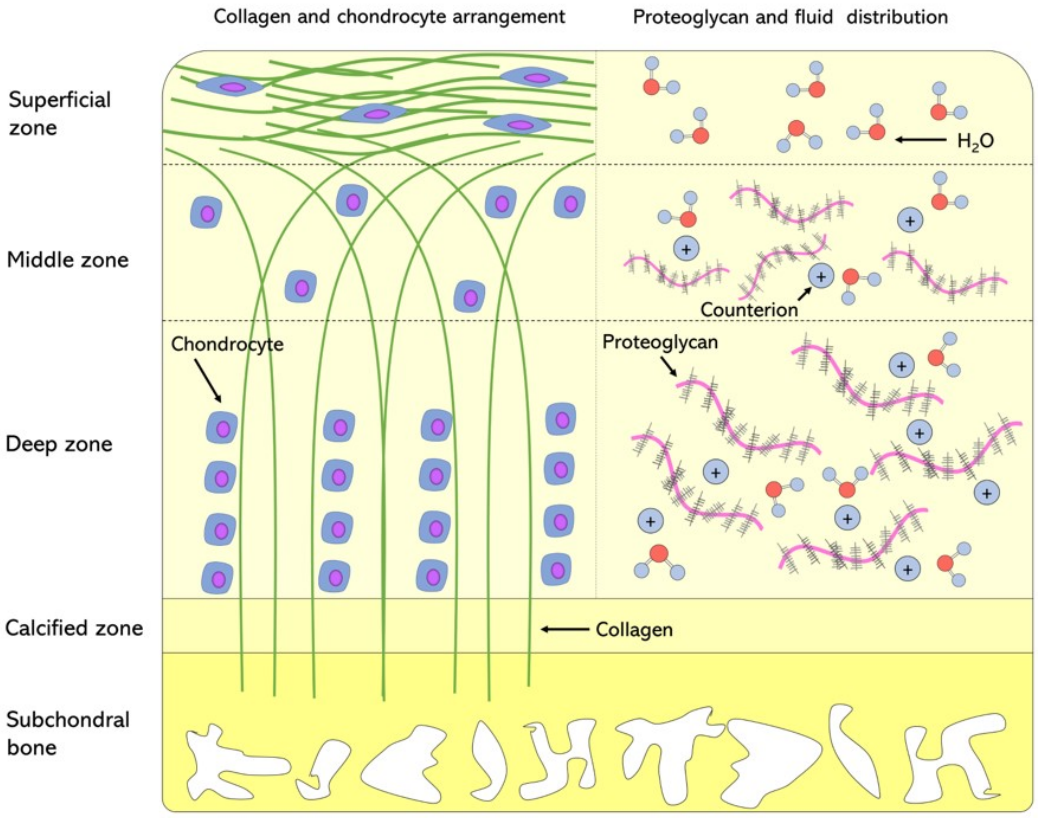

Figure 1.4: Arrangement of key ECM components and chondrocyte distribution. Left: collagen fiber structure and zone-dependent chondrocyte morphology and arrangement. Right: zonal distribution of proteoglycans, associated counterions, and water molecules. Reproduced from (Statham *et al.*, 2022) which is licenced under CC BY.

Firstly, there is the superficial zone, which is composed of collagen II fibres which are highly aligned in the direction of articulation. This layer also has a high density of compacted chondrocytes, however the orientation and form of both the ECM and resident cell types have a zone dependent inhomogenous composition and shape (Kumar *et al.*, 2001).

Below the superficial surface, is the middle zone which acts as a transition zone between the surface region and deeper cartilage zones. The collagen fibres here are thicker and randomly orientated, and chondrocytes adopt a more spherical shape (Guo and Torzilli, 2016). This layer and the deep zone contribute to the ability of articular cartilage to withstand compressive loads. This is due to the high proteoglycan and glycosaminoglycan content within these regions (Sophia Fox *et al.*, 2009). The basic proteoglycan structure consists of a core protein decorated with chondroitin

and keratan sulphate glycosaminoglycans (GAGs). Both types of GAG are polyanionic, causing repulsion between adjacent chains. This repulsion causes the chains to adopt an extended conformation. These proteoglycan aggregates can interact with collagen II, to form an interlinked mesh structure characteristic of this tissue (Sophia Fox *et al.*, 2009).

In the deep zone of the cartilage, the collagen fibrils have the largest diameter and are aligned perpendicularly with the subchondral bone/articular surface which enables a connection to form between the cartilage and the underlying bone through anchoring the fibres within the calcified zone (Sophia Fox *et al.*, 2009). The chondrocytes also align in a perpendicular orientation adopting an elongated cell shape. This zone also has the higher concentration of proteoglycans, which contribute towards its load bearing capacity (Guo and Torzilli, 2016).

The calcified cartilage zone, exists in healthy cartilage to form an interface with bone which enables mechanical integration between the two regions. This interface is a result of the collagen fibrils anchoring into underlying subchondral bone. This calcified zone has a low population of hypertrophic chondrocytes which contribute to the calcification of this matrix by undergoing endochondral ossification (Goldring *et al.*, 2005).

1.4.3 Biomechanical Function of Articular Cartilage

Articular cartilage structure is well adapted for it's function and role in permitting smooth TF articulation and allowing effective load absorption and re-distribution. It is estimated that the average person takes 2 million steps per year, meaning that each knee joint undergoes 1 million loading cycles per year (Weightman, 1976). During walking, peak cyclic stress can reach 4-9 MPa. Articular cartilage also has a low friction coefficient, which permits the ability to withstand the repeated articulations and loading whilst ideally minimising damage to the surface and underlying tissue.

1.4.3.1 Multiphasic theory of articular cartilage

The key biomechanical properties that articular cartilage provides to the knee joint are wear resistance, as well as resistance to both compressive, shear and tensile loads. These biomechanical capabilities can be attributed to multiphasic composition of articular cartilage (Lai *et al.*, 1991). There are various theoretical models for the behaviour of articular cartilage, however the most inclusive model describes cartilage as a triphasic material. The first phase is a solid phase, composed of the densely woven collagen fibrils (15-22% of wet weight) interspersed by proteoglycans (4-7%). The average pore size found in this solid phase is roughly 60Å (Lu and Mow, 2008). The second phase is water, and is referred to as the fluid phase, which makes up 80% of the total (wet) weight of articular cartilage. The third is composed of an array of dissolved ionic species such as Na^{+}, $Ca^{2}+$ and Cl^{-}. All three of these phases act in unison to allow cartilage an ability to withstand very high compressive loads as well as the resultant compressive and shear stresses (Seireg and Arvikar, 1975).

The presence of water within cartilage gives rise to viscoelastic material properties, rather than elastic properties seen in single phase materials. Upon loading, fluid is slowly extruded as a result of the low permeability of the mesh-like cartilage ECM and frictional drag between the fluid and ECM components. This results in an increased osmotic pressure which is responsbile for 95% of the total load bearing capacity of articular cartilage (Soltz and Ateshian, 1998). This redistribution of applied loads, protects the solid phase (cartilage ECM and chondrocytes) from high stresses experienced on a daily basis, giving the tissue substantial longevity.

1.4.3.2 Fixed charge density

As mentioned previously the proteoglycans found in cartilage are decorated with chondroitin sulfate and keratin sulfate, which both contain the negatively charged sulfate (SO3-) and carboxyl (COO-) groups. Due to the high presence of GAGs, cartilage has a high charge density or as is referred to in the literature a fixed charge

density (FCD) (Mlynarik and Trattnig, 2000). As the GAGs are fixed within the tissue, and cannot diffuse to balance a charge disequilibrium this draws an imbalance of counter ions from the extracellular fluid such as Na^+, due to a requirement for electroneutrality (Lu and Mow, 2008). The excess influx of cations, causes an increased osmotic pressure inside the tissue which causes water to enter the tissue (Donnan, 1924). This effect governs many tissue properties such as hydration and ion transport, as well as material properties of the tissue. To determine the existence and contribution of this third phase proposed by (Lai *et al.*, 1991), cartilage has been loaded under hypertonic conditions, which causes the Donnan osmotic effect to be close to zero, negating its effect on cartilages material properties. These experiments revealed a 30-50% contribution of Donnans osmotic pressure to the equilibrium stiffness of this tissue (Flahiff *et al.*, 2002).

1.4.3.3 Biphasic lubrication

The concept of interstitial fluid support is pivotal in the low friction and low wear function of cartilage (Ateshian and Wang, 1995), which is enabled through a mechanism called biphasic lubrication (Forster and Fisher, 1996). Due to the low porosity and permeability of the matrix, upon contact loading the interstitial fluid is pressurised and bears most of the load, minimising the friction between the opposing solid articulating surfaces (Ateshian, 2009) The resulting low friction coefficient is dependent upon a high interstitial fluid pressure, which can be sustained indefinitely if the contact area migrates faster than the velocity of interstitial diffusion into lower pressure areas (Ateshian, 2009; Caligaris and Ateshian, 2008).

1.4.3.4 Biphasic theory and mechanical testing

Due to fact that the biomechanical properties of cartilage *in-situ* depend upon the interaction of this 'triphasic' system, in order to determine its material and mechanical characteristics out of the body it is necessary to take into account all of these contribution in an all-encompassing model. In the basic biphasic theory of cartilage three material properties must be known to characterise the tissue, the Young's modulus E, Poisson's ratio v and the permeability k.

Many mechanical testing configurations are possible for the biomechanical characterisation of articular cartilage. As work contained within this thesis will focus on methodologies to augment the stiffness under compression of decellularised cartilage, methodologies for characterisation of other important biomechanical parameters such as friction and tensile stiffness will not be introduced. As well as the mechanical properties described above, the equilibrium elastic modulus and aggregate modulus (H_A) are two parameters which are of interest for defining the bulk mechanical properties of cartilage. Firstly, an unconfined compression test can be used to determine the equilibrium elastic modulus. The testing set up consists of a cartilage disc, which is subject to compression between two impermeable platens. During compression, fluid exudes radially from the tissue and the tissue can expand laterally. In confined compression an excised cartilage disk is compressed against an impermeable indenter by a permeable platen, within a confined collet or mould, which prevents lateral expansion of the tissue and allows for the determination of the H_A (Armstrong and Mow, 1982).

The advantage of both these methods, is that they provide direct measurement of these parameters and are both simple and cheap to perform. In confined cartilage testing, studies have shown good correlation between biphasic models and experimental data. However, due to the use of an indenter, the presence of high local strains cause concern with regards to the physiological relevance of the model, whereas the smooth platens used for unconfined compression do not cause artificially elevated strain gradients along the articular surface (Park *et al.*, 2003).

Despite the merits of confined and unconfined compression testing, there are limitations of both in terms of the requirement for excision of the cartilage from the site of interest, which limits the application for *in-situ* testing. Furthermore, as will be described later in the thesis, ideally the mechanical testing will be performed on intact osteochondral units, with a focus on the mechanical properties of the cartilage itself. Therefore, either testing the whole osteochondral unit or simply separation of the cartilage from the unit will limit the utility of the mechanical testing.

Mow *et al*. (1989) developed a biphasic method to calculate E, v and k from a single indentation test (Figure 1.5), which measures creep deformation over time (Mow

et al., 1989). The benefit of this methodology is that it is non-destructive, and can be used in our application to investigate cartilage biomechanical properties in the context of an intact osteochondral plug. They later elaborated upon this method in order to permit a calculation of the contribution of FCD to the material properties. This is done by reducing the resultant Donnan osomotic pressure from fixed charge density (FCD) by performing the test in a hypertonic solution, which measures the intrinsic mechanical properties without any FCD contribution. Once both the intrinsic and apparent mechanical properties have been determined, the contribution of FCD can be easily calculated using mathematics based upon a correspondence principle which states that 'the behaviour of a charged hydrated tissue under loading is identical to that of an elastic medium without charge' (Lu *et al.*, 2007).

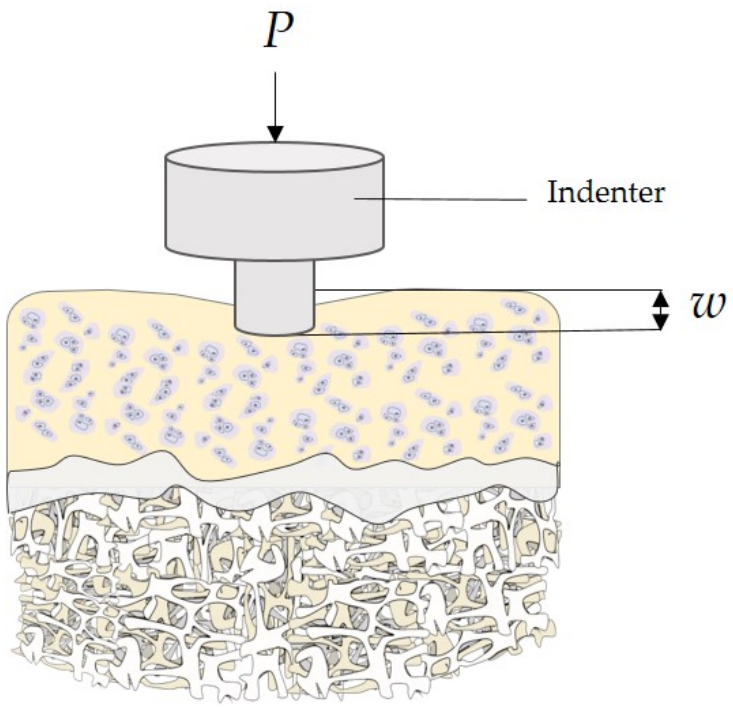

Figure 1.5: Schematic of an indentation test on an osteochondral construct (articular cartilage attached to subchondral bone). Where P = contact force and w = indenter displacement.

1.4.4 Chondrocytes and Cartilage Homeostasis

As described previously, the specialised material properties of cartilage permit longevity of the tissue by preventing damage to the solid phase. A key component in this solid

phase is the chondrocyte cell, which can be found at relatively low cell density compared to other tissues, occupying only 1-5% of the total tissue volume (Bhosale and Richardson, 2008). The intracellular structure of a chondrocyte is detailed in Figure 1.6, and is typical of a cell destined for production of large ECM molecules such as collagen and proteoglycans.

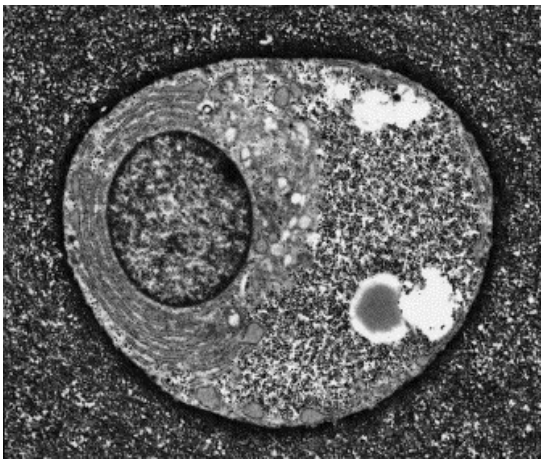

Figure 1.6: Electron Micrograph of an articular chondrocyte. Taken from (Archer and Francis-West, 2003) under licence number 5160280267357.

Within the knee joint two distinctly different chondrocyte forms can be observed depending on whether they are located within the articular cartilage layer or at the epiphyseal growth plate. The principal function of articular cartilage chondrocytes is to maintain a state of homeostasis within the cartilage ECM, balancing anabolism and catabolism. Whereas those located at the epiphyseal plate are responsible for longitudinal growth (Archer and Francis-West, 2003)

1.4.4.1 Articular Chondrocytes

Chondrocytes found in the superficial and middle zone of articular cartilage play an important role in the synthesis of collagen types found abundantly in these zones such as type II, IX and XI as well as proteoglycans. Furthermore, chondrocytes at the superficial layer produce lubricin, which is secreted into the synovial fluid and coats the articulating surfaces allowing near-frictionless articulation as well as to prevent cell and protein adhesion (Jay and Waller, 2014). In the deep zone chondrocytes produce collagen type X as well as Indian hedgehog (Ihh) and Runx2, which all facilitate

the process of calcification of cartilage as well as the differentiation of chondrocytes and osteoblasts (Kwan *et al.*, 1991).

Adult cartilage chondrocytes have a very low turnover rate, which can partially be attributed to the avascular nature of articular cartilage. This means that the chondrocytes rely on diffusion at the articular surface for glucose and metabolite exchange from the blood into the synovial fluid and as a result of this chondrocytes exist in a relatively hypoxic environment. Furthermore, due to the lack of O^2 chondrocytes rely principally on anaerobic respiration (Sophia Fox *et al.*, 2009). In healthy cartilage, the low turnover rate is suitable for the requirements of replacing the collagen and proteoglycans that make up the ECM. Collagen has a half-life of roughly 100 years whereas proteoglycans are more short lived with a half-life of 3 to 24 years (Goldring and Marcu, 2009). In order to maintain a healthy tissue, chondrocytes must balance anabolic and catabolic activities. This balance is governed by both bio-molecular and mechanical influences.

1.4.5 Influence of Biomolecules on Chondrocytes and Cartilage Homeostasis

There are many biomolecule that contribute to controlling healthy cartilage metabolism. These range from cytokines and growth factors to transcriptional regulators.

1.4.5.1 Transforming Growth Factor and SOX-9

Transforming Growth Factor (TGF)-beta is an extracellular cytokine which influences cartilage and chondrocytes for most of their respective lifespans. In chondrogenesis and cartilage development, TGF-β plays a role in the aforementioned chondrogenic condensation by activating fibronectin synthesis. This, in turn downregulates neural cell adhesion molecule (NCAM) permitting the creation of condensation boundaries (Goldring *et al.*, 2005). TGF-β also promotes the differentiation of chondroprogenitor cells into chondrocytes through a SMAD-3 dependent cell signalling cascade (Figure 1.7), resulting in the production of the chondrogenic transcription

factor Sox9, which in turns promotes gene expression resulting in the production of cartilage ECM molecules (Kawakami *et al.*, 2006).

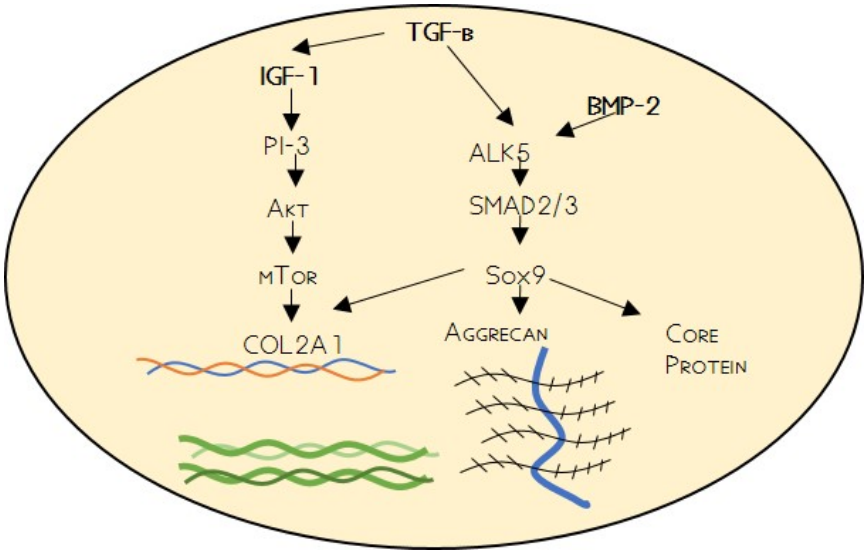

Figure 1.7: Three key signalling cascades within chondrocytes responsible for the healthy homeostasis of articular cartilage. Adapted from (Ashraf *et al.*, 2016).

As well as promoting chondrogenesis, TGF-β also inhibits terminal differentiation to a hypertrophic state. This prevents further matrix calcification, vascularisation, osteoblast formation and bone formation (Kraan *et al.*, 2009). This is what allows an articular cartilage surface to appear on the end of long bones in development.

TGF-β also mediates cartilage catabolism by producing protease inhibitors such as Tissue inhibitor of metalloproteinase (TIMP)-1 (Kraan *et al.*, 2010).

TGF-β is considered as a master *extracellular* regulator of chondrogenesis, but it is important understand how this molecule enables the intracellular regulation of cellular activity to permit healthy homeostatic mechanisms. There is a wealth of literature which associates TGF-β with the transcription factor Sox9, which is considered as the *intracellular* regulator of chondrogenesis. The role of Sox9 in chondrogenesis has been shown in various studies showing that Sox9+/- mice exhibit cartilage hypoplasia (Bi *et al.*, 2001), and Sox9 inactivation at discrete intervals during limb development in mice has revealed that without Sox9 there is no progression to mesenchymal condensation or chondrogenic differentiation (Akiyama *et al.*, 2002).

Given its importance in chondrogenesis, it is important to briefly discuss how Sox9 and TGF-β interact to regulate chondrogenesis. Firstly, TGF-β homo/heterodimers

bind serine/threonine tyrosine kinase transmembrane receptors. This activates an intracellular tyrosine kinase domain which phosphorylates and activates activin receptor-like kinase (ALK)-5, which subsequently phosphorylates SMAD2/3 allowing interaction with a co-SMAD (SMAD4) which permits nuclear translocation of this SMAD complex. Once in the nucleus this SMAD complex can interact with Sox-9 and other promoters and repressors to regulate chondrogenic gene expression (Ross and Hill, 2008; Finnson *et al.*, 2012).

1.4.5.2 Bone Morphogenetic Protein

Similarly to TGF-β, Bone Morphogenetic Proteins (BMPs) regulate gene expression through interaction with type I and type II serine/threonine kinases on the chondrocyte cell surface. Their name arises as a result of their role in endochondral bone formation, and articular cartilage is an intermediate in this sequence. BMPs promote chondrogenesis and chondrogenic differentiation, as well as interacting with Sox-9 downstream, and in this aspect shares similar activities with TGF-β (Kraan *et al.*, 2010). BMPs can also influence chondrocyte extracellular matrix deposition, (Chubinskaya *et al.*, 2008) saw that cultured chondrocytes treated with BMP-2,-4 and -6 demonstrated an upregulated synthesis of aggrecan. Furthermore, like TGF-β, BMPs elicit their chondrogenic response through upregulating Sox9, and it has been shown that BMP activity also enhances the Sox-9 binding to DNA through promoting histone methylation and enhancing NF-Y-p300/CBP complex binding to the Sox-9 promoter region (Pan *et al.*, 2009).

1.4.5.3 Insulin Growth Factor

Insulin Growth Factor (IGF)-1 is another key growth factor, which has important roles in the metabolism of cartilage, and has been studied extensively in both healthy and pathological settings. Its application has been shown to enhance net ECM depositions as well as to decrease catabolism (Sah *et al.*, 1994), and has been shown to play a vital role in the maintenance of the chondrocyte phenotype (Ekenstedt *et al.*, 2006). Through the use of a chronic IGF-1 deficient mouse model, they observed an increased severity of articular cartilage lesions. Furthermore, IGF-1 has been shown to

enhance the regeneration of numerous cartilage defects (Fortier *et al.*, 2002). Taking into account both the effects of TGF-β on early chondrogenesis and IGF-1 in enhancing and maintaining cartilage proliferation, it has been shown that IGF-1 and TGF-1 act synergistically to enhance both proliferation and differentiation, increasing total cartilage formation (Fukumoto *et al.*, 2003).

1.4.5.4 Molecules Responsible for Cartilage Catabolism

As mentioned previously, homeostasis requires a balance of both anabolism and catabolism. In a healthy condition chondrocytes degrade their surrounding ECM in order to replace it with newly synthesised macromolecules (Sophia Fox *et al.*, 2009). Chondrocytes mediate this degradation through the secretion of matrix metalloproteinases (MMPs) such as collagenases, gelatinases, stromelysins and aggrecanases (Saha and Kohles, 2012). Key examples of which can be found in Table 1.1.

Table 1.1: Matrix metalloproteinases found in articular cartilage. Reviewed in: (Rose and Kooyman, 2016)

Matrix Metalloproteinase	Other names	Degrades	Other activities
MMP-1	Interstitial Collagenases	Type I, II and III collagen	Endochondral and intramembranous bone formation in development
MMP-2	Gelatinase A	Type IV collagen	
MMP-3	Stromelysin-1	Type II, III, IV, IX and X Collagen, Fibronectin, Laminin, elastin and proteoglycans	Upregulate other MMPs; presence in cartilage characteristic of OA
MMP-8	Neutrophil collagenase	Dentin	Deficiencies can cause joint inflammation through downregulation of neutrophil apoptosis; presence in cartilage characteristic of OA
MMP-9	Gelatinase B		Angiogenesis; presence in cartilage characteristic of OA
MMP-13	Collagenase III	Degrade type II, IV, IX collagen, proteoglycan	
MMP-14	Membrane-type 1 matrix metalloproteinase	Aggrecan and cadherin	Activates MMP-2, MMP-13; postnatal bone formation

1.5 Mechanobiology of articular cartilage

As well as responding to the presence of biomolecules, cartilage also is responsive to mechanical forces experienced as a result of the applied loads during daily activities. However, these two stimuli are not mutually exclusive.

1.5.1 The Chondron and the Pericellular Matrix

In order to understand how articular cartilage responds to mechanical load, it is essential to first discuss the micromechanical environment surrounding the chondrocyte. Within the ECM, the resident chondrocytes are found individually within 'chondrons', which consist of the cell and a pericellular matrix (PCM) (Figure 1.8). The PCM structure is defined by the presence of type II and VI collagen, proteoglycans, fibronectin, perlecan and biglycan (Poole *et al.*, 1987). It has many functions, but generally it permits a connection between the ECM and the cell, which in turn, allows load transmission to the chondrocyte (Guilak *et al.*, 2006).

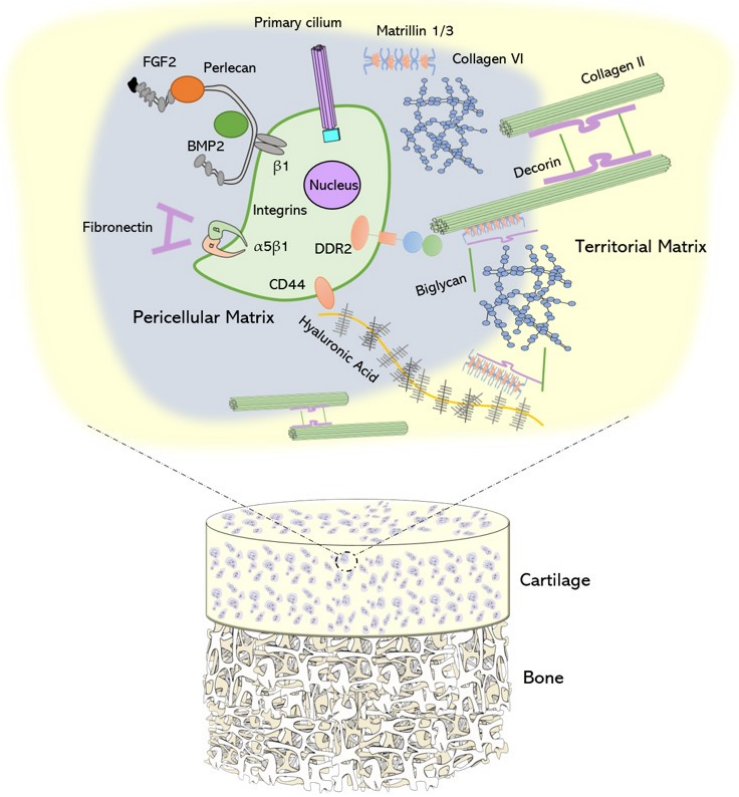

Figure 1.8: Pericellular matrix structure within the context of cartilage structure. Magnified view demonstrates the pericellular matrix and territorial matrix components. Collagen II fibrils, linked by decorin/biglycan, from the ECM can interact directly with chondrocytes through DDR2 receptors on the surface. CD44 also links the chondrocyte to hyaluronic acid, which in turn can associate with collagen VI and II through matrilin 1/3 and biglycans. Cell surface integrins also permit interaction with fibronectin and perlecan, which itself acts as a biomolecule repository of FGF-2 and BMP-2. Primary cilia are also located on the cell surface membrane, which deform in response to mechanical loading. BMP, bone morphogenetic protein; CD, cluster of differentiation; DDR2, discoidin domain-containing receptor 2; FGF, fibroblast growth factor.

In terms of mechanical strength, the Young's modulus of a chondron versus an isolated chondrocyte is 1.54kPA to 0.6kPA (Guilak *et al.*, 1999). Therefore it is hypothesised that due to the PCMs presence, chondrons are stiffer than chondrocytes alone (Zhang, 2014). As well as providing a degree of mechanical support, the PCM acts in part as a 'buffer zone' between the ECM and the chondrocytes and as a filter from molecules interacting with the cells. This is enabled by the fact that molecules have a slower diffusion coefficient and lower diffusivity in the PCM when compared with the ECM (Leddy *et al.*, 2008). This can be attributed to the aforementioned molecules found within the PCM, as well as the presence of basement membrane proteins such as laminins, nidodens, collagen type IV and perlecan (Kvist *et al.*, 2008). Several growth factors are also found in the PCM, which is thought to act as a repository

where they can be activated, get degraded or are transported in or out. FGF-2 has been seen to interact with perlecan, where it plays a role in mechanotransduction (Vincent *et al.*, 2007).

The chondron provides a supportive niche for healthy chondrocyte growth and homeostasis. Isolated chondrons have been seen to grow larger in culture compared to chondrocytes (Larson *et al.*, 2002), produce more type II collagen and proteoglycans (Wang *et al.*, 2010), as well as balancing the catabolic response by expressing less degradative MMP-2, 9 and 13 (Vonk *et al.*, 2010). The matrix components also support chondrogenesis, as perlecan has a binding site for BMP-2 (Jha *et al.*, 2009), and Type VI collagen stabilises the chondrocyte phenotype (Quintero *et al.*, 2008).

One of the primary constituents of this matrix from a mechanosensing point of view are the matrilin (MATN) group of oligomeric matrix proteins. MATNs connect type VI collagen microfibrils to collagen II and aggrecan to form a molecular complex which forms the primary building block of the PCM. Importantly, MATNs connect the PCM to the chondrocyte through an interaction with transmembrane integrins, as well as with ECM molecules such as Type II and IV collagen (Wiberg *et al.*, 2003). These MATNs have been shown to have a vital role in the mechanosensing ability of chondrocyte. For example, a MATN1 deficiency results in a dampened ability to response to mechanical stimuli, judged by the downstream lack of Indian hedgehog (Ihh) signalling (Kanbe *et al.*, 2007).

1.5.2 Response of Articular Cartilage to Mechanical Loads

Mechanical loading is an extremely important stimuli for healthy development of a joint. In fact recent research data indicates that fetal kicking during pregnancy serve a purpose in bone development (Rauch and Schoenau, 2001; Verbruggen *et al.*, 2018). Furthermore, the mechanical environment of the joint plays an important role in defining the joint surface geometry and cartilage thickness (Wong *et al.*, 2003). Post-development, correct mobilisation of the knee joint is vital for cartilage maintenance which is supported by the fact that immobilisation can lead to cartilage atrophy and loss of proteoglycans (Haapala *et al.*, 1999). Conversely, high strain magnitudes

and excessive loading can cause cartilage lesions, injuries and progressive cartilage degradation (Buckwalter *et al.*, 2013).

1.5.3 Mechanisms of Mechanotransduction

There are several suggested pathways by which mechanotransduction can occur (Figure 1.9). Mechanical loading causes a deformation of the cartilage matrix, an increase in hydrostatic pressure and increase fluid flow. This results in tension in the the chondrocyte membrane which consequently distorts the lipid bilayer which results in the opening of stretch activated Ca^{2+} channels (Wright *et al.*, 1996). Due to the low intracellular [Ca^{2+}], there in an influx of cations into the cell which causes further influx through voltage gated Ca^{2+} channels.

There are two receptor types worth mentioning in this instance, the first being transient receptor potential vanilloid 4 (TRPV4) receptors. TRPV4 receptor are highly expressed in chondrocytes, and under compressive loading promote a cartilage anabolic response (O'Conor *et al.*, 2014). Furthermore, Piezo 1&2 channels are also cation permeable ion channels which are activated within 5 ms of loading. However, these channels are involved more so in sensing hyperphysiological and injurious loads, defined by strains higher than 45% (Lee *et al.*, 2014). Upon influx of Ca^{2+} into the cell, a series of calcium-dependent kinase signalling cascades are activated (IP3, DAG and further Ca^{2+} release from intracellular stores) which culminate in activating expressions of genes involved in chondrogenesis such as TGF-β (O'Conor *et al.*, 2014).

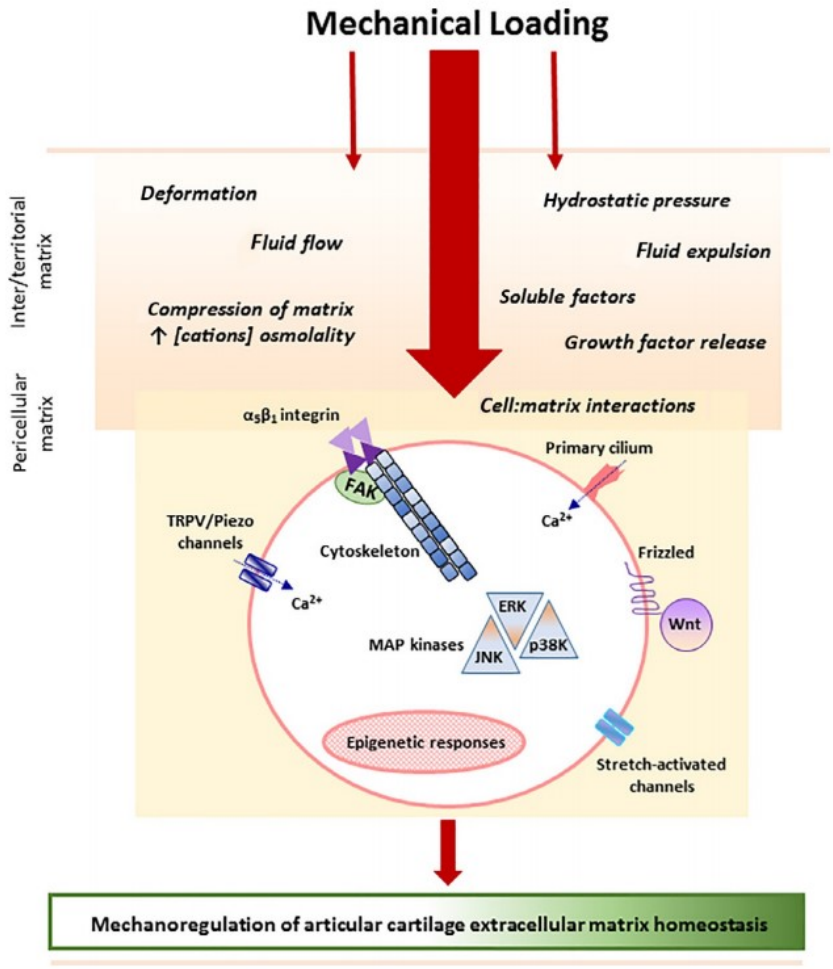

Figure 1.9: Effects of mechanical loading on cartilage matrix and pericellular matrix, as well as how these are transduces intracellularly to permit mechanoregulation. (Taken from (Gilbert and Blain, 2018) under licence number 5396020294678.

On the surface of chondrocyte there are microtubule structures called primary cilium which protrude from the cell surface into the PCM, and these cilia are principal sensors within cartilage mechanotransduction (Jensen *et al.*, 2004). The role of primary cilia is to detect deformation within the cartilage and chondron matrix, and in fact forms a continuous connection between chondrocyte intracellular golgi apparatus, cilia and extracellular collagen fibrils (Poole *et al.*, 2001). Under compression, cilia react through promoting the synthesis of proteoglycans through the release of intracellular Ca^{2+} stores in response to ATP release (Wann *et al.*, 2012), and without cilia this response is not possible which produces cartilage with a significantly reduced mechanical properties (Irianto *et al.*, 2014). Through this pathway, under compressive strain (5% strain, 1HZ, 1hr) Cbp/p300-interacting transactivator with

ED-rich tail 2 (CITED2) becomes activated. CITED2 is involved in suppressing the expression of MMP-1 and MMP-13 (He *et al.*, 2016).

A family of transmembrane heterodimeric proteins called integrins also play a vital role in mechanosensing. These proteins connect the intracellular actin cytoskeleton with molecules located extracellularly. Integrins $\alpha 1\beta 1$, $\alpha 5\beta 1$, $\alpha 10\beta 1$ and $\alpha v\beta 5$ are the principal integrins found in chondrocytes. Upon compressive loading, $\alpha 5\beta 1$ results in the intracellular production of IL-4 which subsequently causes membrane hyperpolarisation (Wright *et al.*, 1997). Upon hyperpolarisation the transcription of aggrecan is activated and MMP-3 transcription becomes inhibited (Millward-Sadler *et al.*, 1999). Furthermore, under cyclic pressurisation (26.7kPA, 0.33Hz, 30mins-3hours) integrins can activate c-Jun N-terminal kinases (JNK) MAP kinase signalling cascade resulting in proteoglycan synthesis (Fitzgerald *et al.*, 2008). However, under compression at 0.1MPa, 0.5Hz, 24h another MAP kinase called p38K is activated and causes the production of nitric oxide and prostaglandin E2, which are pro-inflammatory molecules (Fermor *et al.*, 2002).

1.6 Cartilage Damage

Thus far, we have discussed various mechanisms by which healthy cartilage homeostasis is maintained. In an ideal scenario, cartilage would remain in this healthy state for the remainder of a lifetime. However, due to the fact that the cartilage is in an environment which supports high mechanical loads as well as multiple load cycles it is a tissue susceptible to mechanical injury or in lay terms 'wear and tear'.

1.6.1 Mechanical Injury of Articular Cartilage

As discussed previously, cartilage displays an excellent ability to withstand compressive loads partially due to the water content within the chondral matrix, which in response to a low strain rate, slowly permeates out the matrix allowing hydrostatic pressure to bear the load rather than the matrix. However, in injury the load is applied too fast for the fluid to permeate. Therefore a much greater share of the load is experienced by the solid phase (cells and cartilage matrix). This results in

damage to the cartilage matrix as well as a reduction in its biomechanical function in supporting and transmitting loads (Buckwalter and Mankin, 1998). It is estimated that every year in the United Kingdom that there are 10,000 cartilage lesions severe enough to require surgical intervention (NICE, 2017).

There are several modalities by which articular cartilage can be damaged without any disruption to surrounding tissues. The first of these is through direct blunt trauma to the knee, which can occur for example by falling directly onto a hard surface. Another example is torsional loading which occurs when a joint that is loaded is severely twisted. Finally, there is indirect impact loading which involves injuring the subchondral bone below the articular cartilage. The final two examples are common cases of articular cartilage injury during sport (Buckwalter and Mankin, 1998).

There are three categories which can be used to define articular cartilage injuries, each with different clinical presentation as well as a different capacity for repair and regeneration. The first of these is damage to the solid phase (cells, chondral matrix or subchondral bone) without visible damage to the articular cartilage surface. This has minimal known symptoms, and providing the cellular fraction retains sufficient viability the cells can restore the native composition. Another injury type is of course disruption to the articular surface integrity which includes ruptures and fractures. This results in significant pain, inflammation and a reduced biomechanical function, and depending on various factors including size and location of the lesion this can progress to further cartilage degeneration. The final and most severe injury is an osteochondral fracture which demonstrates damage to both the cartilage and bone layers. This has similar symptoms to the chondral disruptions. However, there is a formation of a fibrin clot which can contribute to neotissue regeneration. However once again, depending on size, location and joint integrity, stability and alignment this type of lesion can progress to further cartilage degeneration (Buckwalter and Mankin, 1998).

Furthermore, there are several determinants which influence the type and severity of lesion experienced by an individual. Naturally, an important determinant is the rate and intensity of the load as well as concomitant muscle contraction which influence

the load experienced by the articular surface. Aside from external factors, there are also unavoidable intrinsic factors such as age of individual as well as natural variability in articular cartilage which are genetically pre-determined, which influence injury type and progression (Buckwalter and Mankin, 1998).

In order to diagnose a cartilage lesion it is important to have a uniform system for the characterisation of injury severity. Historically, two principal systems have been utilised, the Outerbridge and Bauer and Jackson (Bauer and Jackson, 1988). The Bauer and Jackson system is a more descriptive measure, in that it includes information on lesion appearance. This grading system defines lesions on a scale of Grades I through to VI. The Outerbridge system differs from the Bauer and Jackson system through its assessment of the depth of a lesion (Nehrer *et al.*, 1999). More recently, Brittberg and Winalksi (2003) developed a grading system in conjunction with the International Cartilage Repair Society (ICRS) that allows for macroscopic assessment of cartilage lesions. The ICRS grading scale describes 5 grades of cartilage damage from 0 = normal to 4 = severely abnormal. The qualifiers for each grade are described and graphically presented below in Figure 1.10 (Brittberg and Winalski, 2003). Whilst this system has the potential to unify diagnoses and treatment evaluations, there are still a number of macroscopic, histological and imaging based techniques to assess cartilage damage depending on application. The most appropriate system for grading is a contested subject within the field. However, in terms of grading for cartilage repair, Smith et al. (2005) have validated the use of the ICRS scale as well as the Oswestry Athroscopy Score (OAS) as statistically reliable and valid in assessing repair of articular cartilage following autologous chondrocyte implantation (Smith *et al.*, 2005).

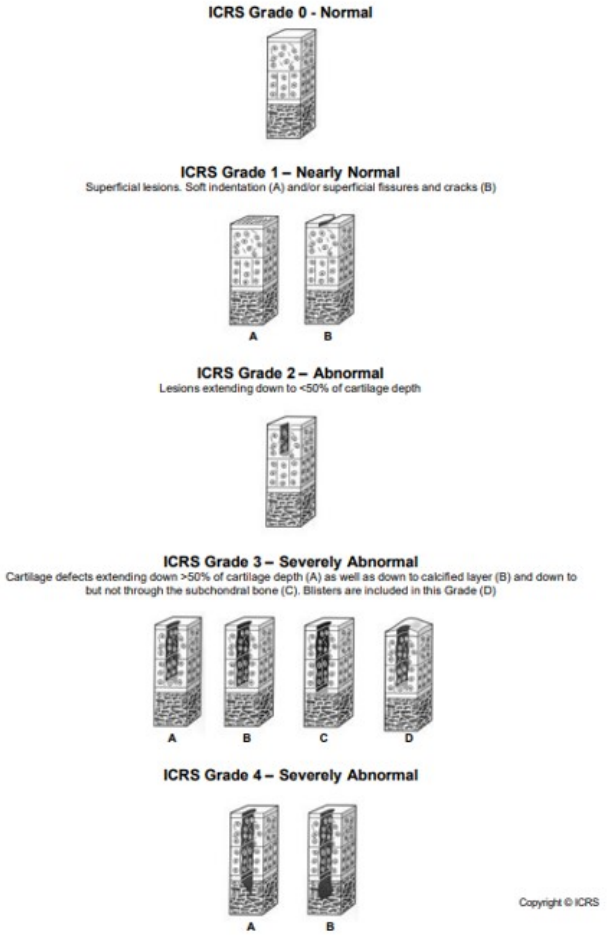

Figure 1.10: ICRS Grading System. Graphical representation of various degrees of cartilage lesions according to the ICRS grading system. (Taken from the ICRS Cartilage Injury Package).

1.6.2 Response to Mechanical Injury

When subject to hyper-physiological loads articular cartilage undergoes significant changes in the extracellular matrix organisation and biomolecular composition of the tissue. In response to acute or repetitive blunt trauma there is a reduction in the proteoglycan concentration (Buckwalter, 1992; Donohue *et al.*, 1983). Furthermore, several *in-vitro* models of acute compressive trauma demonstrate a loss of proteoglycans (Torzilli *et al.*, 1999). These studies also elucidate a disruption to the collagen network, accompanied also by cell death when loads over 15-20MPa were applied (Torzilli *et al.*, 1999).

As mentioned previously, the chondrocyte has an ability to sense changes in the

extracellular matrix composition and has a limited capacity to restore native ECM composition. It is hypothesised that self resolution is only possible if the amount of proteoglycan and collagen loss is within the range of what a chondrocyte can produce. Of course this depends on the percentage of viable chondrocytes remaining after injury (Buckwalter, 1992)

Post-injury, the resident chondrocytes first response is to secrete Interleukin-1-β, which in turn binds the IL-1 receptor I initiating intracellular signalling cascades through nuclear factor kappa B (NF-$\kappa\beta$), p38 and JNK. The final result of this is expression of the inflammatory cytokine Tumour Necrosis Factor-α (TNF-α) (Klatt *et al.*, 2006). In this instance TNF-α activates MMP-1, MMP-2 and MMP-13 expression in chondrocytes, resulting in cartilage degradation (Fan *et al.*, 2006; Tang *et al.*, 2009; Liacini *et al.*, 2003). Furthermore, chondrocytes begin to express TGF-β (Scharstuhl *et al.*, 2002) to increase chondrogenesis to begin regeneration of the joint. However, in some instances there is a lack of control over the TGF-β production, resulting in it's overexpression, which causes a downstream high expression of MMP-13 (Rose and Kooyman, 2016).

In response to injury there is an immune response which derives primarily from resident macrophages in response to the presence of damaged ECM in the synovial fluid. This results in the inflammation of the synovial membrane and release of aforementioned inflammatory mediators. Studies have also shown thickening of the synovial membrane in response to cellular infiltration. In patient with joint injuries the macrophage content of the synovium increases (Bondeson *et al.*, 2010).

1.7 Osteoarthritis of the knee

Thus far, normal homeostasis of articular cartilage has been discussed, as well as some of the changes associated with mechanical injury. Unfortunately, if the previously mentioned conditions which permit restoration of native articular cartilage are not met, there is a potential for the joint to become osteoathritic. OA is a degenerative disease, characterised by the deterioration of joints, which results in significant pain and immobility in those who suffer (Thomas *et al.*, 2013). In the knee, OA principally

manifests itself in the progressive degeneration of the articular cartilage surface. It is estimated that there are currently 8.75 million individuals suffering from knee OA in the UK alone (Mobasheri and Batt, 2016). Phenotypic changes in OA articular cartilage include surface fibrillation, chondrocyte clustering, chondrocyte hypertrophy, increased cartilage calcification and vascularisation of the subchondral bone (Figure 1.11) (Goldring, 2012)

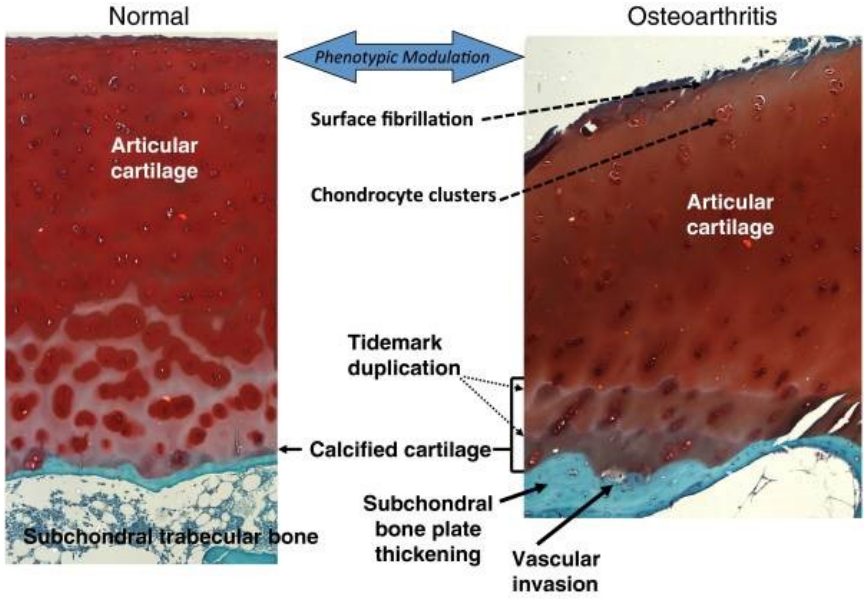

Figure 1.11: Osteoarthritic Cartilage. Histological appearance of healthy articular cartilage (left) and OA articular cartilage stained with Safranin O. (Taken from (Goldring, 2012) with permission for Gratis Reuse).

1.7.1 Inflammation and OA

OA has a plethora of triggers, of both mechanical and biological origins. Previously, the concept of injury based inflammation has been introduced, and this is considered a common trigger for OA and inflammation of the synovial membrane is considered a key contributor towards degradation of the articular cartilage matrix. A schematic summarising some of the principal pathways involved in the propagation of inflammation in articular cartilage and OA is demonstrated below in Figure 1.12 (Chevalier *et al.*, 2013).

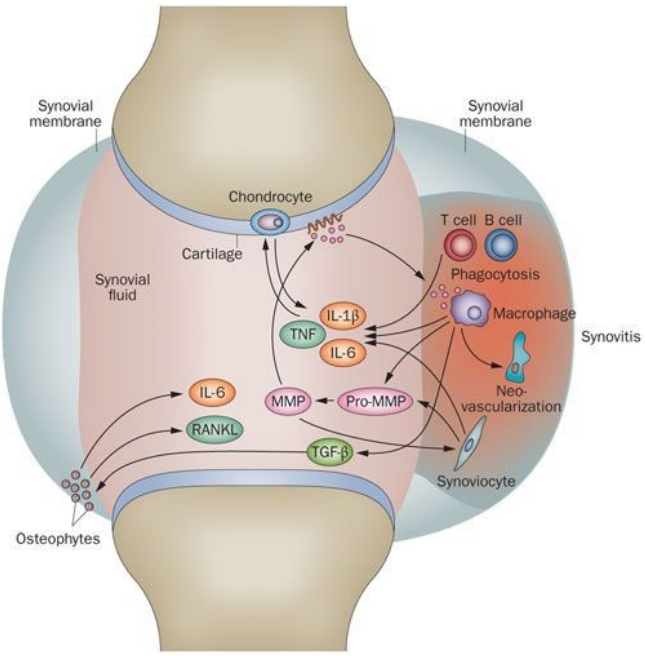

Figure 1.12: Inflammatory cytokines in OA Cytokine production in response to presence of DAMPS in the knee joint. (Taken from (Chevalier *et al.*, 2013) under licence number 5396040906834).

Upon injury, fragments of ECM are released into the synovial fluid in the joint space. In this instance, fragments from the ECM such as hyaluronan can be considered as damage associated molecular patterns (DAMPs) which initiate an innate immune response (Scanzello *et al.*, 2008). Toll-like receptors on the cell surface membrane of synovium macrophages recognise DAMPs, and as a result the macrophages adopt an activated phenotype and subsequently secrete IL-1β and TNF, alongside pro-MMPs (Blom *et al.*, 2007); (Bondeson *et al.*, 2010). IL-1β is a key regulator of cartilage degradation, as it stimulates a catabolic shift in chondrocytes. This involves an increased expression of MMP-13 and A disintegrin and metalloprotease with thrombospondin type I motifs (ADAMTS)-4, and a suppression of aggrecan and collagen synthesis (Fernandes *et al.*, 2002). Furthermore, TNF-α engages in a positive feedback loop with ADAMTS-7 through NF-κB signalling. Increased TNF-α, stimulates ADAMTS-7 which causes articular cartilage breakdown, and as a result also upregulates TNF-α (Lai *et al.*, 2014). Interestingly, chondrocytes in OA cartilage exhibit significantly higher amount of the p55 TNF-α receptor, which may make OA cartilage more sensitive to the effects of TNF-α stimuli (Fernandes *et al.*, 2002).

Finally, it is not only the hyaline surface and the synovium that is affected, the subchondral bone layer also experiences inflammation in the zone of calcified cartilage. This can cause the production of vascular endothelial growth factor (VEGF) as well as other angiogenic molecules which subsequently causes cell differentiation and local MMP production (Bonnet and Walsh, 2005; Sanchez *et al.*, 2005; Pesesse *et al.*, 2011).

1.7.2 Chondrocyte Hypertrophy and OA

As described earlier, unrestricted differentiation of chondrocytes will eventually form bone, and not cartilage. Permanent articular cartilage production relies on the prevention of terminal differentiation (Kraan and Berg, 2012). Hypertrophic chondrocytes at the growth plate have a differing phenotype to resident articular cartilage chondrocytes. They can be characterised by the expression of Type X Collagen, MMP-13, Runx2, VEGF and HtrA1, analogous to the role of this chondrocyte phenotype in endochondral ossification (Kirsch and Mark, 1992; Nurminskaya and Linsenmayer, 1996; Alvarez *et al.*, 2000; Horner *et al.*, 1999; Tsuchiya *et al.*, 2005). There is a large body of work based upon the hypothesis that in OA, chondrocytes acquire the phenotype of a hypertrophic chondrocyte (Kraan and Berg, 2012).

On examination of the characteristic markers of hypertrophic chondrocytes, the basis for their involvement in development of OA is evident. On acquisition of this phenotype, chondrocytes switch towards a degradative phenotype. This involves the aberrant secretion of catabolic enzymes such as MMP-13 and HtrA1 which are responsible for degradation of the articular cartilage matrix (Kraan and Berg, 2012). In fact the expression of MMP-13 has been shown to be increased 40-fold in OA cartilage shown by reverse transcription polymerase chain reaction (RT-PCR) and microarray (Fukui *et al.*, 2008). As described previously, MMP-13 has specific activity towards Collagen III. It has been shown that when comparing healthy and OA cartilage samples, the OA samples have a much elevated level of MMP-13 (Aref-Eshghi *et al.*, 2015). As well as upregulating certain genes involved in OA, genes such as Sox-9 involved in the maintenance of the healthy chondrocyte phenotype have been shown to be downregulated (Hattori *et al.*, 2010).

Following on from this, there are many hypotheses as to how heathy articular chondrocytes acquire this hypertrophic and degradative phenotype. Some studies indicate that it is a result of age-related changes in chondrocytes (Figure 1.13). TGF-β is an essential growth factor in the maintenance of articular cartilage and thereby inhibits chondrocyte hypertrophy. As described previously TGF-β signalling is propagated via downstream phosphorylation of SMAD3. In a SMAD3-KO model, symptoms such as cartilage fibrillation; proteoglycan depletion and mild degeneration were observed accompanied by an increase in the number of hypertrophic chondrocytes (Yang *et al.*, 2001). This can be explained by the fact that in articular cartilage, SMAD2/3 with ALK5 controls cartilage anabolic responses, whereas SMAD1/5/8 and ALK1 control catabolic responses (Finnson *et al.*, 2010). This is significant as these pathways are delicately balanced, therefore inhibiting one pathway causes a phenotype switch towards a catabolic pathway. Interestingly, with age ALK5 and SMAD2/3 phosphorylation decreases in chondrocytes which may explain the skewed homeostatic balance favouring cartilage degradation (Blaney Davidson *et al.*, 2009).

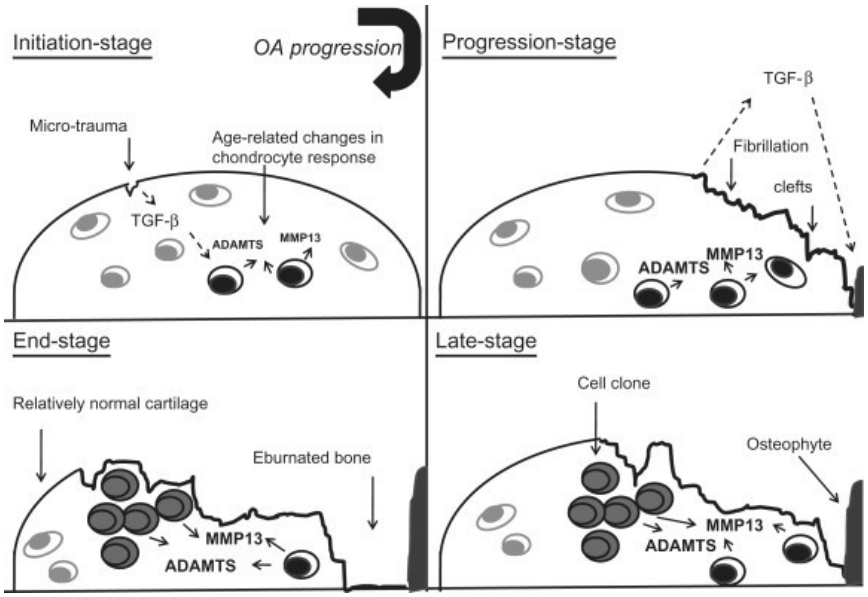

Figure 1.13: Model of hypertrophic like changes and the development of OA. Black cells indicated cells that have acquired a hypetrophy-like phenotype. (Taken from: (Kraan and Berg, 2012) under licence number 5396050081596).

Chondrocyte hypertrophy can also be initiated post mechanical insult. On damage to the cartilage collagen II is exposed, which is detected by DDR2 domains on the

surface of chondrocytes. This activates a switch towards this degenerative phenotype (Xu *et al.*, 2007). This has been investigated further, and may be explained by the fact that collagen II activation of DDR2 increases Runx2 expression (Zhang *et al.*, 2011), which drives chondrocyte hypertrophy. Runx2-KO models have shown a decrease in severity of OA as well as a decreased MMP13 expression (Kamekura *et al.*, 2006).

1.7.3 Mechanical Stress and OA

The final risk factor discussed in this review will be the role of high, hyperphysiological loads in the progression of OA. As alluded to previously, chondrocytes respond to mechanical loads in various ways depending on the magnitude and mode of the load. Unloading or static loading is unfavourable for healthy cartilage homeostasis (Guilak *et al.*, 1994). However, loads within the physiological range applied dynamically are beneficial in promoting and maintaining matrix synthesis and decreasing inflammatory responses (Wong *et al.*, 1999; Torzilli *et al.*, 2011). But when loads occur in the 'hyper-physiological' range, homeostasis is disrupted. When these type of loads are applied dynamically and acutely as in an injury setting, cartilage degradation is favoured (Figure 1.14), as well as resident cell death and the promotion of inflammation (Nam *et al.*, 2009; Ashwell *et al.*, 2013).

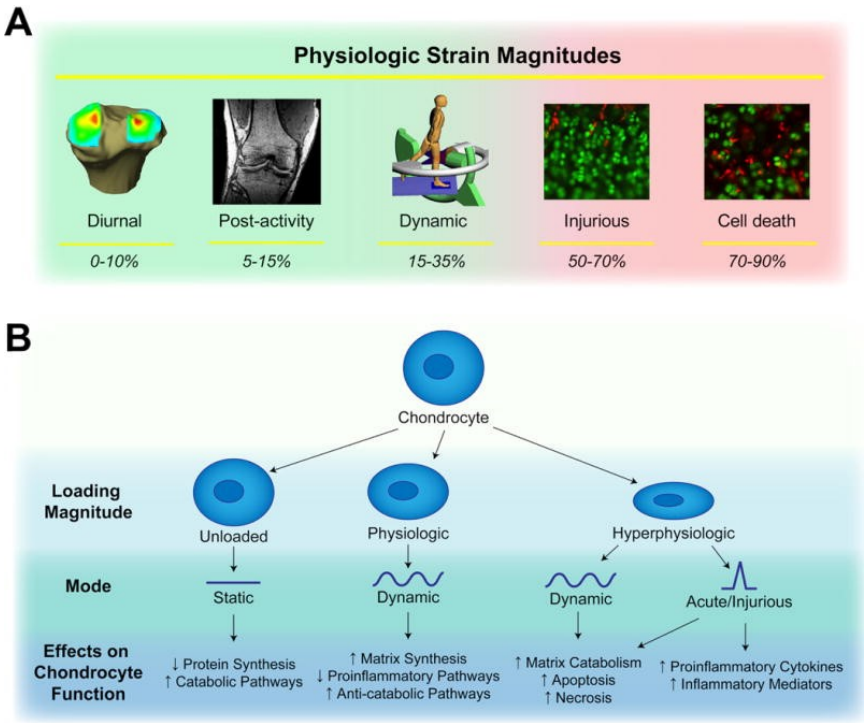

Figure 1.14: Effect of different loading regimes on the anabolic and catabolic function of chondrocytes. Taken from: (Sanchez-Adams *et al.*, 2014) with permission from Springer Nature under licence number 5396050575801.

The development of OA after experiencing 'hyper-physiological' loads is specifically known as posttraumatic osteoarthritis (PTOA), and is estimated to be the cause of 12% of all OA cases (Brown *et al.*, 2006). This is partially due to the subsequent up-regulation of inflammatory regulatory such as IL-1α and IL-1β, and in more severe cases of PTOA there is a greater upregulation (McNulty *et al.*, 2013). This IL-1 signalling causes MMP activity to increase, GAG degradation and further release of the pro-inflammatory mediator Nitric Oxide (NO) (McNulty *et al.*, 2013). Furthermore, upon biomechanical loading there is a release of TGF-β1 which activates HTRA1 serine protease, which disrupts the PCM, causing it to enlarge and suffer a reduction in mechanical properties (Xu *et al.*, 2014).

Finally, as well as articular cartilage fractures, injuries to surrounding soft tissues such as anterior cruciate ligament (ACL) and the menisci can contribute to PTOA (Englund *et al.*, 2009; Dare and Rodeo, 2014). A study of synovial fluid sample from 111 patients suffering from post traumatic ACL tears indicated that levels of IL-1β, IL-6, IL-8 and TNFα were elevated against an uninjured control, most so at day 0-1 post ACL tear (Sward *et al.*, 2012). Furthermore, post-ACL injury, ligament tissue

demonstrated at 1000-fold increase in MMP-13 production and the synovium had a 350-fold increase (Haslauer *et al.*, 2013). This potentially indicates that the soft tissue injuries are a significant source of inflammatory mediators and proteolytic enzymes that contribute to the degradation of cartilage post injury (Lieberthal *et al.*, 2015).

1.7.4 Symptoms of Osteoarthritis

The consequences of OA on patients include pain, which can result in immobilisation and psychological distress, joint stiffness/instability and reduced joint function (Hunter *et al.*, 2008). As cartilage is an aneural tissue, the pain does not result directly from damage to the tissue. However, concomitant changes such as synovitis and bone marrow lesions contribute significantly to knee pain. The aneural nature of cartilage also means that degradation and damage goes undectected until the subchondral bone is exposed and significant degradation has already occurred. Furthermore, inflammatory mediators released in response to the disease can sensitise afferent nerves, which causes previously non-painful activities such as walking to elicit a pain response (Hunter *et al.*, 2008).

Whilst pain is undoubtedly an extremely significant symptom of OA, this chapter will focus more on the impact on the biomechanical function of the tissue, as the biomechanical properties of articular cartilage are intrinsic to healthy knee joint function and longevity. Furthermore, in order to make any substantial recovery from the disease, the native biomechanical properties must be recapitulated.

The resultant damage to the solid phase of articular cartilage causes significant disorganisation and disruption to the fibrillar collagen network which can result in up to a 90% reduction in the tensile modulus of the tissue (Akizuki *et al.*, 1986), as well as the compressive modulus, which decreases with increasing severity of cartilage degradation (Armstrong and Mow, 1982). This interferes with the tissues ability to withstand and transmit compressive loads. Comparison of the mechanics of cartilage at different ICRS grades of OA shows that with increasing severity, the Young's modulus of cartilage decreases (Kleemann *et al.*, 2005). This is likely to be a result of the decreased proteoglycan content seen in OA cartilage (Saarakkala *et al.*, 2010), which results in a greater permeability of the tissue meaning that more of the load

is supported by the solid phase rather than by the osmotic pressure (Pearle *et al.*, 2005). This loss of proteoglycans is complemented by a stiffening of the collagen matrix due preferential deposition of collagen I over collagen II found in healthy cartilage, which has a lower elastic modulus (Silver *et al.*, 2002). The net outcome of this is a stiffer and thinner matrix which ultimately results in a greater load transmission to the subchondral bone, can result in alterations to the subchondral bone structure (Maldonado and Nam, 2013).

Finally, the boundary lubrication at the articulating surface is also drastically affected by the onset of morphological changes to the hyaline cartilage surface such as fibrillation, roughening, ruptures and fissures. Combined with a reduction of the lubricin content of the synovial fluid (Kosinska *et al.*, 2015) this increases the solid-solid contact, as well as friction, resulting in increasing wear and further cartilage damage (Desrochers *et al.*, 2013) . The loss of biomechanical function of a joint can cause health problems such as obesity and immobility which further contribute to the deterioration of joint function. This loss of mobility can cause patients psychological distress due to the loss of physical and mental wellbeing. Consequently, due to the innate importance that the biomechanical properties has on correct joint mechanobiology and function, as well as on patient wellbeing, we believe that when considering treatments for cartilage damage and osteoarthritis it is essential to consider the mechanical properties of the intervention.

1.8 Treatment of OA and Articular Cartilage Damage

If OA is left untreated, and the degradation occurs to a severe extent, total knee athroplasty (TKA) is the recommended solution, and can offer >95% survivorship for 7-16 years (Font-Rodriguez *et al.*, 1997). TKAs prove to be successful interventions in patients over 70 years old, with a lifetime risk of revision of 5% (Bayliss *et al.*, 2017). However, for young and more active patients there is much higher failure rate which could result in a patient requiring several revisions throughout their lifetime. In fact in patients below 55 years old, one study has reported a survivorship of 63% after 10 years (Lee *et al.*, 2014). Patient satisfaction with the intervention, has been

reportedly low. Of a survey of 27,372 TKA patients, 17% of patients were dissatisfied with the outcome (Robertsson *et al.*, 2000).

To delay prosthetic intervention in patients, it seems more effective to treat cartilage lesions earlier on before severe degradation can occur. Popular techniques for treating symptomatic and asymptomatic cartilage lesions are microfracture, osteochondral autografting (mosaicplasty) or allografting as well as autologous chondrocyte implantation (Sophia Fox *et al.*, 2009).

1.8.1 Microfracture

Microfracture is a technique which aims to enhance the regenerative potential of the knee, through releasing bone-marrow-derived MSCs from the subchondral bone layer (Figure 1.15). This is achieved through drilling 1-2 mm diameter holes, 3-5 mm apart in the subchondral bone plate with either a pointed metallic instrument or a narrow calibre drill (Steadman *et al.*, 1997; Chen *et al.*, 2009).

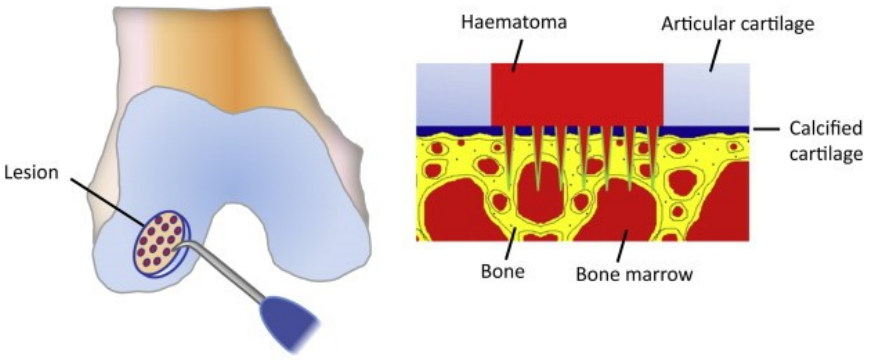

Figure 1.15: Graphical representation of the microfracture process. (Left) Shows the perforation of the subchondral bone through the use of a narrow calibre drill; (Right) Demonstrates the formation of a haematoma – which bears bone-marrow-derived MSCs (Taken from (Hunziker *et al.*, 2015)) with permission from Elsevier under licence number 5396060478178.

This technique has become a popular first-line of treatment due to the low cost and technical simplicity, as well as the reported clinical outcomes (Hunziker *et al.*, 2015). The results of microfracture are essentially filling of the defect which is accompanied by pain relief. Studies have shown that 80% of patients report an improvement in knee pain (Steadman *et al.*, 2003). Furthermore, in terms of functionality of the knee, they report an improvement in the Lysholm score (1-100) from 59 to 89, indicating

a significant improvement in knee function after 7-17 year follow up (Steadman *et al.*, 2003). However, there are several limitations with this treatment, firstly in regards to the inferior fibrocartilaginous repair material in place of the native hyaline cartilage (Nehrer *et al.*, 1999). Furthermore, Steadman's study was carried out on patients under 45 years old, and studies have shown that in elder patients, with a lower capacity for spontaneous regeneration this technique is less effective (Kreuz *et al.*, 2006). Finally, a recent UK clinical consensus suggests that microfracture is less effective for cartilage lesions over $2cm^2$ (NICE, 2017)

1.8.2 Osteochondral Autografting (Mosaicplasty) and Allografting

Osteochondral Autografting or Mosaicplasty is a treatment based on replacing the area of cartilage damage with healthy, autologous native tissue. This technique is utilised for full-thickness lesions and involves the introduction of multiple osteochondral plugs to the lesion site. As demonstrated in Figure 1.16, the plugs are drilled out of non-weight bearing areas of the cartilage and press-fit side by side. The number of plugs depends on the size of the lesion (Hunziker *et al.*, 2015).

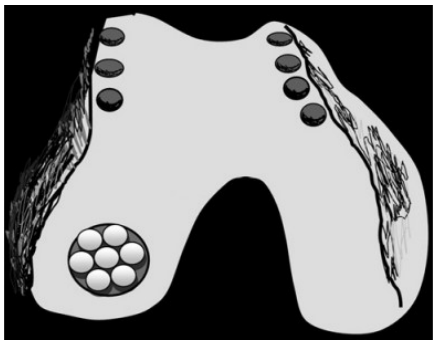

Figure 1.16: Surgical procedure of mosaicplasty. Image demonstrates both the extraction site, as well as the plugs inserted into the lesion site (Bartha *et al.*, 2006)

The advantage of this procedure is that the plugs re-establish the cartilage surface and provide a restoration of previous biomechanical properties of the tissue, meaning that the benefits stretch beyond sole symptom release. Furthermore, due to the autologous nature of this procedure, it only requires a single surgery (Hunziker *et al.*, 2015).

Studies have shown statistically improved outcomes of mosaicplasty over microfracture in terms of ICRS score, reoperation rate and return to sport (Gudas *et al.*, 2012). However, amongst the literature there is discrepancy as to whether there is a difference in clinical outcomes after each treatment, as comparison of functional and MRI outcomes have shown no significant difference (Lim *et al.*, 2012). However, in most instances both report a significant improvements in functional measures and in the Knee Injury and Osteoarthritis Outcome Score (KOOS) (Ulstein *et al.*, 2014).

With this treatment, however, its benefits are also a source of its limitations. The cost of having autologous tissue replacement is the creation of additional lesions elsewhere in an already damaged joint, which may generate additional sites of degeneration within the joint termed donor site morbidity (LaPrade and Botker, 2004). A systematic review into incidence of donor site morbidity after mosaicplasty, which included 1473 knee cartilage defects from 11 studies, showed donor site morbidity in 5.9% of patients (Andrade *et al.*, 2016). There is also a limited amount of donor material, which restricts this technique for smaller lesions (Burks *et al.*, 2006). On top of this, lesions above $3cm^2$ treated with mosaicplasty have demonstrated inferior outcomes (Gudas *et al.*, 2009). Osteochondral allografting operates under the same principles as autografting, apart from the fact that the tissue origin is cadaveric (Czitrom *et al.*, 1986). The benefits are much the same as autografting, with clinical success rates from 65-85% with studies ranging to 10 years follow up (Meyers *et al.*, 1989; Mahomed *et al.*, 1992). However, this technique creates potential complications with the immunogenicity of the grafts (Langer *et al.*, 1978), disease transmission (Mahomed *et al.*, 1992), donor availability and the feasibility of long-term storage of the grafts (Sherman *et al.*, 2014). However, this is an area of interest, with groups demonstrating improved viability and maintenance of chondrogenic gene expression after 7-days post-harvest by maintaining at 37°C (Denbeigh *et al.*, 2021).

1.8.3 Autologous Chondrocyte Implantation

In 1994, Brittberg and colleagues introduced autologous chondrocyte implantation (ACI) into the clinical setting. ACI is a procedure which involves first taking a biopsy of healthy cartilage from a non-load bearing region (Figure 1.17). This cartilage is

subsequently digested to obtain the patients chondrocytes, usually in the scale of 10^5. These are subsequently expanded to generate a cell number of approximately 2-5 x 10^6 cells. These cells are subsequently implanted into the cartilage defect, below a sutured on section of periosteum from the medial tibia (Brittberg *et al.*, 1994).

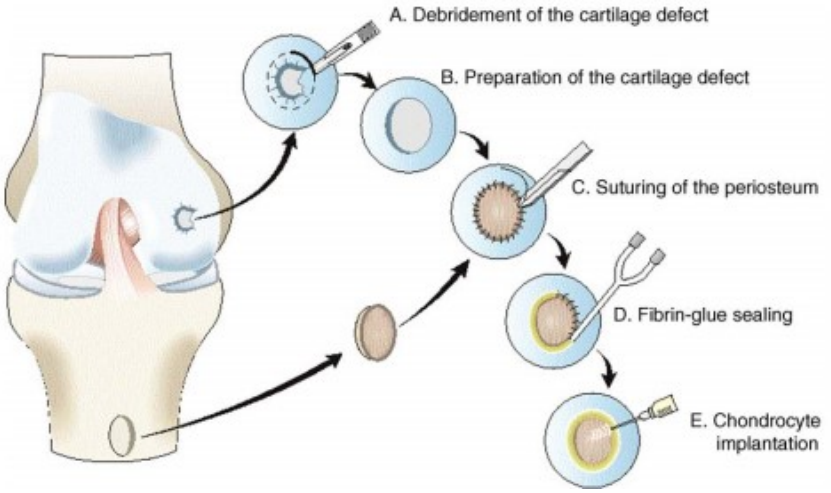

Figure 1.17: Overview of the procedure of 1st Generation ACI. Taken from (Marlovits *et al.*, 2006) with permission from Elsevier under licence number 5396070970791

From this initial study, Brittberg *et al.* (1994) reported that 14 out of 16 patients showed good or excellent results in terms of the pain, swelling and locking of the knee. Furthermore, macroscopic and histologic evaluations took place, and in 73% of cases the repair material was hyaline-like cartilage, the remainder was fibrocartilage (Brittberg *et al.*, 1994). This was supported in when Peterson *et al.* (2000), studied 101 patients who received ACI. In follow ups between 2-9 years after surgery, 93% of patients with single lesions showed good to excellent clinical results, as well as 63% of patients with multiple lesions (Peterson *et al.*, 2000). ACI has been compared with microfracture in a clinical setting over a 2 and 5 years, to show that both show improved short and midterm clinical outcomes (ICRS score, Lysholm, Short Form-36 and Tegner). However there was no significant clinical or radiographic difference between either of the two treatments (Knutsen *et al.*, 2004; Knutsen *et al.*, 2007). This may cause some to argue in favour of using the cheaper, less risky and less traumatic option in microfracture (Hunziker *et al.*, 2015). Despite this, in 2017 NICE recommended ACI for the treatment of asymptomatic cartilage lesions over the size of 2cm^2 (NICE, 2017).

One of the major limitations of ACI, is the necessity for two surgical interventions; one for tissue harvest and the other for cell implantation (Hunziker *et al.*, 2015). Similarly to autografting, some argue against creating further lesions in an already arthritic cartilage (Lee *et al.*, 2000). Another issue is the lack of mechanical competency prior to hyaline cartilage regeneration, as well as the relatively long rehabilitation process (Lee *et al.*, 2017a). Many patients will have significant restriction in independent weight bearing for 6 to 8 weeks (Toonstra *et al.*, 2016). Finally, in terms of the procedure, some have highlighted issues of such as cell leakage from repair site and microtrauma from the suturing (Willers *et al.*, 2005).

1.8.3.1 Generations of ACI

In response to some of the limitations of conventional ACI, a 2nd generation of ACI was developed. As demonstrated in Figure 1.18, in place of the periosteum a bi-layer collagen membrane is utilised. This is advantageous as it reduces the amount of surgical incisions required, and studies have shown a lower incidence of graft hypertrophy than seen with the use of periosteum. Hyaline cartilage was also demonstrated in 70% of repair sites (Haddo *et al.*, 2004). Brittberg conducted a randomised controlled trial into the efficacy of matrix assisted cell implantation (MACI) versus microfracture. After a 2 and 5-year follow up, it was determined that cartilage lesions over 3cm^2 treated with MACI demonstrated clinically and statistically improved outcomes based on KOOS pain and function score and MRI evaluation of structural repair, amongst other measures (Brittberg *et al.*, 2018).

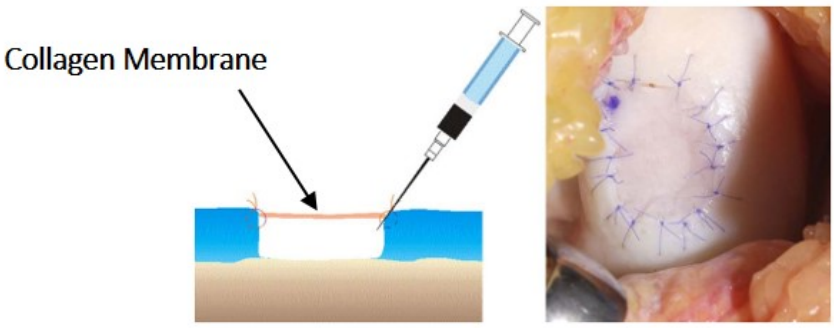

Figure 1.18: Second Generation ACI or Matrix Assisted Chondrocyte Implantation (Adapted from:(Marlovits *et al.*, 2006) with permission from Elsevier under licence number 5396070970791).

However, as with ACI, prior to regeneration there is still limited biomechanical strength. Furthermore, the mantra for successful osteochondral tissue engineering, dictates that for successful regeneration one should use of a 3D scaffold which attempts to emulate the structure properties of the tissue. In this case it's clearly far removed from the native tissue structure (Kon *et al.*, 2013).

In response to these requirements, a 3rd generation of ACI has been developed. This development is defined by a 3D scaffold, pre-seeded with autologous chondrocytes. Usually, after debridement of the lesion the biomaterial is trimmed to fit the lesion size, and is inserted by a press fit (Marlovits *et al.*, 2006). This again eliminates the requirement for periosteal harvest, promotes an even cell distribution throughout the defect and maintains chondrocyte viability and their phenotype (Willers *et al.*, 2005). A 3rd generation MACI device has been compared against microfracture, and the results demonstrated that over two years MACI outperformed microfracture according to Lysholm, Tegner and ICRS scores, in the treatment of larger cartilage lesions (4cm^2) (Basad *et al.*, 2010). This is a conclusion that has been shown in other studies (Brittberg *et al.*, 2018).

Despite promising indications of 3rd generation ACI/MACI, there are still key limitations in the mechanical strength of the repair material. Several studies have investigated the mechanical properties of repair material generated by the ACI and later generations of MACI. Compression testing of ACI repaired cartilage in an equine model demonstrated an aggregate modulus equal to 12% of the native tissue (Strauss *et al.*, 2005). Furthermore, MACI grafts reportedly achieve 15% of the aggregate modulus of native tissue (Lee *et al.*, 2000) Interestingly, (Griffin *et al.*, 2015) report values of up to 70% of the native tissue. However, they suspect this is due to the fact that a long-term implant was used and the use of a large animal model.

1.8.3.2 Rehabilitation post-ACI

Another important variable in the successful implementation of autogolous cell implantation is the post-surgery rehabilitation programme. In the first 6-weeks post implantation the cells are seeded with a collagen membrane and are at their most vulnerable to damage through excessive loading (Hambly *et al.*, 2006), as well as

graft delamination (Reinold *et al.*, 2006). To allow for succesful graft maturation, a conservative programme of progressive weight bearing (WB), culminating with full WB after 12-weeks has been suggested (Hambly *et al.*, 2006).

In the first 7 days post-surgery the key aims are to prevent excessive shear forces on the cell and graft by restricting weight bearing. Constant passive motion between 0 and 30 °for a minimum of 1 hour/day, is suggested to prevent intra-articular adhesions (Mithoefer *et al.*, 2012), to maintain joint mobility and to reduce oedema and pain. Patients may also practice 20% WB exercises using scales and crutches. The patient also is instructed to wear a knee brace, restricting the movement from 0 - 30°(Edwards *et al.*, 2014). In weeks 2-3, the goal is to achieve full and painless passive knee movement, as well as 90°knee flexion and 30% WB, with correct heel to toe gait mechanics. Furthermore, once the surgical wound has healed sufficiently, hydrotherapy is recommended, whereby exercise such as heel raises, squats and step-ups are performed in water, reducing gravity on the joint which mimics an unloaded knee and permits greater range of motion of movement without the contraindications of weight bearing (Edwards *et al.*, 2014). In the 3rd rehabilitation phase (4-6 weeks post surgery), the key aims are to achieve active knee flexion beyond 125°and to progress from 40% - 60% BW. The resistance for the WB exercises in previous phases are increased, and recumbent cycling (less knee flexion) is introduced (Edwards *et al.*, 2014).

By the fourth phase (weeks 7-12), the graft is assumed to be in the proliferative phase of its maturation. Chondrocyte begin to migrate from the implanted matrix and start to fill the defect with a primitive repair tissue. Rehabilitation aims to achieve full WB by week 8, as well as a pain-free cycling and 6-minute walk test without protective knee brace. The patients must demonstrate a proficiency in post-operative rehabilitation exercise, so that these can be continued independently at home.

After 12-weeks the cells begin remodelling the defect, and produce collagen II and aggrecan to fill the defect with a firm matrix. Rehabilitation enters Phase 5 where the goal is to restore healthy gait, the introduction to additional WB exercises such as squats, leg press and lunges. It is in this phase that the patient may return to work (Edwards *et al.*, 2014)

After 6-months, the defect should be begining to mature into a functional tissue, and rehabilitation is focussed on including more intense cardiovascular exercise to restore strength to both the treated and contralateral limb. However, resumption of previous sporting activities must be avoided until 12 - 18 months post-surgery if they subject the knee to high compressive or shear loading (Hambly *et al.*, 2006; Edwards *et al.*, 2014).

The evolution of ACI to MACI, in terms of the inclusion of a 3D scaffold as well as improved athroscopic techniques (Filardo *et al.*, 2011) has reduced the morbidities associated with the procedure and may allow for an accelerated rehabilitation programme, with full WB by 6-weeks (Edwards *et al.*, 2013). Utilising this accelerated approach, patients are able to return to normal gait and daily activities much faster, allowing for improved clinical outcomes (Edwards *et al.*, 2014).

1.9 Osteochondral Tissue Engineering

Given the clinical success of 3rd generation ACI/MACI it appears that cells seeded onto a three dimensional scaffold, which attempts to emulate the native cartilage structure, is an effective solution. In the field of cartilage tissue engineering research this is a well-researched approach. This section of the review will highlight the most successful, as well as features which contribute towards their success.

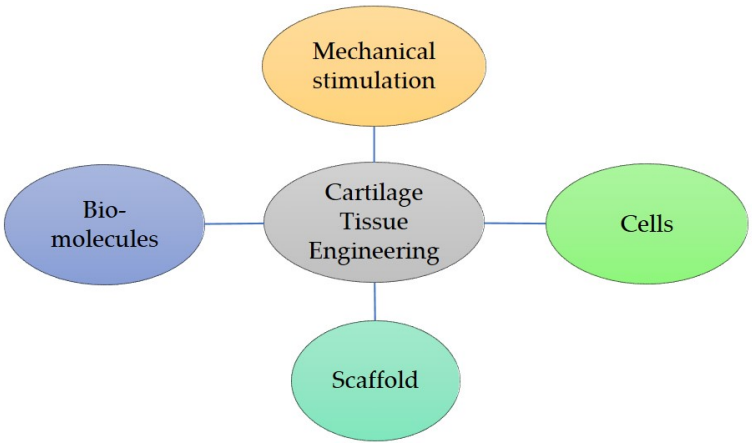

Figure 1.19: The basic paradigm for cartilage tissue engineering

1.9.1 Key concepts in Tissue Engineering

Before discussing the various approaches, it is important to understand the central tissue engineering paradigm (Figure 1.19). Historically, there have been three key elements to the engineering of any tissue. First is the scaffold, which is usually a three dimensional structure made from synthetic or natural biomaterials. Secondly, there are cells, which are responsible for regeneration through their synthesis of ECM. The final element is biomolecules, which when applied to the system can modulate cellular activities (Langer and Vacanti, 1993).

1.9.2 Cells for cartilage tissue engineering

In cartilage tissue engineering there are simply two cell approaches that can be employed 1) seed chondrocytes onto the scaffolds or 2) seed stem cells that have the capacity to differentiate into chondrocytes, as these are the only cell type capable of regenerating articular cartilage.

The application of chondrocytes has been discussed already in respect to ACI. They are an obvious choice of cell due to their restriction to the chondrogenic lineage. Furthermore, they are more abundant than progenitor cells and there are yet to be any severe clinical safety issues with chondrocyte implantation. Furthermore, due to the autologous nature of this cell therapy, problems with immunogenicity are bypassed. That being said, there are still limitations to be considered with this approach in that it requires surgery in order to obtain the cells. There is also phenomena of chondrocyte dedifferentiation during the expansion phase pre-implantation, which is characterised by the production of non-specific proteoglycans as well as collagen type I (Von Der Mark *et al.*, 1977). This is as a result of 2D monolayer culture conditions which does not accurately mimic what the cells experience *in-vivo*. Therefore, efforts must be made pre-implantation to ensure the chondrocyte phenotype is maintained, and this can be done through the application of growth factors such as IGF-1 or TGF-β (Jenniskens *et al.*, 2006; Shakibaei *et al.*, 2006) or through maintaining in a 3D culture environment (Tare *et al.*, 2005). The use of cell aggregate culture in medium containing FGF, has shown the capability of redifferentiating 2D expanded

chondrocytes (Huang *et al.*, 2016).

Another attractive source for cartilage cell therapies are mesenchymal stem cells (MSCs). The basis behind this is that MSCs have chondrogenic potential under the correct environmental conditions, and therefore could differentiate into chondrocytes and repair cartilage defects (Caplan *et al.*, 1997). Therefore, researchers can pre-condition MSCs through culture in a 3D environment along with the addition of growth factors such as TGF-β, FGF and BMPs amongst others, in order to generate chondrocytes for use in cell therapy (Fellows *et al.*, 2016). Alongside their chondrogenic capacity, MSCs have a high proliferative capacity, ease of expansion and extraction from tissues such as bone marrow, adipose tissue and the synovial membrane (Pelttari *et al.*, 2008). Another property of MSCs which makes them attractive from a tissue engineering point of view is that they readily interact with the microenvironment, exhibiting immunomodulatory and anti-inflammatory effects, as well as improvements of native cell viability (Glenn and Whartenby, 2014). Despite this, chondrocytes derived from MSCs synthesis have lower levels of articular matrix molecules (collagen II and aggrecan) than the native tissue, and the repair tissue is more akin to that of the intervertebral disc (Steck *et al.*, 2005). Furthermore, hydrogels seeded with chondrocytes had much improved mechanical properties over gels seeded with MSCs under the same conditions (Mauck *et al.*, 2006). Furthermore, what is termed an MSC is usually a heterogeneous population of cells which may affect reproducibility in cartilage tissue engineering application, when compounded with the fact that during *in-vitro* expansion MSCs have a great capacity for phenotypic drifts (Somoza *et al.*, 2014).

Whilst both cell types offer promising prospects for cartilage tissue engineering, and indeed chondrocytes are used regularly in the clinic for ACI to great success, several iterations upon these two cell types show promising indications for cartilage repair. One such iteration is the application of allogeneic cells, which would remove the necessity for cell harvesting from an individual. This is possible through the use of human juvenile chondrocytes, which are protected from the host immune system due to the lack of cell surface molecules that activate T-cell responses (Adkisson *et al.*, 2010a). This juvenile cell type shows a 100-fold greater rate of GAG

synthesis, production of hyaline cartilage, faster growth rates when compared to adult chondrocytes (Adkisson *et al.*, 2010b). Intriguingly, this cell phenotype also confers a resistance to the inflammatory cytokine IL-1β, due to the enriched levels of CD24 (Lee *et al.*, 2016). Some of these properties, namely increased proliferation and IL-1β resistance are also shared by human iPSC-derived chondrocytes (Lee *et al.*, 2017b). The research into these two approaches is still very much in its infancy but both represent promising solutions to some of the limitations of other cell therapy procedures.

1.9.3 Role of mechanical stimuli in cartilage tissue engineering

Over time the tissue engineering paradigm has had to adapt due to a previous negligence with regards to the resulting biomechanical properties of the engineering tissue. As this review has certainly stressed, it is vital for an intervention to eventually recapitulate the native mechanical properties of the diseased/injured tissue. Therefore, the notion of 'functional tissue engineering' (FTE) was adopted, which places emphasis on the final mechanical properties of the tissue (Butler *et al.*, 2000). Therefore, within this FTE approach, the application of mechanical stimuli to tissue engineering constructs, is considered another essential element to include in the paradigm. As a result of this, various chondrocyte mechanical loading regimes have been studied to determine optimum conditions for cartilage tissue engineering.

As discussed previously, compressive stimuli are important in the maintenance of growth of articular cartilage. This is also true in the field of tissue engineering, dynamic compression of up to 1HZ and 10% have demonstrated beneficial effects in natural, synthetic and hydrogel scaffolds (Mauck *et al.*, 2000; Jung *et al.*, 2008; Kisiday *et al.*, 2009). Interestingly, it has been suggested that as well as mechanically stimulating the cells, compression may act to increase solute transport which is beneficial for cell growth. This too may explain the negative impact of static loading upon cartilage biosynthesis (Zhang *et al.*, 2009). Using a bespoke dynamic compression bioreactor ((Kisiday *et al.*, 2009)) to investigate constructs composed of cells cultured in self-assembling peptide hydrogels has demonstrated a significant increase in GAG

accumulation, equilibrium modulus and dynamic stiffness versus constructs maintained in free-swelling conditions. The values for the equilibrium modulus in mechanically stimulated constructs was 98kPa which is an order of magnitude lower than that of native cartilage (Tatman *et al.*, 2015).

Despite synovial fluid minimising shear forces in an in vivo environment, various studies have investigated effect of shear on cultured chondrocytes. (Jin *et al.*, 2001) found that the application of dynamic shear of 1-3% at 0.01-1Hz resulted in the increased synthesis of cartilage ECM products such as proteoglycans. Therefore, this has been employed in vessels for tissue engineering known as bioreactors. For example, rotating wall bioreactors are capable of applying shear of 0.15Pa (Freed and Vunjak-Novakovic, 1995), which has also been shown to increase GAG synthesis within tissue engineering constructs whilst maintain collagen content (Martin *et al.*, 2000). However, the application of applied shear at 1.6Pa has been shown to increase the production of proinflammatory mediators (Smith *et al.*, 1995), therefore regulated application of shear is important.

The previous studies, utilise uniaxial loading regimes (i.e. compression alone). However, research has demonstrated the benefit of biaxial loading regimes (Meinert *et al.*, 2017). For example, using a custom built bioreactor capable of both compression and shear has shown improved chondrogenesis in MSCs compared with uniaxial loading, in the absence of growth factors (Schätti *et al.*, 2011). Tensile stimulation has also been used to improve the ultimate tensile strength of tissue engineered constructs by 3.3X (Lee *et al.*, 2017a), and through the use of compression and sliding motion it is possible to yield constructs with a comparable equilibrium friction coefficient to articular cartilage (Bian *et al.*, 2010). This work demonstrates the potential and importance of developing bioreactors with physiologically relevant loading regimes in generating biomechanically relevant constructs for articular cartilage repair.

1.9.4 Scaffolds for cartilage tissue engineering

As mentioned previously, in order to ensure chondrocytes maintain phenotype it is favourable to maintain these cells within a three dimensional and mechanically relevant matrix. For cartilage tissue engineering there are a variety of scaffold manufacturing processes. These include matrices derived from synthetic polymers, natural materials, as well as hydrogel scaffolds and acellular native materials. Another important component for tissue engineering is the general properties for scaffolds for tissue engineering, which are summarised in Figure 1.20.

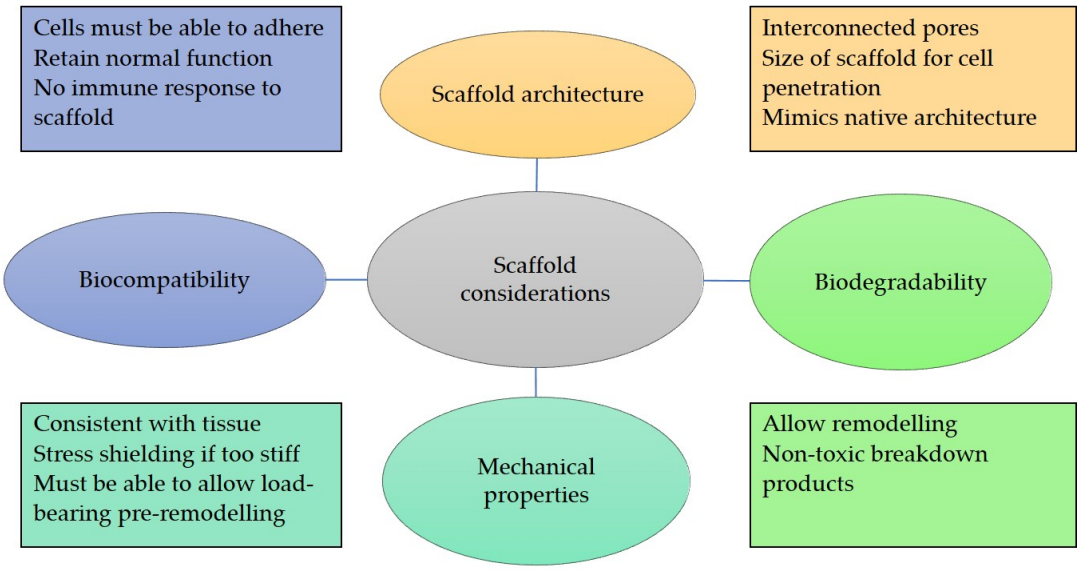

Figure 1.20: Key considerations in scaffold manufacture for tissue engineering Information from: (O'brien, 2011).

1.9.4.1 Synthetic polymer scaffolds

Due to the wealth of polymer processing technology now available, synthetic polymers can be used in cartilage tissue engineering (CTE) research to mimic the microarchitecture of natural tissues. Table 1.2 represents some of the commonly used polymers in tissue engineering as well as their application in cartilage repair.

Table 1.2: Synthetic Scaffold material applications in cartilage tissue engineering

Scaffold Material	Processing method	Evaluation	References
Polylactic Acid (PLA)	3D printed	Similar mechanical properties to cartilage and support cell growth	(Rosenzweig et al., 2015).
Polyglycolic Acid (PGLA)	Sponge with BMSCs + TGFβ	Cartilage regeneration in rabbit joint	Wang et al., (2010)
Polycaprolactone (PCL)	3D printed	Similar mechanical properties to cartilage	Olubamiji et al., (2016)
Polycaprolactone (PCL)	Electrospun and anisotropic	Similar mechanical properties to native cartilage and support cell growth + ECM deposition	McCullen et al., (2012)

These polymers have significant advantages in this application. Firstly, from a translation perspective, all of these materials already have FDA approval for use in humans. Secondly, PLA and PGLA are α-hydroxy acids, which means they contain an ester bond which makes the scaffolds capable of non-enzymatic hydrolysis. The degradation products from this breakdown are non-toxic, which satisfies both the biodegradability and biocompatibility criteria for TE scaffolds. Furthermore, the rate at which the polymers degrade can be tuned to suit the rate of neo-tissue formation by altering the material properties of the polymer (Atala, 2007).

Another clear advantage of synthetic scaffolds is the ability to finely tune structure and properties to yield scaffolds with appropriate biomechanical properties. A polyethylene terephthalate (PET) scaffolds seeded with chondrocytes, achieved a 2.8 MPa compressive modulus after culture, which was higher than their reported value for native cartilage (1.8 MPa) (Finlay *et al.*, 2016).

The use of synthetic materials, also permits the use of advanced fabrication technique, allowing for high precision manufacture of scaffolds capable of recapitulating the complex structure of articular cartilage. Using electrospinning McCullen *et al.* (2012) report an impressive example of an attempt to recapitulate the 3D zonal arrangement of articular cartilage using electrospun PCL arrange in a trilaminar composite scaffold (Figure 1.21) (McCullen *et al.*, 2012).

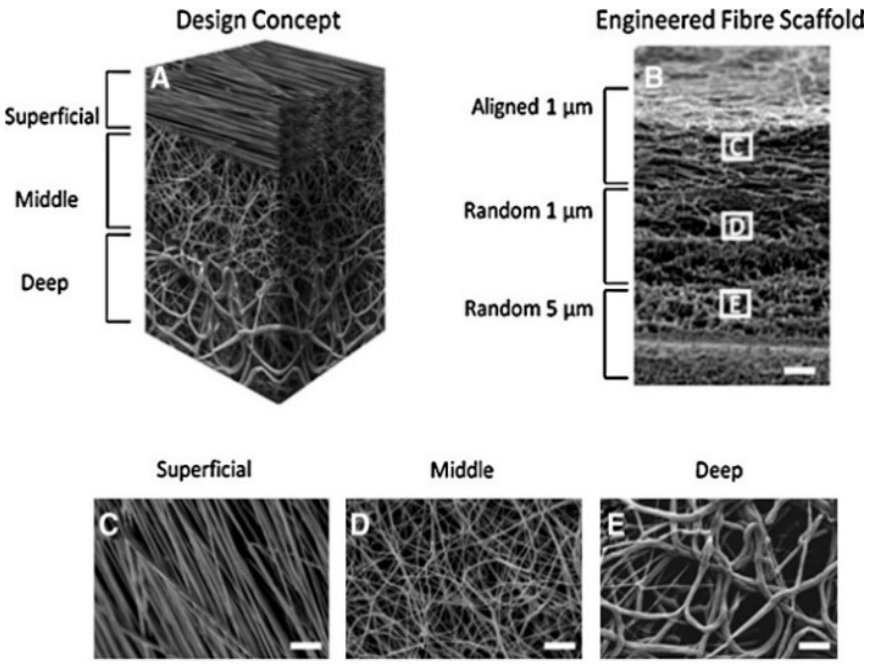

Figure 1.21: Electrospun PCL scaffold to recapitulate native bioarchitecture. Taken from: (McCullen *et al.*, 2012).

These scaffolds supported chondrocyte attachment as well as the production of Collagen II and GAGs. The anisotropic zonal arrangement showed vast improvements versus a scaffold which was homogenous in structure. Furthermore, the scaffold demonstrated similar mechanical properties to that of articular cartilage (McCullen *et al.*, 2012).

3D bioprinting is also an effective biofabrication method in the production of constructs for cartilage tissue engineering. The technique uses bioinks which can be composed of synthetic materials and cellular material. These bioinks are 3D printable, thereby offering the possibility of printing a 3D scaffold with encapsulated cells, or scaffold-less approaches in which the cellular material is deposited in an order to optimise cell-cell interactions (Elhadad *et al.*, 2022). Due to the recent emphasis on platform compatibility, 3D bioprinting can be used following image acquisition of tissue using CT/MRI scanning. Using these images, computer aided design can be as a template for precise bioprinting, allowing accurate replication of the desired replacement tissue. This technique has been used in cartilage tissue engineering to generate constructs capable of mimicking more complex cartilage behaviours, beyond compressive resistance alone. Using hydrogel bioinks (alginate and gelatin

methacryloyl), reinforced with PCL fibres and loaded with MSCs, researchers have produced a scaffold with a compressive modulus approaching that of native cartilage. However, by offsetting the deposition of PCL fibres, it was possible to generate a construct with the tension-compression non-linearity which is also observed in native cartilage. Using a finite element modelling approach, it was predicted that the offset in fibre deposition would allow for maintenance of a higher hydrostatic pressure in the construct compared with the aligned scaffolds, as a result of the ability to resist lateral expansion of the network (Schipani *et al.*, 2020).

Despite these advantages, there are several problems frequently observed with synthetic biomaterial scaffolds, which may have origin in the lack of natural binding motifs, hydrophobicity and failure to precisely recapitulate the bioarchitecture found in cartilage which the chondrocytes are sensitive to. This results in low cell attachment to the scaffolds, lower production of ECM matrix molecules (Chu *et al.*, 1997) which may result in resorption of the scaffold prior to ECM deposition (Frenkel and Di Cesare, 2004). Furthermore, due to the low clearance rates *in-situ* of metabolites from the cartilage, the acidic degradation products can cause a decrease in pH which negatively impacts the cell niche for regeneration (Park and Cho, 2010).

1.9.4.2 Natural biomaterials for cartilage tissue engineering

In order to improve the biocompatibility and the cell adhesive properties of scaffolds, it seems logical to utilise proteins and carbohydrate materials found in articular cartilage such as collagen and hyaluronan (Duarte Campos *et al.*, 2012).

As has been extensively discussed, collagen is naturally found within the articular cartilage matrix, and as well as providing tensile mechanical strength, also displays motifs on its surface which support cell adhesion (Getgood *et al.*, 2009). Collagen II matrices in particular have demonstrated a capacity to maintain chondrocyte phenotype of BMSCs with the addition of TGF-β1 (Awad *et al.*, 2004). Collagen bilayer membranes are already utilised in the clinic in the form of MACI, the success of which has previously been discussed (Basad *et al.*, 2010; Ebert *et al.*, 2011). Chen *et al.* (2009) utilised a collagen sponge material alone to treat cartilage defects in rabbits, which showed improved repair material judged by both MRI and histology (Chen

et al., 2009). Interestingly these scaffolds also report a reduction in inflammatory exudation as well as preventing fibrous tissue growth. Furthermore, collagen can be processed to form a 3D hydrogel, which permit homogenous cell seeding, cell encapsulation as well as the previously mentioned supportive niche for chondrocyte proliferation and matrix synthesis (Mueller-Rath *et al.*, 2010).

Hyaluronic acid (HA) is a prevalent molecule in articular cartilage, and forms the backbone upon which proteoglycan molecules assemble (Sophia Fox *et al.*, 2009). HA based scaffolds are popular for tissue engineering due to their biocompatibility, ability for chemical modification and biodegradability. Similarly to collagen this material can be processed in many ways to form HA sponges, hydrogels and cryogels (Chircov *et al.*, 2018). A clinical product named Cartistem, is based on allogeneic human umbilical cord MSCs (hUCB-MSCs) seeded within an HA hydrogel (Park *et al.*, 2017). Recently, a clinical trial has been completed and the results from a 7-year follow up indicate that the product is safe as well as effective for articular cartilage repair. This conclusion was met based upon histological findings after a year, MRI at 3 years, as well as continuous clinical assessments over 7 years (Park *et al.*, 2017). Composite approaches, which use multiple materials as in native cartilage have been used. A composite hydrogel of collagen, chondroitin sulfate and hyaluronic acid (CCH) was seeded with allogeneic chondrocytes and cultured in a subcutaneous diffusion chamber for 4-weeks to generate ectopic cartilage (Jiang *et al.*, 2018). This construct was subsequently implanted into a cartilage defect within the same animal. They found compared to a collagen hydrogel alone the CCH showed much improved *in vivo* morphological, histological and mechanical properties compared with collagen and defect control (Jiang *et al.*, 2018). This approach appears to support many of the requirements for successful cartilage tissue engineering that this review has thus far discussed, in moving away from homogenous materials and using macromolecules that resemble those found in cartilage.

Another popular natural material used in scaffold approaches for cartilage tissue engineering is fibrin. Although not a component of cartilage, fibrin is a principal macromolecule that makes up blood clots at sites of injury. It is suggested as a potential scaffold material due to its biocompatibility, ability to be remodelled by

cells and retain biomolecules (Wong *et al.*, 2003). The most commonly used application of fibrin in the clinic in relation to cartilage is to aid with fixation of osteochondral fragments and sealing of periosteal flap in ACI (Wysocka *et al.*, 2010). It is especially popular in this application due to its protection of chondrocytes and its malleability. Therefore, studies have used autologous fibrin glue as a 3D carrier for autologous chondrocytes and found that the 'fibrograft' eliminated pain in all 50 patients and arthroscopy showed congruence of graft with host tissue. Despite interesting implications, minimal data was reported in terms of clinical outcome (Wysocka *et al.*, 2010). Fibrin can also be manipulated into hydrogels. The expansion of human fat pad stem cells (FPSCs) in fibrin hydrogels supported sGAG synthesis (O'hEireamhoin *et al.*, 2012). The authors attribute the success of this intervention to the recreation of a microfracture like environment.

Despite the key benefits of the use of natural biomaterials for cartilage tissue engineering such as cell attachment, differentiation and biocompatibility, there are several associated disadvantages. For example, HA and fibrin both have demonstrated low mechanical properties (Kawabe and Yoshinao, 1991), which when applied in the load bearing environment of the knee may lead to graft failure. It is possible, certainly with collagen, to improve mechanical properties through crosslinking (Vega *et al.*, 2017). Another drawback is the susceptibility of natural biomaterials to rapid degradation in response to enzymatic release from cells (Buchta *et al.*, 2005). Finally, there are general concerns over batch variation as well as disease transmission especially collagen from bovine sources (Frenkel and Di Cesare, 2004).

The advantages of both synthetic and natural biomaterials are complementary to each other's weaknesses, therefore a composite approach is becoming a more popular technique for cartilage tissue engineering (Moutos *et al.*, 2007; Wang *et al.*, 2020).

1.9.4.3 Hydrogels for cell encapsulation and delivery

As evident from the previous discussion of biomaterials for cartilage repair, hydrogels have received a lot of interest from the tissue engineering community. Hydrogels are defined by a 3D crosslinked network of a hydrophilic polymers, which have the capacity to absorb water and swell under aqueous condition. As discussed, it

is possible to cross-link natural biomaterials to create polymers making them an attractive tissue engineering solution as they have an ability to mimic the biomolecular content of the ECM. Furthermore, by altering the composition it is possible to alter the porosity of the mesh to permit cell adhesion, migration and proliferation (Slaughter *et al.*, 2009).

Hydrogels have also shown to be an effective delivery vehicle for growth factors as well as cells (Figure 1.22), via an injection. This provides many advantages for cartilage defect tissue engineering due to the potential for a minimally invasive treatment, which can gel in irregularly shaped defects to deliver regenerative factors (Liu *et al.*, 2017).

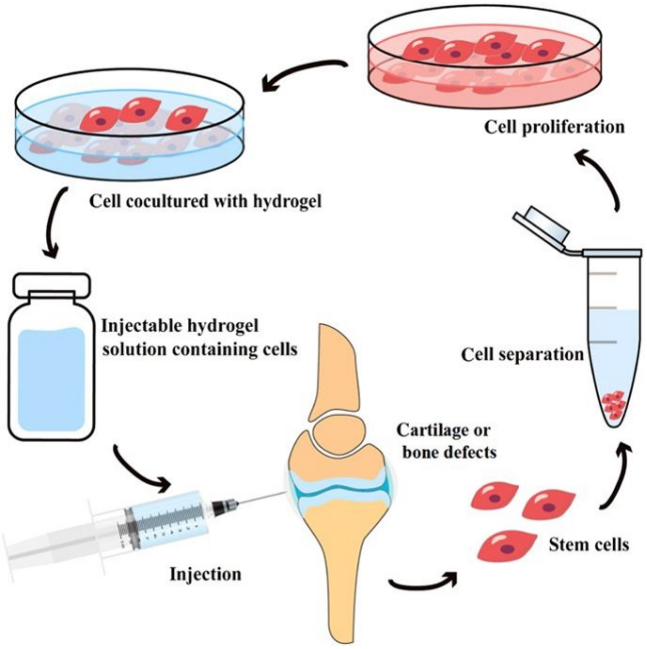

Figure 1.22: Schematic demonstrating the process of delivery an injectable, cell seeded hydrogel Taken from (Liu *et al.*, 2017).

Whilst some of the natural biomaterials that can be used to form hydrogel have been mentioned above it is worth mentioning that many other materials can be used to form cell encapsulating hydrogels such as chitosan, alginate, chondroitin sulphate, poly(ethylene glycol) and self-assembling peptides (Nicodemus and Bryant, 2008). The same key properties that apply for scaffolds (biocompatibility etc.) still apply for hydrogels, however hydrogels also have another distinct and defining property in their method of gelation. As demonstrated in Figure 1.22, the aim is to inject the

hydrogel into the defect as a solution which then forms a gel *in-situ*, therefore a popular approach is formulate a solution which forms a gel in response to physiological conditions. One example can be seen with temperature sensitive hydrogels, which pre-implantation are kept below what is known as the critical solution temperature. Upon injection, the physiological body temperature causes a phase transition, due to a change in the hydration state (Liu *et al.*, 2017).

1.9.4.4 Development of self-assembling peptide technology for cartilage tissue engineering

Self-assembling peptides are a type of hydrogel which have a promising application in tissue engineering. The P_{11}-X family, are a family of self-assembling peptides developed at the University of Leeds, which can assemble into a β-sheet tape structure when a pH trigger is imparted (Carrick *et al.*, 2007). The P_{11}-X family is so called due to the rationally designed sequence of eleven amino acids which make up the peptide. These amino acid residues are generally hydrophillic or hydrophobic with the exception of the three aromatic amino acids which make up a core of tryptophan and phenylalanine residues. Depending on the desired properties of the peptide, the eleven amino acid sequence can vary. Thermodynamics governs self-assembly of this peptide family, whereby assembly is driven by the formation of favourable inter/intramolecular interactions (Kyle *et al.*, 2012).

In powdered form, the peptide exists in a monomeric state, however, if resuspended in buffer of an appropriate pH and at a concentration above the critical concentration for gelation (C*), the peptide will begin to self-assemble. Firstly, from a random coil into a β-strand, which is a conformational transition associated with entropy loss. Upon formation of hydrogen bonds between backbone/sidechains of opposing peptides, the β-sheets subsequently form tapes. Intermolecular interactions between two tapes leads to the formation of a ribbon, which is energetically enabled by decreasing a conformational helical twist to adopt a "saddle" curvature. Finally, several ribbons can stack to form fibrils forming the intact self-assembled peptide structure (Davies *et al.*, 2006).

The Aggeli group at the University of Leeds are responsible for much of the research into this particular peptide family (Aggeli *et al.*, 1997; Aggeli *et al.*, 2003; Bell *et al.*, 2006; Carrick *et al.*, 2007), and have designed and developed over twenty self-assembling peptides which self-assemble based on a variety of triggers (Kyle *et al.*, 2012). These peptides have been implicated in several tissue engineering applications. The first of these was in the treatment of osteoarthritis, where P_{11}-9 was used to restore lubrication to damaged cartilage, due to it's similarity to hyaluronic acid (Bell *et al.*, 2006). Furthermore, the P_{11}-X family has been used in dentistry, where P_{11}-4 was used to promote hydroxyapatite mineralisation as the distance between the glutamic acid residues matched that observed in hydroxyapatite (Kirkham *et al.*, 2007). Both these applications demonstrate the applicability of this peptide family as acellular materials for use in tissue engineering and regenerative medicine.

An important finding in the development of this system for tissue engineering applications was the ability of the peptides to self-assemble at physiological pH, as well as the biocompatibility of these acellular peptides when subject to cytotoxicity testing. These findings have led to the investigation of this material as a matrix for cell encapsulation (Maude *et al.*, 2011). Of the peptides, P_{11}-8 was demonstrated to be the best peptide to support cell growth (Maude *et al.*, 2011).

P_{11}-8 is a glutamine based peptide, and has a positive charge (+2). These properties have made the peptide attractive for combination with the glycosaminoglycan (GAG) chondroitin sulphate (+2 charge) for treatment of intervertebral back pain. This combination reduces the apparent C* of P_{11}-8, and results in an increased shear modulus of the gel compared to the peptide alone. This P_{11}-8/CS system was used to successfully deliver GAG to injured and GAG depleted intervertebral discs. Restoring the native GAG content was shown to be effective in restoring biomechanical properties to the tissue (Miles *et al.*, 2016). Following on from this theme of GAG delivery to depleted tissues, P_{11}-8/CS has been used to improve the biomechanical properties of articular cartilage by restoring the native GAG content (Warren, 2017; Barco, 2017).

Based on the previous data we hypothesise that P_{11}-8/CS could act as a means of

delivering both chondroitin sulphate and therapeutically relevant cell types to damaged cartilage. This may allow for augmentation of biomechanical properties of damaged cartilage, accompanied by regeneration of the tissue supported by the delivered cells. However, the P_{11}-8/CS system has yet to be tested as a hydrogel for encapsulating cells and in it's current form would require significant development to the preparation process to allow for cell encapsulation.

1.10 Decellularisation of xenogeneic tissues

Thus far it has been determined, that the use of a homogeneous scaffold material is a basic approach to regenerate osteochondral lesions, as it is too distant from the native structure. It appears that the incorporation of molecules found within articular cartilage is an effective approach as it permits cell attachment and differentiation. Finally, in order to be a functional intervention it is important to have near-native mechanical properties. One increasingly prevalent technique which may fulfil all of these requirements is the use of decellularised tissues. Decellularisation is described as the process of generating 'like-for-like' tissue replacements by either chemically and/or mechanically removing the cells from a tissue. Upon removal of the cellular material and DNA, what remains is the ECM scaffold structure. There are a variety of techniques used to decellularise a tissue, which are listed below in Table 1.3. Each has slightly different effects on the tissue and tend to be used complementarily to each other to achieve the best results (Gilpin and Yang, 2017).

Table 1.3: Summary of decellularisation techniques and the effects on tissue

Method	Mode of Action	Effect on tissue	Refs.
Physical			
Freezing	Formation of ice within tissue ruptures cell membrane	Potential for ECM damage if frozen too rapidly; Remnant DNA	Xing *et al.*, 2014
Mechanical force/agitation (Shaker/sonication)	Pressure can burst cells as well as agitation. However, agitation is more commonly used to wash/ensure thorough exposure to chemicals	Force may damage ECM	Funamoto *et al.*, 2010
Supercritical CO_2	High applied CO_2 pressures (>7.40Mpa) and temperature (>31.1˚C)	Maintains mechanical properties	Sawada *et al.*, 2008
Chemical			
Non-ionic detergent (Triton X-100)	Interferes with lipid interactions with other lipids or proteins	Efficiency of cell removal is tissue dependent; removes GAGs	Mendoza-Novelo *et al.*, 2011
Ionic detergents (Sodium dodecyl sulfate (SDS))	Denature proteins; solubilises cellular membranes	Removes GAGs	Bolland *et al.*, 2007; Fermor *et al.*, 2015
Zwitterionic detergents (hypo/ertonic)	Osmotic shock causes rupture of cell membrane	Cell lysis	Kheir *et al.*, 2011
Enzymatic			
Trypsin	Cleaves peptides	May disrupt ECM structure with time	Shneider *et al.*, 2016
Endo/exo nucleases	Hydrolyses genetic material	Difficult to remove from tissue	Elder *et al.*, 2009; Gilbert *et al.*, 2006
Chondrotinase ABC	Breaks down aggrecan	Loss of GAGs	Bautista *et al.*, 2016

1.10.1 Decellularised osteochondral scaffolds

This technique has also been developed by many research groups for use in osteochondral tissue engineering, despite difficulties in complete cell removal posed by its dense structure (Wang *et al.*, 2018). Table 1.4 below demonstrates many of the approaches used in fabricating decellularised cartilage/osteochondral grafts.

Table 1.4: Summary of decellularisation strategies for osteochondral/cartilage tissue

Cartilage Decell Method	Description	Evaluation
Devitalised cartilage (Kelley *et al.*, 2002)	Dehydration in ethanol, lyophilisation, Freeze-thaw in liquid nitrogen	Cell fragments remained
Cartilage ECM-derived matrix (Yang *et al.*, 2008)	Pulverised, centrifugation, TritonX-100 in hypotonic, nuclease, made into solution, lyophilised and crosslinked to form a scaffold. Seeded with MSCs and implanted into mice	Cell viability maintained and neocartilage contained GAGs/collagen II
Acellular cartilaginous matrix (Wang *et al.*, 2014).	Freeze dried, Triton X-100, DNase and RNAase. Seeded with adipose stem cells (ASCs).	ASCs became chondrocytes and deposited collagen II; Repair tissue had higher cell density than cartilage and an inhomogenous distribution
Decellularised osteochondral scaffold (Fermor *et al.*, 2015)	Freeze/thaw, waterpik, hypotonic, hypertonic, 0.1% SDS, nuclease	Effective reduction in DNA, Reduced GAGs and biomechanical properties
Chondrofix osteochondral allograft plugs (ZimmerBiomet) (Farr *et al.*, 2016)	Remove lipids and bone marrow elements, soaked in methylene blue under light to inactivate viruses	72% failure and 19.6% survivorship; Age predictive of failure (average 35years); Degen *et al.*, (2016) report acute graft delamination
Decellularised chondrocyte sheets (Wang *et al.*, 2018)	Chondrocytes cultured to form cell sheets, sheets decellularised using 1% SDS	Application to rabbit defect model showed substantial remodelling
Acellular cartilage sheets (Xue *et al.*, 2018) *	1% SDS and lyophilised. Seeded with BMSCs.	Defects showed cartilage-like tissue with satisfactory interface healing after 6-months; ACS-BMSC significantly higher Young's moduli

In the first instances, many attempted to generate scaffolds derived from decellularised cartilage tissue (Kelley *et al.*, 2002; Yang *et al.*, 2008; Wang *et al.*, 2013). Aside from the unsuccessful devitalisation process (Kelley *et al.*, 2002), all have been implanted into animal models and shown relatively successful results. However, more recent work has developed the devitalisation process to yield constructs with a DNA content below the decellularisation threshold (Crapo *et al.*, 2011), however, this also required pre-processing with a laser to engrave channels (Nürnberger *et al.*, 2021). Despite promising indications of the other listed techniques, many involve destruction and reconstitution of the products into a scaffold and this has shown problems with integration and remodelling with the surrounding tissue (Wang *et al.*, 2018). Another strategy is to produce an ECM sheet derived from material synthesised from chondrocytes, and decellularise these sheets. The sheets are subsequently stacked to form ECM derived scaffolds. These have also showed promising results in animal models. However, it appears that a cell seeded approach showed

improved results over acellular scaffolds (Wang *et al.*, 2018; Xue *et al.*, 2018). However, it is worth mentioning that prior to regeneration these scaffolds also have very low mechanical properties.

Most recently, solubilisation of decellularisation cartilage has emerged as a trend in the literature. The solubilised matrices have been used as starting material in the production of extracellular matrix *derived* materials, for example in the production of hydrogels and bioinks (Beck *et al.*, 2016; Setayeshmehr *et al.*, 2021). The bioinks are currently early in development using solubilised decellularised ECM with poly(vinyl-alcohol) to 3D bioprint hydrogels laden with ATDC5 chondrocytes. The inclusion of decellularised material in the hydrogels was beneficial for cell viability, and demonstrated good printability, however the modulus was also inappropriate for restoration of biomechanical properties (Setayeshmehr *et al.*, 2021). Whilst the elastic compressive modulus of the reinforced hydrogels approaches that of articular cartilage (150 kPa), for the application of restoring the complex biomechanical and structural properties of large articular cartilage defects, the authors consider the production of intact decellularised osteochondral scaffolds more valuable (Beck *et al.*, 2016).

Processes have been developed at the University of Leeds to produce decellularised porcine osteochondral scaffolds with near-native structural and functional properties. The inclusion of the subchondral bone, rather than the implantation of the cartilage layer alone, is hypothesised to aid with graft integration and fixation. The one limitation of this study is that the native GAGs are depleted as a result of the process. This leads to an increase in the percentage deformation of the scaffolds under loading (Fermor *et al.*, 2015a).

Thus far, only one decellularised osteochondral scaffold has been tested in a clinical setting. This scaffold is termed a decellularised osteochondral allograft and has been translated into a product known as Chondrofix (ZimmerBiomet). Presumably due to the commercial nature of this product little is divulged into the processing methods to generate the scaffold. However, cadaveric human allografts have had both the lipid and bone marrow elements removed, and become sterilised through soaking in methylene blue and low-dose gamma irradiation (Gomoll, 2013). The results

of the several case reports and clinical series show discouraging results such as a 72% failure rate (Farr *et al.*, 2016), and a 61% survivorship (Johnson *et al.*, 2017). One report into 2 cases, show failure by acute graft delamination (Degen *et al.*, 2016). Despite the concerning results of these trials, it is all based on one scaffold type which has limited information describing its structural/mechanical properties or how it is fabricated. Therefore, it is difficult to discern the cause of failure. Furthermore, the extremely high failure rate reported by (Farr *et al.*, 2016) is likely to be due to their definition of failure, which is the occurrence of damage to the graft. If defining failure by revision, only 38% patients can be categorised as a failure.

One possible hypothesis could be as a result of the low cellular content of the graft. After the study, the graft still had no viable chondrocyte within the articular cartilage layer (Farr *et al.*, 2016). This could be explained by the difficulty which endogenous cells experience in migrating into the cartilage ECM due to the dense nature of the tissue (Wang *et al.*, 2018). Furthermore, studies have shown a correlation between defect size and likelihood of failure with this scaffold (Johnson *et al.*, 2017), therefore if our previous hypothesis is true, the bigger the graft the lower the likelihood of *in-situ* recellularisation.

1.10.2 Recellularisation of decellularised grafts

Due to the relative success of MACI (Brittberg *et al.*, 2018), as well as with naturally derived cell seeded scaffolds (Yang *et al.*, 2008; Park *et al.*, 2017; Xue *et al.*, 2018), a possibility to enhance the regenerative potential of decellularised osteochondral scaffold would be to supply them with regenerative cell types prior to implantation. In fact, studies have demonstrated that decellularised cartilage has chondroinductive properties. MSCs seeded onto these scaffolds showed an increased expression of collagen II, Sox-9 and aggrecan in an *in-vitro* setting (Sutherland *et al.*, 2015),.

A few groups are investigating this possibility, however, due to the small pore size of cartilage it is a challenge to recellularise the scaffold in vivo or in vitro. One group utilised an approach by which they created 30G channels in the cartilage, digested the GAGs, and used centrifugation and vacuum forces to improve recellularisation (Bautista *et al.*, 2016). After 20 days of culture there was infiltration up to 100 µM

into the deep zone, however, much of the rest of the cartilage was left unpopulated (Bautista *et al.*, 2016). Similar results were observed by (Schwarz *et al.*, 2012). Having said this, both the aforementioned studies were in an *in-vitro* setting. Wang *et al.* (2014) pre cultured cartilaginous matrix for 3-weeks with adipose derived MSCs prior to implantation into rabbit articular cartilage defects and found that after 12-weeks implantation the scaffold was completely recellularised (Wang *et al.*, 2014),. The use of dynamic culture environments, such as rotation, usually functions to improve the efficiency of recellularisation (Luo *et al.*, 2016). Furthermore, there is a possibility of including chemoattractive biomolecules to enable homing of endogenous cells to allow a enhanced cell distribution within the scaffold (Bautista *et al.*, 2016).

1.11 Rationale for Decellularised Matrix Assisted Cell Implantation

This review has indicated the clinical need for early intervention therapies for the treatment of cartilage lesions. Whilst ACI and its iterations (MACI) offer an attractive solution, prior to regeneration there is limited mechanical strength, which leads to a slow return to full joint loading. In addition recent evidence indicates that restorative procedures are more effective than purely regenerative solutions (Crawford *et al.*, 2012; Gudas *et al.*, 2013). However, restorative techniques such as mosaicplasty are limited by donor materials and donor site morbidity. Furthermore allografting has difficulties surrounding availability of tissue, immunogenicity and disease transmission. Tissue engineering research has demonstrated exciting applications. In spite of this, a large proportion of these scaffolds fail to recreate the exact bio-architecture of articular cartilage which can have downstream effects upon the biomechanical properties and quality of repair tissue.

We hypothesise that decellularised matrices would be ideal scaffolds to support autologous or allogeneic cell therapies, in the repair of large shallow cartilage lesions. Decellularised matrices offer a like-for-like tissue replacement, with retention of near-native biochemical composition and ECM structure which may provide an

initial recovery of biomechanical function to the compromised articular cartilage. We hypothesise that both seeded cells and endogenous cells will respond to the retained native bioarchitecture, to direct cells and maintain them in the chondrogenic state, resulting in the deposition of appropriate neotissue (hyaline cartilage).

This project aims to continue the development of the decellularised osteochondral scaffolds described by (Fermor *et al.*, 2015a). Whilst material and process development shows extremely promising indications, the scaffolds have several limitations in:

1. Current dimensions not relevant for treatment of large shallow cartilage lesions
2. Observed lack of integration *in-vivo* (Farr *et al.*, 2016)
3. Reduced GAG content and associated increase percentage deformation under loading

Therefore, this project will investigate the adaptation of the scaffold dimensions to treat larger lesions, as well as the efficiency of the existing decellularisation process on larger scaffolds. Furthermore, the potential of these scaffolds to be recellularised with chondrocytes will be studied, with a view to later provide a construct with an improved regenerative/integrative capacity. Articular cartilage has a low porosity and limited pore interconnectivity, making repopulation difficult, therefore, seeding methods will be investigated to improve cell repopulation of these scaffolds. Finally, to improve the biomechanical properties under loading, restoring the GAG content of the scaffolds is a promising place to start. This work will investigate the use of a self-assembling peptide (P_{11}-8) hydrogel to deliver chondroitin sulphate (CS) to the decellularised cartilage. The delivery method and resultant biomechanical properties will be studied.

The ultimate vision for this construct is the combination of a scaffold, cells and P_{11}-8/CS, yielding a scaffold with both improved regenerative and biomechanical properties. Therefore, rather than start with attempting to generate this composite scaffold, the compatibility of the hydrogel with cells will be determined, alongside the rheological properties of the gel. Whilst the ultimate aim is the tri-composite

scaffold, this research will explore the possibility of the use of P_{11}-8/CS with cells as a solitary device. The interaction between the three elements is demonstrated in Figure 1.23.

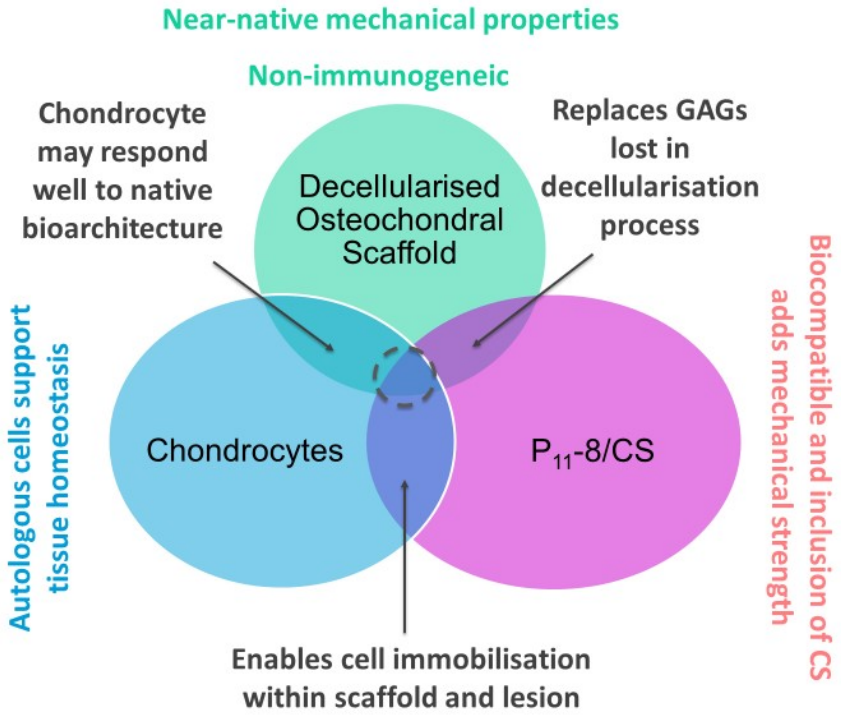

Figure 1.23: Graphic depicting the three interacting elements investigated in this thesis.

This study therefore has the following research questions:

- Would using decellularised porcine osteochondral scaffolds to assist autologous chondrocyte implantation be cost-effective compared with ACI, using a Markov health economics model?
- Is it possible to reproducibly fabricate osteochondral scaffolds of dimensions appropriate to treat large, shallow cartilage lesions? Is the current decellularisation process valid, to remove cells and DNA from the native tissue, whilst maintaining the extracellular matrix content and mechanical properties seen in previous porcine osteochondral decellularisation processes?
- Are self-assembling peptide suitable in terms of rheological and biological properties for the implantation of cells into damaged cartilage?

- Can methods be developed to enhance the delivery of viable cells to decellularised porcine osteochondral scaffolds? Is this method also appropriate for the delivery of P_{11}-8/CS to decellularised scaffolds?
- Does the delivery of P_{11}-8/CS reduce the percentage deformation of decellularised scaffolds?

This thesis will detail the methods used to address these research questions, and the subsequent result of these investigations.

Chapter 2

Materials and Methods

2.1 Materials

2.1.1 Equipment

The equipment used in this project is detailed in the Appendix, Table 9.1.

2.1.2 Consumables

The equipment used in this project is detailed in the Appendix, Table 9.2.

2.1.3 Cell lines

Three cell lines were used; C20A4 human chondrocytes obtained from Sigma Aldrich (SCC041), BHK hamster derived fibroblasts from the Health Protection Agency and murine L929 fibroblasts from the European collection of cell cultures.

2.1.4 Chemicals and reagents

The chemicals and reagents that were used in this project are listed in the Appendix, Table 9.3.

2.1.5 Software

Table 2.1: Details of Software used in this project.

Software	Purpose	Provider
ABAQUS	Assist Finite Element Modelling	**Dassault Systemes** https://www.3ds.com
FeBio	Finite Element Modelling	FEBIO software suite https://www.febio.org
LabView	Indentation test software	National Instruments https://www.ni.com/
MATLAB	Assist Finite Element Modelling	MathWorks Inc
PostView	Assist Finite Element Modelling	FEBIO software suite https://www.febio.org
PreView	Assist Finite Element Modelling	FEBIO software suite https://www.febio.org
Prism	Data analysis	GraphPad SoftWare, USA https://www.graphpad.com
Zen Blue/Black	Image capture	Carl Zeiss AG, Germany https://www.zeiss.co.uk

2.1.6 Glassware

Beakers and duran bottles (100 mL, 1,000 mL and 2,000 mL) were cleaned by immersion in a 1% (v/v) solution of phosphate-free detergent (Neutracon®, Decon Laboratories Ltd) overnight. Following this, glassware was rinsed in tap water, and a final rinse in distilled water to remove any residual detergent. Glassware was then dried and sterilised (180°C for 4 h, as required) by dry heat.

2.2 Methods

The following chapter will detail generic methods used across several chapters and studies. This has detailed methods for operations related to:

- Decellularisation solution preparation (Measurement of pH, Sterilisation, Composition of decellularisation media)
- Histological assessment of osteochondral scaffolds (Fixation, sectioning of paraffin wax samples, stain preparation and staining protocols, brightfield and confocal microscopy)

- Biochemical composition of decellularised scaffolds
- Cell culture for biocompatibility and use in recellularisation studies

2.2.1 General methods

2.2.1.1 Measurement of pH

The pH of decellularisation and histology solutions was measured using a Jenway 3020 pH meter. This was calibrated using pH 4, 7 and 10 standard solutions. To measure the pH of a solution using temperature compensation, both the pH and temperature probe were placed into the solution, whilst 1-12 M hydrochloric acid and sodium hydroxide were used, whilst stirring, to adjust to desired pH.

2.2.1.2 Sterilisation

Depending on the item three different sterilisation procedures were employed:

- **Dry heat sterilisation**. This method was used for equipment that was suitable for dry heat sterilisation such as dissection equipments. Each item was wrapped separately in foil or sealed within a sterilisable tin, and placed in a hot air oven for 4 hours at 180 °C.
- **Moist heat sterilisation**. Items not suitable for dry heat sterilisation (solutions within duran bottles or autoclavable plastics) were sterilised in an autoclave cycle of 20 minutes at 121 °C at a pressure of 103 kPa.
- **Filter sterilisation**. Solutions which were not suitable for heat sterilisation (cell culture aliquots) were filtered through 0.2 µm pore sized filter using a sterile syringe within a class II safety cabinet.

2.2.1.3 Microscopy

For imaging histology samples brightfield miscroscopy was employed using an Axio Imager M2 microscope (Zeiss) with an AxioCam MCr5 digital camera (Zeiss), and operated using Zen blue software (Zeiss). The same microscope and camera were

used for fluorescent microscopy, with the addition of a fluorescent illuminator and appropriate filters for the desired probe detection.

Phase contrast microscopy, for imaging monolayers, was undertaken on a BX51 inverted microscope (Olympus) with an XC-50 Camera (Olympus), operate using Cell B software (Olympus).

2.2.1.4 Confocal microscopy

For confocal microscopy of 3D cell constructs (hydrogels and recellularised scaffolds) a Zeiss LSM880 Inverted confocal laser scanning microscope was used (Zeiss). This is equipped with an Axio Observor.Z1 microscope, a Nano Focusing Piezo Stage and ZL multi S1 Incubator box, set to 37°C, and a selection of lasers (Diode 405 nm, Argon 458, 488, 514 nm, DPSS 561 nm, HeNe 633nm). Additionally, this microscope is equipped with a Airyscan detector for super-resolution imaging.

2.2.2 Acquisition and dissection of porcine legs to obtain femoral condyles

To produce decellularised porcine osteochondral scaffolds, first it was necessary to extract the native tissue. Porcine right hind legs were supplied by a local abbatoir (J Penny & Sons, UK) from immature pigs (approximately 6 months) within 48 hours of slaughter. Figure 2.1 illustrates the process of obtaining both lateral and medial femoral condyles from a whole porcine leg. Briefly, an incision was made laterally to the femur and tibia to expose the knee joint. Following removal of the tissue surrounding the joint, the femur was separated from the tibia by transection of anterior, medial, posterior and lateral collateral ligaments as well as the anterior, posterior cruciate ligaments. The femur was subsequently mounted in a vice, and using a bone saw, both the lateral and medial condyle were obtained and stored at -20°C.

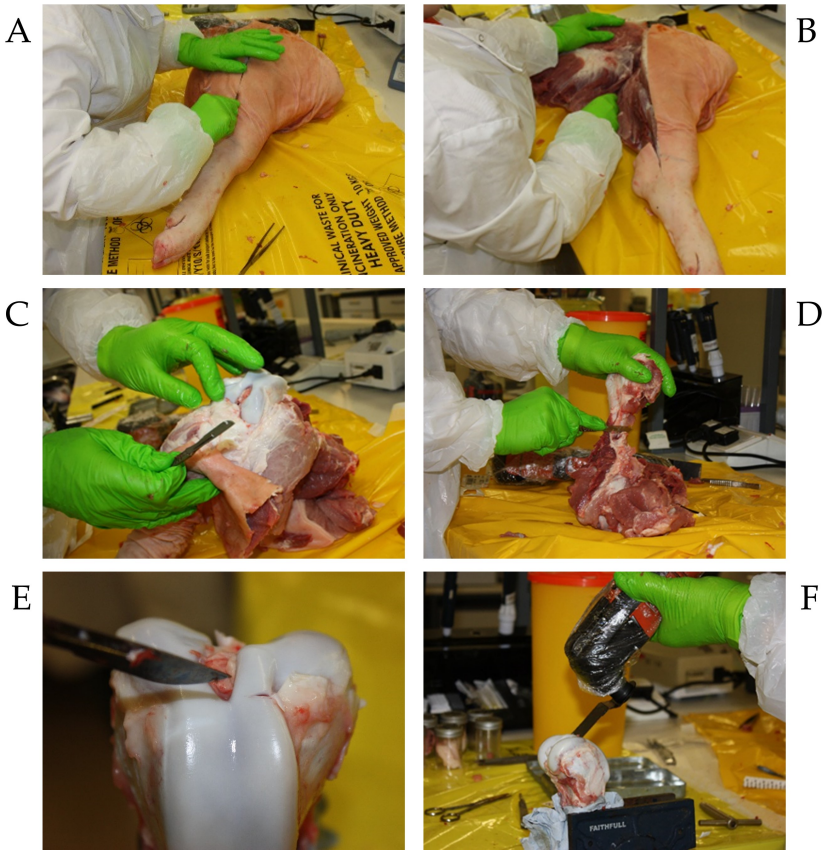

Figure 2.1: Dissection process for obtaining porcine femoral condyles. A) Lateral incision made to detach tissue from knee joint. B) Remove excess tissue surrounding the joint C) Knee joint exposed. D) Strip tissue away from the femur. E) Mount femur in vice use scalpel to create a groove. F) Use bone saw to remove lateral and medial condyles.

2.2.3 Decellularisation solution preparation

2.2.3.1 Phosphate Buffered Saline

A solution of phosphate buffered saline (PBS) solution (2 L) was made using 20 PBS tablets. The pH was adjusted to 7.2-7.4 and autoclaved at 121 °C, 15psi for 20 minutes. Solution was stored at room temperature for no longer than a month.

2.2.3.2 PBS with aprotinin (10 KIU.mL^{-1} aprotinin)

PBS solution was made as in Section2.2.3.1. Immediately prior to use, 1 mL of aprotinin (10 KIU.mL^{-1}) was added per 1L of PBS.

2.2.3.3 Hypotonic buffer (10 mM Tris, 10 KIU.mL^{-1} aprotinin)

Trizma base (2.42 g) was dissolved in 1900 mL of distilled water. The pH was adjusted to 8.0 - 8.2, and the volume was made up to 2 L. Solution was sterilised in autoclave at 121 °C, 15psi for 20 minutes, and stored for up to 1 month. Prior to use 2 mL of aprotinin (10 KIU.mL^{-1}) was added.

2.2.3.4 Antibiotic solution (100 U.mL^{-1} Penicillin and Stretomycin, 5µg.mL^{-1} Amphotericin B

. PBS solution was made as in Section2.2.3.1. Immediately prior to use add 20 mL of 5000 U.mL^{-1} P/S and 20 mL of amphotericin B (250µg.mL^{-1}).

2.2.3.5 SDS in hypotonic buffer (0.1 % w/v SDS, 10 mM Tris, 10 KIU.mL^{-1} aprotinin

SDS solution (20 mL) (Sigma-Aldrich, USA) was added to 1978 mL of sterile hypotonic buffer (Section 2.2.3.3), as well as 2 mL of aprotinin (10 KIU.mL^{-1}).

2.2.3.6 Nuclease solution (50 mM Tris, 10 mM $MgCl_2$, 10 U.mL^{-1} Benzonase

Trizma base (12.2 g) and magnesium chloride ($MgCl_2$) (0.406 g) were dissolved in 900 mL of distilled water, and adjusted pH to 7.5-7.7. This was then made up to 1 L solution and autoclaved at 121 °C, 15psi for 20 minutes. Store for 1 month at room temperature. Immediately prior to use add 40µL Benzonase (from a 250 U.mL^{-1} stock)

2.2.3.7 Peracetic acid solution (0.1 % v/v)

Peracetic acid (PAA) (3.14 mL) was added to 997 mL sterile PBS and adjusted to pH 7.2 – 7.5. Solution was used within 1 h of preparation.

2.2.4 Decellularisation

Tissues were subject to the University of Leeds decellularisation protocol (Fermor *et al.*, 2015a) which is summarised below in Figure 2.2. Briefly, all solutions changes were performed aseptically in a Class II cabinet using aseptic technique. Osteochondral tissue was placed in 150 mL sterile containers, with 125 mL of solution per container. All solutions were pre-warmed to the temperature required for the incubation. During the incubation, all the containers were agitated at 220 rpm in shakers in the incubators, with the exception of the nuclease (80 rpm) and the antibiotic step (200 rpm). All containers were laid horizontally for the incubations, except for the nuclease step where they were vertical. Before each solution change, sample's were sonicated for 10 minutes in a ultrasonic bath (Ultrawave, UK).

The purpose of each step is briefly summarised below:

- *Waterpicking with PBS*: Remove bone marrow
- *Waterpicking with Monosodium citrate (MSC)*: MSC is an anticoagulant used to further remove blood and bone marrow
- *Freeze/Thaw*: Disrupt cells
- *Hypotonic*: Cytolysis
- *Hypertonic*: Plasmolysis
- *Cambridge Antibiotic*: Sterilisation
- *Sodium dodecyl sulphate (SDS)*: Cell removal
- *PBS*: Remove previous solution from scaffolds/washout cells
- *Nuclease*: Digestion of genetic material
- *Peracetic acid (PAA)*: Digestion of genetic material

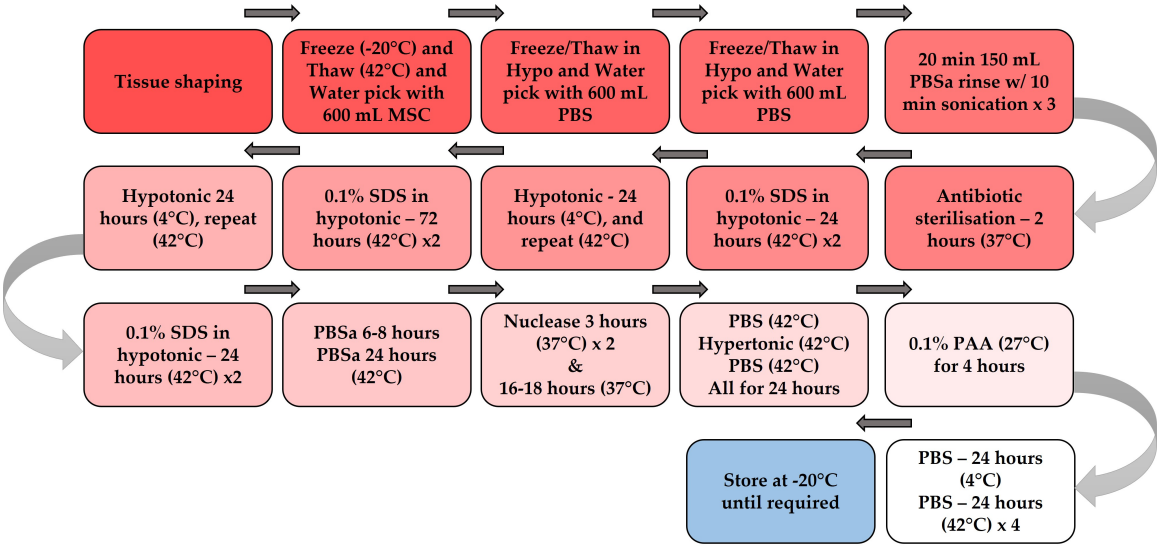

Figure 2.2: Decellularisation protocol. Flow chart demonstrating the decellularisation protocol used for the decellularisation of osteochondral scaffolds

Following the decellularisation, samples were removed from the wash solution and stored at -20 °C until required for quality assessment and additional experiments.

2.2.5 Fixation, Processing and Paraffin wax embedding of native and decellularised osteochondral tissue

Decellularised and native osteochondral scaffolds (n=3) were bisected under sterile conditions as shown in Figure 2.3. One half was used for histology. The tissues were fixed in 10% (w/v) NBF for 48 hours prior to decalcification in 25 mL of 12.5% (w/v) EDTA at pH 7. The osteochondral plugs were decalcified over the period of up to 2-weeks at 45°C with agitation. The EDTA solution was changed every 2 days, until the bone was soft enough to be sectioned.

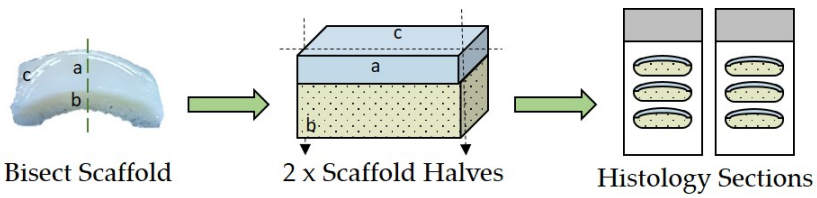

Figure 2.3: Histology for decellularised scaffolds. Producing histology sections from the osteochondral scaffolds. The scaffolds (left) were sectioned in the saggital plane to create two halves (middle) (a, b and c are reference points); 5 µm thick frontal sections were cut from the paraffin wax embedded blocks and were mounted onto the slides

After decalcification, the tissues were placed in plastic cassettes and dehydrated, cleared and wax embedded using a Leica TP 120 automated tissue processor (Leica, Germany). The processor was set to the programme for osteochondral tissues detailed below:

- 1 hour in 70% (v/v) ethanol
- 1 hour in 90% (v/v) ethanol
- 2 hour 20 min in absolute ethanol
- 3 hour 20 min in absolute ethanol
- 4 hour 20 min in absolute ethanol
- Cycles of 1 hour, 1 hour 30 min and 2 hour in Xylene
- Embed in molten paraffin wax for 1 hr 30
- Embed in molten paraffin wax for 2 hour

Following this the tissues were removed from the plastic cassettes, and placed with the face labelled as 'a' in Figure 2.3 against the bottom of the moulds. The mould was then flooded with molten wax and allowed to set overnight at room temperature. The following day the wax blocks were removed from the mould, and any excess wax was trimmed.

2.2.5.1 Sectioning of paraffin embedded blocks

The tissue blocks were subsequently loaded onto the microtome (Leica, Germany) via the cassette clamps. The blade was set to an angle of 5°, and sections of 6 µm were produced which were placed quickly onto the surface of water set to 45-50°C. When the required number of sections had been cut, they were picked up onto Superfrost microscope slides (SLS, United Kingdom) and left to dry on the hotplate overnight at 55-60°C.

2.2.5.2 Dewaxing and rehydration of tissue samples

The slides were then cleared in fresh xylene (Atom Scientific, United Kingdom) for 2 x 10 minutes cycles. Following this, the sections were immersed in 100% ethanol for 3 minutes, 100% ethanol for 2 minutes, 100% ethanol for 2 minutes, 70% ethanol (Fisher Scientific) for 2 minutes and in running tap water for 3 minutes.

2.2.5.3 Dehydration and mounting of stained tissue sections

Following any histological stain, sections were rehydrated. Sections were dipped in 70% (v/v) ethanol for 5 seconds, changed in 100% (v/v) ethanol for 1 minutes, 2 minutes and 3 minutes, before entering xylene for two changes of 10 minutes. After 10 minutes in the final xylene, the slides were removed and allowed to airdry briefly, before mounting coverslips onto each section with DPX mountant (Atom Scientific, United Kingdom).

2.2.6 Histological staining of paraffin embedded osteochondral tissue

2.2.6.1 Haematoxylin & eosin staining of paraffin wax embedded osteochondral tissue

Haematoxylin & eosin staining was performed to stain osteochondral tissue for the presence of cell nuclei and to judge the condition of the extracellular matrix. Slides were taken out of the running tap water as described in Section 2.2.5.2 and immersed into Mayer's haematoxylin for 1 minute. Following this sections were moved into Scott's Tap Water for 3 minutes, and rinsed in running tap water for a further 3 minutes. Then the slides were immersed in eosin for 3 minutes, followed by running tap water for 3 minutes. After staining, the section were dehydrated and mounted as stated in Section 2.2.5.3. Using a light microscope as described in Section 2.2.1.3, images were captured from the superficial and deep cartilage zones, as well as the bone and subchondral bone regions.

2.2.6.2 Safranin O & Fast Green staining of paraffin wax embedded osteochondral tissue

Safranin O & Fast Green staining was performed to assess glycosaminoglycan content in osteochondral tissue. Post rehydration as described in Section 2.2.5.2, slides were then immersed in Weigerts haematoxylin (Atom Scientific, UK) for 3 minutes and washed in tap water for 10 minutes. The sections were then differentiated in 1% acid alcohol for 1 minute, and then washed in tap water for 3 minutes prior to staining in 0.02% (w/v) Fast Green (Sigma-Aldrich, USA) for 5 minutes. The slides were briefly washed in 1% acetic acid and then drained prior to second staining in 0.1% Safranin O (Acros Organics, USA) for 4 minutes. Following the staining procedure, the slides were rehydrated and mounted as mentioned previously in Section2.2.5.3. A light microscope was used to capture images throughout the areas described in Section 2.2.6.1.

2.2.6.3 Sirius red/Miller's elastin staining of paraffin wax embedded osteochondral tissue

Sirius red/Miller's elastin was performed to visualise collagen and elastin. Prepare solutions of 5% (w/v) potassium permanganate in 300 mL in distilled water, 1% (w/v) oxalic acid in 100 mL in distilled water, Weigerts haematoxylin, 1% acid alcohol (5 mL 1% conc. hydrochlorid acid in 495 mL 70% ethanol), 0.1% Sirius red (w/v) in 100 mL picric acid. ost rehydration as described in Section 2.2.5.2

2.2.6.4 DAPI staining

DAPI staining was performed as another method to detect the presence of cell nuclei in osteochondral tissue. Post rehydration as described in Section 2.2.5.2, the sections were immersed in 200mL of DAPI working solution (Sigma-Aldrich, USA) (0.1 $\mu g.mL^{-1}$ in PBS at pH 7.4) at room temperature in the dark for 10 minutes. Following this the slides were washed three times in PBS for 10 minutes in the dark. Each section was then mounted with Dako fluorescence mounting medium (Agilent, USA) and a glass coverslips. Slides were stored in the dark at 4°C prior to imaging to

protect the fluorescence of the samples. Presence of cells will be determined through observation under an upright fluorescent microscope with the DAPI filter.

2.2.7 Biochemical quantification of decellularised tissues

2.2.7.1 Quantification of DNA content

To assess the quality of decellularisation compared to native tissue, DNA quantification was performed as follows.

The cartilage and bone segments were separated and 100-250 mg of decellularised tissue (n=3) or 25-50 mg of native tissue (n=3) was macerated and placed into a bijou. The weight of bijou alone and the bijou with the tissue was recorded in order to determine the wet weight of the tissue. The bijous were subsequently placed in the Modulo D Freeze Drier (Thermo Scientific, UK) to be lyophilised to a constant weight. Following lyophilisation, the total weight of tissue and the bijou was recorded, and the dry weight of the tissue was calculated.

Tissue DNA was extracted and purified using a DNAeasy blood and tissue kit (Qiagen, Germany), following the manufacturers instruction. 180 µL of Buffer ATL and 20 µL of proteinase K was added per 25-50 mg of tissue, and was incubated with agitation for 3 hours at 56°C or until tissue is completely lysed. Volumes of ethanol and buffer AL, proportional to digest volume were used for DNA precipitation.

Following this, the DNAeasy columns were rinsed and the DNA was eluted using buffer AE in an elution volume of 20 µL. In most instances two 200 µL elutions were performed in order to maximise yield. The purified DNA was immediately quantified using a nanodrop spectrophotometer. Prior to this, a standard curve using calf thymus DNA was used to calibrate the instrument. For both the standards and the sample 1 µL of solution was pipetted onto the pedestal and the absorbance was measured at 260nm. The A260/280 was also noted to judge DNA purity.

2.2.7.2 Determining the glycosaminoglycan composition of decellularised scaffolds

2.2.7.2.1 Reagent preparation

- **PBS.** Sterile PBS was made up as described in Section 2.2.3.1.
- **Digestion buffer (5 mM L-cysteine hydrochloride, 5mM Na_2EDTA).** L-Cysteine Hydrochloride (0.788 g) and disodium ethylenediaminetetraacetic acid (1.861 g) were dissolved in 1 L of PBS using a magnetic stirrer. The pH was adjusted to 5.9 - 6.1. This solution was stored for a maximum of 6 months at room temperature.
- **Papain digestion solution (800 kU.mL^{-1} 5 mL.** Papain (4000 kUnits) was dissolved in every 5 mL digestion buffer required using a magnetic stirrer and was used immediately.
- **0.1 M sodium di-hydrogen orthophosphate monohydrate; 250 mL.** Sodium di-hydrogen orthophosphate monohydrate (3.45 g) was dissolved in 250 mL of distilled water using a magnetic stirrer.
- **0.1 M di-sodium hydrogen orthophosphate; 250 mL.** Di-sodium hydrogen orthophosphate (3.55 g) was dissolved in 250 mL of distilled water using a magnetic stirrer.
- **GAG assay buffer; 200 mL.** 0.1 M Sodium di-hydrogen orthophosphate monohydrate (137 mL) was added to 0.1 M di-sodium hydrogen orthophosphate (63 mL). Solutions were stirred with magnetic stirrer and pH was adjusted to 6.8. This solution was kept for no longer than three months.
- **Dimethyl methylene blue (DMB) dye solution; 1L.** 1,9-dimethy methylene blue dye (16 mg) was dissolved in 5 mL ethanol and 2 mL of formic acid. Sodium formate (2 g) was added and volume was increased to 1 L using distilled water. The pH was then adjusted to 3.0 using formic acid solution (1 M)

- **1 M Formic Acid solution; 200 mL.** Formic acid (7.9 mL) was added carefully to distilled water (192.1 mL).

2.2.7.2.2 Papain digestion To detect GAGs, it was necessary to digest the tissue first. Cartilage (50-80 mg) was cut up and lyophilised as mentioned previously in Section 2.2.7.1. Following this, the tissue was digested in 5 mL papain solution (800kU.mL^{-1}) (Applichem) at 60°C for 36-48 hours. Standards of chondroitin sulphate B (200, 150, 100, 50, 25, 12.5, 6.25, 3.125 and 0 µg.mL^{-1}) in assay buffer were used to produce a standard curve.

2.2.7.2.3 GAG assay To quantify the GAG content following complete digestion, the samples were diluted 1 in 50 in GAG assay buffer so that their absorbances fell within the linear region of the standard curve. The standards and diluted unknowns (40µL) were added to a clear flat-bottomed 96 well plate and 250µL of DMB dye solution was added to each well. The plate was slowly rocked on a plate rocker for 2 minutes, before measuring the absorbances at 525 nm using a microplate spectrophotometer (Thermo Scientific, USA). The blank measurements (0 µg.mL^{-1}) was subtracted from all values, and the standard curve was plotted. This was used to interpolate GAG concentrations from the unknown absorbances using linear regression. The dilutions and dry tissue weights were taken into account, giving a final GAG concentration in units of µg.mg^{-1} of dry tissue.

2.2.8 Cell culture techniques

In this study, baby hamster kidney (BHK) cells, mouse immortalised fibroblast cell line (L929) and human articular chondrocytes (C20A4) cells were procured as described in Table 2.1.3. These cells were used for a variety of purposes including biocompatibility, metabolic activity studies, cell seeding studies and 3D culture.

Media was always pre-warmed to 37 °C, and cells were incubated at 37 °C at 5% CO_2 in air. Media changes and cell passaging were performed with aseptic technique in Class II safety cabinets.

2.2.8.1 Cell culture media preparation

For 100 mL of BHK cell culture media 82 mL of Glasgow's minimal essential media (GMEM) (Sigma) was added to; 5 mL of fetal bovine serum (Sera Lab); 10 mL of tryptone soya broth (Sigma), 2 mL of penicillin (5000 $U.mL^{-1}$) / streptomycin (5 $mg.mL^{-1}$) and 1 mL of L-glutamine (200 mM) (Sigma). For 100 mL of L929 and C20A4 media, 87 mL of Dubecco's minimal essential media (DMEM) (Sigma) was added to; 10 mL of fetal bovine serum, 2 mL of penicillin (5000 $U.mL^{-1}$) / streptomycin (5 $mg.mL^{-1}$) and 1 mL of L-glutamine (200 mM).

2.2.8.2 Cell line resurrection

In this study all cell lines were resurrected from liquid nitrogen storage through defrosting of the cryovials in 37°C waterbath. Once thawed, the cells were immediately introduced to a T75 with 13 mL of appropriate cell culture media inside at 37°C. The following day the cells were examined microscopically to confirm attachment and growth. Following this the cell media was replaced in order to ensure complete removal of dimethyl sulfoxide (DMSO).

2.2.8.3 Cell passaging

Once the cells are growing the media was changed every two days for optimal growth. Once the cells had grown to 70-80% confluence, they were passaged. First, the media was removed from the flask and care was taken not to disturb the monolayer. Then the monolayer was washed with 10 mL of PBS without calcium and magnesium, before detaching the cells with 3 mL of trypsin at 37°C and 5% CO2 for 5 minutes. After 5 minutes, the side of the flask was gently hit to dislodge any stubborn cells, and detachment was monitored with the microscope.

To terminate the trypsin activity, 10 mL of fresh cell culture media was added, and pipetted up the sides of the flasks several times to ensure maximum cell detachment and retrieval. The suspended cells were then removed into a 50 mL universal test

tube, and centrifuged and 150 g for 10 minutes to remove the trypsin. The subsequent pellet was resuspended in a 1 mL of fresh cell culture medium and a suitable cell dilution was made.

2.2.8.4 Cell count

In order to quantify the total number of cells, once cells have been detached and resuspended in cell culture media, 50 µL of trypan blue was mixed with an equal volume of cell suspension (1:1 ratio). From this mixture 10 µL was applied into the Countess disposable slide chamber (Invitrogen), the slide was then inserted into the Countess automatic cell counter (Invitrogen) which auto-focuses on the cells and performs a cell count giving the total proportion of live and dead cells in cells per mL. Only the live cell number was used for calculation of seeding densities .

2.2.8.5 Cell cryopreservation

On completion of the study where the cells are required, to allow preservation of cell stocks, remaining cells were prepared for cryopreservation. Remaining cells were expanded to confluency, detached, resuspended and a cell count was performed. Cells were pelleted again (150 g for 10 minutes) and resuspended in a sufficient quantity of cell culture medium with 10% DMSO in order to provide a final cell count of 1 x 10^6 cells.mL^{-1}. Aliquots of the cell suspension (1 mL) were rapidly separated into Cryovials, and placed into a -80°°C freezer in cryofreezing pots containing isopropanol for 24 hours. The following day cells were relocated to the liquid nitrogen cell dewars for long-term storage.

2.2.9 Sterility testing

2.2.9.1 Preparation of thioglycollate broth

Thioglycollate medium USP (11.88 g) was dissolved in 400 mL of distilled water with a magnetic stirrer set to 90°C, until the solution changes colour from straw to purple. The resulting solution was aliquoted in 45 mL portions into 8 narrow

neck glass medicine bottles, leaving the lid loose. The solutions were subsequently autoclaved at 121°C for 15 minutes.

As soon as the autoclave run had finished and the bottles were beginning to cool, the lids were tightly sealed to prevent oxidation of the media. Over time the media settled and a thin pink layer emerged at the top of the solution, the rest of which was straw coloured as pictured in Figure 2.4

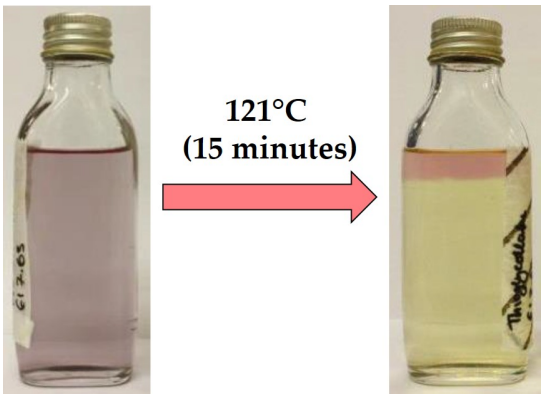

Figure 2.4: Thioglycollate broth. Prior to autoclaving the solutions, the thioglycollate broth appears purple in colour, however post autoclave the solution should appear a straw colour with a pink band at the top. These two layers represent the aerobic (top) and anaerobic (bottom) layers, where the respective bacteria survive

2.2.9.2 Testing the sterility of the decellularised scaffolds

Cartilage and bone samples (n = 3) (approx. 5 mm^2) were aseptically transferred to the broth using a scalpel and forceps. The negative control (sterile broth without tissue), and positive control (contaminated loop) were also included. The broths were incubated at 37°C and the presence of growth was determined visually at 3 and 7 days.

2.2.10 Contact Cytotoxicity

Both L929 and BHK cells were resurrected, and expanded as per Section 2.2.8. Osteochondral scaffolds were sectioned aseptically into thin slices. These slices were attached to the bottom of a 6-well plate with steri-strip, as shown in in Figure 2.5. The tissue was subsequently washed three times with PBS for 10 minutes each wash. Cell suspensions of 250,000 cells/mL were made for both BHKs and L929s. After

the final wash, the PBS was aspirated and 2 mL of respective cell suspensions were added to each well in a 6-well plate. For each cell type, 3 scaffolds were assessed for cytotoxicity in triplicate. For the control groups, there was a cell only control, a negative control with a steristrip with no tissue, as well as a positive/cytotoxic control in which a drop of cyanoacrylate was placed in the centre of the well.

The cells were left to incubate with the tissue for 48 hours in 5% CO_2 at 37 °C. Following the incubation, the plates were viewed under phase contrast to examine changes in cell morphology, cell detachment and for the presence of dead cells especially at the biomaterial-cell interface. Following this initial observation, the media was removed and the surface was gently washed with PBS containing calcium and magnesium. The DPBS was removed and replaced with 2 mL of neutral buffered formalin (NBF) for 10 minutes. After fixation, the wells were stained with Geimsa stain for 5 minutes. The stain was aspirated, and the surface was thoroughly rinsed with running tap water until the waste water runs clear. The biomaterial-cell interface was examined.

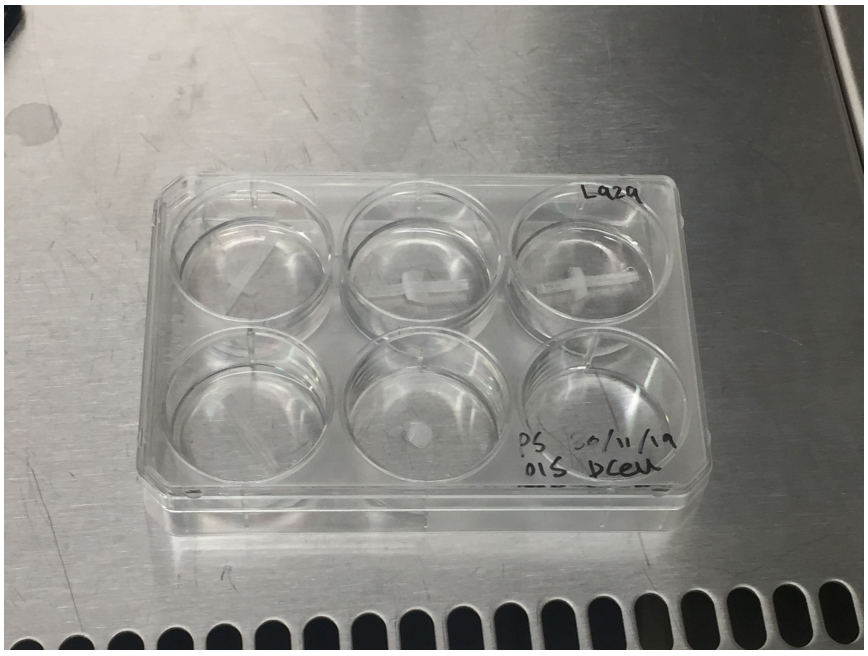

Figure 2.5: Contact Cytotoxicity. Osteochondral slices were attached to the 6-well plate using steristrip. The three bottom control wells contain a steristrip alone control, a cyanoacrylate contact adhesive (positive control for cytotoxicity) and a cell only well (negative control).

2.2.11 Extract Cytotoxicity

Both L929 and BHK cells were resurrected, and expanded as per 2.2.8. Osteochondral scaffolds were sectioned into cartilage and bone portions as mentioned in Section 2.2.9.2. Following this, the tissue as well as a postive (DMEM alone) and negative (DMEM with 40% DMSO) control, were incubated in 3 mL of DMEM for at 37°C and 240 RPM agitation for 72 hours. BHKs and L929s were seeded into 96-well plate at a concentration of 50,000 cells/mL and 125,000 cells/mL respectively. 200 µL of cells were plated, in triplicate and cultured for 24 hours in 5% CO_2 at 37°C.

The next day, the culture media was removed and replaced with 100 µL of double strength media, 100 µL of extract or control to the appropriate wells in triplicate. The cells were incubated with the extract for 24 hours in the previously described cell culture conditions. Following the culture period, and ATP Lite assay was performed in order to assay the effects of the extracts and controls on cell viability.

2.2.11.1 ATP Lite Assay

As per Perkin-Elmer instructions, the media was removed and 50 µL of cell culture media and 50 µL of cell lysis solution were added to each well. In order to lyse the cells, the plates were agitated for 5 minutes on the microshaker. The well contents were carefully transferred into a white 96-well optiplate as well as 50 µL of ATP lite substrate solution. The plate was covered with foil and shook on the microplate shaker for a further 5 minutes. A bunsen burner was then used to remove any bubbles in the wells, and subsequently the plate was left for 10 minutes to dark adapt. After the 10 minutes, the luminescence of each sample was measured using the Chameleon Plate reader.

2.2.12 Statistical analysis

2.2.12.1 Confidence limits

Numerical data were analysed using Prism 7 (GraphPad) and presented as a mean, where $n \geq 3$, $\pm$ 95% confidence limits. The limit was calculated using the following

equations:

$$mean = \frac{\sum x}{n}$$

$$StandardDeviation = \sqrt{\frac{\sum x^2}{n-1}}$$

$$SEM = \frac{SD}{\sqrt{n}}$$

$$95\%C.l = SEM \times t$$

Where t = a mutiplier determined by the n, summarised below in Table 2.2.

Table 2.2: Summary of the effect of sample number (n) on the multiplier (t) for calculating 95% confidence limits.

N (Number of Samples)	T (Multiplier)
2	12.706
3	4.303
5	2.776
10	2.262
25	2.064
50	2.010

2.2.12.2 Comparison of means

In experiments where number of groups = 2, means were compared using a students t-test on Prism 7. When the number of groups > 2, one or two-way analysis of variance (ANOVA) was used to compare multiple means. Tukey's post-hoc test was used to indentify the location of significant differences. Significance was taken at P <0.05.

2.2.12.3 Linear regression analysis

When analysing standard curves, linear regression analyses were conducted in Prism 7 in order to calculate r^2 values. This value (from 0 - 1) indicates the strength of linear relationship, and allows a judge of the reliability in interpolating from a standard curve.

Chapter 3

Cost-effectiveness analysis of decellularised osteochondral scaffolds for cartilage repair

3.1 Glossary

- ACI = Autologous chondrocyte implantation
- CEAC = Cost effectiveness acceptability curve = A method for investigating uncertainty in estimates of cost-effectiveness
- Cost = value of opportunity forgone
- DC-ACI = Decellularised assisted chondrocyte implantation
- ICER = Incremental cost effectiveness ratio = Summary measure of the economic value of an intervention against a comparator
- Investment costs = investment expenditure required to have the facility to manufacture interventions
- NHS = National health service
- Osteochondral allografting
- QALY = Quality adjusted life year
- Recurring costs = operational costs involved in intervention manufacture

- TKA = Total knee arthroplasty
- Utility = A measure of the benefit obtained from an intervention
- WTP = Willingness to pay = The maximum price a customer is willing to pay for a product or service

3.2 Introduction

Due to improved healthcare in the UK, it is expected that by 2039, 25% of the population will be > 65 years old (ONS, 2017). Whilst there are many positives to this estimate, there are also concerns due to the increased incidence of osteoarthritis observed in those over 64 (Prieto-Alhambra *et al.*, 2014). As a result of this, there are many companies and research groups trying to develop and translate cartilage repair interventions to address the issue. Unfortunately, due to problems with reimbursement, several cartilage interventions have had to be withdrawn from the market, namely Chondrocelect (Tigenix) (Negoro *et al.*, 2018). In order to be adopted for use in the NHS and receive reimbursement, an intervention must demonstrate cost-effectiveness in relation to an existing strategy. In the UK the unit of cost-effectiveness is the cost (£)/QALY (quality adjusted life year).

In 2017, ACI received NICE recommendation in the UK, making it available on the NHS for the treatment of symptomatic articular cartilage defects. This appraisal was partially based on an economic evaluation performed by (Mistry *et al.*, 2017), suggesting that ACI was cost-effective compared with microfracture across a range of scenarios. However, as discussed previously there are concerns over biomechanical properties of ACI prior to regeneration, as well as inappropriate repair material.

Therefore, our aim is to develop and translate decellularised osteochondral matrices as scaffolds for autologous cell implantation (referred to as DC-ACI for brevity). In order for translation to be successful, the cost-effectiveness of the intervention against the current 'gold standard' (ACI) must be investigated. Base-case cost-effectiveness analysis required input costs and utilities, which have not been previously determined for decellularised osteochondral scaffolds. Therefore, this study will first investigate and estimate the associated investment and recurring costs of scaffold

production. As the scaffolds are still in the early development stages, there is no clinical data to base utility values on, so the literature will be examined for suitable comparators. Once the input variables have been determined, the cost-effectiveness will be examined using a Markov Model (Sonnenberg and Beck, 1993; Komorowski and Raffa, 2016). This model determines transition of a theoretical patient cohort through health states related to an intervention over time, and is useful in assessments involving stochastic decisions. Following determination of the base-case incremental cost-effectiveness ratio (ICER), stochastic bootstrapping will be performed to determine the uncertainty of the model.

We hypothesis that ACI effectiveness will be improved by use of decellularised scaffolds and that this will ultimately be cost effective. This analysis will help to determine cost and effectiveness parameters which decellularised scaffolds will need to achieve in order to be a financially viable intervention.

3.3 Aims and Objectives

The aim of this study was to determine the cost-effectiveness of decellularised assisted chondrocyte implantation (DC-ACI) compared to ACI. We hypothesise that seeding the autologous cells onto a decellularised osteochondral matrix prior to implantation, will improve patient outcomes. However, differences between the cost and effectiveness between both interventions need to be investigated to determine which is more cost-effective.

The objectives of this study were to:

(i) Determine the investment and recurring costs of the production of decellularised osteochondral scaffolds

(ii) Calculate the selling price of the scaffold and the associated treatment costs

(iii) Design a cost-effectiveness Markov transition state model

(iv) Compare cost-effectiveness of decellularised osteochondral assisted chondrocyte implantation versus ACI

3.4 Model structure

A Markov model (state transition model) was developed in Microsoft Excel, in order to model the transition from primary repair through to permanent repair, no further repair or towards total knee arthroplasty (TKA) (Figure 3.1). Many of the assumptions for later described model inputs for ACI were based on a previous cost-effectiveness analysis performed by (Mistry *et al.*, 2017), which contributed towards ACI's subsequent NICE approval. For the DC-ACI, as no clinical trial data was available, the assumption is that the device would perform similarly in function to osteochondral allografting (OCA), given the near identical structure and treatment methodology.

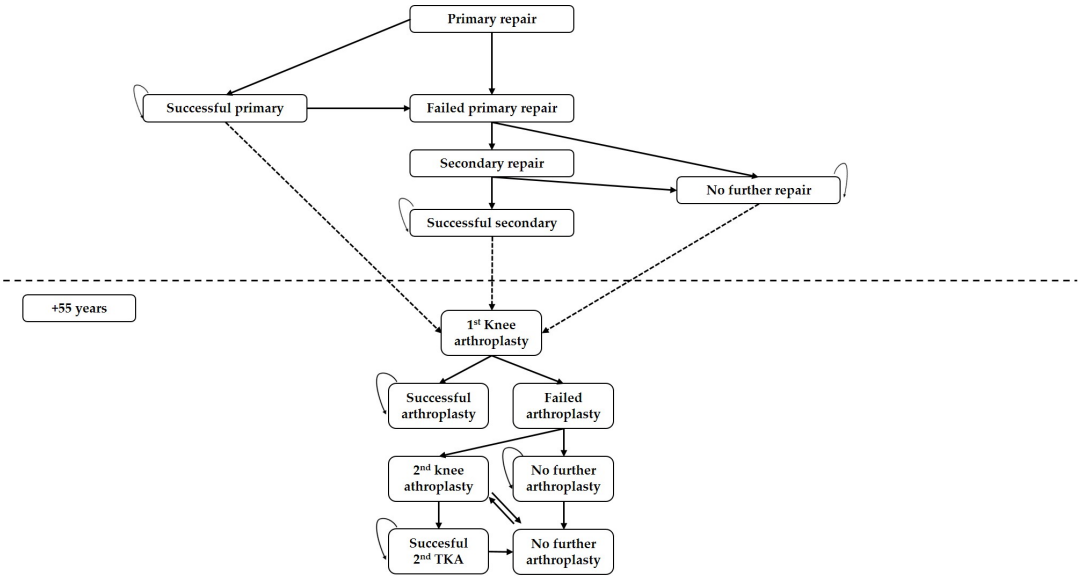

Figure 3.1: Markov Model. Summary of the various health states possible in this model as well as the possibilities for transition between health states. Arrows indicate direction of transition. Where arrows return to the same health state, this indicates a possibility of staying in the health state at a transition point. The dotted line indicates a barrier which cannot be passed until the model reaches 55 years old.

3.4.1 Patients Aged 33-55

This model is made up of two Markov Models run sequentially. The first model describes patients aged 33-55 years old, the second following the same patients from 55-100 years old. This split is based upon several cost-effectiveness studies into both ACI and OCA, whereby prior to the age of 55, patients are not considered for TKA

due to the likelihood of requiring revision surgery (Mistry *et al.*, 2017; Mistry *et al.*, 2019).

3.5 Model Inputs

3.5.1 Costs

3.5.1.1 Recurring costs

The recurring costs for the scaffold were defined as the costs incurred to produce a batch 30 osteochondral scaffolds. It was assumed that each decellularisation run takes 8-weeks (including QC), and that it was possible for a technician (£30,000/year) to produce (60 scaffolds) in parallel based on resource use in each 8-week cycle. It was assumed that this technician would work full-time (35 hours/week) on decellularisation scaffold production. Based on production cost-efficiency calculations (data not shown), taking into account investment costs; demand and resource use, it was determined most cost-efficient for 2 technicians to work together to produce a total of 120 scaffolds in each 8-week cycle.

In order to produce 120 scaffolds, it would be necessary to obtain 60 porcine legs, as it is possible to take and decellularised both the lateral and medial femoral condyles. The cost/leg was obtained from our laboratory accounts (Table 3.2). The cost for the decellularisation solutions was assumed to be the same as for current research laboratory costs. Briefly, the volume of each solution required for 4 runs (4 x 30 scaffolds) was calculated. From this information, the amount of each reagent per wash was calculated, and multiplied by the cost/g. A summary of the individual solution costs is detailed in Table 3.1. It is of note that in this production of this table it was assumed that penicillin/streptomycin (P/S) was preferred over Cambridge antibiotic due to the cost difference. This fact also influenced later protocols used in the experimental section of this thesis.

Table 3.1: Solution costs. Input parameters to the low, base-case and high solution costs

Solution	Volume (L)	Low	Base-case	High
Decell solutions				
PBS	333	£492.84	£ 9,570.42	£13,320.00
MSC	96	£35.74	£66.27	£3,840.00
Hypotonic	93	£5.07	£ 118.92	£3,720.00
Hypertonic	15	£5.07	£119.08	£600.00
Nuclease	50	£550.80	£980.84	£2,000.00
PAA	15	£27.94	£27.94	£600.00
SDS Hypo.	75	£38.66	£200.48	£3,000.00
Aprotinin	0.683	£412.92	£412.92	£27.32
Antibiotic				
Cambridge	6	£2280.00	£2280.00	£2280.00
or				
P/S *	6	£142.26	£143.70	£27,347.32
Total *	**683.68**	**£1,711.30**	**£11,640.56**	**£27,320.00**

The low, base-case and high values were used for solution cost, to allow for downstream sensitivity analysis of costs, this was applied henceforth to all other costs were it was applicable to have a range (Table 3.2). In respect to the solutions, for use in medical device production it is essential that all reagents were of a good manufacturing practice (GMP) grade suitable for biopharmaceutics production. The low-case is if solution were bought in the largest possible bulk order, the base-case is the cost of reagent in it's smallest packaging. The high value is simply £40 per litre of decellularisation solution, a value obtained from consultation with an industry expert.

Finally, in terms of packaging, expert industrial advice was obtained from a company within the decellularisation field, and based on their suggestions and experience a cost for packaging of £30 per scaffold was decided upon. This resulted in a range of recurring costs from £146.18-£359.59 per scaffold.

Table 3.2: Recurring costs. Input parameters to the low, base-case and high recurring costs.

Item	Quantity	Low	Base-Case	High
Summary	Scaffold number	-	120	-
	Decell runs	-	4	-
	Time	-	**8-weeks**	-
Labour	Staff number	-	2	-
	Days	-	40	-
	Hours per day	-	8	-
	Hourly rate	-	£14.42	-
	Total cost	-	**£ 9,230.77**	-
Tissue	Scaffolds/leg	-	2	-
	Number	-	60	-
	Cost per leg	-	£50.00	-
	Total cost	-	**£3,000.00**	-
Solutions	Scaffold number	-	120	-
	Total cost	**£1,711.30**	**£11,640.56**	**£27,320.00**
Packaging	Scaffold number	-	120	-
	Cost per scaffold	-	£30	-
	Total cost		**£3,600.00**	
Total cost	**120 scaffolds**	**£17,542**	**£27,471**	**£43,151**
	£/scaffold	**£146.18**	**£228.93**	**£359.59**

3.5.1.2 Investment costs

The initial investments costs were determined based on the resources required for two technicians to the produce 120 decellularised osteochondral scaffolds every 8-weeks. This equipment is listed in Table 3.3, and includes equipment for the dissection of porcine legs, the decellularisation run and subsequent quality assessment.

The low-cost investments were taken from our laboratories accounts ledger. For the base-case costs, quotes for the same (or same specification if initial product discontinued) equipment at the rate as of (29/05/2020) were used. This was to account for the cost of setting up this laboratory with current prices, and full retail prices. The high case costs were estimated by using multiplier based on the difference between the low and base-case. In calculation of the final selling price (Table 3.4), these costs were amortised to 20% of the total cost, to account for the cost over the lifetime of

the equipment.

Table 3.3: Investment costs. Input parameters to the low, base-case and high equipment investment costs.

Item	Low	Base-case	High
37 ˚C Incubator	£9140.00	£9,140.00	£10,861.96
4 ˚C Incubator	£9140.00	£9,140.00	£10,861.96
Bench top autoclave	£8000.00	£8,000.00	£9,507.18
Bench top vice	£19.99	£24.99	£29.70
Cell culture centrifuge	£1750.00	£2,050.00	£2,436.22
Cell culture incubator	£3289.00	£6,135.00	£7,290.82
Cell sens software	£292.50	£292.50	£347.61
Centrifuge	£2590.00	£3,392.00	£4,031.05
Class II safety cabinet	£5000.00	£12,940.00	£15,377.87
Computer for nandodrop	£514.00	£618.99	£735.61
Deionisation cartridge	£190.40	£190.40	£226.27
Dremmel	£43.62	£94.50	£112.30
Dremmel bits	£11.99	£11.99	£14.25
Duran bottles	£155.60	£246.30	£292.70
Freezer (-4 ˚C)	£177.00	£273.34	£324.84
Fridge	£235.07	£384.15	£456.52
Histology water bath	£391.35	£630.00	£748.69
Hot air steriliser	£1188.65	£1,951.00	£2,318.56
Inverted microscope	£11980.00	£11,980.00	£14,237.01
Labconco freeze drier	£7005.00	£7,005.00	£8,324.73
Microtome	9060.00	£9,060.00	£10,766.89
Mortar and Pestle	£15.15	£53.33	£63.38
Nanodrop	£2709.17	£8,164.79	£9,703.02
Olympus fluoro microscope	£7087.96	£9,660.00	£11,479.93
Olympus microscope camera	£5946.20	£5,946.20	£7,066.45
Oscilatting bone saw	£279.00	£286.80	£340.83
pH meter	£128.87	£565.00	£671.44
Pipette	£85.00	£299.00	£355.33
Platform shaker	£1949.32	£2,995.08	£3,559.35
Pretreatment cartridge	£59.20	£59.20	£70.35
Scale (Kern)	£694.00	£1,025.00	£1,218.11
Scalpel	£5.45	£6.87	£8.16
Slide drying rack	£589.00	£1,305.00	£1,550.86
Sonicator	£542.00	£703.78	£836.37
Stirrer	£189.00	£260.00	£308.98
Tissue processor	£16795.00	£16,795.00	£19,959.15
Vortex	£143.00	£208.22	£247.45
Water purification	£3486.55	£3,486.55	£4,143.41
Waterpic	£57.03	£61.22	£72.75
Wax dispenser	£779.00	£2,145.00	£2,549.11
Wax oven	£710.00	£935.00	£1,111.15
Total	**£112,424.07**	**£138,521.20**	**£164,618.33**

3.5.1.3 Determining selling price

The recurring and investment costs were utilised in the calculation of the final scaffold selling price (Table 3.4), and the cost of overheads were set at 100% of the production costs. Costs included here include laboratory rent, based on industrial consultation that separate laboratories would be required for solution preparation, decellularisation and quality assessment. The suggested price for these was £30,000, again based on expert advice. The consumable costs per scaffold was based on internal recurring laboratory costs per user.

The costs of regulatory approval, pre-clinical and clinical trials were based on range of costs from expert opinion. These costs were amortised over 20 years, based on the lifetime of a patent. Distribution costs were calculated as double the production and development costs.

When accounting for a low profit margin (5.5%), a selling price was calculated between £1,586.02 - £2,563.74.

Table 3.4: Selling price. Input parameters to the low, base-case and high scaffold final selling prices.

Cost Item	Low value	Base case	High value
Tissue	£50.00	£50.00	£50.00
Reagents	£14.26	£97.00	£227.67
Product labour	£76.92	£76.92	£76.92
Lab rent	£115.38	£115.38	£115.38
Consumables	£6.58	£6.58	£6.58
Packaging	£30.00	£30.00	£30.00
Product cost	**£293.15**	**£375.90**	**£506.56**
Regulations	£100,000.00	£125,000.00	£150,000.00
Pre clinical	£500,000.00	£750,000.00	£1,000,000.00
Clinical	£1,500,000.00	£1,750,000.00	£2,000,000.00
Total	£2,100,000.00	£2,625,000.00	£3,150,000.00
Amortisation (20 years)	£105,000.00	£131,250.00	£157,500.00
Cost per scaffold	**£134.62**	**£168.27**	**£201.92**
Investment cost	£153.72	£191.99	£ 228.16
Amortised Investment (20%) cost	**£30.74**	**£38.40**	**£45.63**
Recurring Product + Investment cost	£323.90	£414.29	£552.19
Overheads	£293.15	£375.90	£506.56
Total production and overheads cost	**£617.05**	**£751.79**	**£1,013.12**
Production and development cost	£751.67	£920.06	£1,215.04
Distribution costs	£751.67	£920.06	£1,215.04
Total cost	**£1,503.33**	**£1,840.13**	**£2,430.08**
Selling price (5.5% profit)	**£1,586.02**	**£1,941.33**	**£2,563.74**
Scaffold profit	£82.68	£101.21	£133.65
Yearly profit	**£64,492.96**	**£78,941.45**	**£104,250.56**

3.5.1.4 Treatment costs

The selling price determined in Table 3.5.1.3 was used in the calculation of the cost of implementing the use of DC-ACI in the NHS versus ACI (Table 3.5). The exact ACI scaffold cost was unknown, assumed to be included in the final scaffold price (Table 3.6).

For both comparisons the cost incurred in the surgical procedure were considered equal. The procedure consists of a two-step surgical procedure. The first procedure is the endoscopic harvest of articular cartilage, which is always performed arthroscopically, regardless of downstream size of scaffold implantation. The cost of this

surgery was obtained from NHS costs for 2018-19. The base-case value was based on a weighted average of the outpatient costs. The low cost is based on an 'intermediate knee procedure from non-trauma, 19 years and over, with a complications and co-morbidity (CC) score of 0-1, given the (human resource group) HRG code of HN24C. The high score is the cost of a non-elective short stay following this surgery, which has the HN24A code and represents a CC score of 4+, but represents only 13% of the total cases. The second procedure is the implantation of the seeded scaffold into the knee joint. This is more commonly (60%) performed with an open surgical technique (HN23A-C), with the other 40% performed arthroscopically. Therefore, the base case reflects the weighted average cost of the total population surgical procedure distribution. The low case reflects the best case scenario of an arthroscopic day-case (>22%). Studies have shown arthroscopic implantation of ACI can be used to treat cartilage lesions of up to 7cm^2, with a range of 1-3 nights in hospital (Edwards *et al.*, 2014). The high case represents the cost of a non-elective stay with an open surgical technique. The surgical cost for both treatments was assumed to be equal.

For the intermediate cell expansion phase for DC-ACI, the base-case cost was obtained from a prior cost-effective analysis (Mistry *et al.*, 2017) for DC-ACI. Here it states a range of costs from £16,000 for use of Chondrocelect, to £4,125 for the cost of cell expansion from the OsCell site at the Robert Jones and Agnes Hunt Hospital in Oswestry. The OsCell value was used as our base-case cost as all that is states a base cost for cell expansion, whereas the Chondrocelect value was used for the high value in case of having to leverage off that technology. For ACI, despite (Mistry *et al.*, 2017) using Chondrocelect as their base-case cost, we decided to use the cost of another ACI intervention of Chondrosphere which is cheaper at £10,000, as Chondrocelect no longer has marketing authorisation in the UK (Armoiry *et al.*, 2019).

We assumed that recovery and NHS resource usage post DC-ACI followed the same model as osteochondral allografting (OCA) (Mistry *et al.*, 2019). The key difference between this and ACI recovery, is an emphasis on physiotherapy over rehabilitation.

Table 3.5: NHS Cost. Parameters determining final cost of DC-ACI treatment for NHS.

Category	Item	Low	Base-case	High
Materials	**Scaffold**	**£ 1,586.02**	**£ 1,941.33**	**£2,563.74**
Surgery 1	**Biopsy**	**£ 1,719**	**£ 1,871**	**£2,104**
	All athroscopic	*Day case CC (0-1)*	*Weighted*	*Short stay CC (0-1)*
Cell expansion	**Cell culture**	**£4,125.00**	**£4,125.00**	**£ 16,000.00**
		Oscell	*Oscell*	*Chondrocelect*
Surgery 2	**Implantation**	**£ 1,719**	**£ 2,845.39**	**£ 4,741**
		Day case CC (0-1) Athroscopic	*Weighted*	*Non-elective short stay CC (0-1)*
Recovery	Rehab cost	£203.14	£203.14	£203.14
	Rehab use	3	3	3
	Total rehab	**£609.42**	**£609.42**	**£609.42**
Outpatient	Outpatient cost	£130	£130	£130
	Outpatient use	1	1	1
	Total outpatient	**£130.30**	**£130.30**	**£130.30**
Phsyiotherapy	Cost	£132.00	£132.00	£132.00
	Use	8	8	8
	Total physio	**£1,056.00**	**£1,056.00**	**£1,056.00**
	Total cost	**£10,944**	**£12,579**	**£27,205**

Table 3.6: Procedural Costs. Calculating the final implementation costs of ACI

Category	Item	Low	Base Case	High
Materials	**Scaffold**	**N/A**	**N/A**	**N/A**
Surgery 1	**Biopsy**	**£1,719**	**£1,871**	**£2,104**
	All athroscopic	*Day case 0-1*	*Weighted*	*Non-elective short stay (0-1)*
Cell expansion	**Cell culture**	**£4,125.00**	**£10,000.00**	**£16,000.00**
		Oscell	*Chondrosphere*	*Chondrocelect*
Surgery 2	**Implantation**	**£1,719**	**£2,845.39**	**£4,741**
		Day case 0-1 Athroscopic	*Weighted*	*Non-elective short stay*
Recovery	Rehab unit cost	£385.99	£385.99	£385.99
	Rehab use	8	8	8
	Total rehab	**£3,087.92**	**£3,087.92**	**£3,087.92**
Outpatient	Outpatient cost	£130	£130	£130
	Outpatient use	1	1	1
	Total outpatient	**£130.30**	**£130.30**	**£130.30**
Total cost		**£10,781**	**£17,935**	**£26,063**

3.5.2 Utility

In this model, DC-ACI was assumed to be as effective as ACI. Base-case values were used as in the (Mistry *et al.*, 2017) paper. For sensitivity analysis, a range of utility values were used from the literature and are detailed in Table 3.7.

Base-case utility values for cartilage repair were obtained from an economic evaluation of ACI versus microfracture based on data from a clinical trial by (Saris *et al.*, 2009). Prior to first repair, (Gerlier *et al.*, 2010) report a utility value of 0.654 based on a clinical trial of ACI versus microfracture (Saris *et al.*, 2009). It was assumed that the utility prior to second repair (cartilage defect) was equivalent. The utility value was slightly higher for the no further repair health state, likely due to the medication provided and the receipt of slight improvement from the initial treatment. The variability in reported utilities in the literature ranging from 0.41 (Derrett *et al.*, 2005) to 0.8 (Clar *et al.*, 2005). The authors claim that the value (0.8) is implausibly high, therefore was not used as the base-case and hence was used as extreme values in the stochastic model.

Upon transition into the successful repair health state, utility value rises to 0.760 in the first year and 0.817 from the second year onwards (Gerlier *et al.*, 2010). This takes into account the first year of repair, rehabilitation and recovery of function. The sources used for the extreme values in this instance reflected the low (Derrett *et al.*, 2005) and high (Clar *et al.*, 2005) values from the 'prior to first repair' health state. As mentioned previously, second repair utilities reflect the primary repair utility values.

For the utility values concerning knee athroplasties, the base-case data was obtained from (Dong and Buxton, 2006). Besides these values, it was assumed that the utility value following successful knee replacement was equal whether first or second repair. Furthermore, the no further TKR health state utility value was assumed equal to the no further repair health state during cartilage repair.

Table 3.7: Utility Inputs. Low, base-case and high utility values used in this evaluation. Instances where colours match indicate usage of the same utility values.

Parameters	Low	Base-case	High
Prior to first repair	0.41	0.654	0.8
Source	*Derett et al. (2005)*	*Gerlier et al. (2010)*	*Clar et al. (2005)*
Succesful repair	0.64	**Year 1:** 0.760 **Year 2 plus:** 0.817	0.9
Source	*Derett et al. (2005)*	*Gerlier et al. (2010)*	*Clar et al. (2005)*
No further repair	0.645	0.691	0.721
Source	*Mari et al. (2016)*	*Gerlier et al. (2010)*	*Losina et al. (2014)*
Prior to second repair	0.41	0.654	0.8
Source	*Derett et al. (2005)*	*Gerlier et al. (2010)*	*Clar et al. (2005)*
Succesful second repair	0.64	**Year 1:** 0.760 **Year 2 plus:** 0.817 **Year 3 (ACI):** 0.654	0.9
Source	*Derett et al. (2005)*	*Gerlier et al. (2010)*	*Clar et al. (2005)*
No further repair	0.645	0.691	0.721
Source	*Mari et al. (2016)*	*Gerlier et al. (2010)*	*Losina et al. (2014)*
Before knee replacement	0.377	0.615	0.68
Source	*Jenkins et al. (2013)*	*Dong and Buxton (2006)*	*Konopka et al. (2018)*
Succesful knee replacement	0.671	0.78	0.872
Source	*Jenkins et al. (2013)*	*Dong and Buxton (2006)*	*Ara and Brazier (2010)*
Second repair	0.377	0.56	0.61
Source	*Jenkins et al. (2013)*	*Mistry 2017 (Gerlier)*	*Konopka et al. (2018)*
Succesful second	0.631	0.78	0.872
Source	*Mari et al. (2012)*	*Dong and Buxton (2006)*	*Ara and Brazier (2010)*
No further TKR	0.41	0.691	0.721
Source	*Derett et al. (2005)*	*Gerlier et al. (2010)*	*Losina et al. (2014)*

3.5.3 Transition probabilities

The transition probabilities are used in the Markov Model to determine the proportion of patients moving between health states each year cycle. In all instances transition probabilities were derived from the clinical studies survival data below in Table 3.8.

Table 3.8: Health state transition probabilities and assumptions. Data is provide for source literature of the assumption for each health state, alongisde the patient number, the follow up time frame, as well as the assumption made from the literature.

Treatment	Health State(s)	Source	Patients	Timeframe	Assumption
DC-ACI					
	Failure/Reoperation	Levy *et al.* (2013)	122	13.5 median	50.8% of reoperations have revision surgeries
	Primary repair	Familiari *et al.* (2017)	1036	5 years	86.7% survival at 5 years
	Successful primary	Familiari *et al.* (2017)	1036	10 years	78.7% survival at 10 years
	Second repair	Horton *et al.* (2013)	33	5 years	79% revisions survive at 5 years
	Successful second	Horton et al. (2013)	33	10 years	61% survival at 10 years
M-ACI					
	Failure/Reoperation	Biant *et al.* (2014)	104	10.4 years	25.9% patients underwent revision surgery
	Primary repair	Nawaz *et al.* (2014)	827	5 years	78.2% survival at 5 years
	Successful primary	Nawaz *et al.* (2014)	827	10 years	51% survival at 10 years
	Second repair	Ogura *et al.* (2019)	53	5 years	71% survival at 5 years
	Successful second	Ogura *et al.* (2019)	53	10 years	53% survival at 10 years

Similarly to the utility values, for DC-ACI, studies into osteochondral allografts were used to predict DC-ACI graft survival and health state transitions. These survival rates were first converted into progression probabilities using the formula below:

$$r = -(ln(1 - P))/t \tag{3.1}$$

Where r = progression rate, t = time and P = survival percentage.

The progression rates could subsequently be converted into transition probabilities using the below equation:

$$P_{transition} = 1 - exp(-rt) \tag{3.2}$$

Tables 3.9 and 3.10 show the calculated transition probabilities for DC-ACI and ACI for both age groups (33-55 years & 55-100 years).

Table 3.9: Transition probabilities (33-55 years). Transition probabilities used in the Markov model to determine progression between health states for DC-ACI and ACI for the first cohort of 33-55 year olds.

Decellularised-ACI (33-55 years)

From\to	Succesful primary	Second repair	Succesful second	Non-surgical	Death
Primary Repair	0.971	0.013	0.000	0.014	0.002
Succesful primary	0.976	0.011	0.000	0.012	0.002
Second repair	0.000	0.000	0.952	0.046	0.002
Succesful second	0.000	0.000	0.950	0.048	0.002
No further repair	0.000	0.000	0.000	0.998	0.002
Death	0.000	0.000	0.000	0.000	1.000

ACI (33-55 years)

From\to	Succesful primary	Second repair	Succesful second	Non-surgical	Death
Primary Repair	0.952	0.012	0.000	0.035	0.002
Succesful primary	0.941	0.013	0.000	0.044	0.002
Second repair	0.000	0.000	0.932	0.066	0.002
Succesful second	0.000	0.000	0.937	0.062	0.002
No further repair	0.000	0.000	0.000	0.998	0.002
Death	0.000	0.000	0.000	0.000	1.000

Table 3.10: Transition probabilities (55-100 years). Transition probabilities used in the Markov mode for DC-ACI and ACI treatments, for the second cohort of 55-100 year olds. TKR = Total knee replacement, PKR = Partial knee replacement.

Decellularised-ACI (55-100 years)

From\to	Successful primary	Second repair	Successful second	No further repair	First TKR	First PKR	Successful first TKR	Successful first PKR	Further knee replacement	Successful further KR	No further knee replacement	Death
Successful primary	0.894	0.004	0.000	0.004	0.007	0.007	0.000	0.000	0.000	0.000	0.000	0.084
Second repair	0.000	0.000	0.870	0.046	0.000	0.000	0.000	0.000	0.000	0.000	0.000	0.084
Successful second	0.000	0.000	0.874	0.015	0.013	0.013	0.000	0.000	0.000	0.000	0.000	0.084
No further repair	0.000	0.000	0.000	0.902	0.007	0.007	0.000	0.000	0.000	0.000	0.000	0.084
First TKR	0.000	0.000	0.000	0.000	0.000	0.000	0.901	0.000	0.006	0.000	0.002	0.091
First PKR	0.000	0.000	0.000	0.000	0.000	0.000	0.000	0.901	0.006	0.000	0.002	0.091
Successful first TKR	0.000	0.000	0.000	0.000	0.000	0.000	0.882	0.000	0.011	0.000	0.016	0.091
Successful first PKR	0.000	0.000	0.000	0.000	0.000	0.000	0.000	0.882	0.011	0.000	0.016	0.091
Further knee replacement	0.000	0.000	0.000	0.000	0.000	0.000	0.000	0.000	0.000	0.884	0.021	0.095
Successful further KR	0.000	0.000	0.000	0.000	0.000	0.000	0.000	0.000	0.011	0.878	0.016	0.095
No further knee replacement	0.000	0.000	0.000	0.000	0.000	0.000	0.000	0.000	0.000	0.000	0.905	0.095
Death	0.000	0.000	0.000	0.000	0.000	0.000	0.000	0.000	0.000	0.000	0.000	1.000

ACI (55-100 years)

From\to	Successful primary	Second repair	Successful second	No further repair	First TKR	First PKR	Successful first TKR	Successful first PKR	Further knee replacement	Successful further KR	No further knee replacement	Death
Successful primary	0.868	0.004	0.000	0.034	0.005	0.005	0.000	0.000	0.000	0.000	0.000	0.084
Second repair	0.000	0.000	0.850	0.066	0.000	0.000	0.000	0.000	0.000	0.000	0.000	0.084
Successful second	0.000	0.000	0.868	0.038	0.005	0.005	0.000	0.000	0.000	0.000	0.000	0.084
No further repair	0.000	0.000	0.000	0.906	0.005	0.005	0.000	0.000	0.000	0.000	0.000	0.084
First TKR	0.000	0.000	0.000	0.000	0.000	0.000	0.901	0.000	0.006	0.000	0.002	0.091
First PKR	0.000	0.000	0.000	0.000	0.000	0.000	0.000	0.901	0.006	0.000	0.002	0.091
Successful first TKR	0.000	0.000	0.000	0.000	0.000	0.000	0.882	0.000	0.011	0.000	0.016	0.091
Successful first PKR	0.000	0.000	0.000	0.000	0.000	0.000	0.000	0.882	0.011	0.000	0.016	0.091
Further knee replacement	0.000	0.000	0.000	0.000	0.000	0.000	0.000	0.000	0.000	0.884	0.021	0.095
Successful further KR	0.000	0.000	0.000	0.000	0.000	0.000	0.000	0.000	0.011	0.878	0.016	0.095
No further knee replacement	0.000	0.000	0.000	0.000	0.000	0.000	0.000	0.000	0.000	0.000	0.905	0.095
Death	0.000	0.000	0.000	0.000	0.000	0.000	0.000	0.000	0.000	0.000	0.000	1.000

3.5.4 Mortality

At each transition state, the probability of transition to a death state was included. One probability was used for patients in the 33-55 age bracket (0.0018), which was calculated by mortality data from the Office for National Statistics (ONS) National Life Tables (2016-2018). Briefly, the deaths (per 10,000) were calculated, then using the equations detailed in Section 3.5.3 a progression and transition probability were calculated.

The same process was conducted for the 55+ age bracket (0.0840), however, for the patients in either TKR or PKR health states an additional probability of 0.007 and 0.011 were added in line with data from (Mahomed *et al.*, 2005) into mortality following TKR and PKR.

3.6 Results

3.6.1 Base-case cost-effectiveness

One thousand patients began the model in the primary repair health state at an age of 33, and remain in this knee repair model until the age of 55 years old. At 55 years old it is estimated that patients with cartilage damage or osteoarthritis are eligible for knee replacement. The total cost and utility outcomes after the model were calculated and are represented below in Table 3.11. The DC-ACI treatment had a cost £6,293.66 cheaper than ACI, whilst providing 2.5 QALYs more. This calculated an incremental cost effectiveness ratio (ICER) of -£2,535.69, which indicates that DC-ACI dominates ACI and is therefore more cost-effective. To account for the fact that transitions could occur at any time during a cycle, a half-cycle correction was applied to the first and final years of each model, giving an ICER of -£2,222.30. Given these initial base-case data, it suggest that DC-ACI is cost-effective compared to ACI, and falls beneath the £20,000-£30,000 per QALY suggested NICE threshold.

Table 3.11: Base-case cost-effectiveness. ICER is presented with and without half-cycle correction.

Without correction		COSTS	OUTCOMES	NET BENEFIT
DCOCACI		£ 24,373.80	14.51	£ 410,897.83
ACI		£3 0,840.29	11.96	£ 327,925.57
Incremental		-£ 6,466.49		
		for	2.6	QALYs
ICER		-£ 2,535.69	per QALY	
Half cycle corrected		COSTS	OUTCOMES	NET BENEFIT
DCOCACI		£ 24,034.35	14.33	£405,956.59
ACI		£30,565.52	11.39	£311,257.68
Incremental		-£ 6,531.17		
		for	2.9	QALYs
ICER		-£ 2,222.30	per QALY	

3.6.2 Sensitivity analysis

A sensitivity analysis (Table 3.12) was conducted to study the effect of input parameters on the cost-effectiveness. Firstly, the variation in utility was investigated. In the scenario where successful repair with DC-ACI yielded no QALY gains, DC-ACI still dominated ACI. The same result occurred using a high utility value for successful repair following ACI, and this was applied alongside the previous low DC-ACI utility. The price of the treatment, however, had more of an influence on the cost-effectiveness.

The base-case cost for DC-ACI (Table 3.4) assumes that GMP reagents for decellularisation are bought in small quantities, and that all investment costs were the recommended retail costs. However, the high case takes into account the assumption that solutions cost £40/L, investment costs rise, and that overheads, regulations and developments costs are overestimated. In this scenario the incremental cost is

£20,682.88 compared with ACI, giving an ICER of £7,037.57. The effect of reducing the cost of ACI to the low cost (assumes a cell cost of £4,125.00 without scaffold costa) has less of a dramatic effect on the ICER (£1,817.98). Whereas matching the cost of the DC-ACI and the ACI to the base case DC-ACI value, yielded an ICER of £867.04.

NICE suggest that the discount rate can severely affect long term economic models due to a progressively diminished benefits. Decreasing the discount rate 2% from 3.5%, yielded a slightly lower incremental cost reduction with a great increase in the incremental QALYs. Testing the sensitivity of the model to the transition probabilities, didn't cause any change to the DC-ACI domination of ACI.

The results of this analysis show that neither cost or utility extremes alone will raise the ICER above the NICE willingness to pay (WTP) threshold. However, by matching the transition probabilities related to entering/remaining in the successful primary health state, the ICER exceed the NHS WTP threshold. The WTP threshold was also exceeded when combining low DC-ACI utility with high ACI utility or a high DC-ACI cost.

Table 3.12: Sensitivity Analysis. Scenarios were created in which input variables were modified. Scenarios were grouped by input variables of: utility, cost, discount, transition probabilities and a combination on input variables. Green boxes indicate that the scenario resulted in an ICER that was below the NICE WTP threshold. Red box indicates that the scenario resulted in an ICER above the NICE WTP threshold. The * indicates a scenario where the incremental cost and incremental QALYs are negative, in which instance the ICER value is not relevant, and assessment of cost-effectiveness relies on graphical methods (Figure 3.2

Sensitivity analysis:	Incremental costs:	Incremental QALYs:	ICER:
Base-case	-£ 6,531.17	2.9	DC-ACI dominates
Utility			
Low utility for DC-ACI succesful repair (0.640)	-£ 6,531.17	0.6	DC-ACI dominates
High utility for ACI succesful repair (0.9)	-£ 6,531.17	2.3	DC-ACI dominates
Low DC-ACI utility and High ACI utility ($1^{st}/2^{nd}$ repair)	-£ 6,531.17	-0.1	*
Cost			
High cost DC-ACI (£27,204)	£ 20,682.88	2.9	£ 7,037.57
Low cost ACI (£10,780)	£ 4,604.34	2.9	£ 1,817.98
Identical treatment cost (DC-ACI base case)	£ 2,519.62	2.9	£ 867.04
High cost DC-ACI + Low cost ACI	£ 32,556.97	2.9	£ 11,077.85
Discount and transition probabilities			
Decreased discount to 1.5% (from 3.5%)	-£ 3,058.92	7.4	DC-ACI dominates
Lower limit transition probability DC-ACI successful primary	-£ 7,846.48	0.3	DC-ACI dominates
Upper limit transition probability ACI success from primary	-£ 6,920.90	2.8	DC-ACI dominates
Combination			
DC-ACI TP's equal for successful primary and successful primary to successful primary	-£ 9,384.96	-0.5	*
No DC-ACI utility improvement, ACI utility 0.950	-£ 6,531.17	-0.2	*
Low utility and High cost DC-ACI	£ 20,682.88	0.6	£ 36,763.67

In such scenarios, when there is a reduced cost but also a loss in utility, the ICER is

positive, but the results belong in the south-west (SW) quadrant of the cost-effectiveness plane Figure 3.2. This shows that the variables highlighted in red (Figure 3.12 are on, or above the threshold to pay.

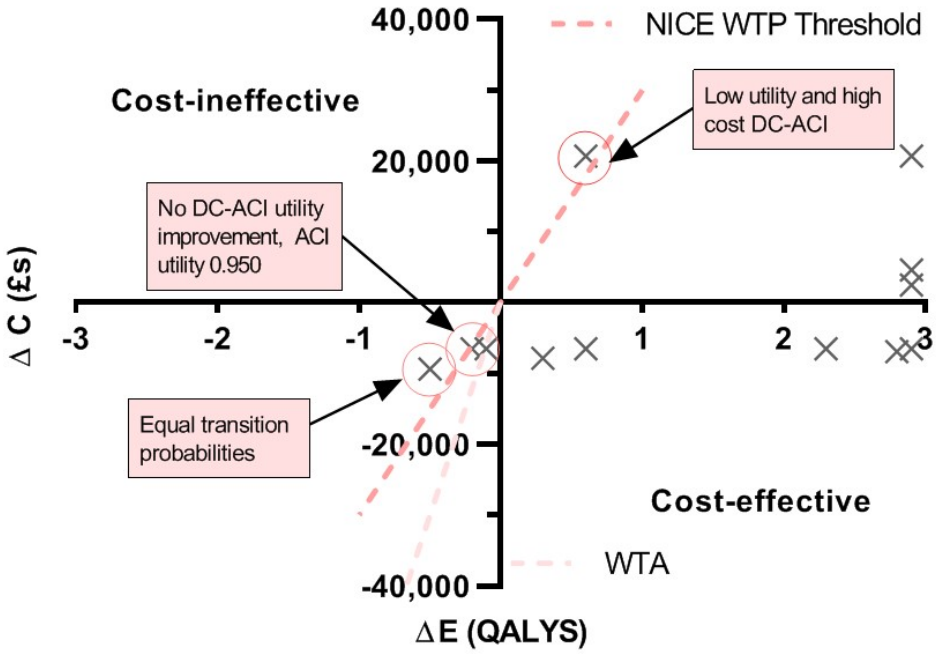

Figure 3.2: Sensitivity analysis results plotted on a cost-effectiveness plane. Red dotted line represents the NICE £30,000/QALY threshold, whilst the pink 'kink' represents a willingness to accept (WTA) threshold (= 2x WTP). All points found below the lines are determined cost-effective, and vice-versa. *delta* C describes the change in cost (£), whilst *delta* E (QALYs) described the gain or loss of QALY's.

3.6.3 Probabilistic Markov Model

In the inputs for this model, there is of course uncertainty around the costs, transition probabilities and utilities. As a result, for all of these inputs a mean and standard deviation value was calculated from the low, base-case and high values. These were used as a input for a probabilistic model, whereby 10,000 simulations were run using random values from each parameters distribution.

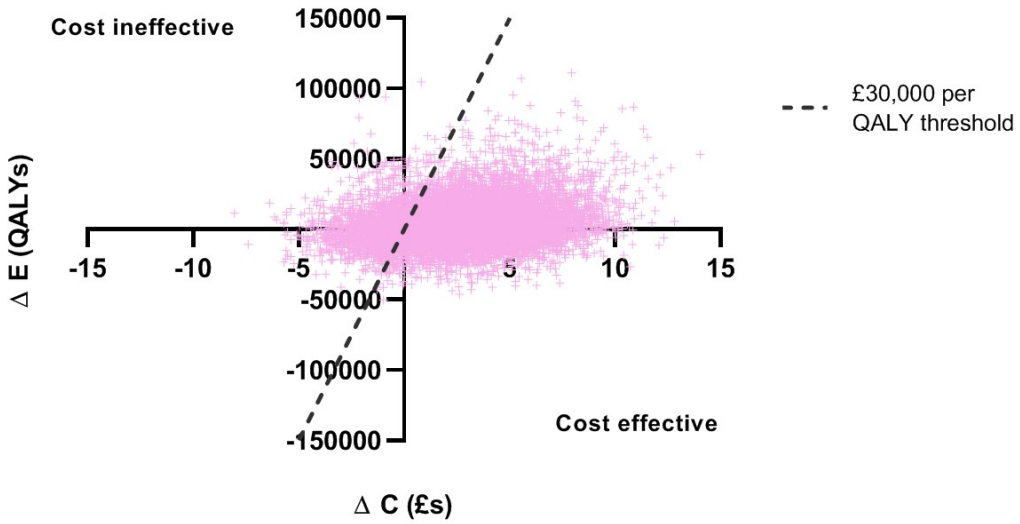

Figure 3.3: Stochastic cost-effectiveness plane. Results of 10,000 simulations using values from the distribution of extreme values around the base-case. *delta* C describes the change in cost (£), whilst *delta* E (QALYs) described the gain or loss of QALY's. The black line described the upper limit of NICE threshold value for willingness to pay.

From the probabilistic model in Figure 3.3, it can be observed that the majority of the simulations fall beneath the £30,000/QALY threshold used by NICE. The variability in cost is seen to span from -£50,0000 to £100,000. This is accompanied by a variability in effectiveness, with change in QALYs ranging from -7 to 14 QALYs. Averages were taken for the Δ C and Δ E, giving an average incremental cost of £3,828 and an average QALY gain of 2.7, yielding an ICER of £1,370.

This data is supported by the cost-effectiveness acceptability curve (CEAC) in Figure 3.4. This technique estimates the probability of improved cost-effectiveness of DC-ACI versus ACI at a range of willingness to pay thresholds. This CEAC shows that aside from a extreme low values for WTP, DC-ACI has a higher probability of being cost-effective (80%) when compared with ACI.

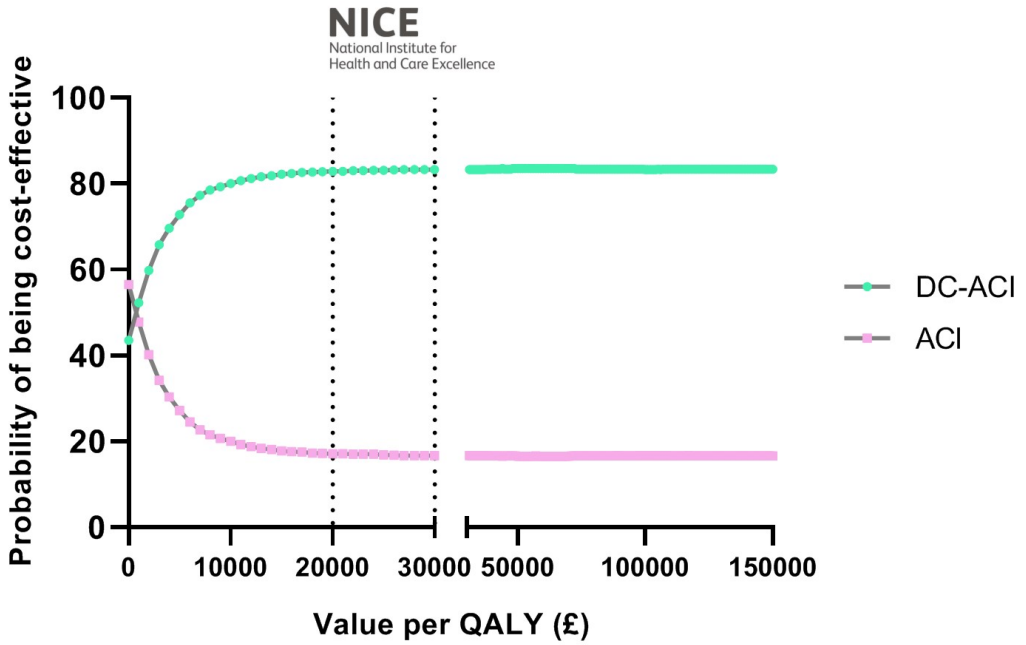

Figure 3.4: Cost-effectiveness acceptability curve (CEAC). Dotted region indicates the NICE range of WTP.

3.7 Discussion

Data from this cost-effective analysis indicates that DC-ACI would be a more cost-effective approach than ACI with an ICER of -£2,535.69 (-£2,222.30 with half-cycle adjustment (HCA)). This is supported by the stochastic model in which only 525/10,000 samples were over the NICE WTP threshold of £30,000, and the average ICER was £1,370. Finally, the cost-effectiveness acceptability curve (CEAC) demonstrates that in the NICE WTP threshold £20-30,000, DC-ACI is 80% likely to be cost-effective. Taken at face value, these data provide promising indications for the translation of decellularised scaffolds as matrices for cell therapy implantation and repair of articular cartilage.

As well as evaluating the cost-effectiveness, this study enabled estimation of the selling price of the decellularised scaffold as £1,941.33 in the base-case scenario (Table 3.4). Cost of scaffold production (recurring and investment costs) only made up 21% of the final cost. The rest of the cost was made up of overhead, development and distribution costs. The main variability around the cost was dependent on scale.

When bought in bulk, large savings can be made on reagents, this was reflected in the variability of the production costs. Furthermore, investment costs were variable depending on price and condition of purchased equipment (second hand or brand new).

The cost of the interventions had a large influence over the ICER. Although in most scenarios the ICER for DC-ACI remained under the threshold, variability in the cost is likely. Therefore it is an important consideration especially if decellularised scaffold production is at a small scale with inefficient manufacture processes, as discounts on bulk reagents would not be as great and costs would be nearer the extreme.

There are several caveats to this analysis that must be discussed. The first, and most important of these is the fact that the model inputs, especially utility and transition probabilities are based on the assumptions from clinical studies relating to OCA rather than DC-ACI specific clinical data. This was necessary as decellularised scaffolds are still early in development, however, of course it must be reiterated that these are assumptions, and further clinical studies would need to be performed to validate this model. Despite this, the data gives an indication for success rates, costs, and utility that should be an aim for studies.

Following on from this, due to hypothesised mechanisms of action, it was assumed that recellularised osteochondral matrices would perform similarly to osteochondral allografts. Certainly, this is an optimistic assumption, and as will be discussed later the transition probabilities derived from this data have an influence on the final ICER. However, this is the realistic aim for the technology, and the abundance of clinical data surrounding it made it a suitable assumption for the purposes of this study.

The final caveat, is that the cost of each treatment is an estimation based on several sources of information. The cost of reagents was based on purchasing records from our laboratory, the NHS costs for both treatments were based on similar treatments for the knee and the costs of translation (overheads, regulatory, packaging etc.) was based on advice from an unnamed adviser from the industry. Although these are estimations, the uncertainty surrounding these costs was covered in stochastic model.

Given these caveats, there are several interesting findings from this study. As described previously the ICER is -£2,222.30, which dominates ACI. Even taking into account the uncertainty surrounding the model the ICER still shows DC-ACI is more cost-effective than ACI. Unsurprisingly, cost variance between the upper and lower limits for DC-ACI and ACI have a drastic effect on the incremental costs for DC-ACI, in all instances changes whereby DC-ACI is higher and/or ACI is lower, DC-ACI becomes incrementally more costly. Interestingly, by matching the cost of the treatments, DC-ACI is incrementally more costly (£2,519.62). However, despite these changes in the incremental costs, due to the incremental QALYs gained (2.9) the ICER is still below the WTP threshold. When combining the extremes of DC-ACI (low utility and high cost), the ICER was above the WTP threshold (£36,763), demonstrating that variability within the DC-ACI input parameters must be controlled to ensure cost-effectiveness..

The sensitivity analysis in Table 3.12 aims to examine the inputs which contribute to the cost-effective nature of DC-ACI. Changing the DC-ACI successful repair utility to the low extreme values reported in clinical studies, causes a 2.3 QALY reduction. However, the net incremental QALYs are still 0.6 against ACI, despite utility for DC-ACI being akin to no improvement from the base-case utility. The reasons for this are likely due to differences in the transition probabilities between the two treatments.

The key discrepancies between the transition probabilities of the two treatments are demonstrated below in Figure 3.5. DC-ACI, has a higher probability of transitioning into successful first/second repair (0.817/0.780) alongside a higher probability of remaining in this health state. However, ACI has a higher probability of transitioning into a no further repair state (utility 0.691).

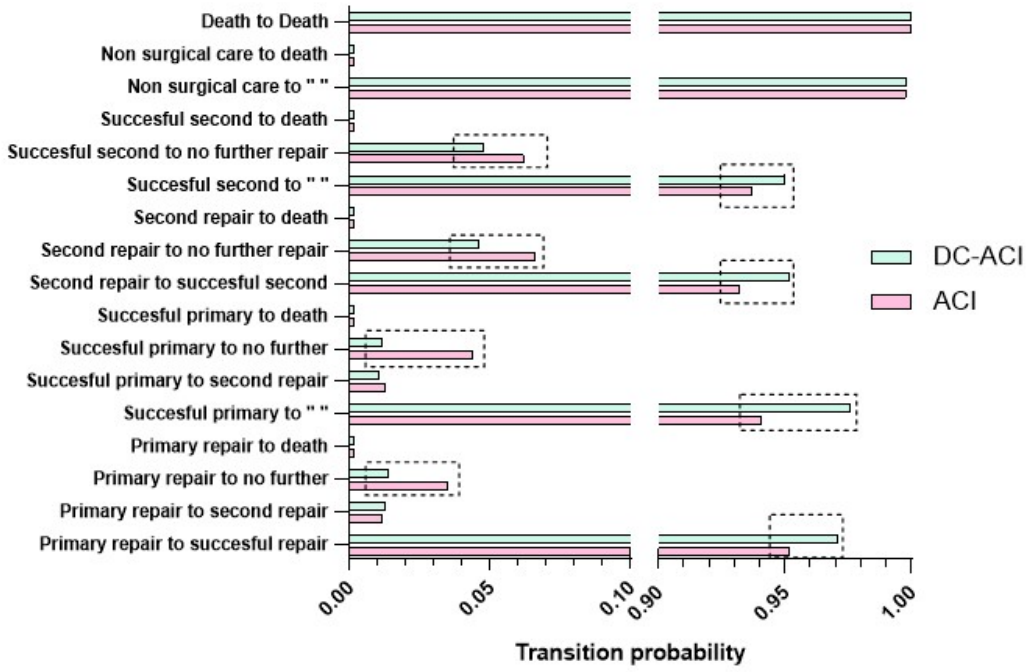

Figure 3.5: Transition probabilities comparison. Health state transitions are stated on the Y-axis. Dotted boxes indicated areas of the greatest discrepancy between transition probabilities.

This is illustrated in Figure 3.6, which shows that by 55 years, the percentage of patients in a successful primary repair state with DC-ACI is 73.30% versus 52.70% in ACI. The key difference between the two distributions of patients is in the percentage of patients in the no further/non-surgical repair health state. The same is true in the 55 years + group.

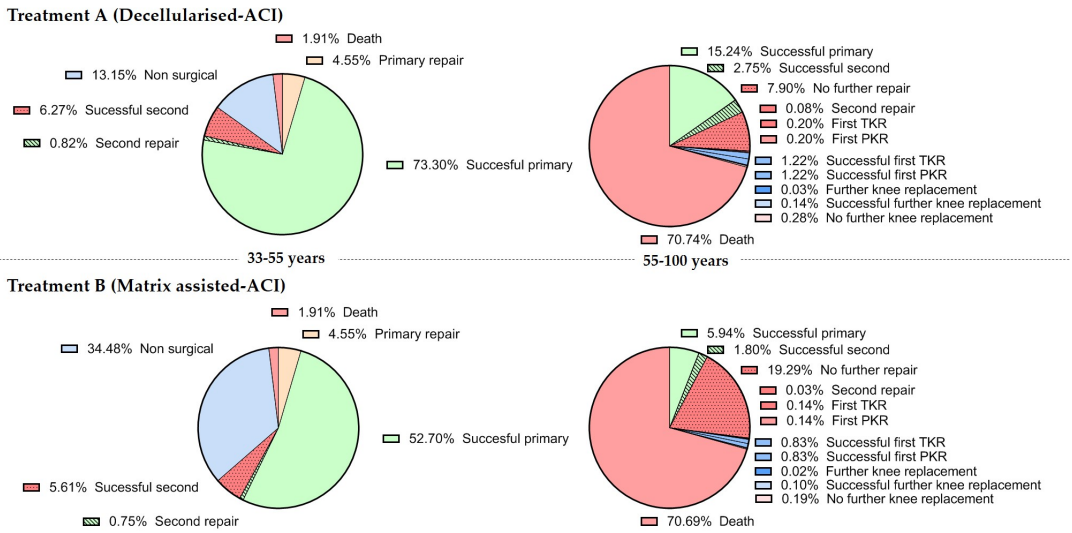

Figure 3.6: Health state distribution comparison between DC-ACI and ACI at 35-55 and 55+ years.

Given this information, the transition probabilities were altered to the limits in the sensitivity analysis. Interestingly, neither the lower limit of the DC-ACI transition to successful primary nor the upper limit of ACI changed the outcome of the cost-effectiveness analysis. This is due to the fact that the lower range of transition probabilities for DC-ACI, are similar to the base case ACI results. As both sets of transition probabilities were based a range of clinical results, this was the best information that was available to work with. However, it may highlight another limitation of this work, in that the variation appears to be greater for the ACI results than in the DC-ACI.

Although outside of the limits of the parameter ranges, when the transition probabilities of DC-ACI and ACI were matched for only two of the key transition probabilities highlighted in Figure 3.5 (successful primary repair and staying in successful primary repair) both the incremental QALYs reduced to -0.5. As the incremental costs were also negative, the ICER cannot be used, and instead the results were plotted on a cost-effectiveness plane (Figure 3.2), which demonstrated that in this particular scenario the ICER for DCI-ACI was above the NICE WTP threshold, making it unlikely to be cost-effective by NICE standards.

Conditions that also challenged the cost-effectiveness nature of DC-ACI were low utility of DC-ACI to a degree in which there was no significant improvement in

utility despite transition to a successful primary/secondary health state. Combined with a utility for successful repair following ACI of 0.950, caused the scenario to be on the border of the WTP threshold (Figure 3.2). Using a symmetrical WTP threshold for the south-west quadrant, is a practice which is up for debate. Authors argue that when a loss of utility is concerned, there is a willingness-to-accept (WTA) threshold, whereby the loss of utility is valued higher than the gain of utility (O'Brien *et al.*, 2002). They estimate that WTA is 2 x the WTP, and therefore, instead of a symmetrical WTP threshold in the SW quadrant there should be a kink equal to the WTA threshold. If applied in this scenario Figure 3.2, the low DC-ACI utility combined with high ACI utility scenario is no longer cost-effective. Despite the apparent disparity in the WTA and WTP from clinical studies, it is argued that from a societal health perspective a symmetrical threshold above and below the X-axis is most appropriate. Overall, the factor which had the greatest influence over the ICER of DC-ACI was the transition probabilities that effected 'patients' staying within the 'successful primary' health state. This leads on to another limitation of this HTA. Due to the previously discussed lack of clinical data, the transition probabilities had to be calculated using survival rates which had been obtained from papers (summarised in Table 3.8) (Horton *et al.*, 2013; Levy *et al.*, 2013; Biant *et al.*, 2014; Nawaz *et al.*, 2014; Familiari *et al.*, 2018; Ogura *et al.*, 2019). Assumptions were also made where data was not given, for example, where 78% of interventions were successful, 22% were considered failures. Then using data which stated 48% of patients had second repairs following OCA (Levy *et al.*, 2013), it was assumed 52% had no further repair. Whilst this seemed like a justifiable calculation, it is based on assumptions rather than clinical data.

3.8 Conclusion

Overall, this body of work aimed to investigate the cost-effectiveness of DC-ACI versus current standard treatment of ACI. The process required determination of the selling price of decellularised scaffolds (£1,941.33), and assumed utility similar to osteochondral allografting. Using our estimations and assumptions the ICER of DC-ACI for cartilage repair was -£2,222.30, indicating that DC-ACI is cost-effective

compared to ACI. Results from stochastic models and cost-effectiveness acceptability analysis also determined that even with the given uncertainty of the model the intervention was 80% likely to be cost-effective within the NICE WTP threshold. The model has inherent limitations, due to the requirement for assumptions in terms of DC-ACI utility and transition probabilities. However, this study highlights the requirement for clinical trials into decellularised scaffolds, as well providing target costs and utilities in order to achieve translation of a cost-effective intervention for cartilage repair.

Chapter 4

Optimisation and characterisation of decellularised osteochondral sheets for use in the treatment of large (>2cm^2) cartilage lesions

4.1 Introduction

The first experimental aim of this PhD research is the development of an osteochondral scaffold of appropriate dimensions for the treatment of large, shallow cartilage lesions.

The decellularisation process for porcine osteochondral tissue has been developed and optimised at the University of Leeds, to produce decellularised and biocompatible osteochondral pins (Fermor *et al.*, 2015a). The dimensions of these pins were 9 mm diameter and 12 mm length, which was required for a interference fixation of the plugs in the intended lesion site. However, this shape is not suitable for large and shallow lesions, characterised by a depth of < 5-8 mm and a total area of > 2 cm^2. A key property of such lesions is a lack of sclerotic bone changes, and ACI has shown excellent midterm results for lesions of this nature (Peterson *et al.*, 2003), likely due to the minimal demand for bone regeneration. Decellularised cartilage scaffolds have potential to act as a biologically and biomechanically relevant scaffold for cartilage repair. However, previous scaffolds show a lack of endogenous

cell repopulation, which has been observed and cited as a failure mechanism (Farr *et al.*, 2016). Therefore, it is hypothesised that a combination of ACI with a decellularised osteochondral scaffold of these dimensions will provide great quality tissue regeneration for large and shallow lesions.

The most appropriate scaffold dimensions were determined based on the characteristics of lesions which are treated most frequently, James Richardson's group at the Robert Jones & Agnes Hunt Orthopaedic Hospital (RJAH) in Oswestry, were pivotal in the development and subsequent NICE approval of ACI in the United Kingdom. They detail a prognostic study conducted into 170 ACI treated patients, which collected data on the characteristics of the cartilage lesions presented by patients pre-ACI (Dugard *et al.*, 2017). Their data showed that the median size of cartilage lesions was 4 cm^2. Furthermore, this study was conducted on patients presenting with lesion grades II-IV (ICRS scale), which encompasses mid-thickness lesions to full cartilage depth lesions. The rationale in this project with decellularised scaffolds, is for use in treating full thickness cartilage lesions without underlying bone damage (grade III), which can range from 2-4 mm in depth. Therefore, a scaffold depth of 5 mm was chosen initially to allow for full thickness cartilage repair, with a subchondral bone section to allow integration into lesion site. This is in line with the dimensions of commercially available Chondrogide®(Geistlich, UK) (20 mm x 30 mm).

Previous work from our group has shown successful decellularisation, sterility and cytocompatibility of osteochondral pin scaffolds (9 mm (diameter), 12 mm (depth) (Kheir *et al.*, 2011; Fermor *et al.*, 2015a). However, altered fluid dynamics within decellularisation vessels can affect decellularisation efficacy (Simsa *et al.*, 2019) and other studies have demonstrated variable detergent penetration and cell removal efficiency with different sized tissues (Lovati *et al.*, 2016). Therefore it is important to validate the existing decellularisation process with scaffolds of the proposed dimensions to treat large, shallow cartilage lesions.

As has been discussed in Section 1.8.3, a key limitation of 1st generation ACI is the lack of biomechanical strength prior to regeneration. Prior work has been conducted by (Kheir *et al.*, 2011), investigating the biomechanical function of decellularised

porcine osteochondral grafts. When subjected to indentation testing, the decellularised cartilage exhibited a 3-fold increased deformation (1.42 mm) when compared with native tissue (0.47 mm) under 1N of load. A similar significant increase in deformation versus the native tissue has also been observed in decellularised bovine scaffolds (Fermor *et al.*, 2015b).

Since these studies there have been significant advances in the decellularisation process as well as in biomechanical testing capabilities and material property derivations, allowing for calculations of permeability and equilibrium elastic modulus (Pawaskar *et al.*, 2010; Abdelgaied *et al.*, 2015). Such parameters have been studied for native bovine cartilage (Fermor *et al.*, 2015b), however there was no corresponding equilibrium moduli determination for decellularised samples. Determining these material properties for the decellularised porcine osteochondral scaffolds, with the latest process and dimensions, will provide valuable insight into the mechanical properties of the scaffolds versus other cartilage tissue engineering scaffolds. In order to determine the equilibrium elastic modulus and permeability it is important that assumptions of the biphasic model are met. A key assumption is a percentage deformation below 20%. Therefore, a low-load indentation set up will be used in order to keep the deformation below this limit for both native and decellularised samples.

As well as mechanical properties, it is hypothesised that decellularised scaffolds can provide benefit in terms of providing a native biochemical niche to support the cellular response to these matrices (Crapo *et al.*, 2011). Research by (Sutherland *et al.*, 2015) has indicated that lyophilised matrices retain bioactivity, and may be chondroinductive. Factors contributing to this ability, are of course molecules of the extracellular matrix such as collagen II. When processed into a hydrogel, cells have been shown to increase GAG accumulation, collagen II deposition and increase chondrogenic gene expression compared to collagen I hydrogels (Bosnakovski *et al.*, 2006). Similar effects have been seen with chondroitin sulphate (David-Raoudi *et al.*, 2009). Pericellular matrix components are also hypothesised to have a positive effect on chondrocyte growth, as isolated chondrons show improved growth versus chondrocytes alone (Larson *et al.*, 2002), such as collagen VI (Smeriglio *et al.*, 2015), perlecan

(French *et al.*, 2002) and hyaluronic acid (Akmal *et al.*, 2005). As well as promoting chondrogenesis, matrix molecules such as fibronectin, collagen II, collagen VI and vitronectin can enhance cell attachment to the matrix (Loeser, 1993). Previous studies from our group have characterised the effect of decellularisation on collagen and glycosaminoglycan (GAG) content of these scaffolds (Fermor, 2013), however, the presence of some of the previously mentioned matrix molecules have yet to be elucidated and would provide a wealth of insight into the bioactivity of these scaffolds.

An in-depth characterisation of these decellularised scaffolds will allow a greater understanding of their suitability as both biomechanically functional and bioactive scaffolds to support both healthy tissue repair and function.

4.2 Aims and Objectives

4.2.1 Aims

(i) To adapt the existing dimensions of the porcine osteochondral scaffolds to be appropriate for treating large shallow cartilage lesions.

(ii) To characterise scaffolds to validate decellularisation efficacy in terms of DNA removal, histological appearance and biocompatibility.

(iii) To further characterise the porcine decellularised scaffolds to judge their ability to support the survival, proliferation and maintenance of phenotype of seeded cells.

(iv) To characterise biomechanical properties of porcine decellularised scaffolds versus native osteochondral tissue.

4.2.2 Objectives

(i) Determine the clinically relevant dimensions for large, shallow cartilage lesions.

(ii) Determine the best means of reproducibly manufacturing porcine scaffolds of chosen clinically relevant dimensions.

(iii) Subject the scaffolds (clinically relevant dimensions) to the existing decellularisation process.

(iv) Investigate the efficiency of decellularisation through quantification of the total DNA and through histological examination.

(v) Characterise the retention of glycosaminoglycans through Safranin O and Fast Green staining, as well as biochemical quantification with the dimethymethylene blue GAG assay.

(vi) To determine the direct and indirect biocompatibility of the new scaffolds through contact and extract cytotoxicity testing *in-vitro*.

(vii) Select a suite of biomarkers associated with cartilage extracellular and pericellular matrix, as well as biomolecules.

(viii) Investigate biomolecule retention in the matrices through immunofluorescent/histochemical staining and imaging, to judge the ability of the matrices to support cell attachment, proliferation and chondrogenic differentiation.

(ix) To determine the biomechanical properties of the decellularised scaffolds through indentation creep testing, to provide baseline data to later judge interventions against.

(x) Derive permeability and equilibrium modulus using biphasic model

4.3 Materials and Methods

4.3.1 Tissue shaping

Porcine right legs were acquired and dissected as described in Section 2.2.2. The femoral condyles were shaped to 20 x 20mm square, 5mm deep osteochondral sheets using calipers, a hacksaw and a Dremel 8220 (Dremel, USA). The resulting shape is illustrated in Figure 4.1. The tissue was treated with 400 mL applications of PBS and monosodium citrate (37°C) using a Waterpik WP120 (Waterpik, USA), in order to remove bone marrow from the tissue. Osteochondral sheets were subsequently decellularised according to the protocol described in Section 2.2. Following decellularisation, the scaffolds were stored at -20°C until required for downstream analysis.

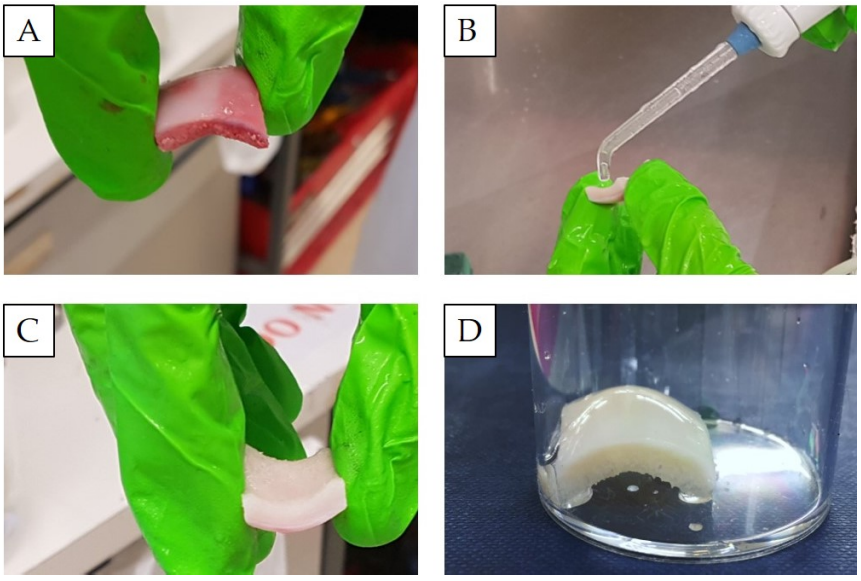

Figure 4.1: Shaping, waterpicking and decellularisation of porcine native osteochondral scaffolds. A) Shaped native osteochondral tissue B) Waterpik treatment C) Clean bone post-Waterpik D) Decellularised osteochondral sheet.

4.3.2 Quality assessment

4.3.2.1 Biochemical Quantification

Following decellularisation, the scaffolds underwent assessment to determine the efficacy of decellularisation. Native tissue was obtained, dissected (as described in

Section 2.2.2) and shaped to the same dimensions as the decellularisation treated scaffolds, and used as a positive control.

- **Total DNA content**. Native and decellularised scaffolds were thawed at 37°C for 30 minutes. Scaffolds (n = 3) were separated into bone and cartilage using a scalpel, then chopped into smaller pieces, lyophilised and digested overnight. The following day the DNA was extracted and quantified using the Nanodrop spectrophotometer as described in Section 2.2.7.1.
- **GAG content**. Native (n = 3) and decellularised samples (n = 3) were thawed at 37°C and the cartilage was shaved off the bone using a scalpel. The cartilage was chopped into smaller pieces, lyophilised and digested with papain for 48 hours. After this digestion period the samples were assayed with DMMB dye against a set of standards at 525 nm as described in Section 2.2.7.2.3.

4.3.2.2 Histological assessment

Native (n = 3) and decellularised (n = 3) scaffolds were bisectioned to expose the middle of the scaffolds. Following this the scaffolds were fixed in 10% NBF for 48 hours and processed for histology as described in Section 2.2.5. The sections were stained with H&E, Safranin O and Fast Green and DAPI as described in Sections 2.2.6.1, 2.2.6.2 and 2.2.6.4.

4.3.2.3 Biocompatibility

Decellularised scaffolds (n = 3) were separated into bone and cartilage portions and subject to the following biocompatibility assessment.

- **Sterility**. Bone and cartilage portions were incubated in thioglycollate broths for 1 week as described in Section 2.2.9.2. Sterility was determined through observation of the colour and opacity of the broth compared with a positive (non-sterile broth) and negative (sterile broth).
- **Contact cytotoxicity**. Slices of bone and cartilage were attached to the bottom of 6-well plate, and incubated with BHK and L929 cells as described in Section

2.2.10. Post-fixation with 10% NBF, cells were stained with Geimsa stain, and biocompatibility was determined through qualitative analysis of cell morphology, survival and growth up to the scaffold surface.

- **Extract cytotoxicity**. Bone and cartilage portions were diced and placed in sterile DMEM for 48 hours with agitation at 37°C, along with a negative (DMEM alone) and positive control (DMEM with 40% DMSO). Following the incubation period extracts were applied to a L929 or BHK cell monolayer, and the cells were assayed for cell viability as described in Section 2.2.11.

4.3.3 Immunofluorescence staining of decellularised scaffolds

Decellularised and native samples had been previously processed, fixed and paraffin embedded as in Section 4.3.2.2. These blocks were sectioned the day before staining, so that the sections were fresh. The following day, the sections were dewaxed in xylene and rehydrated through changes of 100% and 70% ethanol to water. Following this, depending on the desired antigen the sections were subject to a immunolabelling regime as detailed below in Table 4.1.

Slides were first subject to antigen retrieval (if required), followed by blocking for 1 hour in the serum of the animal the secondary antibody was raised in. Following this the slides were incubated with the primary antibody applied at a volume of 100 µL per section, at a dilution specified in Table 4.1. After the 1 hour incubation (R.T.P) the slides were subject to 3 x 5 minute washes in tris buffered saline (TBS), prior to incubation with the secondary fluorescent antibody. Negative (no primary) and isotype controls were used in order to verify the staining.

Table 4.1: Details of primary and secondary antibodies, antigen retrieval methods and blocking steps used for immunofluorescent labelling. NGS = normal goat serum, RT = room temperature, Ms = mouse, Rb = rabbit.

Antigen	Antigen retrieval	Block	Primary Ab	Isotype	Secondary Ab
Chondroitin sulphate	Trypsin (30 secs) Proteinase K (20 mins)	10% NGS 1 hour	Anti-CS (Ms) (1:200) 1 hour (RTP)	IgM (35.6 mg/mL)	GαMs 1:200 1 hour (RTP)
Collagen II	None	Dual endogenous block 2% Milk in TBS 1 hour	Anti-Col II (Ms) (1:200) 45 mins (RTP)	IgG1 (3 mg/mL)	DAKO Anti-Ms HRP DAB+ Substrate chromogen
Collagen VI	Overnight incubation in citrate buffer (pH = 6)	10% NGS 1 hour	Collagen VI (Rb) (1:400) 12 hour (4°C)	IgG (1.2 mg/mL)	GαRb 1:200 1 hour (RTP)
Fibronectin	Trypsin (30 secs) Proteinase K (20 mins)	10% NGS 1 hour	Anti-FN (1:150) 1 hour (RTP)	IgG (10 mg/mL)	GαMs 1:200 1 hour (RTP)

To visualise the presence or absence of cell nuclei sections were stained with DAPI as in Section 2.2.6.4. Cover slips were mounted onto the sections using DAKO fluorescent mountant, and samples were imaged the same day under fluorescent filters as in Section 2.2.1.3.

4.3.4 Immunohistochemical staining of decellularised scaffolds

Decellularised and native samples had been previously processed, fixed and paraffin embedded as in Section 4.3.2.2. These blocks were sectioned the day before staining, so that the sections were fresh. The following day, the sections were dewaxed in xylene and rehydrated through changes of 100% and 70% ethanol to water. Following this, depending on the desired antigen the sections were subject to a immunolabelling regime as detailed below in Table 4.1.

Slides were first subject to antigen retrieval (if required), followed by blocking by adding drops of Dual Endogeneous Enzyme Block to each section until section was covered and incubated for 10 minutes. Then 2% milk in TBS was applied to cover each section, and incubated for 30 minutes. Then two 5 minute washes in TBS were performed. Then the primary antibody was added to each section at the desired concentration (Table 4.1) and incubated for 45 minutes, followed by two 5 minute TBS washes. Following this a drop of DAKO HRP from the relevant source (Table 4.1) was added to each section and incubated for 30 minutes. Three washes in TBS were performed after the incubation. Then one drop of DAB+ chromagen system (20 µL liquid DAB and 1 mL substrate buffer) was added to each section and incubated

for 10 minutes. The sections were then washed four times in distilled water, followed by a 5 second incubation in haematoxylin. The sections were washed in running tap water until the water ran clear, and immersed in Scott's tap water for 1 minute. Following this, the sections were dehydrated as in Section 2.2.6.1, and mounted for visualisation using brightfield microscopy.

4.3.5 Indentation Studies

4.3.5.1 Creep Indentation

In order to investigate the compressive properties of decellularised cartilage compared to native tissue, creep indentation was performed. Cylindrical 9 mm osteochondral pins were extracted from native and decellularised tissues (n = 6). All native tissues were stored at -20°C upon dissection, and thawed for pin extraction and indentation. The studies were conducted using an in house manufactured low load indentation rig (Figure 4.2).

The set up consists of a linear variable differential transformer (LVDT), which measured displacement over a range of 10 mm, with a sensitivity of 0.4 µm. The output of the testing apparatus was voltage (V) and load (N) over time. Displacement data was recorded using LabView software (2012) at a sampling rate of 5 Hz. The displacement data is eventually used to calculate the percentage deformation.

The load applied to the pins was 0.11 N, which was determined by the weight of the fibreglass load shaft, the load cell and acrylic load cell holders. These components were manufactured in order to allow a low load set up, resulting in deformation of the cartilage below 10%, to satisfy requirements for finite element modelling to determine biomechanical properties. This load was applied to the cartilage surface by a flat 2.5 mm diameter stainless steel indenter. This indenter size was chosen, as it was less than or equal to one-third of the sample diameter, which was essential to allow expansion and fluid flow in both axial and lateral directions (Mow *et al.*, 1989; Korhonen and Saarakkala, 2011).

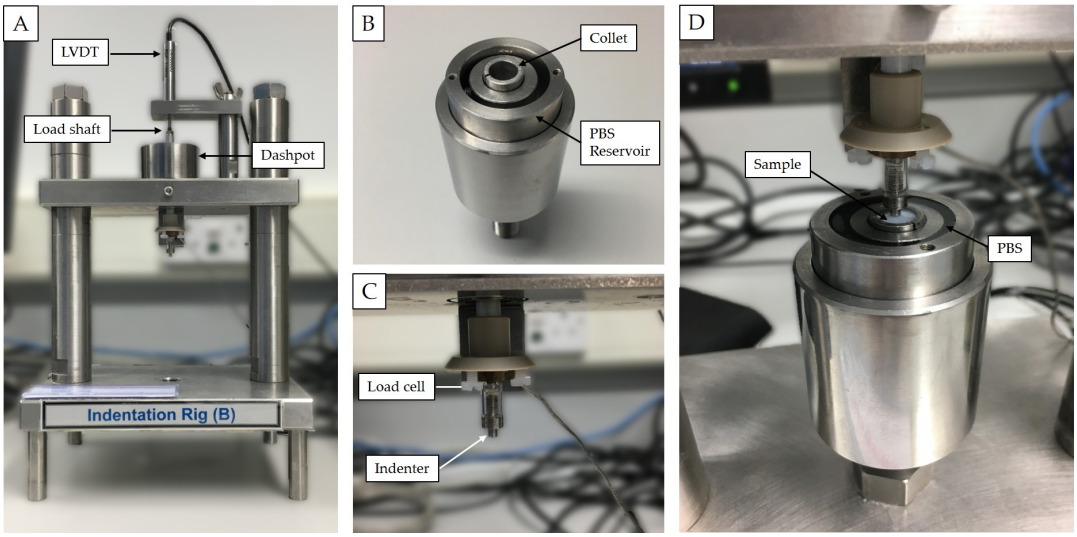

Figure 4.2: Indentation rig set up. A) Indentation rig B) Sample pot and collets C) Load cell and indenter D) Indentation test.

4.3.5.2 Calibration

Prior to measurement of the samples the linear variable differential transformer (LVDT) and load cell were calibrated. The LVDT was calibrated using stainless steel slip gauges of known thicknesses. The indenter tip was rested at the zero position which was 51 mm above the platform (using 50 mm and 1 mm slip gauges) and the voltage was recorded using LabView programme. After 15 seconds of equilibration, the next step heights were iteratively ntroduced up to 53 mm in the following sequence 1.005 mm, 1.010 mm, 0.020 mm, 0.050 mm, 0.100 mm, 0.200 mm, 0.500 mm, 1.000 mm, 1.500 mm, 2.000 mm. From this position, the process was reversed through the same sequence back to the zero position. The LabView programme was stopped, and average voltages were calculated for each displacement position and used to plot a calibration graph.

The load cell was also calibrated by resting the indenter tip on the stainless steel slip gauge and adding calibrated masses to the load shaft in 10 g increments up to 40 g. At 40 g, the process was reversed the process back to 0 g. The LabView programme was stopped and average voltages were calculated for each load.

4.3.5.3 Cartilage indentation testing

To perform the experiment, pins were held within a collet and submerged in PBS (Figure 4.2 D) to maintain tissue hydration throughout the test. The cartilage surface was raised by a spacer so the cartilage surface was just below the lip of collet. This collet was placed within a large specimen holder within the indentation test rig, and raised so that the distance between the indenter tip and the cartilage surface was 1 mm.

To begin the test the indenter was released and made contact with the cartilage surface in under 40 ms. The test was run for 1 hour, which was sufficient time for all samples to reach equilibrium. The voltage and load measurements were recorded, and the calibration data was used to interpolate displacement distance from voltage.

4.3.5.4 Cartilage thickness measurements

The cartilage percentage deformation was calculated as:

$$\frac{\text{Indenter displacement (mm)}}{\text{Unloaded cartilage thickness (mm)}} \times 100 \tag{4.1}$$

The unloaded cartilage thickness was measured for each specimen. The scaffolds were bisected and an image was taken at a consistent distance alongside a ruler with 0.5 mm graduations. These images were subsequently processed in ImageJ. Using the line selection tool, a line was drawn over a 5 cm distance on the caliper scale, then using the set scale function under the 'Analyze' toolbar the known distance was set as 5 cm. A line was drawn from the cartilage surface to the cartilage-bone interface and using the measure function the distance was calculated. Six measurements were taken across the width of the cartilage, and the mean thickness was calculated.

4.3.6 Finite element determination of biomechanical properties

The creep deformation and cartilage thickness data obtained previously was used to model the equilibrium elastic modulus and permeability of both the native and

decellularised cartilage. The equilibrium elastic modulus is a measure of an objects resistance to deformation when stress is applied at equilibrium. Permeability is a measure of the rate at which a substance can pass through a material. A three-dimensional axisymmetric biphasic poroelastic finite element model, developed in FEBio created by (Abdelgaied *et al.*, 2015; Gopu *et al.*, 2017), was used to derive these properties. This biphasic model assumes isotropy, homogeneity, infinitesimal strain, constant permeability and a frictionless indenter tip.

The model is made up of a 3°slice of a flat 2.5 mm diameter indenter contacting a 9 mm diameter cartilage plug (Figure 4.3), with a thickness defined by cartilage thickness data measured from experimental studies. The model was opened in ABAQUS (Dassault Systèmes Simulia Corp, Version 6), and the dimensions of the indenter and tissue geometries were defined, and each part was meshed (Figure 4.4).

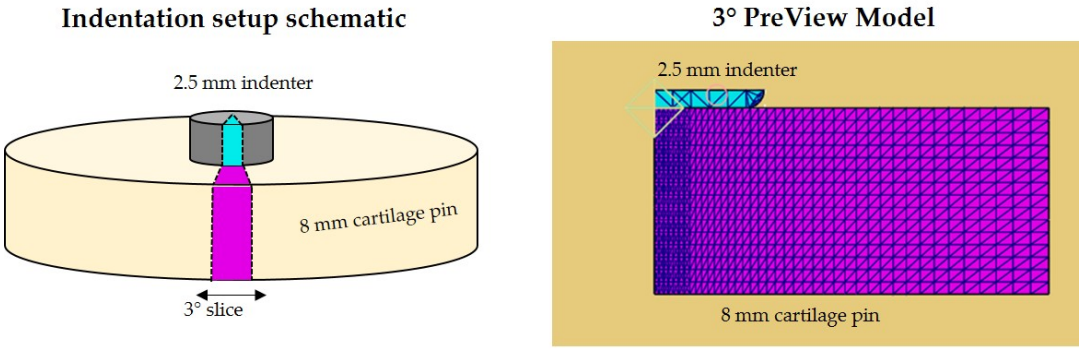

Figure 4.3: Schematic of the indentation set up. Set up in relation to the respective 3°indenter and cartilage pin model on PreView software.

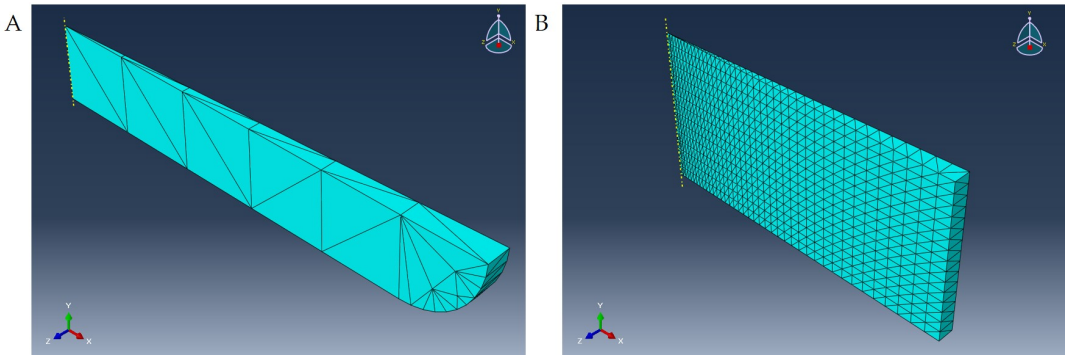

Figure 4.4: Axisymmetric indentation modelling geometries meshed in ABAQUS. A) 1.25 mm indenter part B) 4.5 mm cartilage part.

The meshed model files were imported into PreView, and the indenter was modelled

as a a rigid body whilst the tissue was modelled as a poroelastic material. Following this boundary conditions were added to the tissue (Figure 4.5). The front face of the tissue was assigned with a Fixed Y boundary condition as this is a segment of a 360°plug meaning this face would be supported by tissue. Assuming the bone as a rigid body the bottom face of the tissue was assigned zero displacement in X, Y, Z. Finally the outer portion of the tissue was assigned a fixed fluid pressure to allow free fluid flow from the tissue. Biphasic contacts were also added to the bottom face of the indenter and top face of the tissue.

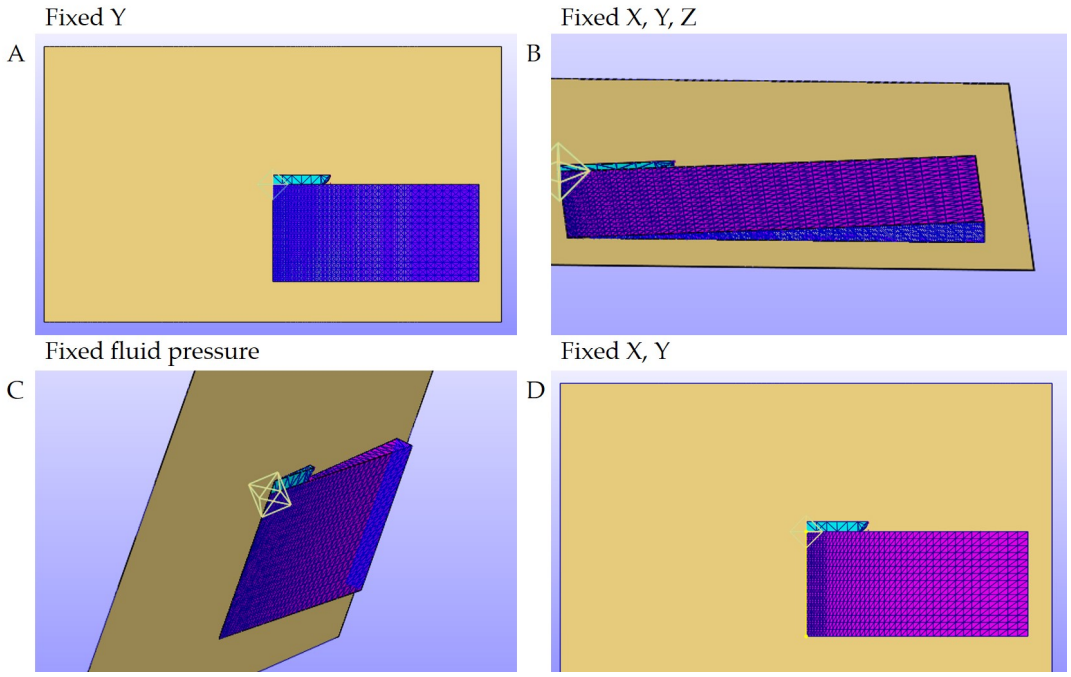

Figure 4.5: Boundary conditions assigned to FE model. A) Fixed Y added to face of tissue B) Fixed X, Y, Z added to bottom face C) Fixed fluid pressure added to the outer circumference portion D) Fixed X, Y condition added to edge on axis of symmetry.

As the model reflected a 3 °portion of the experimental set up, 1/120th of the experimental load was applied (9.56 x 10^{-4}N) in the FE model. The Poisson's ratio was assumed to be zero with a water content of 80%. Using MATLAB (MathWorks Inc, USA) the final 30% of the experimental creep deformation curve was matched with the FE model curve. The program ran iterations of different starting material properties until the curve fitting reached a maximum R^2 value. An R^2 above 0.75 is considered acceptable for tissues, however, in this study all R^2 were > 0.9. The material properties (equilbrium elastic modulus and permeability) which gave the maximum R^2 after curve fitting were recorded.

4.4 Results

4.4.1 Producing scaffold of appropriate clinical dimensions

For MACI applications, decellularised scaffolds of 20 x 20 x 5 mm were identified as more clinically relevant. Figure 4.6 shows the production of porcine osteochondral (OC) sheets. Tissues were successfully and reproducibly shaped with relative ease using the procedure outlined in Section 4.3.1.

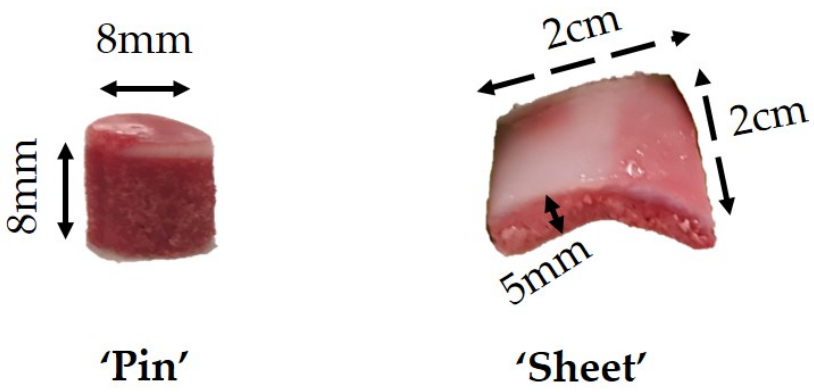

Figure 4.6: Comparison of osteochondral scaffold dimensions

4.4.2 Removal of cells and DNA

The porcine OC sheets were decellularised using an existing process (Section 2.2.4) and decellularisation efficacy was validated.

Follow decellularisation, cartilage DNA content was significantly reduced (23.6 ng.mg^{-1}) compared to the native (823.0 ng.mg^{-1}, p<0.0005 T-test). This falls below the 50 ng.mg^{-1} decellularisation criteria established by (Crapo *et al.*, 2011). The DNA in bone was also significantly reduced (Decell: 60.5 ng.mg^{-1}, Native: 387.5 ng.mg^{-1}, p < 0.0005 T test), however the DNA content was just above the 50 ng.mg^{-1} threshold.

This quantitative data is supported by the H&E comparison of the native and decellularised samples. In Figure 4.7C cells can be seen through the superficial and deep zone cartilage layers within the chondrons, whereas in the decellularised tissue these chondrons are empty. The same is true for the bone portions, indicating

successful decellularisation.

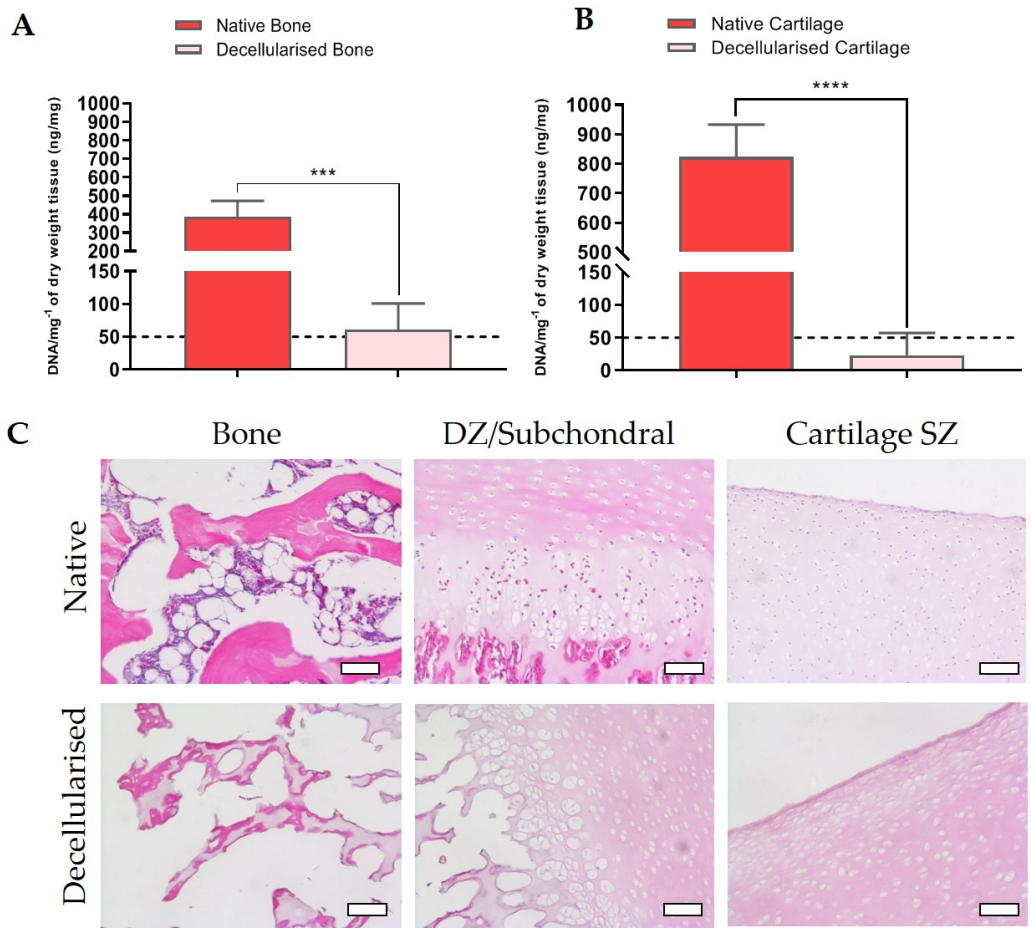

Figure 4.7: Assessment of decellularisation. DNA assay results comparing native and decellularised bone (A) and cartilage (B) segments. Error bars = +/- SD. Unpaired T-test performed. *** = $p < 0.0005$, **** = $p < 0.0001$. C) H&E staining of native and decellularised bone and cartilage segments. Cell nuclei are blue and the extracellular matrix is stained pink. DZ = deep zone and SZ = superficial zone. Scale bars = 100 µm

In order to confirm the decellularisation, a DAPI stain for cell nuclei was performed as shown below in Figure 4.8. As seen in the H&E, the decellularised sample was clear of cell nuclei. However, in the decellularised sample, there was a DAPI signal in the lower subchondral bone portion. Whether these are artefacts, autofluorescence, collapsed pericellular matrix or cellular remnants is unknown.

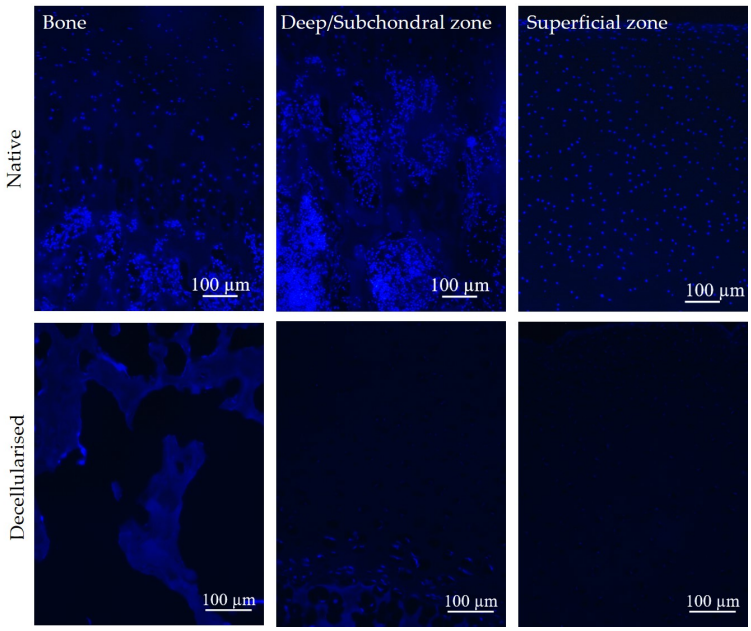

Figure 4.8: DAPI staining. DAPI staining for cell nuclei (blue) within the decellularised osteochondral scaffolds. Scale bars = 100 µm.

4.4.3 Retention of extracellular matrix components in porcine decellularised scaffolds

Following initial confirmation of decellularisation, it was important to determine the extracellular matrix components which are retained within the matrices post-decellularisation. Extracellular matrix components and biomolecules were selected based on the desired application of this scaffold alongside cells and a self-assembling peptide. These functions were defined as a ability to withstand compression, support cell attachment and differentiation.

4.4.3.1 Effect of decellularisation on the GAG content of the scaffold

The GAG content of porcine decellularised cartilage (Figure 4.9) was significantly reduced ($p < 0.0005$) compared to native porcine cartilage. This result is supported by the Safranin O and Fast Green staining, which showed a complete depletion of the GAGs throughout all superficial, middle and deep zones of the cartilage layer following decellularisation. There appeared to be some GAG retention in the upper subchondral bone layer, which coincided with the area of histological cell remnants/debris in (Figure 4.8).

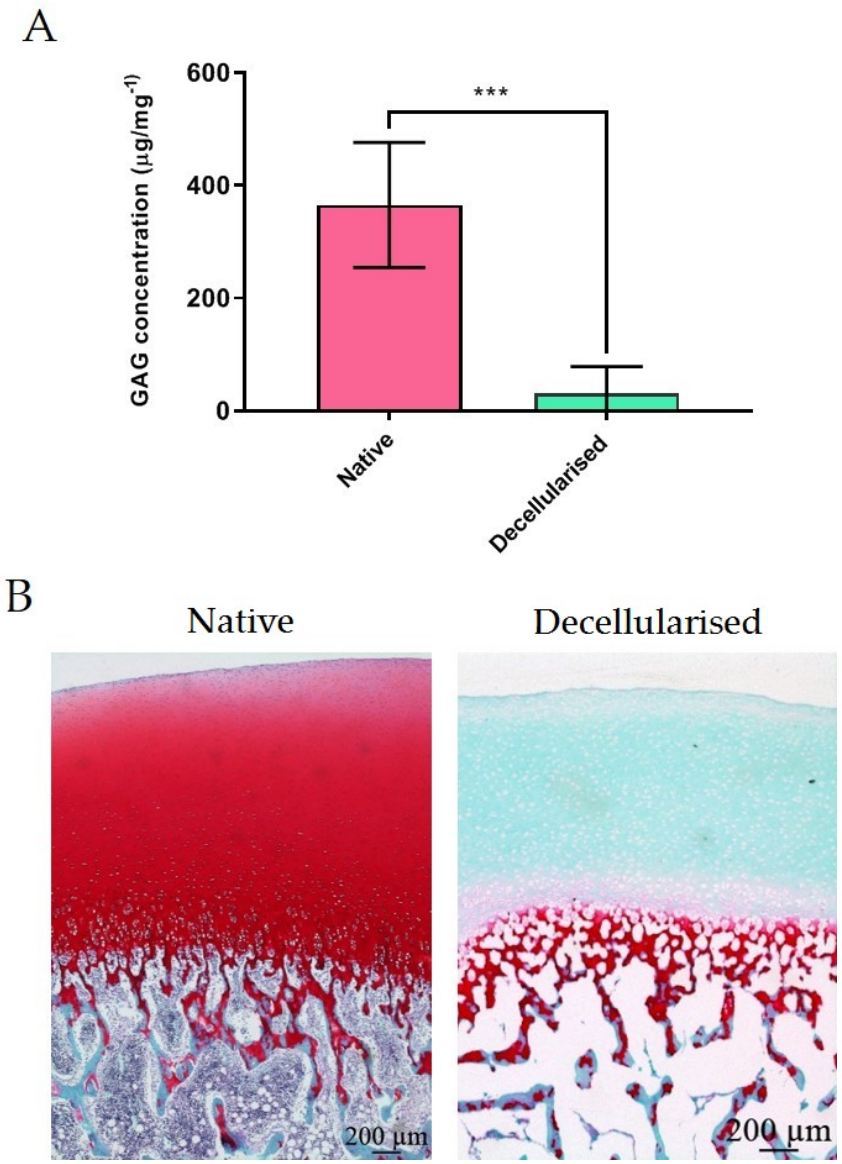

Figure 4.9: Assessment of GAG content of decellularised osteochondral sheets post-decellularisation. A) Mean GAG content (n=3) of native cartilage versus decellularised cartilage. Error bars = ± 95% C.I. *** = $p < 0.0005$ (Unpaired t test). B) Safranin 0 and Fast Green staining of native (left) and decellularised samples. Scale bar = 200 µm.

Neither the DMMB assay nor the Safranin O and Fast Green staining investigated the quantity or distribution of chondroitin sulphate specifically. Therefore, it was labelled and visualised in the decellularised samples using immunofluorescence staining.

As shown previously, the native cartilage samples showed strong Safranin O staining, indicating a consistent presence of proteoglycans throughout the cartilage depth. The chondroitin sulphate immunofluorescence staining matched this pattern, with

positive staining in the ECM throughout the cartilage depth with stronger staining local to the chondron (Figure 4.10).

The decellularised samples showed some retention of proteoglycans in the Safranin O staining. However, significant proteoglycan loss was observed in the mid-deep zone. The immunofluorescence images, showed weaker ECM CS staining. However, the staining was still relatively strong surrounding the chondron. In the middle-deep zones, this staining surrounding the chondron was lost, in keeping with the areas with weak Safranin O staining.

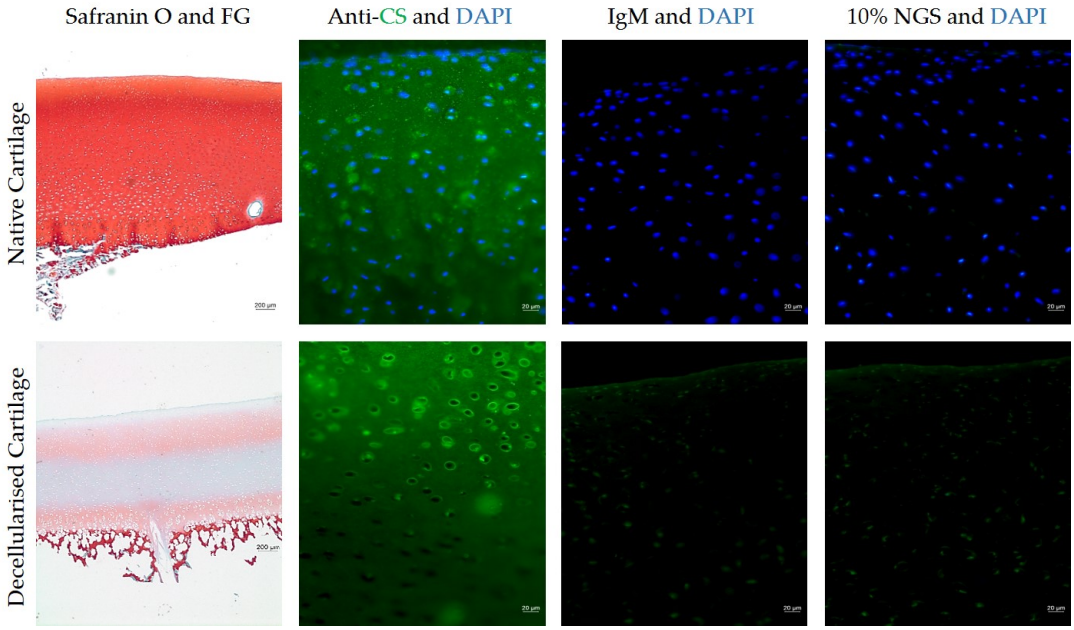

Figure 4.10: Chondroitin sulphate staining of decellularised osteochondral tissue. Representative images of native (n = 3) and decellularised (n = 3) osteochondral scaffolds labelled with anti-chondroitin sulphate, alongside isotype (IgM) and normal goat serum (NGS) control sections. Staining visualised with a goat anti-mouse 488 secondary (green). Immunofluorescent (IF) staining was compared with Safranin O and Fast Green staining for proteoglycans. Nuclei stained with DAPI (blue). Scale bars = 20 µm for IF and 200 µm for histology.

4.4.3.2 Collagen II

As mentioned previously, collagen II is a prevalent biomolecule in cartilage, providing a smooth surface for articulation and resistance to tension in the direction of articulation (Guo and Torzilli, 2016). Both reagent and isotype controls showed limited background staining in both the native and decellularised samples (Figure 4.11).

In the native sample, the staining was strongly present throughout all zones of cartilage, with slightly higher intensity observed in the subchondral bone portion and in the superficial zone. This pattern was also exhibited in the decellularised samples. More detail of the alignment of the collagen fibres can be observed by the Sirius Red staining under polarised light (Figure 4.12). The native and decellularised samples appeared to have similar alignment and intensity of collagen fibres throughout all zones of the cartilage.

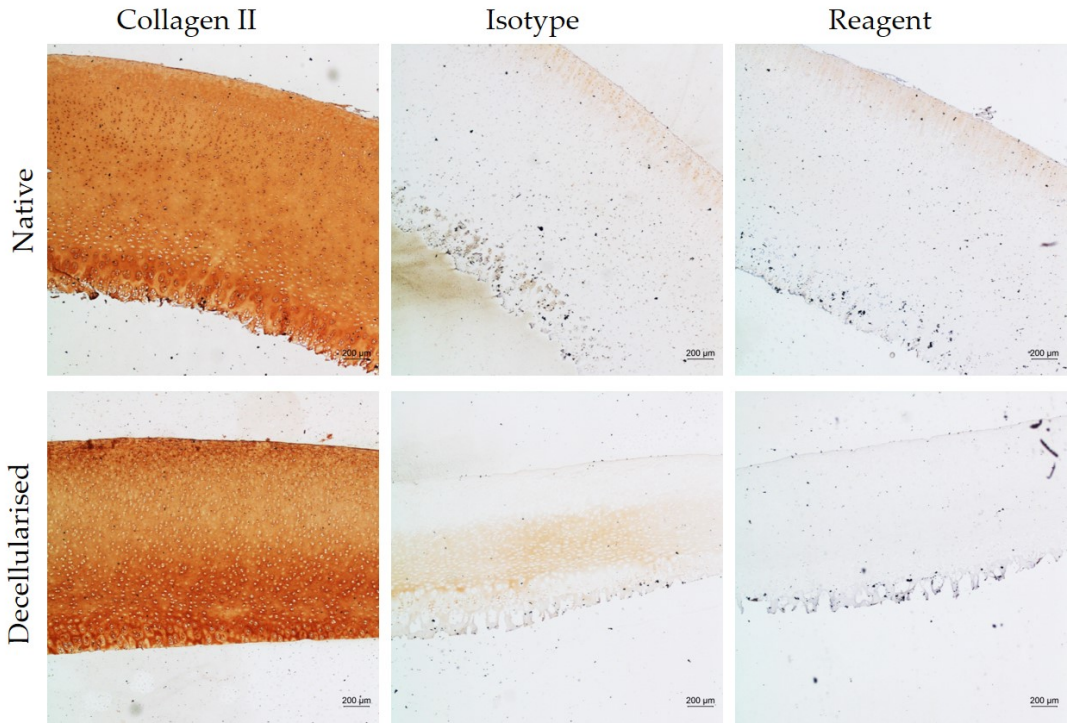

Figure 4.11: Collagen II staining of decellularised osteochondral tissue. Representative images of native (n = 3) and decellularised (n = 3) osteochondral scaffolds stained with anti-collagen II, alongside and isotype and diluent only control sections. Staining visualised with a DAB chromagen system. Scale bars = 200 µm

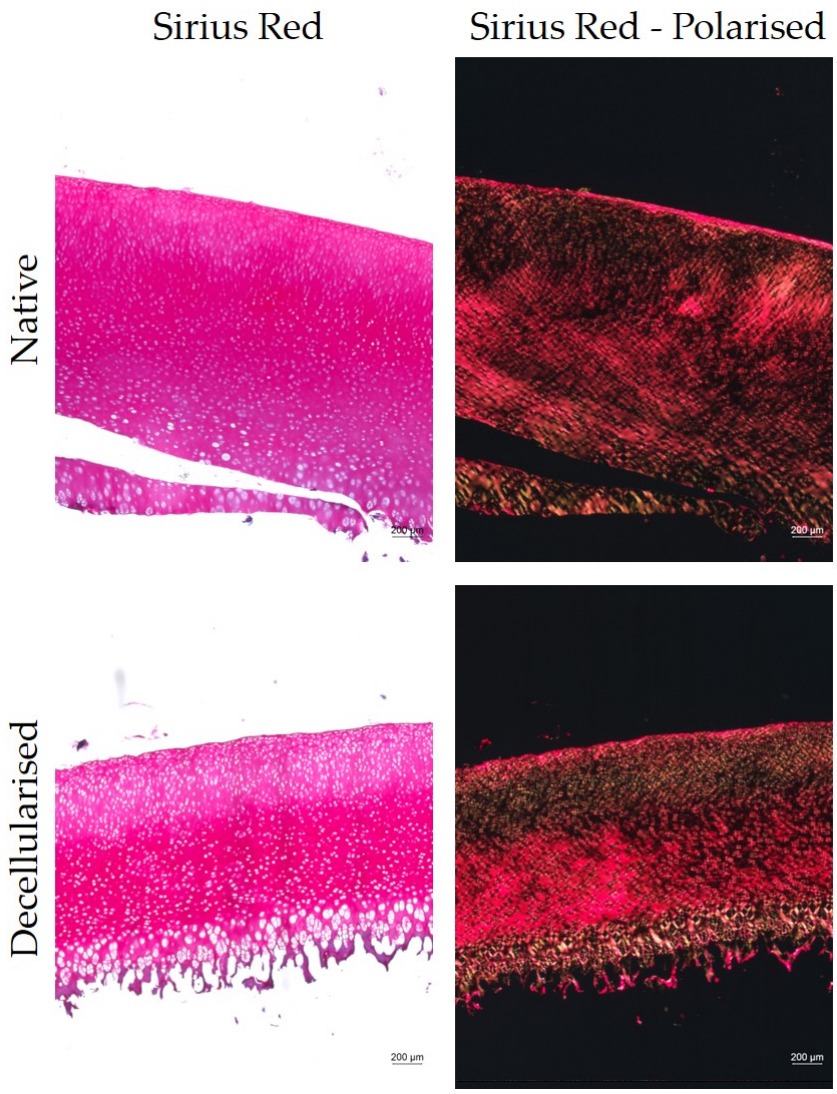

Figure 4.12: Sirius red staining of decellularised osteochondral tissue. Representative images of sirius red stained native and decellularised osteochondral tissue. Sections were stained and visualised under both brightfield (left) and polarised light (right) to view collagen alignment. Scale bars = 200 µm.

4.4.3.3 Collagen VI

Collagen VI is a component of the PCM, and therefore plays an important role in mechanotransduction and protection of the chondrocyte from excessive mechanical loads (Guilak *et al.*, 2006). The native samples (Figure 4.13) showed localised fluorescence surrounding the chondron with staining within the chondron as well. It appeared that staining was more prominent in the superficial and middle zones. A similar pericellular staining pattern was evident in the decellularised samples, however, fluorescence was absent from the inside of the chondron. Both IgG and reagent

controls exhibited no background staining.

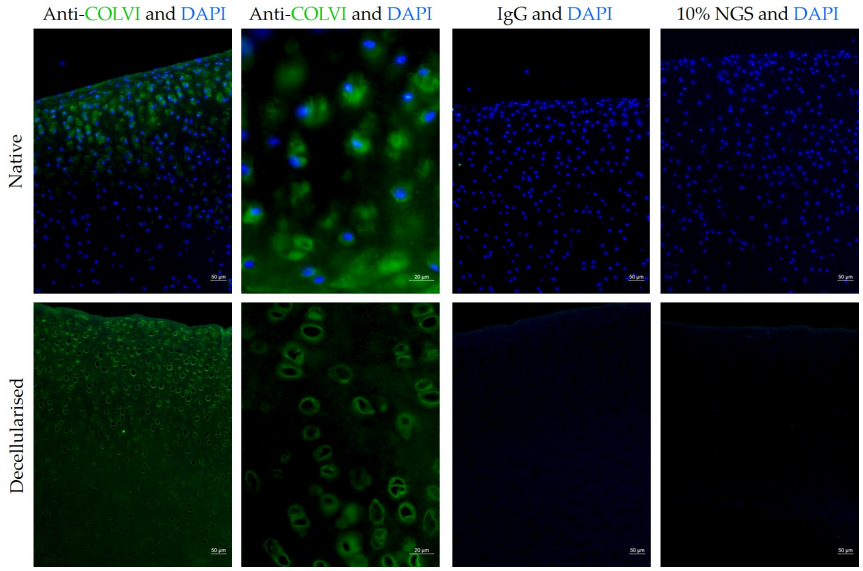

Figure 4.13: Collagen VI staining of decellularised osteochondral tissue. Representative images of native (n = 3) and decellularised (n = 3) osteochondral scaffolds stained with anti-collagen VI, alongside and isotype (IgG) and normal goat serum (NGS) control sections. Staining visualised with a goat anti-mouse 488 secondary (green). Nuclei stained with DAPI (blue). Scale bars = 50 µm and 20 µm for increased magnification images.

4.4.3.4 Fibronectin

In relation to the application of decellularised osteochondral scaffolds alongside autologous cells, it was deemed important to determine the presence of known cell attachment motifs within the cartilage ECM, such as fibronectin (Loeser, 1993).

The native cartilage H & E was used a reference to contextualise the section (Figure 4.14). Fibronectin was present in the ECM in native cartilage as well as the PCM surrounding the cell. However, in the decellularised samples the intensity of ECM fibronectin staining was reduced, showed no difference to the isotype control. The staining surrounding the cell had also disappeared. Indicating that processing led to a loss of detection fibronectin in decellularised osteochondral scaffolds.

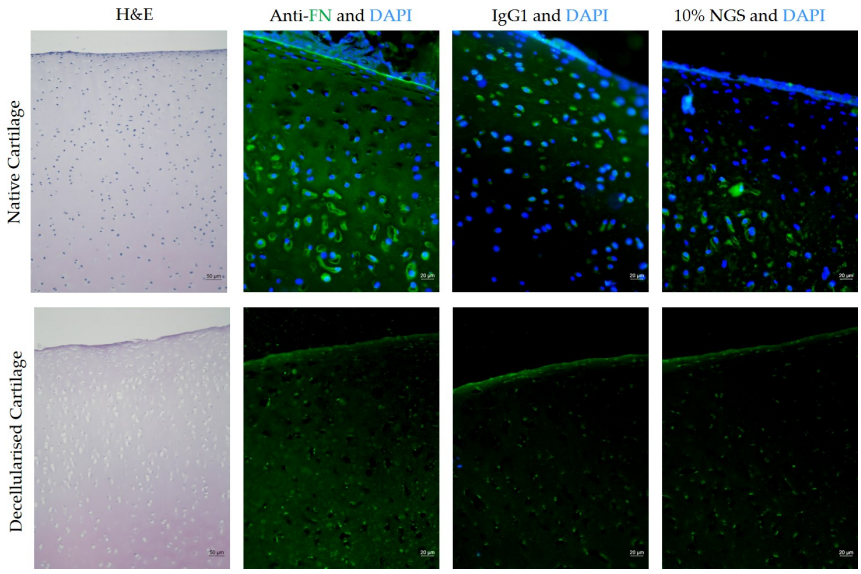

Figure 4.14: Fibronectin staining of decellularised osteochondral scaffolds. Native (n = 3) and decellularised (n = 3) osteochondral scaffolds stained with anti-fibronectin, alongside and isotype (IgG1) and normal goat serum (NGS) control sections. Staining visualised with a goat anti-mouse 488 secondary (green). Immunofluorescent (IF) staining was compared with haematoxylin and eosin stain. Nuclei stained with DAPI (blue). Scale bars = 20 µm for IF and 50 µm for histology.

4.4.4 Biocompatibility testing of decellularised osteochondral sheets

4.4.4.1 Sterility testing

Prior to cytotoxicity testing, it was necessary to perform sterility testing of the decellularised scaffolds alongside control cultures. The results depicted in (Figure 4.15) show that in the positive control at both day 7 and day 3, the broth was cloudy which is indicative of bacterial contamination. However, in the broths of the negative control and of the decellularised samples this was not observed, which suggested that the scaffolds remained sterile throughout the decellularisation process.

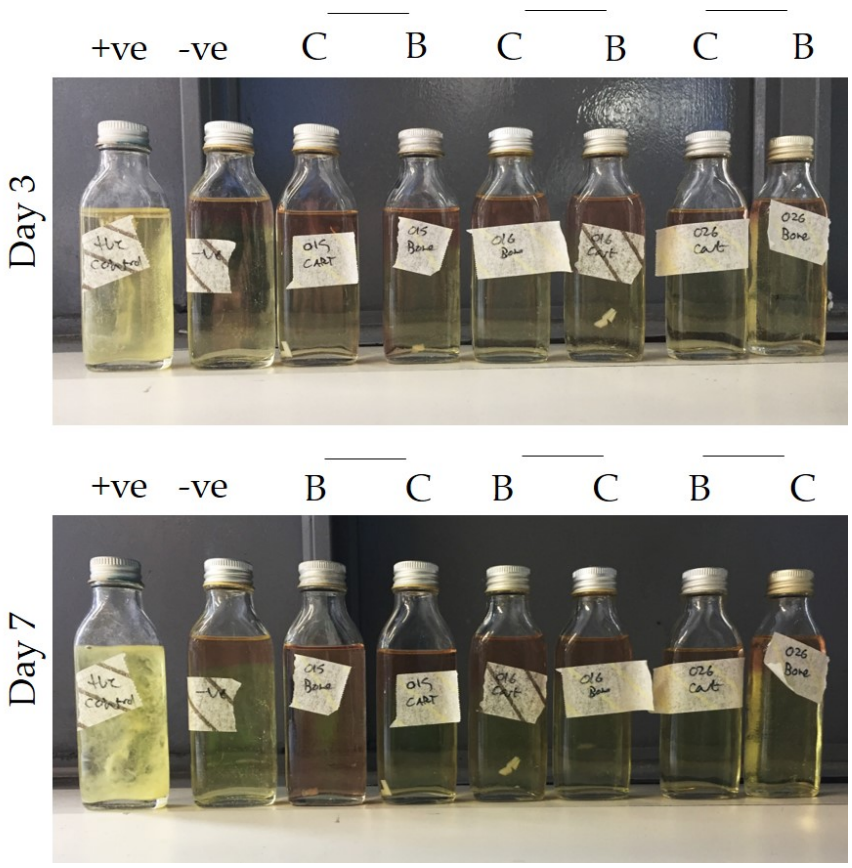

Figure 4.15: Assessment of sterility of decellularised scaffolds using thioglycolate-broths. Scaffolds and controls were incubated at 37 °C, and images were taken at Day 3 and Day 7 to examine the presence of bacteria. Samples denoted with a B are bone, and with a C are cartilage. The linking line represents bone and cartilage from the same osteochondral plug (n=3).

4.4.4.2 Contact cytotoxicity assay

The BHK/L929 cell alone and steristrip controls were used as negative controls for cytotoxicity, and show cells with normal morphology and growth surrounding the material. However, the positive cyanoacrylate showed cells of a non-viable morphology in the immediate vicinity of the material, as well as lack of cell growth surrounding the perimeter of the material. The BHK (Figure 4.16) and L929 (Figure 4.17) cells grew up to the interface with the decellularised cartilage and bone samples, and showed no signs of detrimental change in cell morphology of growth characteristics. The decellularised scaffolds did not induce cytotoxicity upon direct contact with cells.

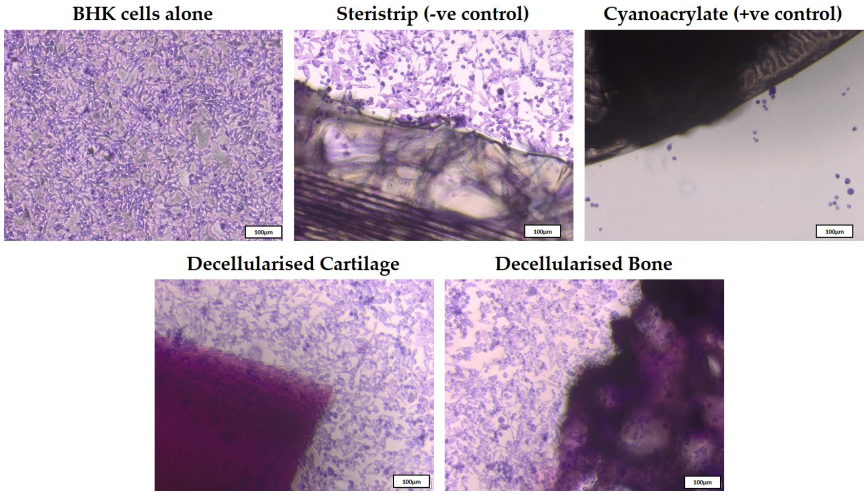

Figure 4.16: Contact Cytotoxicity Assay with BHK cell line. BHK cells were incubated with +ve and -ve controls as well as decellularised osteochondral material (n=3) for 24 hours. Cells were then fixed, stained with Geimsa and visualised under a light microscope. Scale bars = 100µm

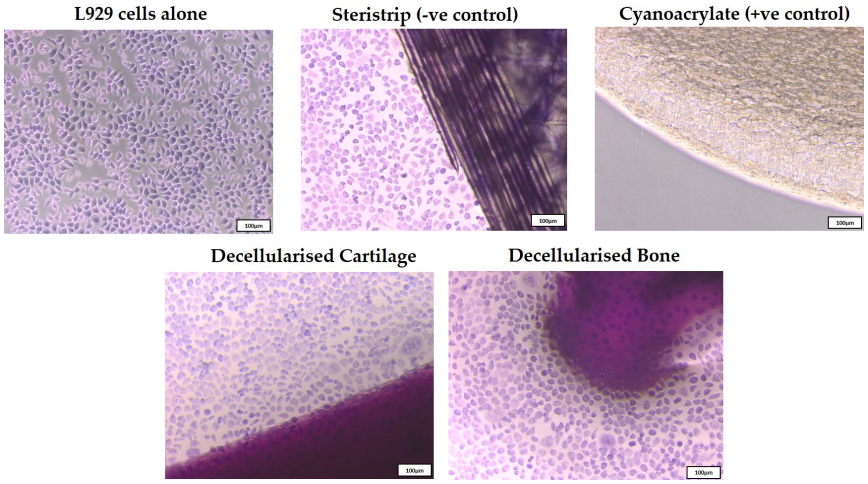

Figure 4.17: Contact Cytotoxicity Assay with L929 cell line. L929 cells were incubated with +ve and -ve controls as well as decellularised osteochondral material (n=3) for 24 hours. Cells were then fixed, stained with Geimsa and visualised under a light microscope. Scale bars = 100µm

4.4.4.3 Extract cytotoxicity assay

Cytotoxicity of the scaffold extracts was also investigated, to ensure no SDS or any other cytotoxic components from the decellularisation process were retained in the scaffold. This was performed with both BHK and L929 cells, and Figure 4.18 shows that in both instances there was no significant difference between the cellular response to the extracts of the scaffolds when compared with the media alone control. However, in the positive control for cytotoxicity (40% DMSO) there was a significant reduction ($p<0.0001$).These results, in conjunction with those shown in Figure 4.4.4.2 and Figure 4.4.4.1, indicate biocompatibility of the scaffolds.

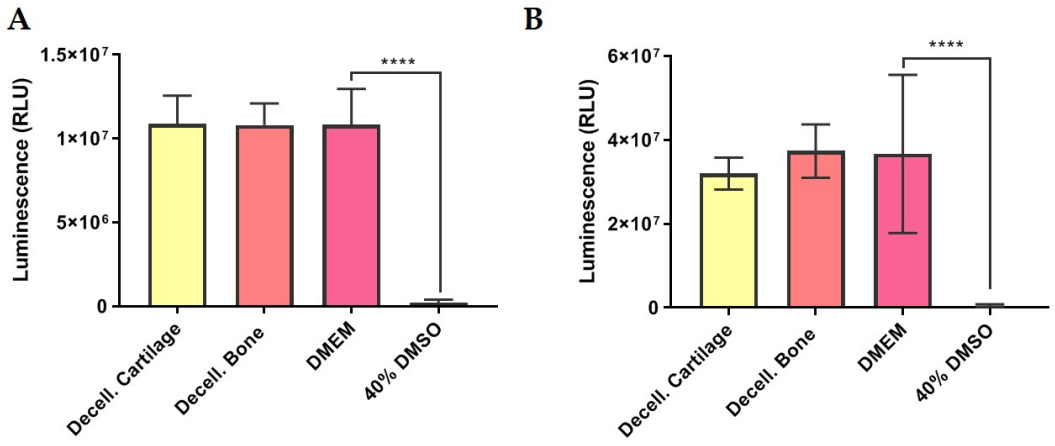

Figure 4.18: Extract cytotoxicity of decellularised scaffolds with A) BHK cells and B) L929 cells. Data presented as mean ±95% C.I. 1-way ANOVA performed with post-hoc Tukey's test. **** = p<0.0001.

4.4.5 Mechanical characterisation of decellularised cartilage

4.4.5.1 Calibration

Calibration of the indentation rig showed a linear relationship between displacement and output voltage with $R^2 = 1$ (Figure 4.19). The equipment was therefore set up correctly to generate experimental data, and displacement could accurately be derived from voltage.

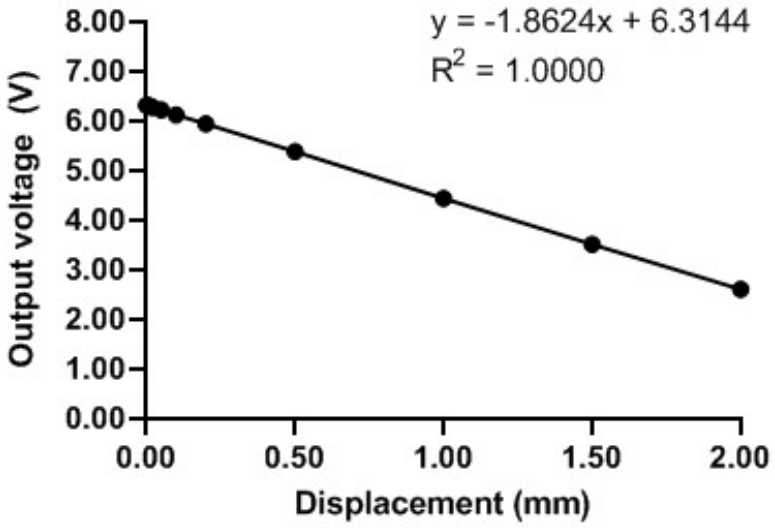

Figure 4.19: LVDT calibration. Output voltage (V) versus displacement (mm) calibration graph, determined with standard height slip gauges. Conversion factor determined from the displayed straight line equation.

4.4.5.2 Determining percentage deformation

Native and decellularised samples were subject to indentation testing as described previously (Section 4.3.5.3), the voltage over time was recorded and using the conversion factor the displacement was calculated. The percentage deformation over time traces are displayed below in Figure 4.20. All samples displayed an initial rapid deformation period, followed by a reduced gradient approaching equilibrium, and all reach equilibrium within the 1 hour time period. The results showed much more variation with the decellularised samples compared with the native controls.

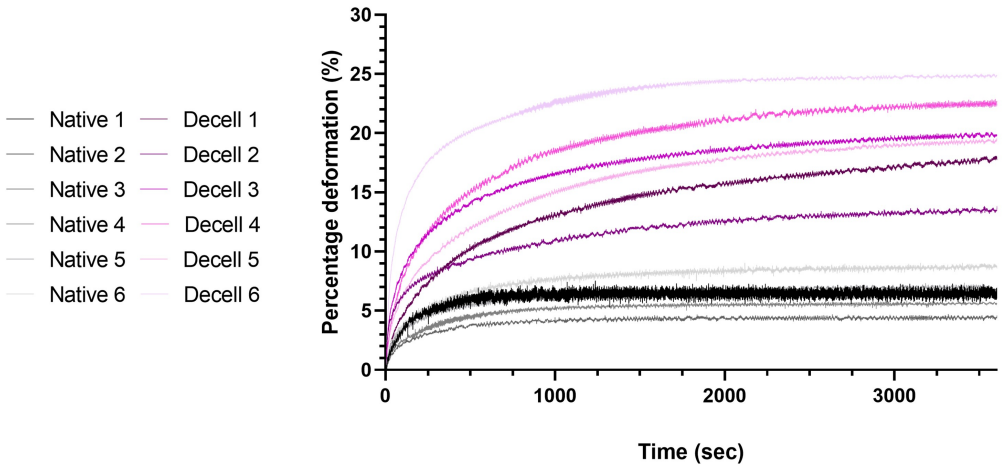

Figure 4.20: Percentage deformation profiles of native versus decellularised samples. Native (n = 6) porcine osteochondral pins and decellularised (n = 6) porcine osteochondral pins were subject to indentation testing. The percentage deformation results are displayed against time. The greyscale lines represent the native samples, whereas the coloured lines represent the decellularised samples.

The percentage deformation after 1 hour was determined, to give the maximum percentage deformation (Figure 4.21). Decellularised porcine osteochondral pins showed a significantly higher ($p < 0.001$) maximum percentage deformation when compared with the native porcine cartilage.

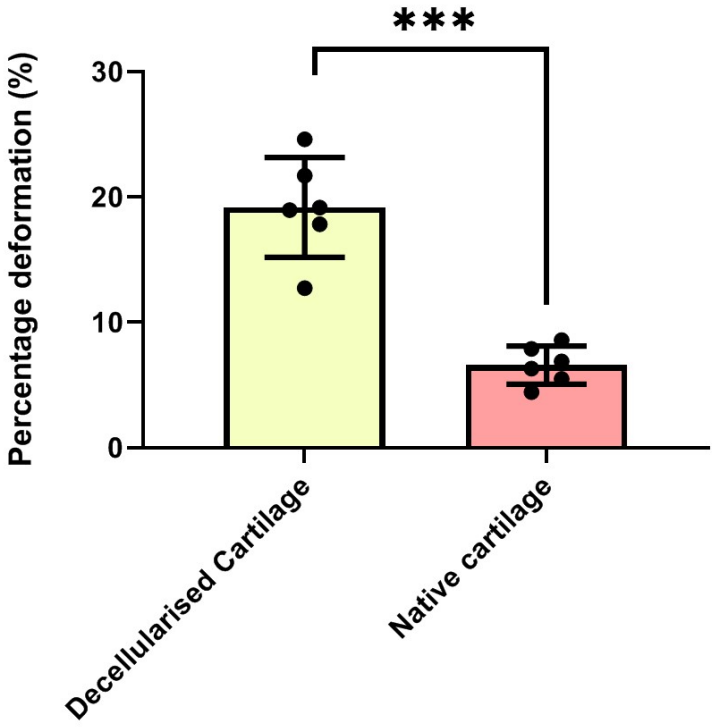

Figure 4.21: Maximum percentage deformation of native and decellularised porcine osteochondral pins. Percentage deformation values were subject to an Arc-Sin transformation, and statistical analysis was performed on the transformed data, prior to back transformation. Bars represent mean, and dots represent individual data points. Error bars = 95% C.I. An unpaired t-test was performed on the transformed data. *** = p <0.001.

Samples from the indentation test were used for subsequent GAG assays and Safranin O and Fast Green (Saf O/FG) staining to determine GAG content and distribution in each sample. From the Saf O/FG staining in (Figure 4.22A), it shows high GAG density and distribution throughout the cartilage. However, the decellularised samples showed no staining for GAGs. Furthermore, from the GAG assay (Figure 4.22B) a significant ($p < 0.0001$) reduction in GAG content is observed in the decellularised samples.

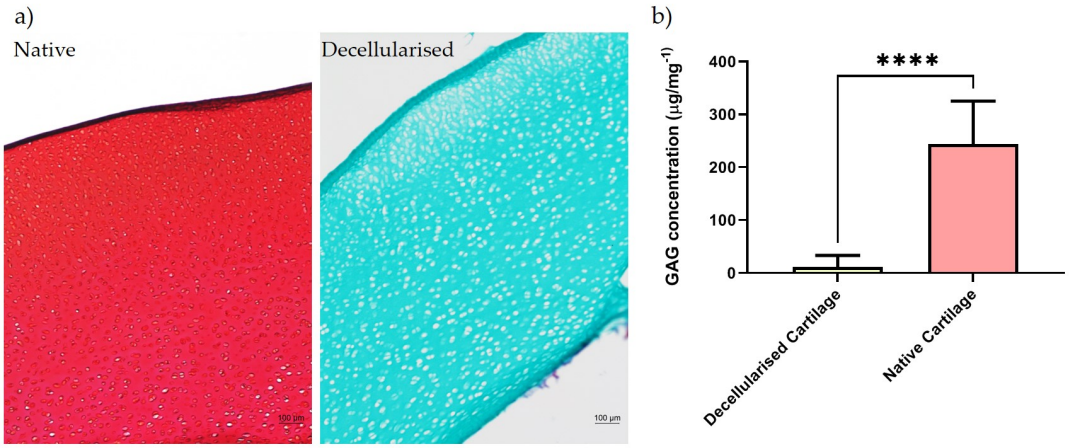

Figure 4.22: GAG content of native and decellularised porcine osteochondral scaffolds following indentation testing. Unpaired t-test performed. **** = $p < 0.0001$.

4.4.5.3 Computational determination of material properties

The equilibrium elastic modulus of decellularised cartilage was significantly lower ($p < 0.001$) than the native cartilage, with mean moduli of 0.065 MPa and 0.235 MPa respectively (Figure 4.23). The permeability results showed no significant difference between the two groups. The decellularised samples showed great variation in this parameter over an order of magnitude (2.7×10^{-15} - 5.8×10^{-14}), compared with the native samples (0.9 - 1.7×10^{-14}).

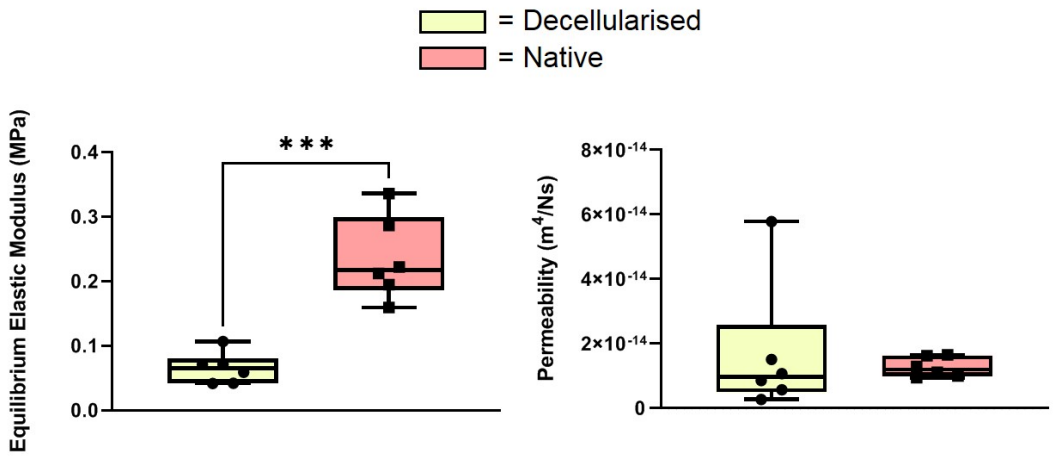

Figure 4.23: Derived material properties of decellularised osteochondral scaffolds. A) Equilibrium elastic modulus and B) Permeability from experimental native (n = 6) and decellularised (n = 6) cartilage. Box represents the interquartile range, the line represents the mean, and the 'whiskers' demonstrate the range of the results. An unpaired t-test was performed. *** = $p < 0.005$.

4.5 Discussion

4.5.1 Decellularised sheet production and assessment

The existing OC porcine decellularised scaffolds were difficult to produce and were not suitable for the treatment of larger lesions. Here, OC sheets were prepared successfully at dimensions of 20 (length) x 20 (width) x 5 mm (depth). The process of shaping these scaffolds from the femoral condyles was much more reproducible, unlike the previous method of producing plugs where in the final processing step one might irreversibly damage a scaffold due to malalignment during the coring out process. Furthermore, the existing decellularisation process was shown to be efficacious in the removal of cells and DNA from the cartilage portion of the OC sheets (Figure 4.7; Figure 4.8).

Despite the H&E and DAPI staining which showed a removal of cells from the bone portion, the DNA assay results in Figure 4.7C show that the DNA content in the bone is just above the 50 ng.mg^{-1} threshold stated by (Crapo *et al.*, 2011) at 60.5 ng.mg^{-1}. The threshold value is stated for dsDNA only, whereas the assay used measures total DNA content. Although not stated in the literature, it is likely that a sample at the 50 ng.mg^{-1} threshold of dsDNA would have a total DNA content above this threshold. The effect of xenogeneic DNA on host immune responses is widely documented (Arzi *et al.*, 2015), however, the justification behind the 50 ng.mg^{-1} threshold is not reported. Therefore, it is not known what the effect of an additional 10 ng.mg^{-1} of DNA would have over scaffold performance. In fact some commercially available decellularised grafts surpass this threshold such as GraftJacket (Wright Medical Group, USA) which is an allograft dermal matrix which has a DNA content of 134.3 ng.mg^{-1}, and has been shown to have good clinical outcomes for rotator cuff repair (Dopirak *et al.*, 2007; Johnson *et al.*, 2020).

Future work should be performed surrounding this threshold, generating experimental validation of the limit as well as tolerances and the impact of surpassing it. Furthermore, PicoGreen is an assay which measures dsDNA content and has been used to measured DNA content of biological tissue (Gilbert *et al.*, 2009). Further

confirmation of the relationship between total DNA content and dsDNA using this method could determine if the samples are truly below this value. Overall, this result was deemed acceptable due to the lack of cells shown in the histology and it's proximity to the threshold.

On closer inspection of a small region of the deep cartilage zone/subchondral bone region, a signal was detected in the DAPI staining (Figure 4.8). The signal appears morphologically different from the cells seen in the native samples. Aside from qualitative morphological assessment it is difficult to determine the identity of such remnants. The DAPI signal was very faint, indicating either autofluorescence from the tissue or collapsed pericellular matrix. Autofluorescence is clear in the decellularised bone DAPI staining, therefore it is possible for calcification in the subchondral bone region to generate similar regions of autofluorescence. Additionally, the retention of pericellular matrix components in decellularised samples is shown in the COLVI staining (Figure 4.13).

Another explanation of the weak DAPI signal may be low traces of fragmented genetic material which has not been fully removed. As shown in the DNA assay data (Figure 4.7) the level of DNA was below the threshold of the 50 ng.mg^{-1} of dry weight tissue stated by (Crapo *et al.*, 2011) for decellularised tissues. Therefore, it is difficult to anticipate the effect if any of such remnants. Furthermore, many studies suggest that due to the dense nature of the cartilage ECM, it can be considered to be immunepriviledged (Bolano and Kopta, 1991). This is a contentious issue in the field as has evidence supporting both sides of the argument (Arzi *et al.*, 2015).

4.5.2 Extracellular matrix retention

Previous studies have shown the effective decellularisation of cartilage can adversely effect the GAG content and therefore the tissues biomechanical function (Fermor *et al.*, 2015a). A significant ($p<0.0005$) reduction in GAGs was also seen in this study.

The retention/loss and location of chondroitin sulphate specifically was of interest, due to it's contribution to the compressive stiffness of cartilage. Regions of strong CS signal matches areas of GAG/Proteoglycan (PG) staining from the Safranin O and

FG staining (Figure 4.10) in both native and decellularised samples. Similarly, areas of GAG/PG loss correlated with areas of CS loss, indicating no preferential retention of CS over bulk PG/GAGs.

The labelling of CS did highlight pericellular retention of CS in the decellularised samples superficial zone. The pattern of retention in the superficial zone may be due to stronger interactions with collagen in the denser collagen-PG mesh. In a study where chondrons and chondrocytes were isolated and separated, chondrocytes alone had a positive signal for CS staining indicating direct interaction with the cell (Wang *et al.*, 2008). In the decellularised samples in the current study, CS staining was only evident in the superficial zone around the PCM borders (Figure 4.10).

Decellularisation effected collagen VI retention similarly to CS. Collagen VI was retained in the borders of the PCM, but removed from the inner-PCM (Figure 4.13). Similarly to CS, Collagen VI was retained predominantly in the superficial and upper middle zone. It is likely that removal of the chondrocytes during decellularisation, caused a removal of the immediately associated PCM molecules (Collagen VI and CS).

There is also a possibility that, as with the cells, SDS plays a role in the removal of these components, either directly through protein denaturation or indirectly through denaturing interacting proteins. SDS treatment (0.1%) has been used as a method to deplete GAGs from cartilage (Warren, 2017).

It is currently unknown whether the retention or loss of these molecules could affect the role of the PCM in protecting the chondrocytes from high mechanical loads (Statham *et al.*, 2022). For the bulk tissue properties, the GAG loss is expected to have similar effects on the mechanical properties as seen in (Fermor *et al.*, 2015a). Future aims of this project are to replenish the lost GAG content through incorporation of the SAP-GAG hydrogel. Furthermore, it has been well documented that, over time, chondrocytes immobilised on scaffolds slowly deposit GAGs (Hsu *et al.*, 2006). Investigating the implantation of decellularised scaffolds that have been recellularised with autologous chondrocytes in a rabbit defect model (Li *et al.*, 2019) have shown recovery of GAG content compared to native controls. The increased GAG content

was also accompanied by a recovery in the Young's modulus, therefore it is possible that a reduced GAG content pre-implantation could be mitigated following either a pre-implantation culture period or subsequent repopulation *in-situ*.

The reduction seen with proteoglycans/GAGs in Figures 4.10 and 4.13 following decellularisation was not observed with collagen II (Figure 4.11). Both the native and decellularised samples had intense staining throughout the tissue. The Sirius red staining under polarised light (Figure 4.12) further confirms collagen maintenance following decellularisation. This is consistent with other studies using SDS to decellularise cartilage (Kheir *et al.*, 2011; Bautista *et al.*, 2016).

As mentioned previously, repopulating scaffolds with cells could allow improve GAG content as well as integration times. An important consideration in cell seeding, is cell attachment, therefore staining was performed for fibronectin (Figure 4.14). It appears that the amount of fibronectin was reduced between the native and decellularised cartilage. However, both isotype and reagent controls have autofluorescence therefore it is difficult to make any firm conclusions. In decellularised blood vessels, fibronectin was retained at similar levels to untreated samples (Simsa *et al.*, 2019). Fibronectin is usually present at low levels in cartilage ECM (Chevalier, 1993), therefore, more sensitive methods may be required to determine differences in fibronectin such as ELISA or western blotting.

4.5.3 Sterility and cytocompatibility

Following the characterisation of the scaffolds (DNA/cellular content and ECM structure) it was then important to demonstrate their biocompatibility. Figure 4.15 confirmed the sterility of these scaffolds, through a week long incubation in nutrient broths. It was not expected that new dimensions would have any bearing over the sterility of the scaffolds. However, a concern when adapting the dimensions from a plug (8 mm diameter) to a sheet (width 2 cm) was complete removal of SDS and PAA from the matrix.

Removal of cytotoxic components was confirmed by the negative contact and extract

cytotoxicity results with both L929 and BHK cell lines, in accordance with ISO 10993-5 (*Biological evaluation of medical devices – Part 5: Tests for in vitro cytotoxicity* 2009). This confirms that the new dimension of the scaffold do not affect the efficacy of reagent washout using the existing process.

Both the sterility and contact cytotoxicity data demonstrate cytocompatibility of the scaffolds *in-vitro*. Whilst these methods are based upon ISO10993-5, it is important to note, that prior to claiming biocompatibility it would be necessary to conduct *in-vivo* biocompatibility tests. Importantly, these results give a positive indication to progress with these *in-vivo* models, such as subcutaneous implantation in xenogeneic models, to further confirm biocompatibility of the scaffolds.

Cytocompatibility of these scaffolds confirms the suitability of these scaffolds for use in later *in-vitro* recellularisation studies. Additionally, it suggests that the scaffolds could be suitable for use as a scaffold to support cell therapies.

4.5.4 Material property determination

The percentage deformation of porcine decellularised cartilage was significantly higher than the native cartilage ($p<0.001$) (Figure 4.21). This result has been shown previously in a comparison of decellularised bovine cartilage against native controls, however the load was much greater than this low load set up (Fermor *et al.*, 2015a). Furthermore, data for native and decellularised porcine cartilage demonstrates a lower equilibrium modulus for decellularised versus native parencite (Elder *et al.*, 2017). The origin of this increased deformation is likely in the GAG removal demonstrated in Figure 4.22.

The finite element modelling results appeared to support the result observed in Figure 4.21. The calculated mean equilibrium elastic modulus of decellularised porcine cartilage was 0.065 MPa, which was significantly lower ($p<0.001$) than the value for native cartilage (0.235 MPa) (Figure 4.23). These values for elastic equilibrium modulus match values reported in the literature for articular cartilage from bovine articular cartilage (Laasanen *et al.*, 2003) ($\approx$ 0.23 MPa) and (Woodfield *et al.*, 2004) (0.27 MPa). For human articular cartilage the values can range from 0.1 - 2.0 MPa

depending on the test and location of cartilage (Mow and Guo, 2002).

There is a 3.6x reduction in the equilibrium modulus of the decellularised samples compared with the native. As seen previously over the test (Figure 4.20), the decellularised samples reach equilibrium after greater displacement compared with the native samples. The equilibrium elastic modulus is dependent on water content of cartilage, the reduction of GAGs following the decellularisation process allows more volume to be occupied by fluid. Increased water content has also been shown to correlate with greater permeability, a combination of both allows greater fluid flow out of the cartilage under a defined load, greater deformation and hence a lower elastic equilibrium modulus (Mansour, 2003).

Given the above assumptions, it is unexpected that the predicted permeability is not significantly higher for the decellularised samples (1.7^{-14} m^4/Ns). The higher variation seen in the permeability data, especially for decellularised scaffolds is likely the cause of this. The modelling data together indicates a reduced GAG content and equilibrium elastic moduli, with no significant changes in permeability. The permeability values obtained for native cartilage in this study (9.4 - 16.5 x 10^{-15} m^4/Ns) compare well with unpublished data from our laboratory using an identical set up and modelling assumptions. Furthermore, the native and decellularised permeability fall in a similar region to human articular cartilage (1.13 x 10^{-15}) (Athanasiou *et al.*, 1991). Previous research comparing decellularised and native meniscus tissue saw no significant difference in predicted permeability when the Poisson's ratio was assumed to be 0. However, when an assumed Poisson's ratio of 0.1 was input, a significant increase in permeability with the decellularised menisci was observed (Abdelgaied *et al.*, 2015). It is important to note that these material properties depend on several assumptions such as equal permeability throughout the tissue and a defined water content of 80%. Furthermore, the permeability assumption is only valid for small deformations of < 10-15% of the cartilage thickness, however only 50% of the decellularised specimens meet this criteria (Figure 4.20. Whilst this is informed on previous data, accuracy could have been improved by inputting individual water content values for each sample based on weight before and after lyophilisation.

4.5.5 Conclusions

This work delivered an effective method to produce cytocompatible decellularised osteochondral scaffolds that have retained the majority of the native cartilage structure and composition. There was a loss of GAGs and therefore a reduced biomechanical stiffness. However, work in later chapters will look to mitigate this GAG loss through recellularisation and self assembling peptide + GAG delivery to the scaffolds. These scaffolds have potential for use in MACI with relevant dimensions, cytocompatibility and natural tissue composition and architecture.

Prior to this, the ability of self assembling peptidse + GAG on it's own, to support cell viability and phenotype will be evaluated, alongside the material properties.

Chapter 5

Self-assembling peptides for cell delivery

5.1 Introduction

As described previously (Section 1.9.4.3), hydrogels have received a lot of interest in the field of cartilage tissue engineering, owing to their biocompatibility and porous framework. This permits an ability to deliver cells and/or growth factors in a minimally invasive manner to cartilage lesions via injections (Slaughter *et al.*, 2009). A promising solution in the field of injectable hydrogels are self-assembling peptides (SAPs). These are peptide molecules which have been rationally designed to self-assemble into stable higher order structures under controllable physiological conditions (Barco *et al.*, 2018). These have attracted attention in the field of tissue engineering due to their ability to deliver both bioactive molecules and cells to support tissue regeneration (Moore and Hartgerink, 2017). An example of a specific system is the P11-X family of SAPs. This family of peptides contain an odd number (11) of residues, in order to drive antiparallel beta sheet formation. In terms of the amino acid structure of these peptides, they have amino acids which alternate between polar and non-polar, so to ensure stable β-sheet formation. Furthermore, the central amino acids are hydrophobic and on the same side to propagate ribbon formation. Finally, the presence of charged residues gives a trigger for self-assembling based upon protonation and deprotonation (Barco *et al.*, 2018). This family of peptides has

been investigated at the University of Leeds (Aggeli *et al.*, 1997) for cartilage and intervertebral disc tissue engineering applications. The P11-8 peptide (Figure 5.1) can support cell growth over a period of 14-days (Maude *et al.*, 2011) and also has been used alongside the GAG chondroitin sulphate (P_{11}-8/CS), in order to restore GAGs lost in early stage OA (Barco, 2017; Warren, 2017).

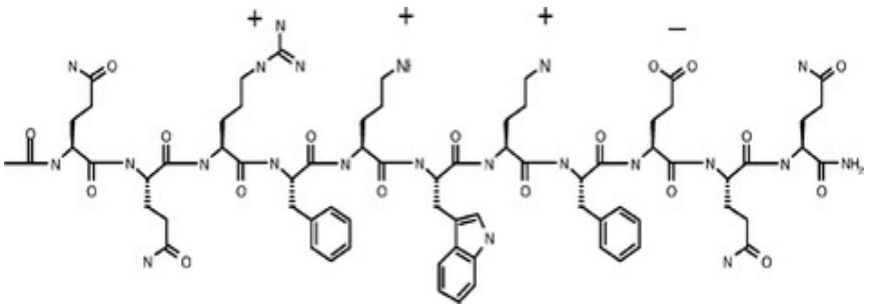

Figure 5.1: P_{11}-8 self-assembling peptide structure

.

As previously shown in Figure 4.9, a consequence of the decellularisation process is a removal of GAGs from the cartilage. Therefore, the P_{11}-8/CS system described by (Barco *et al.*, 2018) may be an effective solution to replenishing the GAGs lost in scaffold decellularisation. Furthermore, previous work has established the capability of the P_{11}-8/CS peptide to support cell growth (Maude *et al.*, 2011). Therefore, if the hydrogel could be used to encapsulate cells within the decellularised matrix, this would overcome the limitations of ACI in terms of cell retention in the scaffold and lesion site. Finally, from a translational perspective, it is beneficial to be able to deliver both elements in a single step procedure.

5.2 Aims and Objectives

5.2.1 Aims

(i) Adapt the exisiting self-assembly process to encapsulate cells

(ii) Develop assays to assess cell viability within P_{11}-8/CS

(iii) Determine the potential of P_{11}-8/CS to support cell growth, viability, and maintenance of the chondrogenic phenotype

5.2.2 Objectives

(i) Adapt the existing process for the production of acellular P_{11}-8/CS production to include cells and cell culture media, whilst still making a gel of comparable integrity and reproducible quality as the acellular gels.

(ii) Validate ATPlite, AlamarBlue and LIVE/DEAD cell viability assays with P_{11}-8/CS encapsulated cell cultures

(iii) Assess cell viability and quality of gel formation using new gel preparation method

(iv) Determine cell viability within the gel over time (14-days)

(v) Use RT-qPCR to probe chondrogenic genes from primary porcine chondrocytes encapsulated in P_{11}-8/CS

5.3 Materials and Methods

5.3.1 Encapsulation of cells within the P_{11}-8/CS system

5.3.1.1 Iteration 1

The P11-8 peptide (Amino acid sequence: QQRFOWOFEQQ) was synthesised and provided by CS Bio (USA) (Purity: 0.9, Counterion: TFA), and the chondroitin sulphate (54,000 $gmol^{-1}$) was obtained from shark cartilage and provided by Sigma Aldrich (USA). Prior to gel preparation cells were cultured to confluency as described in (cell culture methods). For 10mg.mL^{-}1 gel at a 1:1 ratio of P_{11}-8/CS, 10mg of CS was weighed out to be eventually combined with 11mg P11-8, to account for peptide purity. For other concentrations the same ratio is followed, and the peptide ammount is always multiplied by 1.1X to account for the peptide purity. However, prior to combining the two components, a cell suspension of the desired concentration was produced.

To make 6 x 100 µL gels (Figure 5.2), 1mL of stock solution was produced to account for any pre-gelation. Firstly, 500 µL of cell suspension was introduced to resuspend

the CS component. Following this 500 µL was introduced to the P11-8 component to resuspend the powder. Then, the CS-cell suspension was added to the P11-8-cell suspension and mixed briefly, before aliquoting 6 x 100 µL gels into a 96-well plate. These were left to equilibrate for 3 hours, prior to further addition of 100 µL of cell culture media for long-term culture.

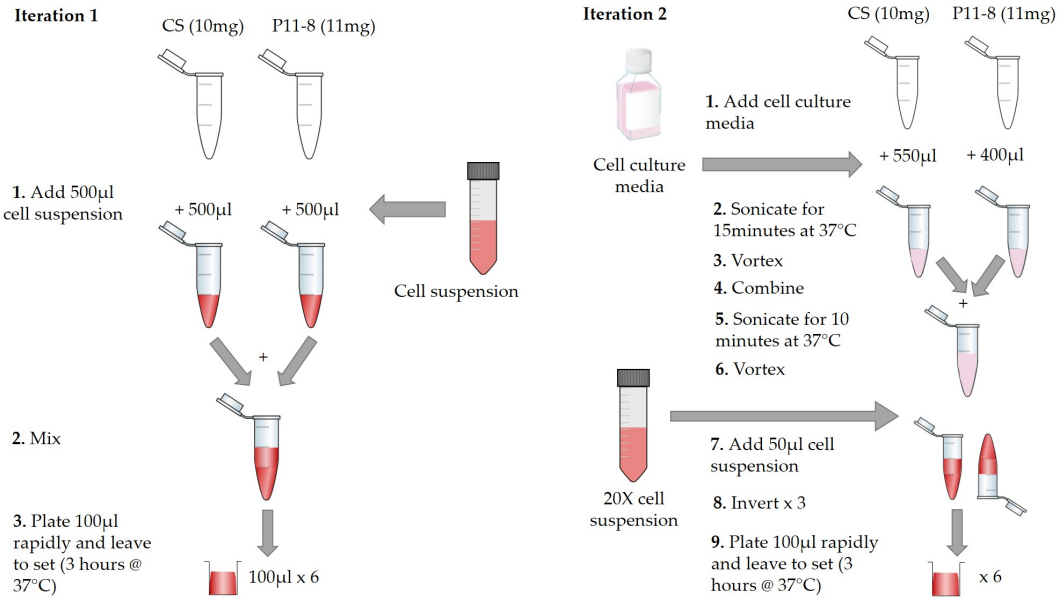

Figure 5.2: Development of the cell encapsulation technique. The graphic demonstrates the two iterations described in Iterations 1 and 2

5.3.1.2 Iteration 2

Due to complications with early gelation, and lack of reproducibility, an alternative preparation protocol was developed. Both iterations are shown above in Figure 5.2. The aim was still to produce 1 mL of a 10mg.mL^{-}1 stock solution of P_{11}-8/CS-Cells. The quantities of each component remained consistent. However, the CS component was resuspended in 400 µL of warm (37°C) cell culture media, and left to sonicate for 10minutes at 37°C. Simultaneously, the P11-8 was resuspended in 550 µL of cell culture media, and was also left to sonicate at 37°C.

Following this, the P_{11}-8 was vortexed for 30 seconds to fully resuspend the peptide and break up any gelated material, and the CS was vortexed for 5 seconds. These two solutions were combined to make 950 µL of P_{11}-8/CS in cell culture media, and sonicated for a further 10 minutes. Whilst sonicating, the cells were detached

from the T75 flask and a cell suspension 20X the final desired cell density was produced. Following the sonication, the P_{11}-8/CS solution was vortexed and 50 µL of cell suspension was added to make 1 mL in total. Working quickly, the solution was inverted gently 3 times and 6 x 100 µL gels were plated into a 96-well plate and left to set for 3 hours prior to addition of 100 µL of cell culture media. Although the process was optimised for P_{11}-8 concentrations of 10 mg.mL^{-1}, as a result of gel dissolution during initial culture experiments, the peptide concentration was increased to 20 mg.mL^{-1} to produce stiffer gels capable of staying intact during media changes.

For clarity, unless stated otherwise Iteration 2 will be used for the rest of this work.

5.3.1.3 Previous P_{11}-8/CS preparation process: Lyophilised method

In order to compare the peptide preparation process developed in this work (Iteration 2), comparisons were made with the previous method for acellular P_{11}-8/CS preparation (Warren, 2017). For brevity, this will be referred to as the lyophilised method.

For the lyophilised method, peptide (22 mg) and chondroitin (20 mg) were separately weighed in eppendorf in the same ratio as in the previous method. The peptide and chondroitin sulphate were resuspended in 500 µL of 1M sodium acetate buffer (pH = 4), and vortexed for 30 seconds each, vials were combined and vortexed for 30 seconds, followed by sonication for 5 minutes at 37 °C. The vials were placed in the -80 °C freezer for 1 hour, and then lyophilised overnight in the freeze drier. The following day, the freeze dried suspension wass rehydrated with 950 µL of cell culture media, and vortexed for 30 seconds. Immediately after vortexing, 50 µL of cell suspension at 20 times desired final cells.mL^{-}1 was added and gently resuspended throughout the mixture, and 100 µL cell encapsulated gels were dispensed into a 96-well plate. Gels were left to equilibrate for 3 hours at 37 °C, prior to addition of a further 100 µL of cell culture media.

5.3.1.4 Preparation of fully hydrated, cell seeded collagen hydrogels for use as 3D controls

As a positive control for 3D cell culture and encapsulation commercial rat tail collagen 1 (Lonza, CH) was used, following manufacturers instructions. Briefly, gels were used at a composition ratio of: 80% (v/v) rat tail type I collagen, 10% (v/v) MEM, 5.8% (v/v) neutralisation solution and 4.2% (v/v) of cells resuspended at appropriate concentration in media.

Prior to mixing the individual reagents inside the Class II Safety Cabinet, they were kept cool by placing them in an ice box, this slowed down the gelation process. This process is very time-dependent as with the P_{11}-8/CS system, therefore an emphasis was made to work quickly.

The collagen was added first to a 30 mL universal tube, followed by the MEM. The universal was gently swirled in order to mix the two solutions, care was taken not to introduce any air bubbles that may disrupt the gel formation. Following this, the collagen was neutralised with the provided neutralisation solution, the mixture then changed colour from yellow to a dark peach colour. The cells were resuspended in the media swiftly, and swirled in order to evenly distribute the cells throughout the gel. The solution was then distributed into 100 µL aliquots within the 96-well plate, and left for 10 minutes to set prior to adding 100 µL cell culture media.

5.3.2 Cell Viability Assessment

5.3.2.1 Optimisation of Alamar Blue Incubation Times

For the cell viability measurements alamarBlue (Biorad, USA) reagent was used. Prior to use in subsequent experiments it was necessary to determine the optimum alamarBlue incubation times for 100 µL 3D hydrogels. Collagen hydrogels were used for this optimisation, due to the reproducibility of the method compared to the P_{11}-8/CS at the time. Briefly, following encapsulation of cells in the collagen hydrogels at 100,000, 200,000 and 400,000 cells/gel, gels were left to set for 10 minutes as described previously. Following this, cell culture media was added, followed by the

addition of alamarBlue at a volume 10% of that of the entire well (200 µL). Four 96-well plates were set up for incubation times of 0, 2, 4 and 6 hours. After the desired incubation time, 100 µL of media with alamarBlue was removed from the well into a new 96-well plate. The absorbance was subsequently measured at 570 and 600nm.

In order to calculate the percentage of alamarBlue reduced the equation below was used:

$$\frac{(O2xA1) - (O1 - A2)}{(R1xN2) - (R2xN1)} \times 100$$

Where O1 = molar extinction coefficient (E) of oxidized alamarBlue (Blue) at 570 nm* O2= E of oxidized alamarBlue at 600 nm, R1 = E of reduced alamarBlue (Red) at 570 nm, R2= E of reduced alamarBlue at 600 nm, A1 = absorbance of test wells at 570 nm, A2 = absorbance of test wells at 600 nm, N1 = absorbance of negative control well (media plus alamarBlue but no cells) at 570 nm, N2 = absorbance of negative control well (media plus alamarBlue but no cells) at 600 nm.

5.3.2.2 alamarBlue Timecourse of encapsulated L929s and C20A4 cells

L929 cells were encapsulated in P_{11}-8/CS at a density of 4 x 10^5 cells/cm^2. Collagen hydrogels were seeded at the same density, one group spiked with SDS (250 µg.mL^{-1}) (negative cytocompatibility control) and one without (positive cytocompatibility control). Media was changed every 3 days. At each timepoint (Day 1, 7 and 14) there were two 96-well plates, one for alamarBlue measurements and the other had a optical bottom (Starstedt, UK) for Live/Dead imaging. After the addition of 10% of alamarBlue to each well, it was left to incubate for 6 hours as previously optimised. Following this 100 µL was removed and absorbance measured at 570/600nm.

A identical test set up was employed for the assessment of C20A4s, following this study.

5.3.2.3 Live/Dead Assay of encapsulated L929s and C20A4 cells

As mentioned above, at each timepoint there was also a plate for Live/Dead (Thermofisher, USA) assessment of viability. 1 hour before the end of the alamarBlue assay the media on the gels was replaced with a solution containing media as well as calcein AM and ethidium homodimer (1 µL of calcein and 2 µL of ethidium in 4mL cell culture media). The staining solution was incubated with the gels on a shaker for 1 hour at 37 °C. Following this, the solution was removed as 3 x 5 minute PBS washes were performed. After the last wash the plate was visualised on a LSM700 confocal laser scanning microscope at 20X magnification.

5.3.3 Gene expression analysis

5.3.3.1 Extraction of chondrocytes from viable porcine cartilage

Viable porcine legs were obtained from J Penny & Sons on the day of slaughter, and transferred into a Class II cabinet. The procedure for dissection was identical to that detailed in Section 2.2.2, except, this was conducted in a sterile manner which entailed several adjustments. A large piece of foil was sterilised alongside the dissection equipment as described in Section 2.2.1.2. The sterile aluminium foil was used to cover the surface inside the safety cabinet, and the porcine leg was placed on this sterile surface. Throughout this process sterile gloves were worn.

Iodine was applied to the lateral side of the knee, and the skin and soft tissue were cut using a sterile scalpel blade to expose the femoral condyles. At this step, using a scalpel, as much articular cartilage as possible was removed from the condyle and placed into a sterile bijou. Following this, other lab members were notified to ensure use of the animal tissue was maximised.

In a clean Class II cabinet, cartilage was washed with PBS until the PBS ran clear. The tissue was subsequently minced into small sections to increase the surface area for digestion and placed into another sterile bijou. The tissue was weighed, in order to calculate the ammount of collagenase to add. 5 mL collagenase (Sigma-Aldrich, USA) (600 units) aliquots were made up previously in DMEM. For each gram of

cartilage, one 5 mL aliquot of collagenase was thawed and combined together in a 50 mL falcon. The falcon was attached horizontally to a shaking platform in a 37 °C incubator O/N.

The following day, the digest was ran through a 100 µm cell strainer (Greiner Bio One, UK) and placed on top of a 50 mL falcon tube. Effort was made to keep large undigested material in the digest tube. The remaining tissue was vigorously washed with PBS to free additional cells, and the wash fluid was also passed through the filter. This process was repeated twice until the PBS ran clear. Finally, PBS was run through the filter to wash any remaining cells attached to the filter.

Following this, the sample was centrifuged at 250 rpm, and the material transferred to a new falcon to remove debris and fat. This was then centrifuged at 1400 RPM for 6 minutes. The supernatant was removed and the pellet was resuspended in 10 mL of supplemented high glucose DMEM (10% FBS, P/S, L-G). The cells were subsequently cultured in a T-75 flask until 90% confluent, with media changes every 3-days. Confluent cells were passaged up to P3 with cell aliquots cryopreserved throughout the process for use in later studies.

5.3.3.2 Culture set up

Porcine chondrocytes were expanded under chondrogenic conditions in chondrogenic media (2 mM L-Glutamine, 50 µg.mL^{-1} P/S, 0.1% ITS, 50 µg.mL^{-1} vitamin C, 0.1 µmol dexamethasone, 1mM sodium pyruvate) with 5 ng.mL^{-}1 FGF-2 (Peprotech, UK). Briefly, cells were seeded at an initial density of 25,000 cells/cm^2, at confluence flasks were left a further 4 days before passaging.

Once sufficient cell numbers were obtained, cells were transferred to 10 cm^2 petri dish coated with 2% agarose to initiate aggregate culture. 15 million porcine chondrocytes were added to each dish in a total volume of 15 mL. The dishes were left overnight on orbital shakers at 60 RPM at 37 °C and 5% CO_2, after which the dishes were left to culture statically in chondrogenic media with 10 ng.mL^{-}1 TGF-beta (Peprotech, UK) for 6 days.

Following the aggregate culture, aggregates were aspirated and centrifuged at 180

RCF for 10 minutes to remove culture medium. Aggregates were disassociated with 0.25% trypsin-EDTA for 20 minutes. The trypsin was removed and aggregates were further disassociated with treatment of 1000 units of collagenase for 90 minutes. The resulting suspension was passed through a 70 µm cell strainer (Greiner Bio-One, UK).

The cell suspension was concentrated in 50 µL to give a final concentration of 400,000 cells/gel.

5.3.3.3 RNA extraction

At each timepoint, RNA was extracted for use in qPCR. For monolayer cultures, 1 mL of TRIZOL (4°C) was added to each petri dish, and a cell scraper was used thoroughly to detach cells. The suspension was collected into a micro centrifuge tube for subsequent extraction.

The cell laden hydrogels were triturated using a p100 pipette and the plate was placed onto microplate shaker for 5 minutes and then the gels were transferred into a 10 mL universal and vigorously resuspended using warm cell culture media. Following this, 200 µL of media was added to each well, and placed on microplate shaker for a further 5 minutes and the resulting solution was added to the universal. This extra step was used to collect any further cells to enhance downstream RNA yield. The cell/gel suspension was then centrifuged at 150 RCF for 10 minutes, and the supernatant was gently removed as to not disturb the pellet. The resulting cell/gel pellet was resuspended in 1 mL of cold TRIZOL and vortexed for 30 seconds to break up cells.

Both monolayer cells and gel encapsulated cells were incubated in TRIZOL for 10 minutes. After the incubation, 200 µL of chloroform was added to each tube, and the tubes were shook by hand for 30 seconds and then incubated on ice for 2 minutes. The samples were then centrifuged for 15 minutes at 4 °C, and the clear aqueous portion was transferred into a fresh 1.5 mL micro-centrifuge tube. An equal volume of TRIZOL was added ($\approx$ 700 µL) and the sample was incubated on ice for 30 minutes. Following this, 200 µL of chloroform was added, shaken by hand and incubated on

ice for 2 minutes. The samples were centrifuged at 12000 g for 15 minutes at 4 °C.

The aqueous portion again was removed and transferred to a fresh micro-centrifuge tube, and 500 µL of isopropanol was added, mixed in by inverting. The samples were then incubated on ice for 30 minutes, followed by centrifugation for 30 minutes at 12000 RCF at 4 °C. The supernatant was removed, with care taken not to disturb the pellet. In order to remove contaminants from the TRIZOL extraction the pellet was washed with 75% ethanol, by carefully adding 1 mL followed by centrifugation at 7500 RCF for 5 minutes. The ethanol was removed carefully, and the wash step was repeated.

The pellet was then resuspended in 50 µL of nuclease free water, and then incubated in Turbo DNAase (ThermoFisher) for 30 minutes at 37 °C to remove any DNA in the sample. The DNAase treated RNA was then purified using an RNA clean-up column (New England Biolabs, USA), as per the manufacturers instructions. The resultant purified RNA was tested on the nanodrop for purity and RNA yield. In each 20 µL elution, a minimum concentration of 30 ng/ul was required, as well as A260/280 and A260/230 ratios above 1.8. RNA was stored at -20 °C until required for reverse transcription.

5.3.3.4 Reverse transcription

RNA was thawed on ice, whilst a cDNA synthesis mastermix was formulated as below (Table 5.1).

Table 5.1: Mastermix formulation for cDNA synthesis

Reagent	Volume	Concentration
10x Buffer RT	2 µL	1x
dNTP mix	2 µL	0.5 mM
RNase inhibitor (10U/µL)	1 µL	10 units per reaction
Random primer	1 µL	5 µmol M
Anchored oligo dT primer	1 µL	1 µmol M
Omniscript reverse transcriptase	1 µL	4 units per reaction
Mastermix total volume	7.2 µL	
Template	12.8 µL	50 ng to 2 µg
Final volume	20 µL	

To a 0.2 mL PCR tube, 7.2 µL of master mix was added. The volume of RNA template to add was calculated to synthesise 500 ng of cDNA. Depending on the concentration of the RNA template and therefore volume added, an appropriate volume of water was added to the PCR tube make the total volume to 20 µL. The RNA template was added, and the samples were briefly vortexed for 5 seconds. The samples were collected at the bottom of the tube via a brief micro-centrifugation, then were placed in PCR thermocycler which was run for 60 minutes at 37 °C (lid temperature 50 °C). Following the synthesis, the cDNA was stored at -20 °C until required.

5.3.3.5 Quantitative PCR

A suite of primers was chosen to investigate the chondrogenic response of chondrocytes within the P_{11}-8/CS hydrogels (Table 5.2). Cartilage oligomeric protein (COMP) was chosen as a general marker of chondrogenesis. Aggrecan was selected as indicator of the PG deposition response to encapsulation. Collagen I (COL1A2) and II (COL2A1) were chosen to assess the quality of collagen expression (favouring fibro/hyaline cartilage formation). Two reference gene's were chosen for improved

reliability and these were β-actin (ACTB) and Peptidylprolyl Isomerase A (PPIA). The sequences (forward and reverse primers) as well as the optimal concentration are described below in Table 5.2, and were designed and optimised previously by Natalie Fox (iMBE).

Table 5.2: Primer sequences and concentrations.

Gene of interest	**Forward Primer**	**Reverse Primer**	**Primer concentration (nM)**
ACAN	CTT CTG CTT CCG AGG TGT CTC	GCT GCG ACT TCT GTC GTC TC	500 nM
ACTB	CTC CTT CCT GGG CAT GGA ATC	ATC TTG ATC TTC ATC GTG CTG G	250 nM
COL1A2	CGG CAA AGT TGG AGG TAC TG	ATC TCC AGT TGG GCC CTT TC	250nM
COL2A1	CAG GAT GGG CAG AGG TAT AAT G	TCC TTT CTG TCC CTT TGG TC	166nM
COMP	CAA GGC CAA CAACAA GCA GGT TTG	CCC ACG GTA TTG ACG CAT AC	250nM
PPIA	GTC TCC TTC GAG CTG TTT GC	ACC ACC CTG GCA CAT AAA TCC	500nM

Depending on the concentration of the primers, a master mix was formulated as described in Table 5.3. Each sample (n = 3 biological repeats) was run in triplicate, and due to space in the 96-well plate, one plate was run for each gene, and each plate had every sample on it. Therefore, it was essential to make sufficient master mix for 90x reactions.

Table 5.3: Primer concentration specific mastermix formulation for 90x reactions.

Primer concentration (nM)	**166 nM**	**250 nM**	**500 nM**
Primer F (50 µmol M	7.47 µL	11.25 µL	22.5 µL
Primer R (50 µmol	7.47 µL	11.25 µL	22.5 µL
Water	1020.06 µL	1012.5 µL	990 µL
Sybr Green	1125 µL	1125 µL	1125 µL

The mastermix was briefly vortexed and microcentrifuged prior to adding 24 µL to each well of the 96-well PCR plate. Subsequently, 1 µL of cDNA template was added, and the plates were centrifuged to collect the sample at the base of the well. Optical lids were attached and the plate was loaded into the qPCR machine (Mx 3000P, Stratagene). The machine was set up so that all wells were scanned for SYBR green, with ROX as the reference dye. The thermal profile was set up as below:

1. Cycle 1: (x1)
    - 5 minutes - 95 °C
2. Cycle 2: (x40)
    - 10 seconds - 95 °C
    - 30 seconds - 60 °C
    - 60 seconds - 95 °C
3. Cycle 3: (x1)
    - 30 seconds - 60 °C
    - 30 seconds - 95 °C

Following completion of the cycle, the cycle threshold (CT) values were exported and the dissociation curves were examined to ensure correct and specific primer melting points (Tm).

5.3.3.6 Quantitative PCR Analysis - delta delta CT method

Gene expression was determined using the delta delta CT method ($\Delta\Delta CT$), whereby relative fold expression = $2^{-\Delta\Delta CT}$. $\Delta\Delta CT$ was calculated as: Δ**CT Day** x (CTref mean - CTgene of interest (GOI)) - Δ**CT Day 0**. As two reference genes were used, the CT values of PPIA and ACTB were averaged. The data was represented as a relative fold change compared to the Day 0 control for both the peptide encapsulated cells and the monolayer.

For statistical analysis, unpaired T-tests were performed on the ΔCT data, as it is not appropriate to perform on the relative fold expression $2^{-\Delta\Delta CT}$. For graphical purposes however, $2^{-\Delta\Delta CT}$ data was plotted.

5.3.4 Rheology

Hydrogels, by definition, are material compositions which form suspensions in water. This makes investigation of material bulk properties difficult. However, rheology can be used to measure the contribution of both the solid and liquid component, separately and together, towards the hydrogel material properties. The properties of the solid component are reflected in the storage/elastic modulus (G'), and the loss moduls (G") reflects the properties of the fluid component. These values are linked together by the phase angle (δ), which defines whether overall the material has more "solid-like" properties (lower phase angle) or "fluid-like" properties (higher phase angle). Rheological testing was performed in this study to assess the G' and G" of P_{11}-8/CS gels, as well as the phase angle, resulting from the process developed in these studies versus the previous (lyophilised) method.

5.3.4.1 Sample preparation

Due to the encapsulation of cells, gels were previously left for 3 hours prior to addition of cell culture medium. However, previous acellular P_{11}/CS gel preparation methods incorporate a 24 hour equilibration period, to allow for improved gel stiffness. As the intention of incorporating P_{11}-8/CS in the decellularised composite scaffold is to improve the resistance to deformation under compression, it was of

interest to investigate the effect of preparation methods incorporating cell culture medium (Section 5.3.1.2) on stiffness of the gels. Due to restrictions surrounding using of samples containing biological material on the rheometer, all gels were prepared without cells.

The stiffness of gels formulated using three different preparation methods were compared. The first group contained gels (20 mg.mL^{-}1) formulated using the Iteration 2 method described in Section 5.3.1.2, and was referred to as '3 hour equilibration'. This was compared with a '24 hour equilibration' group, which used the same protocol, except with a 24 hour incubation period at 37 °C. Gels were made at a volume of 800 µL.

The rheological properties of these gels were compared to a previously optimised method for acellular gel preparation. P_{11}-8 and chondroitin sulphate were resuspended in 1 M sodium acetate buffer (pH = 4) (20 mg.mL^{-}1), vortexed for 30 seconds, combined and sonicated for 5 minutes at 37 °C. Following this samples were frozen for 1 hour at -80 °C. The frozen monomeric P_{11}-8/CS solutions were lyophilised overnight. The following day the lyophilised P_{11}-8/CS was resuspended in 130 mM (Na+/K+/Cl-) solution at pH = 7.6), and the gels were left to equilibrate for 24 hours at room temperature.

5.3.4.2 Rheometer set up

The rheological assessment was carried out on a Malvern Kinexus Rheometer (Figure 5.3), using the rSpace for Kinexus software. The rheometer was set up with a plate-plate geometry of diameter 25 mm and gap height of 0.03 mm with 200 µL sample required per test. Temperature was maintained at 37 °C and a solvent trap was used to minimize evaporation of the peptide samples. Loaded samples were left for 15 min to equilibrate before testing.

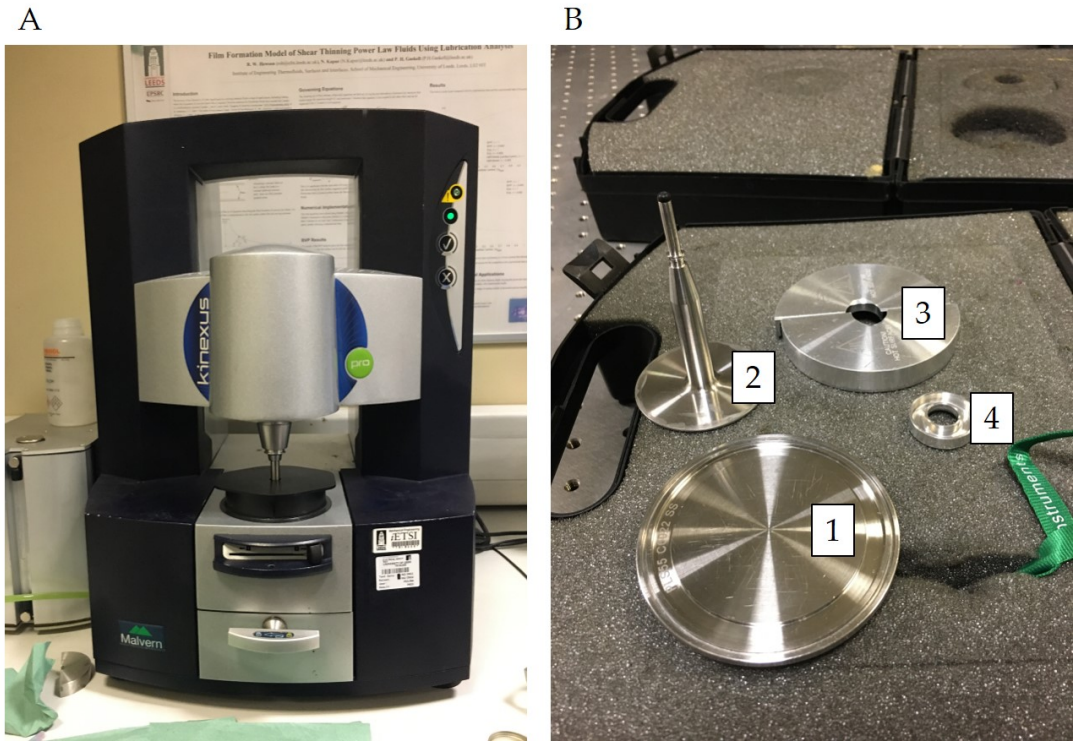

Figure 5.3: Rheometer set up. A) Malvern Kinexus Rheometer set up for test. B) Test components 1) Sample plate with solvent trap 2) 25 mm compression plate 3) Heat trap 4) Solvent trap for compression plate.

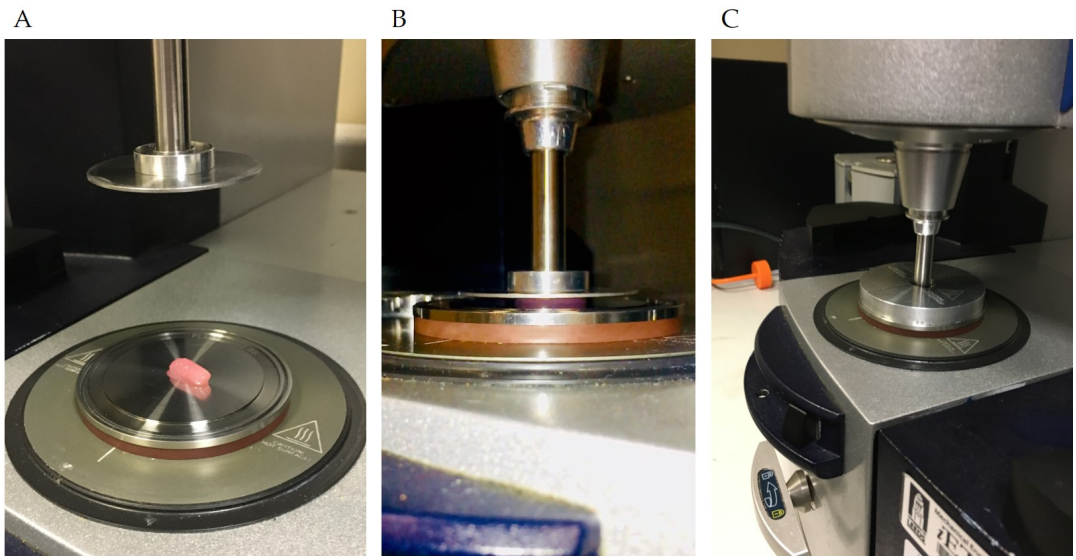

Figure 5.4: Rheology test. A) 200 µL sample on plate, pre-compression to correct gap height B) Compressing to correct gap height C) Test configuration.

5.3.4.3 Amplitude sweep

Prior to performing the frequency sweep it was necessary to determine the linear viscoelastic region (LVER) of the samples. Two amplitude sweeps were performed,

using a range of shear strains from 0.01-100% , at either 1 or 20 Hz. A strain value (0.6%) where both the G′ and G″ were found in the LVER for all three groups was chosen as shown in Figures 5.5 and 5.6.

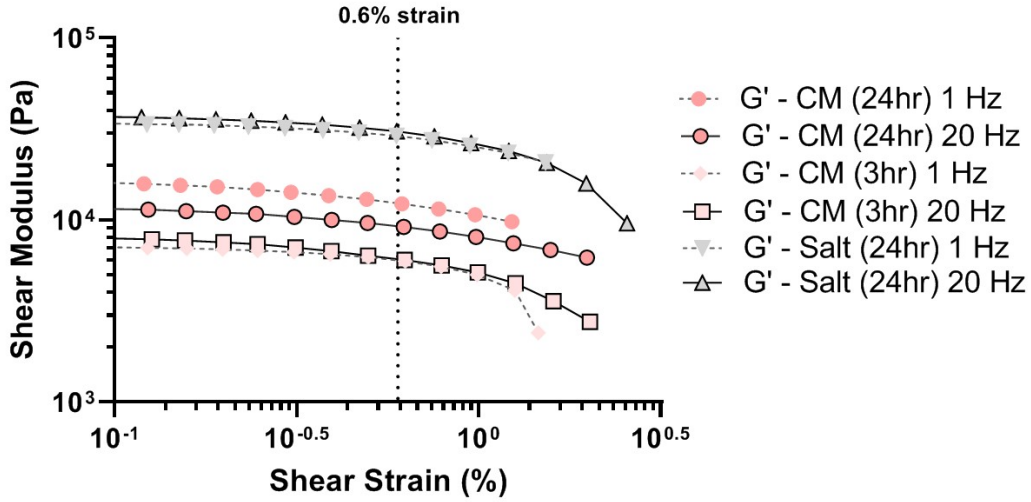

Figure 5.5: G′ data from a strain amplitude sweep. Test was performed at 1 and 20 HZ for the P_{11}-8/CS resuspended in salt solution (24 hour equilibration), or in culture medium (CM) (3 and 24 hour equilibration).

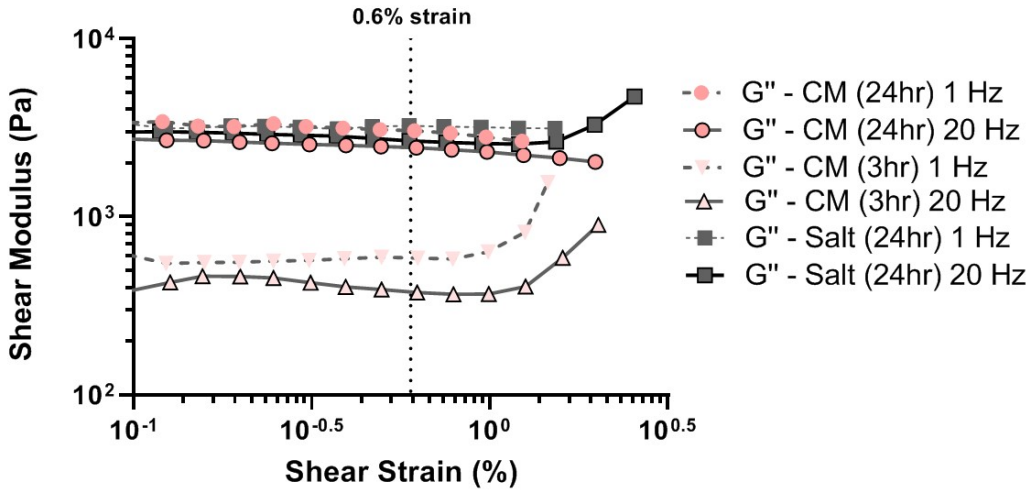

Figure 5.6: G″ data from a strain amplitude sweep. Test was performed at 1 and 20 HZ for the P_{11}-8/CS resuspended in salt solution (24 hour equilibration), or in culture medium (CM) (3 and 24 hour equilibration).

5.3.4.4 Frequency sweep

Once the strain of 0.6% was chosen, 200 µL of sample was pipetted onto the plate, and the Rheometer was set to the desired gap of 0.03 mm. The sample was then left

to equilibrate for 15 minutes as described previously. Then a frequency sweep was carried out, at 0.6% strain, over a range of oscillation frequencies (1 - 20 Hz). The average G', G" and phase angle across all frequencies was recorded and averaged.

5.3.5 Transmission electron microscopy

To assess the fibril formation and interconnectivity in different preparations of P_{11}-8/CS, transmission electron microscopy (TEM) was used. This technique allows high resolution imaging at high magnification. TEM was performed on a JEOL 1400 electron microscope. Hexagonal copper electron microscope (EM) grids (400 mesh) were pre-coated with a carbon film from mica sheets prepared in house. Each grid was placed with the carbon side in contact with each peptide for 1 minute, then any excess peptide was blotted on filter paper. The grids were then negatively stained with aqueous 2% (w/w) uranyl acetate for 20 seconds, and the excess was blotted on filter paper. The grids were then left to dry for 24 hours, before imaging with the TEM operating at 80 kV. Images were taken at 12,000 and 40,000x magnification in order to capture bulk and fibril structure.

5.4 Results

5.4.1 P_{11}-8/CS gel preparation methods

Upon confirming decellularisation and cytocompatibility of the decellularised scaffolds, the next stage was to develop the P_{11}-8/CS cell encapsulation device. In order to function as a scaffold come cell-delivery devices, both rheological properties and ability to support cell survival and growth are essential.

5.4.1.1 Gelation

Prior to determining cell viability within the hydrogel, it was first necessary to optimise the encapsulation technique to produce consistent cell seeded hydrogels. As described in Figure 5.2, the initial method (Iteration 1) produced inconsistent gels due to inappropriate mixing of the two solutions as well as premature self-assembly

within the eppendorf prior to plating the gels. In the acellular preparation of these gels, there is vigorous vortexing to allow consistent mixing of the P_{11}-8 and CS components. However, due to the addition of cells early in the preparation process this was not possible due to concerns surrounding the effects on cell viability. Therefore, in Iteration 2 (Figure 5.2), in place of cell suspension, the powders were initially resuspended in cell culture media alone. Furthermore, greater volumes of cell culture media were added to P_{11}-8 to reduce the critical gelation concentration (C*) of the peptide, allowing for longer working times. As both components were resuspended in media alone it was possible to vortex the individual components, and subject each to sonication at 37°C for 15 minutes, to increase the working time. These were the combined, vortexed and sonicated for a further 10 minutes. After this time the gel solution had not assembled and was manipulatable. The cells were then added in a small volume of 50 µL, which was 20X the desired final cell density, and inverted 3 times to evenly distribute the cells. As depicted in Figure 5.7, the P_{11}-8/CS-Cell composite self-assembled. The lack of a meniscus on the surface of the inverted gel, further proves assembly over water tension holding the gel in place. This approach was consistent and reproducible, and was used for the remainder of the project.

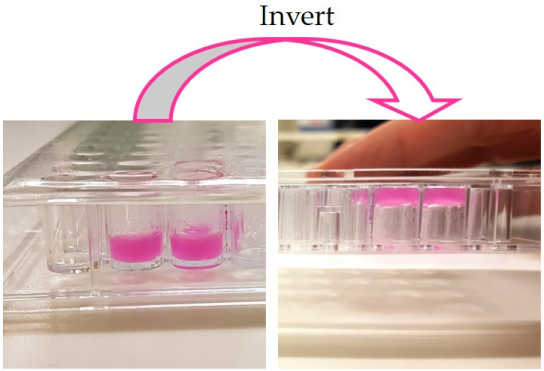

Figure 5.7: Gelation of the P_{11}-8/CS cell encapsulation device with the improved preparation iteration

5.4.2 Rheology

Whilst ability for self-assembly in culture medium is an encouraging sign, the effect of cell culture media on the peptide rheological properties has not been investigated. P_{11}-8/CS was reconstituted in cell culture media (Iteration 2) and left for either 3 or

24 hours to equilibrate. These gels were compared to the method used for acellular gel production, which involved re-suspending the peptide in a 130mM salt solution which simulates interstitial fluid salt concentration.

Comparing the elastic component (G'), both the salt and DMEM (24 hr) gels showed a significantly stiffer G' than the 3 hr DMEM samples (Figure 5.8). The G' of the 24 hr DMEM samples was slightly higher than the salt solution samples, however, this difference was not significant. In terms of the viscous component (G") the salt solution samples have the highest modulus, followed by the DMEM 24 hr, and the DMEM 3 hr. However, there was no significant difference between the three groups.

As well as the differences seen in the G'/G", there are significant changes in the phase angle which provide interesting insight into the differences in the behaviour of the two hydrogel preparations. The phase angle of the salt solution samples was significantly higher than both DMEM samples, which both had a similar phase angle. This indicates that the hydrogels prepared with DMEM exhibit more solid/elastic-like behaviour, whereas the gels prepared in the salt solution exhibit more liquid-like behaviour under this stress.

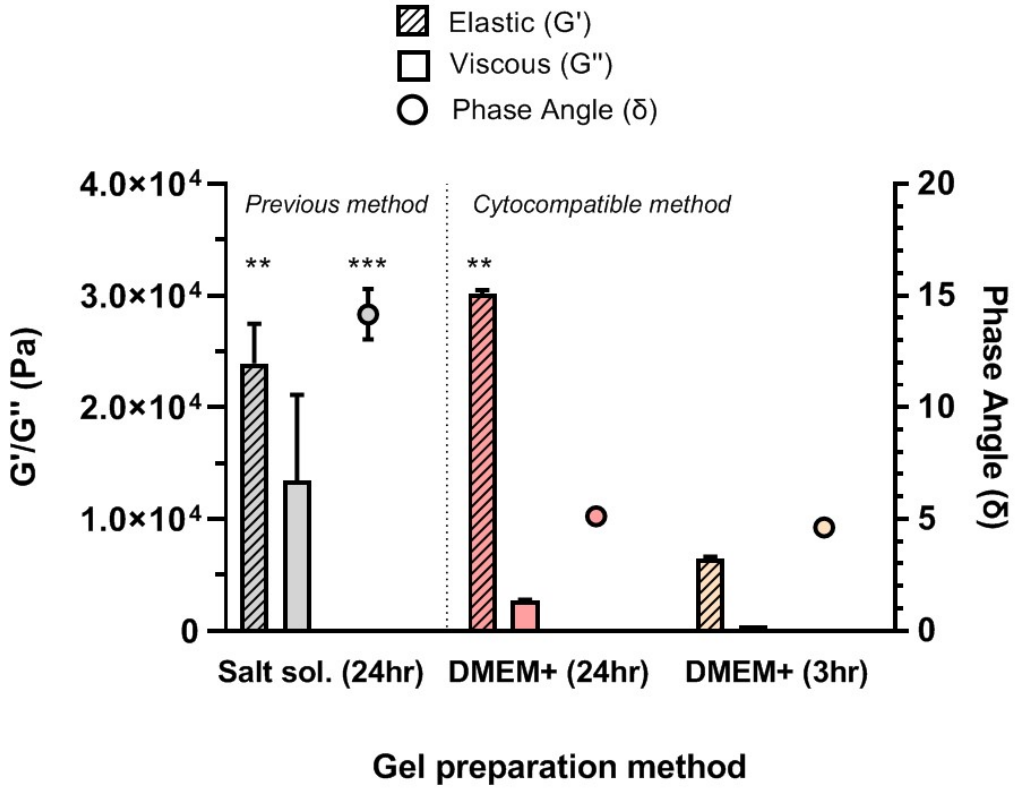

Figure 5.8: Shear properties of P_{11}-8/CS hydrogels prepared using cytocompatible preparation methods. P_{11}-8/CS were reconstituted in supplemented culture medium (CM) and left to equilibrate for 3 hours (n = 3) or 24 hours (n = 3). These were compared against previously used methods for acellular P_{11}-8/CS preparation and delivery, which involved P_{11}-8/CS reconsitution in 130 mM salt solution, followed by 24 hour equilibration at RTP (n = 3). The elastic (G') and viscous (G") moduli were collected, as well as the phase angle (δ). 2-way ANOVA performed, followed by Tukey's multiple comparisons test (** indicates p <0.005, and *** indicates p <0.001 compared to DMEM 3 hr).

5.4.3 TEM

In order to further investigate the rheology results, TEM was employed to determine the effects of both gel equilibration time and the choice of solvent on the gel microstructure.

TEM imaging revealed structural differences at 24 hours versus 3 hour equilibration times. Dark regions in Figure 5.9 represent the P_{11}-8/CS aggregates negatively stained with uranyl acetate. Under both magnifications it is possible to see that there is a higher density of peptide aggregates after 24 hours compared with just 3 hours of equilibration.

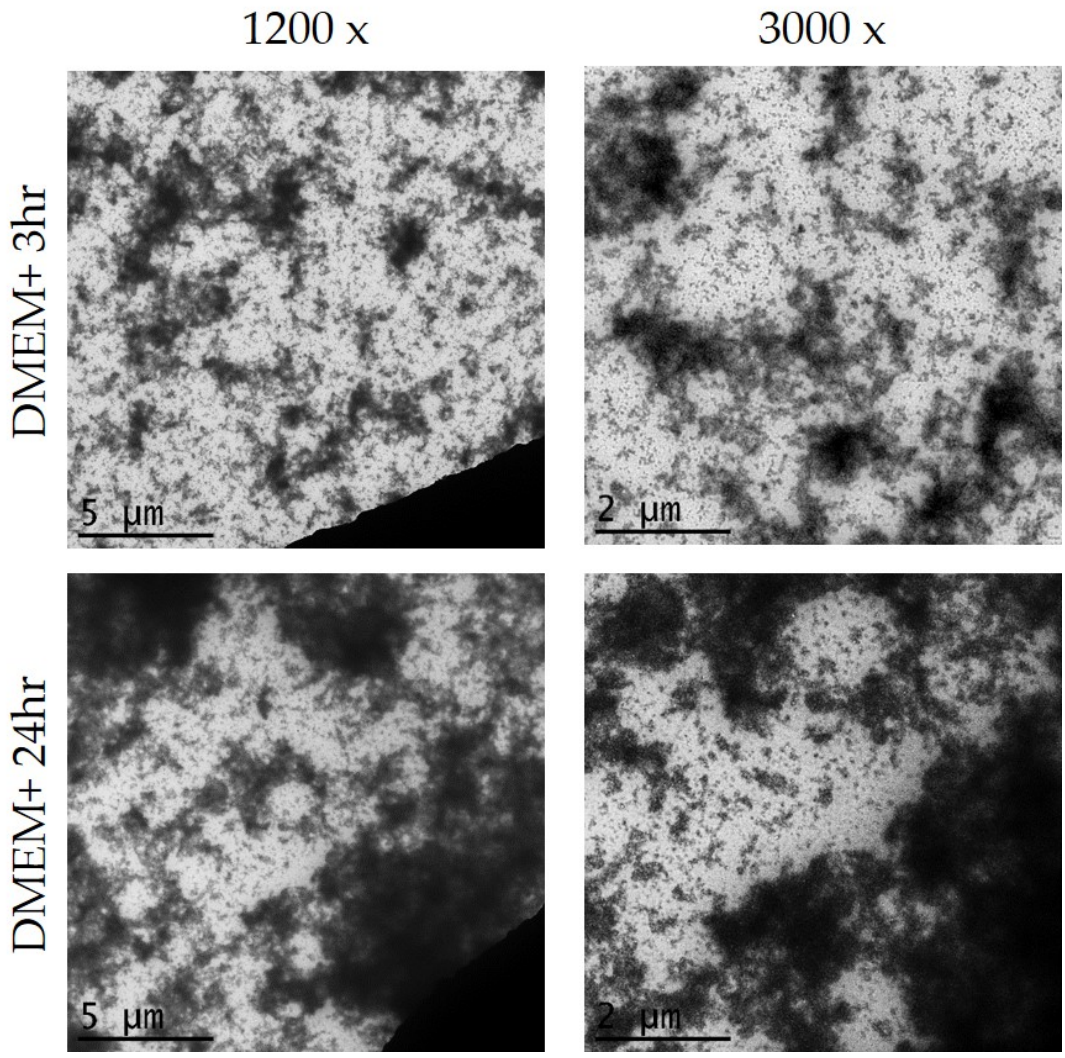

Figure 5.9: Effect of equilibration time on P_{11}-8/CS hydrogels, reconstituted in DMEM. Images captured on the TEM at 1200x and 3000x magnification. Scale bars = 5 µm for 1200x magnification, and 2 µm for 3000x magnification.

Whilst low magnification gives an insight into the 'bulk' structure, at higher magnifications it is possible to get a greater understanding of the effect of both solvent composition and equilibration time on gel nanostructure and interactions. At 12,000x magnification (Figure 5.10), after 24 hour of equilibration there is a more defined fibre structure than at 3 hours, in the media samples. In the 24 hour samples, it is possible to see well defined peptide fibrils, fibril bundles and fibril interconnectivity, demonstrating the ability of cell culture medium to support correct gelation mechanisms. This is accompanied by the presence of denser peptide regions, indicating increased self-assembly as seen in Figure 5.9. In the lyophilised sample, it is possible to clearly observe both the peptide-peptide interactions, as well as the association

with the chondroitin sulphate (darker regions) at the junctions between peptide fibrils.

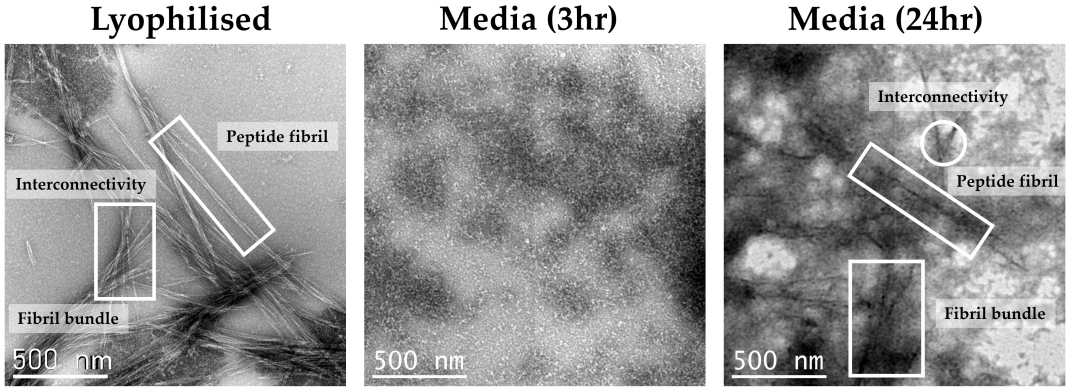

Figure 5.10: Comparison of P_{11}-8/CS hydrogel preparation at 12,000x. Images represent 12,000x magnification TEM micrographs of peptides prepared following the 'lyophilised', and media (3/24 hour equilibration) protocols. Key features of P_{11}-8/CS are labelled in the images.

5.4.4 Cell Viability within P_{11}-8/CS

5.4.4.1 alamarBlue optimisation

In order to evaluate cell metabolic activity, it was first necessary to develop an assay capable of detecting this. AlamarBlue was chosen as a non-destructive method of investigating this parameter. Optimisation of incubation time was essential with this reagent, to ensure the samples had absorbance within the linear range of detection. Figure 5.11B shows that there is only a linear response in % reduction of alamarBlue when incubated for 6 hours. This is supported by Figure 5.11A which shows that across all cell densities a 6 hour incubation is needed to differentiate between them. As a result of these findings a 6 hour incubation was used for subsequent viability measurements.

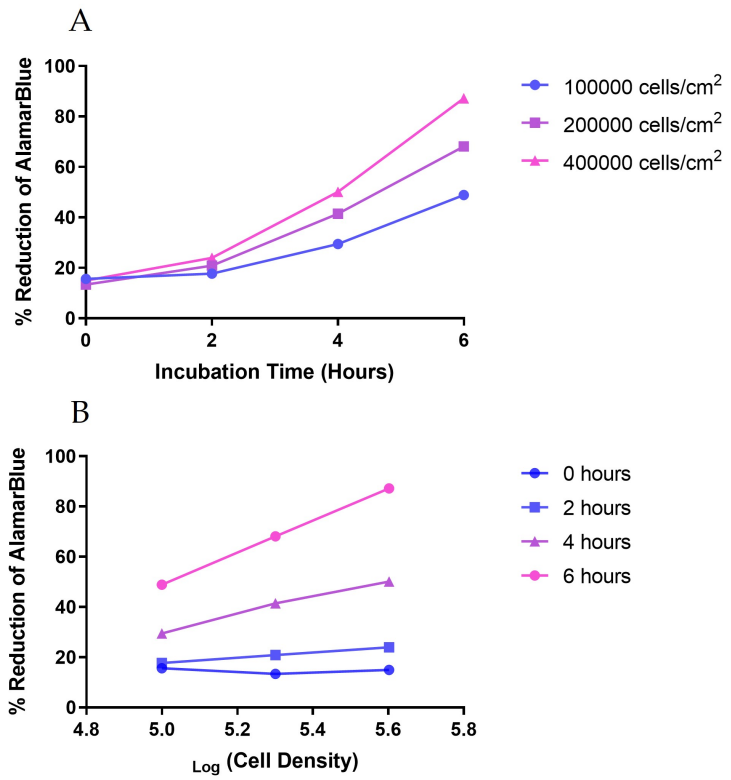

Figure 5.11: alamarBlue incubation time optimisation. A) Demonstrates the % reduction of alamarBlue at different cell densities. B) Demonstrates the % reduction of alamarBlue at different incubation times

5.4.4.2 Preparation Method

Having determined a novel means of encapsulating cells within the P_{11}-8/CS hydrogel, its ability to support growth was compared initially with a previous method used for the delivery of acellular P_{11}-8/CS to porcine femoral condyles (lyophilised method). As described previously, this involves freeze drying the peptide solution at a low pH, and resuspending the powder with cell suspension.

It is evident from Figure 5.12A that despite lyophilisation and hence removal of most liquid, the acidity of the sodium acetate buffer has lowered the pH of cell media in the hydrogel, as it showed a distinct yellow colour. This observation was quantified in Figure 5.12B, where the previous method showed a significantly lower metabolic activity ($p < 0.0005$) compared with Iteration 2. In fact the lyophilised group showed no detectable metabolic activity. Both methods showed a significant reduction compared to the collagen hydrogel.

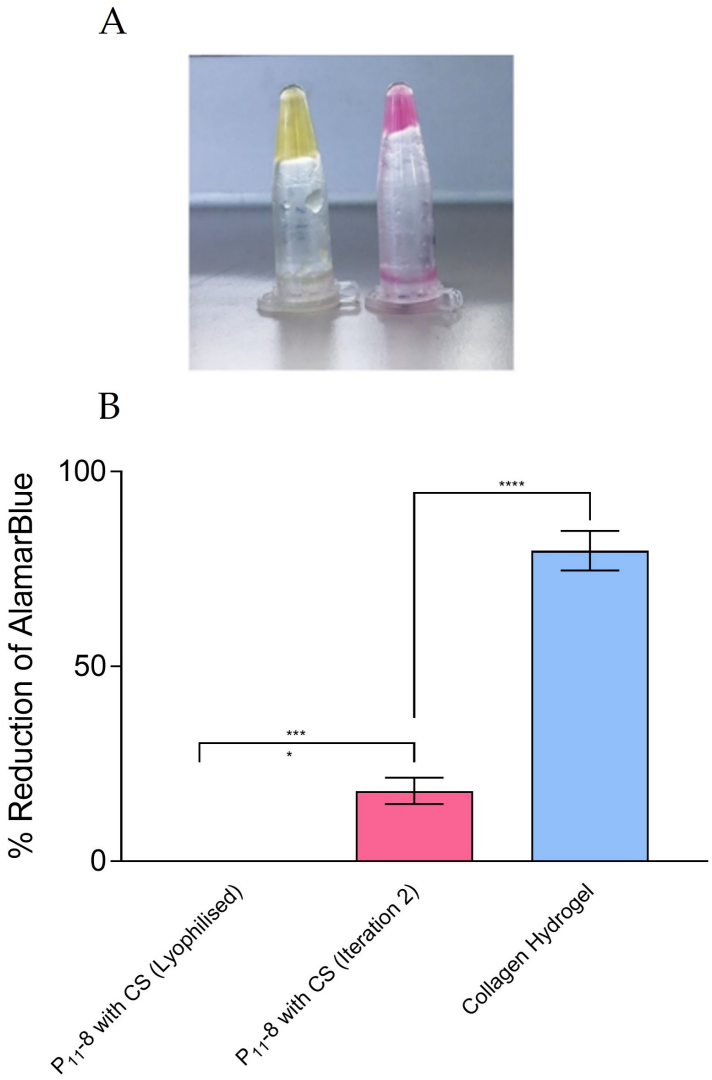

Figure 5.12: Metabolic activity comparison of newly developed P_{11}-8/CS preparation method (Iteration 2) compared with previous method (lyophilised). A) Photograph of cells encapsulated in P_{11}-8/CS gels, prepared using, newly developed method (left) and previous method for delivering acellular gels (right). B) Comparison of cell metabolic activity of L929 cells (1.7 x 10^6 cells/gel), in differing gel preparation methods, compared to a collagen hydrogel. Error bars = $\pm$95% confidence intervals. Significance determined by 1-way anova, followed by Tukey's post-hoc test, performed upon Arc-Sin transformed data (*, **, *** and **** detail that, P > 0.05, 0.005, 0.0005, 0.0001 respectively.

5.4.4.3 L929 fibroblast cell line

To study the ability of P_{11}-8/CS (Iteration 2) to support cell growth and metabolic activity, a timecourse experiment was performed (Figure 5.13). P_{11}-8/CS encapsulated cells had a significantly higher metabolic activity than the negative control (Collagen + SDS), at all timepoints. However, collagen hydrogel encapsulated cells also showed a significantly higher cell metabolic activity than both other groups. At day

7, there was an observed drop in metabolic activity in the collagen group, and an increase of the P_{11}-8/CS group, which resulted in no significant difference at this timepoint. The P_{11}-8/CS seemingly increased in cell metabolic activity over time, however, this difference was not significant. The SDS treated collagen gels, demonstrated very low metabolic activity at Day 1, which was reduced further to 0% at day 7 and 14. These findings, were observed also in the confocal images in Figure 5.13B. In the collagen hydrogel there was a high density of viable cells, which exhibited a rounded morphology. The P_{11}-8/CS showed a much lower cell density, however, there was still a low proportion of dead cells. Cell morphology still represented the fibroblastic shape, however, there were not as many cell-cell interactions as seen in the collagen gel.

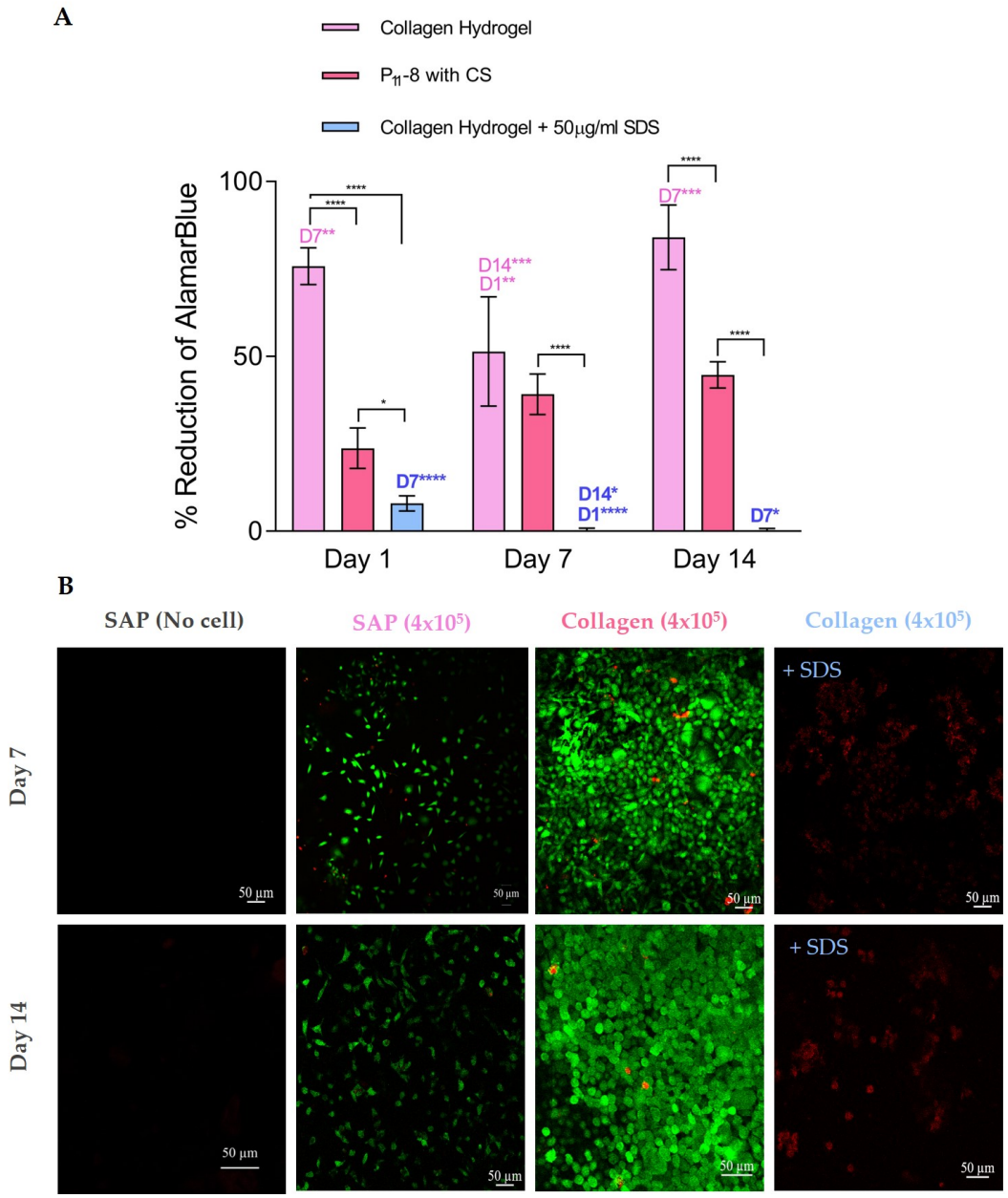

Figure 5.13: Cell viability within the P_{11}-8/CS hydrogel. A) Cell viability measurements for encapsulated L929s versus +ve (Collagen hydrogel) and –ve (Collagen + SDS) controls (n = 6). 1-way ANOVA performed, with Post-hoc Tukey's Test. Error bars +/- 95 % CL. * = $p<0.05$, ** = $p<0.005$. B) LIVE/DEAD confocal imaging of encapsulated L929s at 7 and 14 day timepoints (n=5). Scale bars = 50 µm.

5.4.4.4 C20A4 chondrocyte cell line

Following initial proof of cyto-compatibility with L929 fibroblast cells, the cyto-compatibility of P_{11}-8/CS with a more application relevant human chondrocyte cell line (C20A4).

The cell metabolic activity of C20A4 cells, as determined by alamarBlue reduction

(Figure 5.14), was slightly lower than seen with L929s. However, at Day 1 and 14, there was no significant difference in metabolic activity of cell encapsulated in P_{11}-8/CS and the collagen hydrogel. In all instances the test conditions showed significantly higher metabolic activity than the SDS treated hydrogels.

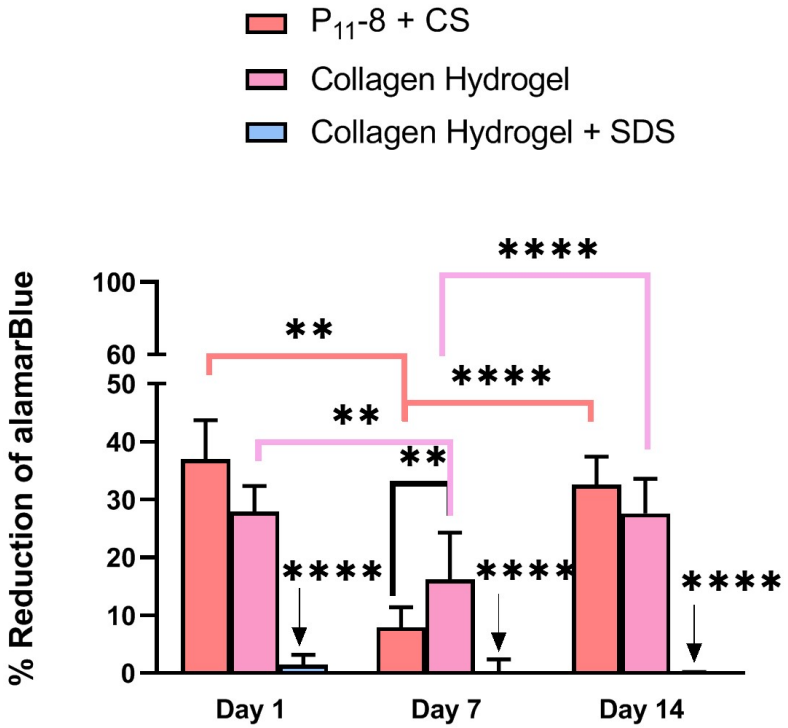

Figure 5.14: Metabolic activity of C20A4 chondrocytes encapsulated within the P_{11}-8/CS hydrogel. Metabolic activity measurements for encapsulated C20A4s versus +ve and –ve controls (n=5). Arrows pointing to collagen hydrogel + SDS group, indicate a significant reduction versus the two groups. Black bars demonstrate significant differences between different groups within the same timepoint. Coloured bars demonstrate significant differences between timepoint for one group. Raw data was subject to Arc-Sin prior to a 2-way ANOVA statistical analysis. Data presented is in the untransformed form. Error bars +/- 95 % CL. ** = $p<0.005$, **** $p < 0.0001$.

The LIVE/DEAD images in Figure 5.15 support the metabolic activity data shown previously. By Day 14 there is a high density of viable chondrocytes in both the P_{11}-8/CS and collagen hydrogel control, which are absent from the negative (SDS) control. This cell confluency increases from seed, to high confluency by the final timepoint in both seeded hydrogels. The P_{11}-8/CS and collagen alone controls, demonstrate a lack of autolfluorescence.

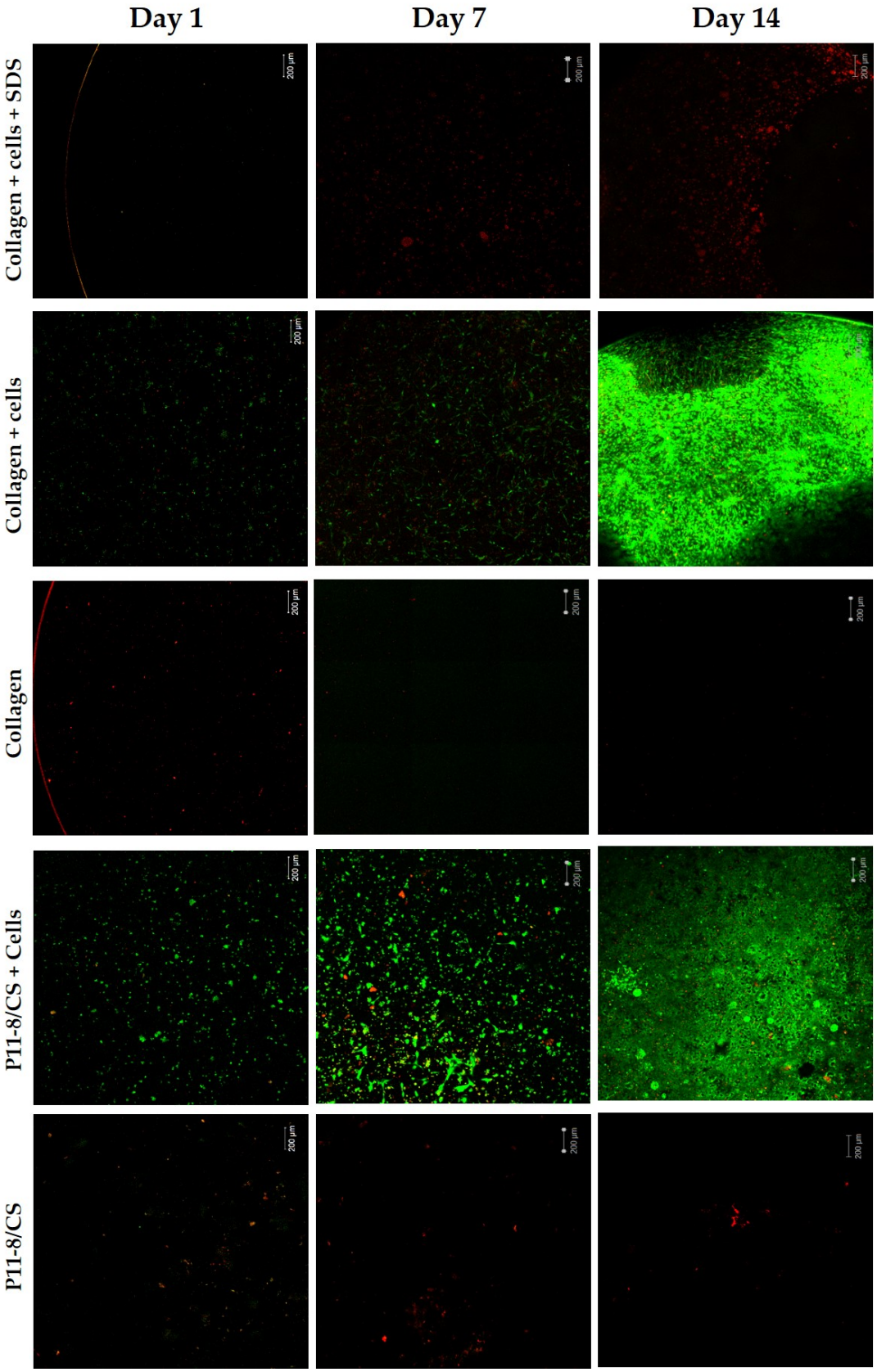

Figure 5.15: Cell viability of C20A4 cells encapsulated within the P_{11}-8/CS hydrogel. LIVE/DEAD confocal imaging of encapsulated L929s at 7 and 14 day timepoints (n=5). Scale bars = 50 µm.

5.4.5 Gene expression of encapsulated chondrocytes

5.4.5.1 Suitability of cell types for gene expression studies

Following demonstration the ability of P_{11}-8/CS to support cell metabolic activity and viability, the effect of encapsulation on chondrogenic gene expression was investigated. Preliminary experiments with the human chondrocyte cell line (C20A4) demonstrated no cycle threshold (CT) value for the genes probed, indicating a lack of chondrogenic gene expression in detectable quantities. Therefore the decision was taken to use primary porcine chondrocytes to see if these would express the genes of interest (GOI). Porcine chondrocytes were either expanded in monolayer or subject to aggregate culture prior to analysis. The purpose behind aggregate culture was to redifferentiate the 2D expanded chondrocytes. In Figure 5.16, the gene expression of collagen II and aggrecan are upregulated 10,000 and 50,000x respectively when chondrocytes are cultured in aggregate versus monolayer. COMP showed a smaller upregulation of 50x, whereas Collagen I showed no difference in expression between the monolayer and aggregate culture.

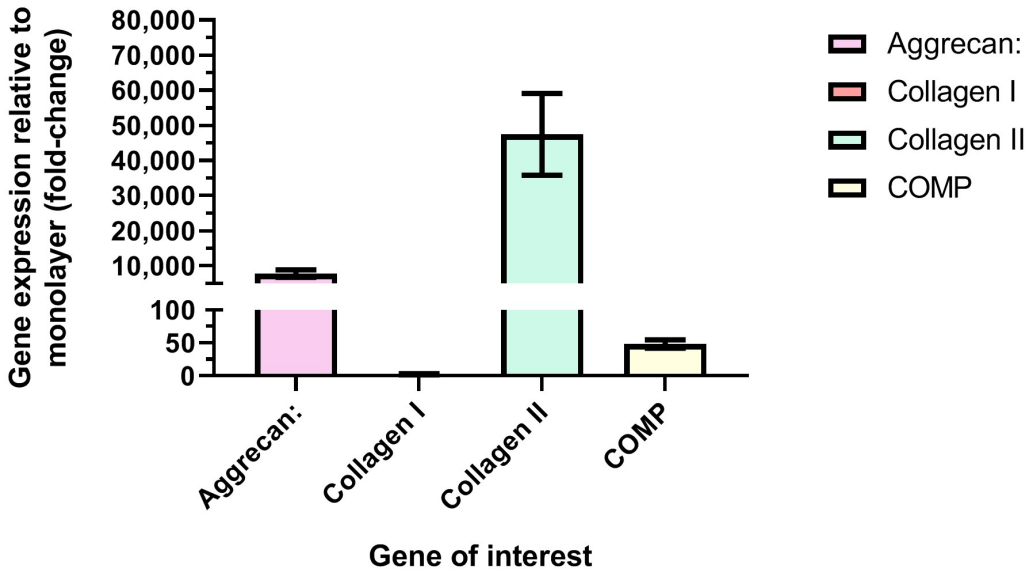

Figure 5.16: Effect of culture method on gene expression in chondrocytes. Fold change of chondrocytes cultured in aggregate (n = 3) is representative relative to chondrocytes cultured in monolayer alone (n = 3). Error bars = +/- SD.

5.4.5.2 Gene expression profile of porcine chondrocytes encapsulated in P_{11}-8/CS hydrogels

Following the optimisation of the cells for use in the gene expression study, the aggregates were dissociated and seeded as single cells into P_{11}-8/CS hydrogels and onto monolayers. The expression of genes associated with chondrogenesis was investigated.

The aggrecan (ACAN) gene expression data in Figure 5.17A demonstrates no significant difference at day 7 between the monolayer and the encapsulated cells, whereas by day 14 and day 21 there is a significant increase in expression in the encapsulated cells. This trend is observed in both the collagen II (COL2A1) and cartilage oligomeric protein (COMP) expression, however, at day 7 for COL2A1 and COMP there is a significantly lower expression in the encapsulated cells versus the monolayer. For collagen I, there is a significantly higher expression in the monolayer samples at day 7, and no significant difference between the two groups at day 14 or 21.

Over time, expression of the ACAN and COMP signficantly increases from Day 7-14, and Day 14-21. Whereas expression both collagen types only showed a significant increase between Day 7 and 14.

The Collagen II:I ratio was calculated at each time point (Figure 5.18), and shows that over time the ratio increases for P_{11}-8/CS encapsulated cells. By Day 14 and 21 the ratio is higher for the encapsulated cells than the monolayer, indicating a more healthy chondrocyte phenotype.

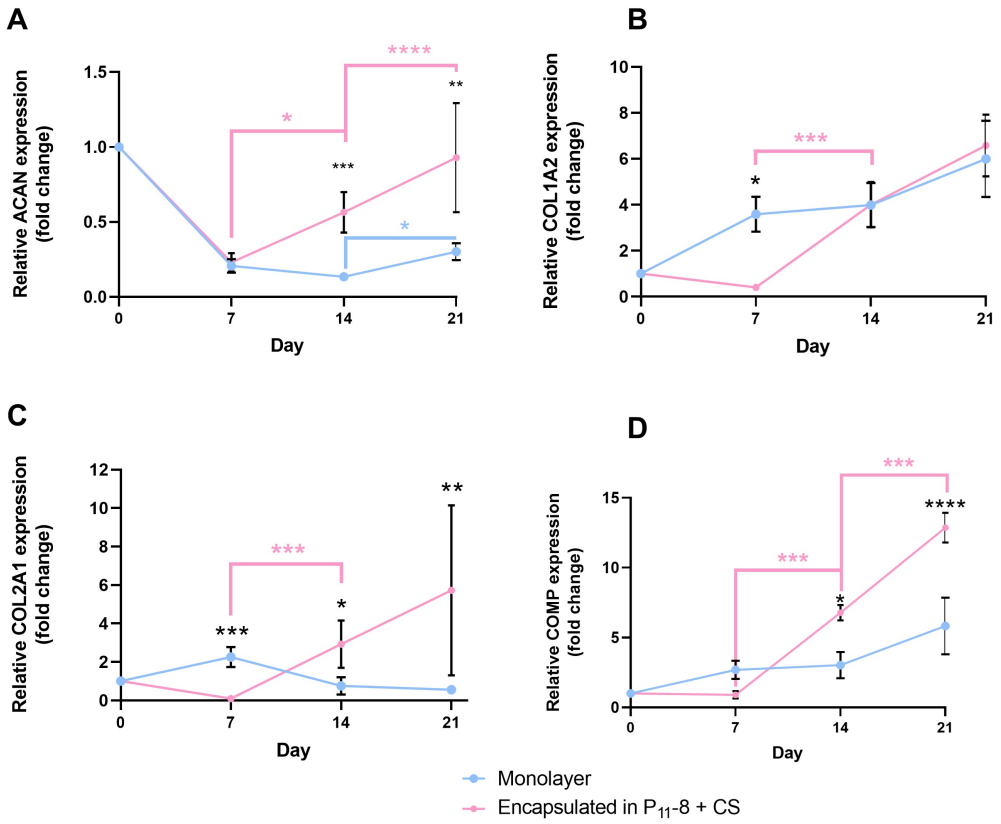

Figure 5.17: Gene expression profile of porcine chondrocytes cultured encapsulated in P_{11}-8/CS hydrogels compared with monolayer culture over 21 days. Gene expression is expressed as relative fold expression compared to Day 0 cells pre-seeding/encapsulation, with mutiple reference genes ACTB (β actin) and PPIA (Peptidylprolyl isomerase). A) ACAN (aggrecan), B) COL1A2 (collagen I), C) COL2A1 (collagen II) and D) COMP (cartilage oligomeric protein). Relative fold expression was calculated as (2^{ddCT}). A 2-way ANOVA was performed on the ddCT values, with a post-hoc Tukey's test for multiple comparisons, to assess significant differences both between the expression between materials and over time (* = p <0.05, ** = p <0.005, *** = p <0.001, **** p <0.0001). Error bars = +/- S.D.

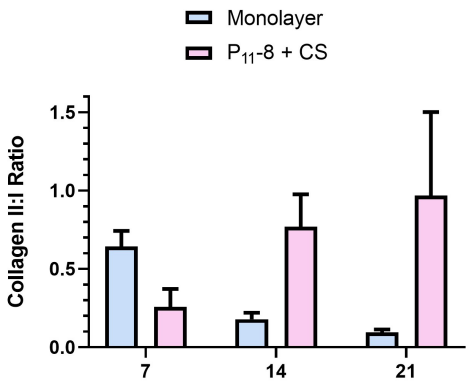

Figure 5.18: CollagenII:I expression ratio in porcine chondrocytes cultured encapsulated in P_{11}-8/CS hydrogels compared with monolayer culture over 21 days. Gene expression is calculated as relative fold expression compared to Day 0 cells pre-seeding/encapsulation, with mutiple reference genes ACTB (β actin) and PPIA (Peptidylprolyl isomerase). To calculate the ration, the fold-change of COL2A1 was divided by COL1A2. Relative fold expression was calculated as (2^{ddCT}). Error bars = +/- S.D.

5.5 Discussion

5.5.1 Development of P_{11}-8/CS as cytocompatible matrices

Previous work with P_{11}-8 has investigated the applicability to be used in conjuction with cells (Maude *et al.*, 2011). However, all work focussed on P_{11}-8 in conjunction with CS has been concerned with acellular gels (Barco *et al.*, 2018). Therefore, this chapter firstly aimed to develop the P_{11}-8/CS gelation process to include cells, to further characterise the cellular response to the gels and to assess the effect of new production methods on gel properties.

The main difficulty in translating the method used by previous lab members was the inclusion of cells, which meant less vigorous mixing as this could have negative effects on cell viability. Therefore the first method that was attempted (Section 5.3.1.1), involved resuspending both the P_{11}-8 and CS in equal volumes of cell suspension, followed by tituration with a pipette to mix, and delivery of 100 µL gels. The main problem encountered was the lack of sufficient mixing of the two components, which resulted in clumpy and inhomogeneous gels. Therefore, it was decided that mixing was essential, and that addition of the cells in a small volume just before gel delivery would allow vortexing and sonication without damaging the cells. This resulted in the method described as Iteration 2 (Section 5.3.1.2) which was utilised for the following studies, as it allowed for the formation of self-supporting gels as depicted in Figure 5.7.

5.5.2 Encapsulation of cells within P_{11}-8/CS

In order to determine the effects of the entire preparation method on cell metabolic activity, a suitable assay needed to be developed. Prior experiments with the AT-Plite assay had shown unreliable results, likely due to the inability to efficiently lyse the cells when encapsulated in a hydrogel. Therefore, alamarBlue was chosen as a reporter that does not rely on cell lysis. The 3D encapsulation of the cells meant a longer incubation time was needed in order to detect an accurate reduction in

alamarBlue. However, at 6 hours a linear relationship between cell density and % reduction of alamarBlue was observed in Figure 5.11.

Following optimisation of the cell metabolic activity assay, two preparation methods of cell encapsulation in P_{11}-8/CS hydrogels were compared. The metabolic activity of the encapsulated cells was compared against the RAFT 3D cell culture system (Lonza, UK), which is a collagen based hydrogel. This acted as a positive control for 3D cell encapsulation, and growth. The new process (Iteration 2) developed in Section 5.3.1.2 showed a significantly improved metabolic activity when compared to the previous method for acellular P_{11}-8/CS preparation. However, when compared to the positive control, there was a significant reduction ($p < 0.0001$) in metabolic activity (Figure 5.12). The practical significance of the reduced metabolic activity P_{11}-8/CS is unclear from this result alone, as the comparison is an established 3D culture and expansion model.

The origin of this reduced metabolic activity in the lyophilised samples may be in the preparation method. In order to keep the peptide in a monomeric form prior to lyophilisation, the peptide is reconstituted in pH 4 sodium acetate (1 M). The solution is subsequently lyophilised overnight to remove the buffer. However, it could be that residual sodium acetate salts remain in the gel solution causing a decreased pH. From the macroscopic image in Figure 5.12, it is evident that the lyophilised method results in a acidic pH in the gel, due to the yellow colour of the phenol red in the DMEM. The effect of this acidity appears to be a reduction in cell viability. Lowering the extracellular pH from 7.2 to 5.8 has been shown to reduce cell viability by 70% (Teixeira *et al.*, 2018). Despite the lower metabolic activity, from a translational perspective the reconstitution of the lyophilised powder was a much simpler process, therefore may still be compatible for acellular gel production depending on the application.

The metabolic activity timecourse data and LIVE/DEAD staining (Figure 5.13A) provides a better insight into the reduced metabolic activity observed previously in the P_{11}-8/CS hydrogels. As seen in Figure 5.12B, there is still a significant reduction in metabolic activity compared with the collagen hydrogels at Day 1 and Day 14. However, at Day 7 there is no difference between the two encapsulation

methods. Although not significant, there is an improvement in metabolic activity over the 14 day period in the P_{11}-8/CS and collagen gels. The difference in viability is demonstrated in the LIVE/DEAD images in Figure 5.13B. There is a much greater cell density in the collagen hydrogels, indicating greater cell proliferation and hence metabolic activity. The improved metabolic activity in the collagen hydrogels is likely a result of the presence of cell attachment motifs (Manferdini *et al.*, 2022). In the P_{11}-8/CS samples, whilst there is a much lower cell density, there is very little cell death. The L929s appear to exhibit healthy fibroblast morphology in both collagen hydrogels and P_{11}-8/CS when compared with the literature (Nargang *et al.*, 2014; Kumar *et al.*, 2016; Montalbano *et al.*, 2018).

These data appear to show viability of L929 cells within P_{11}-8/CS. However, there appears to be a discrepancy in proliferation or metabolic activity between the two models. This is a phenomenon which has been observed in the literature in other 3D models. For example, when comparing the culture of a JIMT1 breast cancer cell line in matrigel and a 3D polyHEMA scaffold against 2D culture, (Hongisto *et al.*, 2013) observed a 1.9 fold faster proliferation rate in matrigel and a 7.2 fold slower proliferation rate in the 3D polyHEMA scaffold. In this instance, the authors cite nutrient exposure as a possible reason for the discrepancy. Additionally, others research has shown that modulus of the hydrogel can affect proliferation rates (Goldshmid and Seliktar, 2017). The research showed that cells cultured in low modulus hydrogels (G' = 100 - 250 Pa) showed higher proliferation rates compared with cells cultured in higher modulus gels (G' = 500 - 2000 Pa). The G' of the collagen used in this study has been reported as 5 kPA (Kayal *et al.*, 2019), whereas the P_{11}-8/CS measured around 30kPa (Figure 5.8). In order to fully determine the cause of the lower metabolic rate observed in the P_{11}-8/CS, further material and composition testing should take place investigating nutrient availability, cell attachment and cyto-compatibility with the individual gel components.

Whilst the metabolic activity data with L929 cells provides a first investigation into the feasibility of encapsulating cells within P_{11}-8/CS hydrogels, L929s are not a relevant cell for the end application. Therefore, the experiment was repeated but with a

human chondrocyte cell line (C20A4) . Firstly, compared with the L929s the percentage reduction of alamarBlue was much lower for the collagen hydrogel, and was slightly lower for the P_{11}-8/CS (Figure 5.14). It is apparent that the metabolic activity of chondrocytes encapsulated in P_{11}-8/CS resembled the positive control closely. At Day 1 and Day 14 there was no significant difference between the two groups. The only significant difference was seen at Day 7 where there was a reduction versus the collagen hydrogel ($p < 0.005$). Both the P_{11}-8/CS and collagen hydrogel groups demonstrated a significantly reduced metabolic activity ($p < 0.005$) at Day 7 compared with Day 1 and 14. This reduction at Day 7 had been seen previously in Figure 5.13 in the collagen hydrogel group. Both groups with the C20A4 cells recover from the drop in metabolic activity by Day 14 however.

The LIVE/DEAD images in Figure 5.15 support the results seen in the metabolic activity results. When compared with the L929 images Figure 5.12B, it is evident that there is a much more equal cell density across all timepoints. In both the P_{11}-8/CS and collagen hydrogel groups there is minimal cell death at Day 1, 7 and 14. In the P_{11}-8/CS only control there is some autofluorescence under the red channel, therefore it is difficult to discern whether there is cell death or autofluorescence alone in the P_{11}-8/CS samples. By Day 14 both groups are over confluent, whereas with the L929 only collagen gels had reached this level of confluence.

The similarity between the metabolic activity of the chondrocytes in either the collagen or P_{11}-8/CS gels, could have it's origin in a lower metabolic activity of the chondrocytes encapsulated in collagen hydrogel compared with the L929s. It is difficult to delineate the exact cause of this reduction in metabolic activity, however, as described previously different cells respond differently to differing 3D environment. From this experiment it appears that C20A4 cells have a lower metabolic activity in collagen than L929, whereas P_{11}-8/CS appears to a similar culture environment for both cell types.

Comparing the cell morphology between the hydrogels, it appears as if the chondrocytes encapsulated within the collagen hydrogel exhibit a fibroblast-like morphology by Day 7, with protrusions extending out into the hydrogel. In the P_{11}-8/CS gels the cells appear more rounded, although there are some cells with protrusions. Healthy chondrocytes *in-situ* exhibit a rounded morphology and clustering (Buschmann *et al.*, 1992), and more recent literature has described chondrocytes with processes to be an abnormal morphology (Karim *et al.*, 2018). Similar results have been observed in a study comparing different strength of agarose gels (2% vs 0.2%), they observed by Day 7 cells cultured in the softer gel exhibited more processes. Interestingly, they saw that increased FBS concentrations exacerbated this effect. Following this assumption, it could be said that the chondrocytes exhibit a healthier morphology in the P_{11}-8/CS hydrogels. However, there is little in the literature describing the morphology of C20A4 and how this differs from primary chondrocytes. Therefore, further work should investigate morphological changes of primary cells in the two hydrogel systems.

Overall, if cell expansion was an important factor to consider for the end application, another system may be more effective. However, chondrocytes *in-situ* have a low proliferative phenotype, therefore this is not an essential factor in our investigation. This data shows that P_{11}-8/CS is a suitable matrix for cell delivery in terms of maintaining cell viability over a 14-day period.

5.5.3 Chondrogenic gene expression of P_{11}-8/CS encapsulated cells

Pilot studies (data not shown) demonstrated that when RNA was extracted from C20A4 cells, there was no detectable expression of any indicators of chondrocyte behaviour (Aggrecan, Collagen I and II or COMP). Therefore, a decision was made to use primary porcine chondrocytes in order to have a base gene expression to determine any differences resulting from culture environment. Due to the high cell numbers required for this experiment, passaging of the primary porcine cells was necessary. Therefore, to reinstate chondrogenic gene expression an aggregation step was carried out based on a protocol from (Huang *et al.*, 2016). From Figure 5.16, it is evident that aggregate culture resulted in a substantial increase in the expression

of genes associated with chondrogenesis, especially collagen II and aggrecan. However, for collagen I there was only a negligible increase. This was a positive result, as collagen I expression can cause fibrocartilaginous repair with inferior biomechanical properties.

In the timecourse, by day 14 and 21 all three chondrogenic markers showed a significant increase versus the monolayer (Figure 5.17). The introduction of chondrocytes to a 3D environment is an established method of promoting chondrogenic gene expression (Bonaventure *et al.*, 1994; Caron *et al.*, 2012). Despite the upregulation of the anabolic genes, at these same timepoints (day 14 and 21), there is no significant difference in the collagen I expression between the monolayer and cells encapsulated in P_{11}-8/CS. This provides early indications that cells encapsulated in the peptide gel, have a tendency towards expression of biomolecules for the regeneration of a relevant hyaline cartilage repair material. However, further experiments assaying biomolecular deposition would have to be carried out before this hypothesis could be substantiated.

The relative gene expression is compared to day 0 cells that have just been dissociated from the 6 day aggregation step in the presence of TGF-β. By Day 21 in the P_{11}-8/CS gels, the ACAN expression had recovered to the same level as post-aggregation. Whereas COL2A1 and COMP increased 5- and 9-fold respectively above the D0 cells post-aggregation. Interestingly, at Day 7 the P_{11}-8/CS groups relative gene expression drops to below 1 across all four genes. This correlates with the observed reduction in metabolic activity in Figure 5.14. Therefore, there is a potential that transfer from 2D to P_{11}-8/CS causes a drop in metabolic activity in chondrocytes. This drop in viability however is not detected at Day 1 but Day 7. Further timepoints could be conducted to delineate at what time point the metabolic begins to drop. More importantly, once stabilised the metabolic activity and gene expression recover by Day 14 and 21.

The chondro-inductive nature of the P_{11}-8/CS may be a result of several factors. As mentioned previously, it may simply be the switch from 2D to 3D environment which has caused the upregulation of chondrogenic genes (Bonaventure *et al.*, 1994; Caron *et al.*, 2012). There is also a possibility that the gene expression originates

from the presence of chondroitin sulphate within the P_{11}-8/CS. Several studies have shown benefits to cell viability and gene expression with the inclusion of CS into the hydrogel systems (Hwang *et al.*, 2007; Chen *et al.*, 2016; Li *et al.*, 2018). Following this observation, a proof of concept experiment was conducted into the effect of CS omission from the hydrogel system (Figure 5.19). Whilst with P_{11}-8 the cells were still viable, when CS was added there was a significantly higher cell metabolic activity at Day 1.

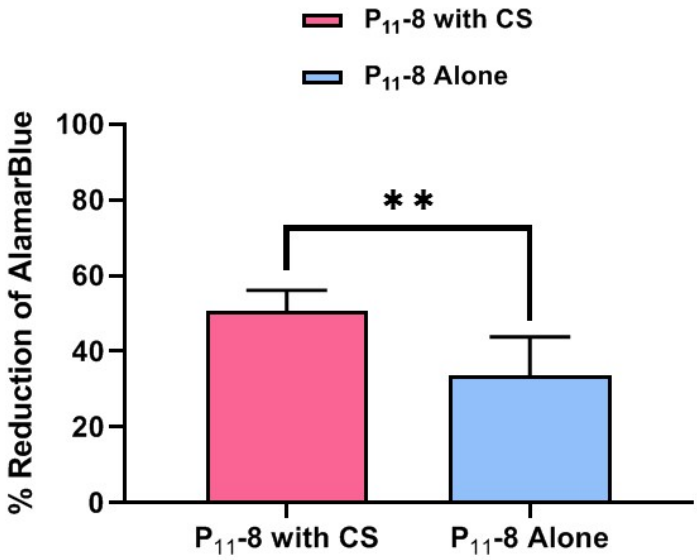

Figure 5.19: Proof of concept experiment comparing metabolic activity in P_{11}-8 with and without CS. C20A4 cells were encapsulated in P_{11}-8 with (n = 6) and without CS (n = 6) as in Section 5.3.2.2. Raw data was subject to Arc-Sin transformation, and an unpaired t test was performed ** = p <0.005. Error bars = +/- S.D.

Several theories exist as to why CS improves the viability and/or gene expression of chondrocytes *in-vitro*. Studies have shown that CS can sequester growth factors and extend their half-life (Varghese *et al.*, 2008). Another hypothesis that the addition of CS adds mechanical stability to the hydrogel. This is partially based on the contribution to the native cartilage compressive strength, and a study demonstrating that an increased stiffness of hydrogels significantly improves chondrogenesis (Li *et al.*, 2016). This was observed through an increase in the elastic and viscous shear modulus with addition of GAG at a ratio with P_{11}-8 of 1:2 (Miles *et al.*, 2016). Future work into this system, should extend this experiment up to day 21 and see if this effect sustains over time. Furthermore, rheological assessment of the hydrogels with and

without CS, could provide further insight into the improved cell behaviour.

Furthermore, the aggregation step clearly increased the chondrogenic expression of the chondrocytes (Figure 5.16). However, what has not been demonstrated here is the ability of the P_{11}-8/CS to re-differentiate chondrocytes. Therefore, future work should investigate the gene expression of chondrocyte post 2D expansion, to see if the same trend is observed.

5.5.4 Effect of preparation method on P_{11}-8/CS behaviour and microstructure

The cell metabolic activity and gene expression data give evidence for the capacity for P_{11}-8/CS hydrogels to act as a cell delivery device. However, the rheological and structural properties of the hydrogels are as important in the ability of the gels to support cell encapsulation and to potential restore biomechanical properties of decellularised or GAG depleted cartilage under compression.

Whilst media is an essential component to maintain cell viability in this system, it is unknown how this affects peptide self-assembly and the downstream mechanical properties. Studies have investigated the rheological and microstructure of the P_{11}-X family of peptides in cell culture medium (Maude *et al.*, 2011), however, at the time of writing no study is yet to investigate these parameters in relation to P_{11}-8/CS. Furthermore, usually with the P_{11}-8/CS system, the gels are left overnight to equilibrate before downstream investigation. However, as explained previously in Section 5.3.1.2, an equilibration time of 3 hours was chosen in order to maintain cell viability. Following the discovery that cell viability was not affected by extending the equilibration time to 24 hours (data not shown), the effect of this extra equilibration time was also examined.

The rheological data (Figure 5.8) showed that the G' is unaffected by resuspension in supplemented DMEM (DMEM+) compared with the lyophilised method, when left for 24 hours to equilibrate. Without this period of equilibration the G' is significantly reduced. There appears to be a reduction in G", however this was not significant compared against the 3 or 24 hour equilibration groups. The phase angle

however, was significantly higher than both when peptide was reconstituted in the salt solution, indicating a more elastic behaviour of the P_{11}-8/CS samples in media. Whether this effect was due to the suitability of the solvent for permitting peptide self-assembly and equilibration, or simply a result of the 24hr equilibration is still unknown. When comparing the 3 and 24 hour DMEM+ groups, there was a significantly higher G' in the 24 hour group. In future studies a 3 hour lyophilised control should be included, to isolate the influence of DMEM+ on the rheological properties alone.

In terms of the pH of the solvents, DMEM has a pH of approximately 7.4, and the salt solution was 7.6. Furthermore, the salt concentration of DMEM is approximately 110 mM sodium chloride, whereas the salt solution was 130 mM sodium acetate. Both of these concentrations approach values stated in the literature, for permitting favourable beta-sheet assembly (Carrick *et al.*, 2007). Therefore, it is likely that maintenance of these pH values and ionic strength are important in buffer composition.

It is also likely that the supplementation of the DMEM with 10% FBS; P/S and L-Glutamine would have an effect over this assembly. However, from the data provided it was not possible to draw conclusions on which component may or may not contribute to the G' of the P_{11}-8s/CS gels. In order to further elucidate the contribution of these additional components, an exclusion study would need to be performed by eliminating the supplements and performing rheological testing. Of greater interest than the other elements would be the elimination of FBS. From a translational perspective the use of FBS is undesirable due to both health and regulatory risks, therefore, performance of the gels from both a rheological and cytocompatibility perspective in the absence of FBS would be important to ascertain.

Studies into the rheology of hydrogels, demonstrate a relationship between the G'/G", and have related the ratio to applicability in tissue engineering applications (Jamburidze *et al.*, 2017). This study reported that their hydrogels had a ratio of approximately 10, which was in line with their literature values reported for tissues such as the pancreas and liver (Zhang *et al.*, 2007). In this study, for the hydrogels which had been reconsituted in DMEM the ratio of G'/G" was 12.44 and 11.20 for the 3hr and 24hr equilibrated gels respectively. However, the lyophilised sample reconstituted

in the salt solution had a G'/G" ratio of 1.79.

Finally, although not investigated in this work, one potential limitation of the use of GAGs is the potential for leaching from the hydrogel over time, which may impact the rheological properties of the hydrogel, causing further disruption to the structural integrity of the material and potentially mobilisation of cells out of the region of interest. Such disruption may also leave encapsulated cells susceptible to high and injurious loads. Previous work investigating P_{11}-12 with GAG, demonstrated a 8% GAG leakage out of an intervertebral disc within the first 24 hours (Miles *et al.*, 2016). Additionally, the P_{11}-X family has been shown to demonstrate shear-thinning properties, which are beneficial in terms of application and handling of the peptide (Warren *et al.*, 2021). However, upon delivery to the articular cartilage in a synovial joint, rather than an intervertebral disc, the various loading-unloading cycles may have a detrimental effect on hydrogel integrity. Such an effect may further increase the propensity of chondroitin sulphate to leach out of the region of interest. Future work should investigate GAG leaching from the hydrogels in the Iteration 2 formulation, first in culture plate then in a more dynamic environment.

5.6 Conclusion

Overall, this data shows that it is possible to adapt the P_{11}-8/CS process to support the cell viablity of both L-929, C20A4s cell lines and the chondrogenesis of primary porcine chondrocytes. Furthermore, this change in ability to support cell viability does not impact the rheological properties or gelation of P_{11}-8/CS.

Chapter 6

Enhanced Decellularised Matrices

6.1 Introduction

At the time of writing, one of the only clinical studies into the application of decellularised osteochondral plugs was of a Zimmer Biomet product, known as Chondrofix. The results were discouraging, with 72% failure rates reported by (Farr *et al.*, 2016) and cases of acute graft delamination (Degen *et al.*, 2016). There is limited information regarding their decellularisation process and additional processing methods which could be causing these high failure rates. We previously hypothesised that this failure was due to ineffective host cell migration into the scaffold, based on findings by (Farr *et al.*, 2016) reporting a lack of viable chondrocytes in the graft. Therefore, a strategy to improve outcomes may be the repopulation of these decellularised xenogeneic matrices with autologous chondrocytes. However, the aforementioned limited chondrocyte mobility and low cartilage porosity remain obstacles in the *in-vitro/vivo* recellularisation of articular cartilage.

Although several groups have published on the recellularisation of cartilage derived ECM or reconstituted decellularised cartilage tissue, much fewer have investigated the recellularisation of intact decellularised cartilage tissue specifically. There is a clear distinction to be made here as cartilage derived and reconstituted ECM does not retain the native articular cartilage zonal arrangement and hence avoids many of the difficulties of recellularisation. These scaffolds also lack many of the benefits of an intact ECM structure on biomechanical performance and the cell response. In general, two approaches have been employed to improve recellularisation of intact

decellularised scaffolds; 1) increasing the permeability of the cartilage matrix or 2) the use of dynamic seeding methods.

To permeabilise cartilage for cell penetration, one study used a combination of treatments with alkali and chaotropic agents to disrupt and decellularise cartilage samples. The results yielded a tissue with a much increased pore size which facilitated passive cell infiltration into the matrix (Schwarz *et al.*, 2015). Other studies have created 310 µm channels from the deep zone into the mid-zone of the cartilage alongside chondroitinase-ABC (chABC) treatment in order to disrupt the proteoglycan mesh in the cartilage ECM (Bautista *et al.*, 2016). This enzyme specifically cleaves chondroitin sulphate which makes up a large proportion of this mesh. This created both physical and enzymatic disruption to the tissue integrity. Once seeded, the scaffolds were subject to centrifugation as well as vacuum to encourage even cell distribution and penetration into the scaffold. Their results indicated that cells did occupy the channels. However, in areas without channels cells only penetrated 100 µm into the deep zone with lower penetration still into the superficial and middle zones. With regard to the enzymatic treatment, there was no improvement in recellularisation over scaffolds treated with PBS, likely due to the fact that decellularisation processes tends to deplete proteoglycans without enzymatic intervention (Fermor *et al.*, 2015a). This indicates that the enzyme concentration was too low meaning that not enough GAG was disrupted, or that GAG disruption is not sufficient to improve recellularisation. As well as chondroitinase, collagenase treatment has been investigated and has been shown to improve migration of cells from the surrounding tissue into implanted scaffolds (Seol *et al.*, 2014).

Creation of channels that penetrate into the cartilage matrix have been employed in another study, whereby the inclusion of 7 x 400 µm channels using an ablation needle, as well as rotational culture, permitted cell distribution throughout the depth of the tissue, demonstrating increases in GAG/DNA ($ng.mg^{-1}$) after 10 days culture. However, it must be noted that no radial migration of chondrocytes was observed from the channels into the tissue (Luo *et al.*, 2016). A subsequent study, saw the culture extended to 28 days, showing improved recellularisation and colonisation of the channels, as well as extensive biomolecular deposition. Interestingly, in this

study they compared decellularised scaffolds derived from skeletally mature and immature porcine tissue. It was observed that cell proliferation was improved in skeletally mature tissues, and that repair tissue from mature tissues more accurately replicated the native cartilage structure and zone dependent mechanical properties (Luo *et al.*, 2017). Laser ablation is another technique which has been employed for the controlled disruption of the articular cartilage, to increase cell penetration throughout the scaffolds. This method was used to create 8 x 970 µm channels in the cartilage. Once seeded with chondrocytes, the scaffolds were implanted into rabbits for 8-weeks, after which there were significant recoveries in GAG and DNA content as well as the Young's modulus, whereby the values exceeded those of the native tissue prior to decellularisation.

A key concern in the further disruption of decellularised cartilage is the effect on the mechanical properties of the tissue. Indeed the digestion with chondroitinase yielded cartilage with a reduced equilibrium modulus (Bautista *et al.*, 2016). Furthermore, collagenase treatment has been shown to decrease the aggregrate modulus and increase permeability of articular cartilage (Grenier *et al.*, 2014). Interestingly, the creation of channels has been shown in numerous studies to not affect the compressive modulus of decellularised scaffolds (Juran *et al.*, 2015; Luo *et al.*, 2016).

In order to improve cell seeding efficiency, homogeneity and penetration into scaffolds, many tissue engineers prefer dynamic seeding rather than passive seeding. Methods such as rotational seeding employ hydrostatic forces, whereas vacuum seeding creates negative pressure differentials, encouraging cell penetration into the scaffold. Many groups have been able to create vacuum set up's from basic lab materials, an example of which is depicted in Figure 6.1 (Griffon *et al.*, 2011). Results from this method saw an increased total number of chondrocytes in the centre of the scaffold with a greater overall observed uniformity of cell seeding. (Tan *et al.*, 2012) also developed a vacuum seeding set up using just a syringe and a luer lock.

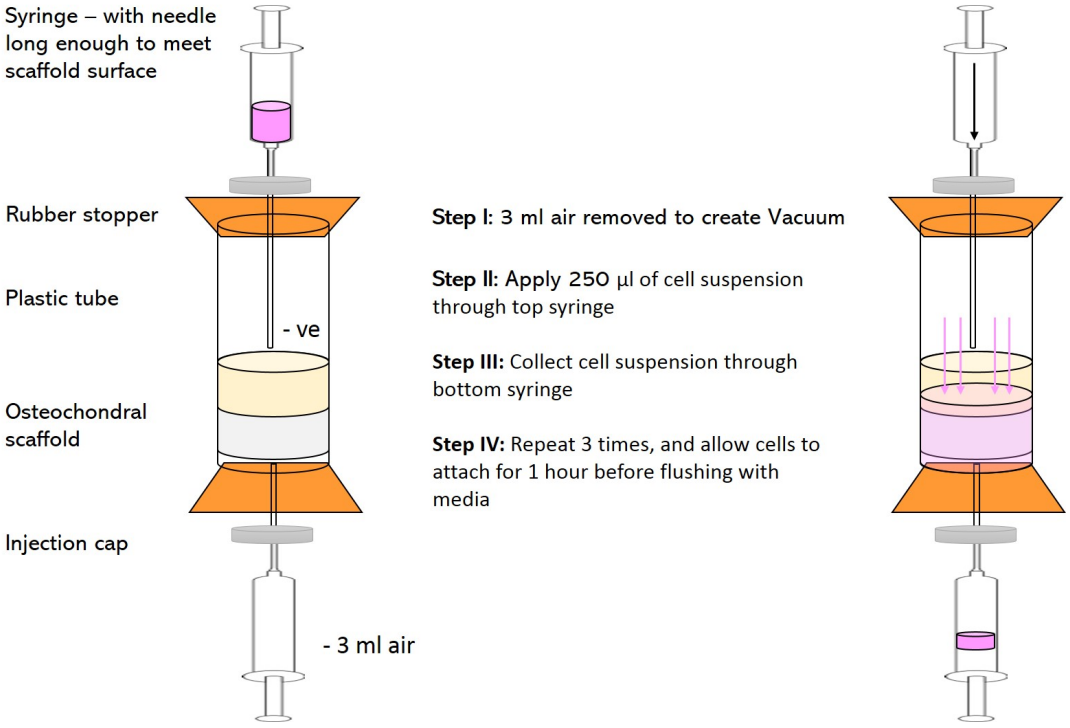

Figure 6.1: Interpretation of vacuum cell seeding method described by (Griffon *et al.*, 2011).

In this chapter, the permeability of decellularised cartilage to chondrocyte cells will be investigated and compared with cartilage samples treated to increase permeability. As well as modifying the cartilage samples, this chapter will detail the development of simple and active seeding methods, which allow cell penetration whilst maintaining the ability for clinical translation.

Another limitation for decellularised scaffolds is the reduction in GAGs and subsequently the biomechanical properties under compression. Therefore, upon discovery of the optimal method for cell delivery, this same method will be used to assess the delivery of P_{11}-8/CS to the cartilage, in an attempt to restore the GAG content. Then based on the hypothesis that GAG delivery will restore the biomechanical properties of cartilage, the decellularised cartilage with P_{11}-8/CS samples will be subject to indentation testing to determine the benefit of this treatment on the resistance to deformation.

6.2 Aims and Objectives

6.2.1 Aims

- Investigate the recellularisation of decellularised porcine scaffolds with C20A4 via active seeding methods and cartilage permeabilisation
- Assess the quality of recellularisation based on depth of penetration, distribution, cell viability and restoration of DNA content
- Attempt to deliver P_{11}-8/CS to the decellularised porcine scaffolds using optimised method for recellularisation

6.2.2 Objectives

- Assess baseline condition for the recellularisation of untreated decellularised scaffolds via static seeding methods and judge success using histology, alongside LIVE/DEAD imaging to determine cell penetration depth and viability.
- Generate channels in the cartilage surface to physically disrupt the ECM. Investigate active seeding methods of injection, vacuum seeding, and centrifugation
- Determine the optimum concentration, incubation time and incubation conditions of osteochondral scaffolds with collagenase, to generate sufficient degradation to allow cell penetration.
- Evaluate lyophilisation method to generate a reproducible method for consistent scaffold seeding. Investigation into cell penetration and viability will be performed as above.
- Elect best process for cell seeding, and optimise for the delivery of P_{11}-8/CS to decellularised cartilage
- Optimise fixation methods P_{11}-8/CS in decellularised cartilage for cryoembedding.

- Using fluorescently tagged P_{11}-8/CS as well as Safranin O and Fast Green staining, assess success of P_{11}-8/CS delivery to cartilage
- Use indentation testing to investigate the percentage deformation of P_{11}-8/CS restored decellularised scaffolds

6.3 Materials and Methods

6.3.1 Recellularisation of decellularised scaffolds

6.3.1.1 Processing of decellularised sheets

Post-decellularisation, the scaffolds were stored at -20 °C until required. Subsequently, the scaffolds were thawed for 30 minutes at 37 °C. In order to maximise the use of each sheet, an 8 mm biopsy punch was used to produce 4 osteochondral plugs with a diameter of 8 mm and a depth of 5 mm. This was performed as shown in Figure 6.2 using aseptic technique in a Class II safety cabinet.

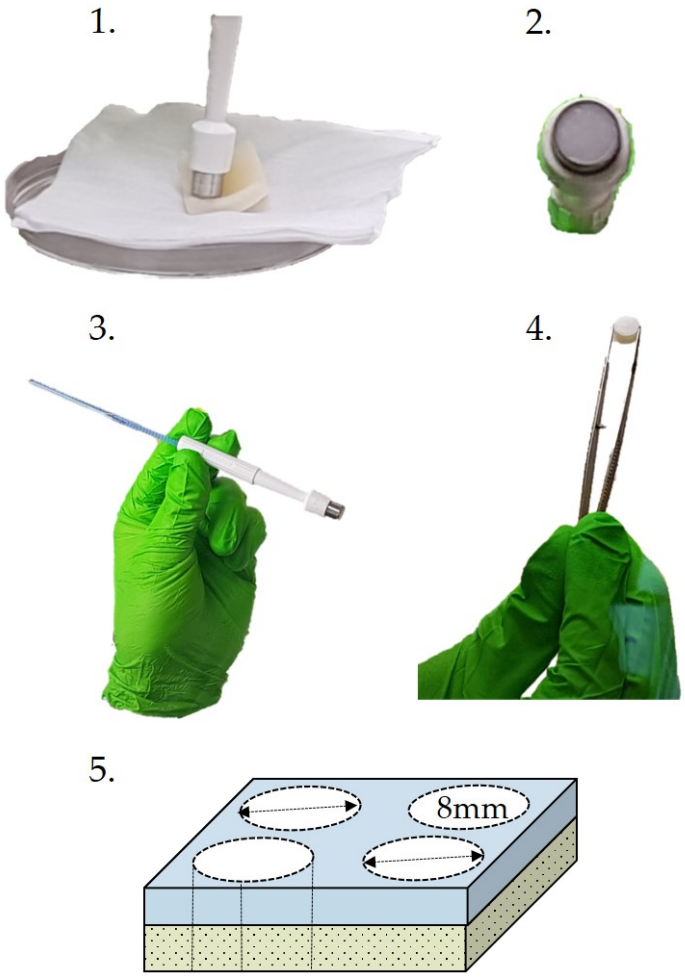

Figure 6.2: Processing of decellularised sheets to generate plugs for culture. 1) 8mm biopsy punch used to extract plug from sheet. 2) Osteochondral plug captured within the biopsy punch is removed 3) using a sterile loop resulting in a 8mm plug. 5) From a 2cm2 sheet it was possible to get 4 plugs which were used as matched pairs.

6.3.2 Seeding chondrocytes onto decellularised plugs using active seeding methods

A C20A4 human chondrocyte cell line (Sigma-Aldrich Ltd) was resurrected and expanded according to Figure 2.2.8. Once confluent, cells were detached and resuspended at a concentration of 10 million/mL. One set of scaffolds was left as an unseeded control (n=4). The three seeding conditions investigated were static seeding, vacuum seeding and a cell injection.

6.3.2.1 Static seeding

Prior to any cell delivery, the scaffolds were left for 30 minutes at 37 °C to dry, allowing maximum potential cell suspension uptake. For the static seeding group, 100 µL of the cell suspension (1 x 10^6 cells per scaffold) was carefully pipetted onto the cartilage surface and incubated for 2 hours at 37 °C, 5% CO_2, to allow the cells time to attach to the scaffold without drying out completely. This was previously optimised (data not shown). Following this the wells were gently filled with 1.5mL of DMEM (10% FBS, 2% P/S, 1% L-glutamine), taking care to not disturb cells on the superficial layer of cartilage.

6.3.2.2 Injection seeding

The second method of seeding that was investigated was via a cell injection (n=4) beneath the superficial zone. For each sample, 100 µL of the cell suspension was aspirated into the syringe and 10 x injections (approx. 10 µL per injection) were administered below the superficial zone into the cartilage.

6.3.2.3 Vacuum seeding

For the third seeding method of vacuum, a pump and vacuum chamber were obtained, set up pictured below in Figure 6.3. Briefly, cell seeding rings were produced from 8mm biopsy punches, and inserted into the top of a sterile eppendorf lid in order to ensure a tight seal. Subsequently 100 µL of the cell suspension was applied to the inside of the seeding ring onto the cartilage surface, and the constructs were placed into a 6-well plate within the vacuum chamber. The pump was then activated until the internal pressure was equal to -90 kPa, at this point the vacuum was rapidly released to atmospheric pressure, this cycle was repeated 6 times. This process was based on previously published research from (Solchaga *et al.*, 2006). Following the vacuum seeding the samples were also incubated for 2 hours at 37 °C, 5% CO_2. After this incubation, the scaffolds were removed from the seeding rings and 1.5 ml of supplemented DMEM was added. Media was replaced for fresh media every 3 days.

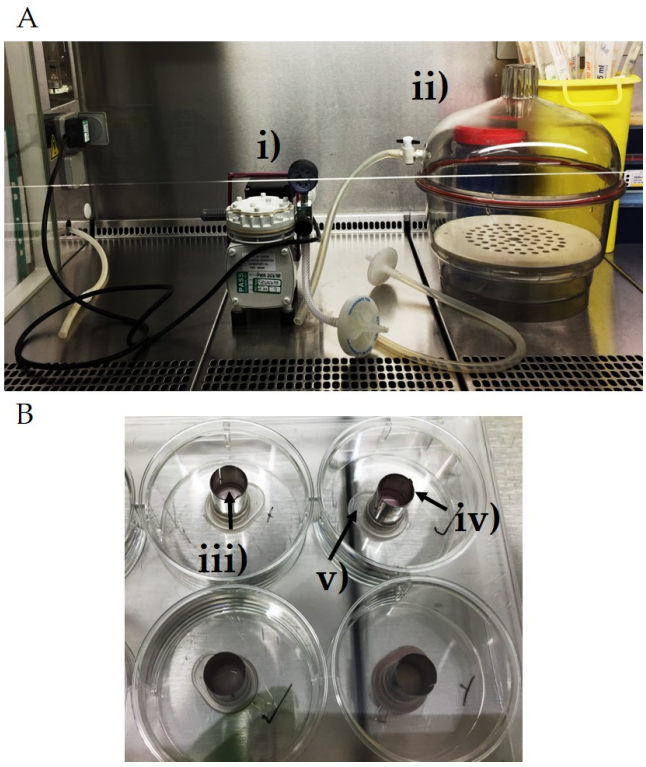

Figure 6.3: Vacuum seeding set up. A) Class II safety cabinet with pump (i) and vacuum chamber (ii). B) Osteochondral plugs (iii) sealed within seeding ring (iv) enclosed within a sterile eppendorf lid (v) to ensure tight fit.

6.3.3 Active seeding methods with decellularised scaffolds with channels

To investigate the effect of creating channels on the seeding efficiency of decellularised cartilage, a 25 gauge (G) needle was used to create 9 channels from the cartilage surface to the top of the bone compartment in decellularised osteochondral scaffolds prepared as in Section 6.3.1.1. This process was performed in an Biological safety cabinet, using sterile forceps to manipulate the scaffolds, and a sterile needle to create the channels.

6.3.3.1 Vacuum and channels

The scaffolds with channels were subsequently seeded using the process described in Section 6.3.2.3 and cultured for 7-days total. Sampling occurred at Day 1 (n = 3) and Day 7 (n = 3), where histology, metabolic activity assessment and DNA quantification were performed as described in the following sections (Sections 6.3.6, 6.3.7, 2.2.7.1).

6.3.3.2 Centrifugation and channels

Scaffolds were produced as described in Section 6.3.1.1. Using sterilised forceps scaffolds were placed in sterilised 1.5 mL eppendorf tubes. 1 x 10^6 C20A4s in 300 µL were delivered to the scaffolds within the eppendorf. The tubes were sealed, and transferred to a centrifuge set at 37°C, where the cell suspension and scaffolds were spun at 1500 RPM for 5 minutes. Following this, the tubes were transferred back to the biological safety cabinet, where any pellet in the tube was resuspended using a P200 pipette. The centrifugation and resuspension process was repeated, until a total of three cycles had been performed. After the final cycle, the scaffolds were removed from the eppendorf and placed into a 48-well plate. The remainder of the tube contents was applied to the surface of the scaffolds before culture for 7-days. Sampling occurred at Day 1 (n = 3) and Day 7 (n = 3), where histology, metabolic activity assessment and DNA quantification were performed as described in the following sections (Sections 6.3.6, 6.3.7 2.2.7.1). The controls in this study were untreated scaffolds (n = 3), statically seeded scaffolds (n = 3), statically seeded scaffolds with channels (n = 3) and channelled scaffolds seeding via centrifugation method (n = 3).

6.3.4 Matrix Disruption methods

6.3.4.1 Collagenase digestion

Collagenase was diluted at desired stock concentration of 125 units.mL^{-1} in DMEM with 1% P/S. Prior to storage at -20°C, the solution was passed through a sterile filter.

Two separate collagenase digestions were performed, the aim of the first digestion was to investigate the effect of lower concentrations of collagenase on decellularised cartilage. Following on from this, the second digestion investigated a higher concentration. The experimental method for each digestion is described below.

1. Collagenase was diluted to 62.5 and 31.25 units.mL^{-1} solutions. Decellularised

scaffolds (n=6) were incubated with either the high, low or no collagenase solution for 30 minutes at 37 °C. To stop the digestion, scaffolds were subject to 3 x 5 minute washes with 4 °C sterile PBS. These scaffolds were divided into two groups for 1 day and 16 day follow up, as well as a cell only (n=3) and untreated (n=3) control groups. Day 1/16 scaffolds in the high and low collagenase group, as well as the cell only control were seeded with 1 million C20A4 cells/scaffold, and culture was performed as described in Figure 6.3.2. At the desired timepoint scaffolds were processed for LIVE/DEAD staining (as described in Section 6.3.5, H&E staining (Sections 2.2.6.1) and alamarBlue cell viability assay (Section 6.3.7).

2. Decellularised plugs were extracted (n=24) from the sheets and divided into two groups (n=12; n=12). Within each groups scaffolds were either left untreated (n=3), or incubated with 125 units.mL^{-1} collagenase solution for 45 mins (n=3), 90 mins (n=3) or 120 mins (n=3). One group (12 scaffolds total) was agitated during the incubation and the other was left static (12 scaffolds total). The reaction was terminated as described above, and the scaffolds were processed for H& E staining (Section 2.2.6.1).

6.3.4.2 Lyophilisation

6.3.4.2.1 Optimisation Decellularised plugs (n=3) were extracted from a decellularised sheet (Section 6.3.1.1), and placed into pre-weighed sterile bijous in a Class II safety cabinet. The weight of the tube and scaffold was recorded. The scaffolds were placed into the freeze drier (ModulyoD, Thermo Savant), and the weight was recorded and photos were taken every 30 minutes until the weights reached a consistent value. The weight loss (mg) was plotted against time, and a hyperbola was fit with the data in order to interpolate the time point at which 25, 50, 75 and 100% of water was removed.

According to the time taken to reach varying degrees of lyophilisation determined previously, decellularised scaffolds were lyophilised to 0% (n=3), 25% (n=3), 50% (n=3), 75% (n=3) and 100% (n=3) lyophilised. Post freeze drying the bijou lids were tightened to prevent uptake of moisture. These scaffolds were subsequently seeded

with 1 million cells as described in Section 6.3.2. The following day (24 hours later), scaffolds were taken out of culture and processed for LIVE/DEAD and alamarBlue viability measurements.

Data shown in Figure 6.20 demonstrated that 100% lyophilisation with a higher media volume was the only condition which caused any disruption to the tissue so this method was taken forward. Therefore, subsequent optimisation studies were performed with this scaffolds type with the analysis described in sections (Sections 6.3.6, 6.3.7, 2.2.7.1).

6.3.5 Live/Dead Viability Assessment of C20A4 cells seeded onto decellularised plugs

Following all aforementioned seeding methods, the scaffolds were incubated in supplemented DMEM at 37 °C, 5 % CO_2 for 24 hours. After this time period the scaffolds were bisectioned, and using a sterile scalpel a thin section was removed from the central cut surface (Figure 6.4). This section was subsequently incubated in DMEM with ethidium homodimer-1 (1:2000) and calcein-AM (1:4000) from a LIVE/DEAD cell viability kit (ThermoFisher Scientific, USA) for 1 hour.

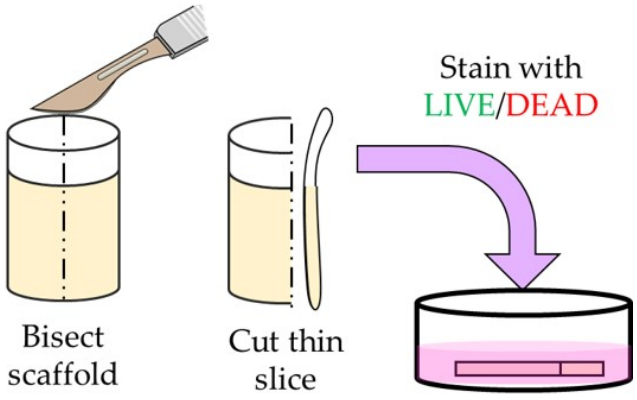

Figure 6.4: Illustration demonstrating method of bisecting scaffold, and removal of a section for LIVE/DEAD staining.

Following staining, sections were subject to 3 x 5 minute PBS washes, prior to mounting onto an optical bottom petri dish for visualisation on the confocal microscope as described in Section 2.2.1.4. In addition, images were captured in a tile scan spanning the width of the scaffold and the depth of the cartilage to the subchondral

bone. As well as this, the several images were taken in the Z-position in order to encompass the 3D distribution of seeded cells. Images were processed on Zen Image processing software (Zen black, Zeiss, DE) and subject to a maximum intensity projection to bring all Z-positions into one frame.

6.3.6 Assessment of cell penetration

As well as LIVE/DEAD viability staining, sections of cell seeded tissue were paraffin wax embedded as described in Section 2.2.5 and stained with haematoxylin and eosin Section 2.2.6.1. In order to distinguish between reseeded cells and any residual cell debris from decellularisation, C20A4's were labelled with Vybrant Dil cell-labelling solution (Thermo Fisher Scientific, USA). Briefly, cells were diluted to 1 million cells/mL, and 5 µL of Vybrant cell labelling solution was added per mL and incubated for 20 minutes at 37 °C and 5 % CO_2. The cells were subsequently washed via 3 cycles of; centriguation at 1500 RPM for 5 minutes, followed by resuspension in warm media. The location of the labelled cells was determined via fluorescence microscopy. Briefly, following paraffin wax embedded and sectioning, section were dewaxed, rehydrated and mounted with a cover slip and fluorescence mountant. Sections were imaged at 553/570 nm (excitation/emission) with brightfield to contextualise the location within the scaffold.

6.3.7 AlamarBlue viability assessment of seeded decellularised matrices

Prior to viability assessment, an incubation time optimisation was performed on scaffolds seeded with C20A4 cells, following protocol detailed in Section 5.3.2.1. On the day of viability assessment, the media was replaced with fresh media, and 150 µL (10%) of alamarBlue reagent was added. The cell seeded scaffolds were incubated for 24 hours at 37 °C and 5 % CO_2. The following day, 100 µL of media was removed and placed into a 96-well plate. The absorbance was read at 570 and 600 nm and the reduction of alamarBlue was determined using the equation described in Section 5.3.2.1.

6.3.8 GAG delivery to osteochondral matrices

Lyophilised decellularised scaffolds (n = 3) were prepared as described previously (Figure 6.20). Prior to GAG delivery, scaffolds were placed in 1.5 mL microcentrifuge tubes. A 10 mg.mL^{-1} P_{11}-8/CS solution was made according to Section 5.3.1.2, and 500 µL was applied to the cartilage surface of each scaffold. Immediately, the microcentrifuge tubes were sonicated for 10 minutes in order to prevent gel assembly. Following this, scaffolds were incubated with the gel solution overnight at 37 °C. The control for this study was decellularised scaffolds, which were lyophilised and rehydrated in media alone.

6.3.8.1 Indentation testing

Following overnight incubation in P_{11}-8/CS (n = 5) or media (control) (n = 5), scaffolds were subject to indentation testing, following an identical procedure to that described in Section 4.3.5.3. Data was transformed to give percentage deformation data.

6.3.8.2 Fixation in EDC

In order to rapidly fix as much of the P_{11}-8/CS in the decellularised plugs as possible, a short fixation period was required. Therefore, 1-ethyl-3-(3-dimethylaminopropyl)carbodiimide hydrochloride (EDC) (Sigma Aldrich, USA) was used as a fixative. A working solution was made up immediately before use containing 0.57 g of EDC, 0.07 g of N-Hydroxysuccinimide (NHS) (Thermo Fisher Scientific, USA) and 0.22 g of 2-(N-morpholino)ethanesulfonic acid (MES) (Sigma Aldrich, USA). The mixture was reconstituted in 20 mL of deionised water.

Prior to use with the seeded scaffolds an optimisation took place with P_{11}-8/CS gels alone. In each cryo-mould, 200 µL of P_{11}-8/CS was pipetted into the centre, and 1 mL of EDC fixative or NBF was added. The samples were kept at 4°C for the length of the fixation. After intervals of 30, 60, 120, 180 minutes the fixative was removed, optimal cutting temperature compound (OCT) was added and the samples were frozen at -70 °C for at least an hour.

6.3.8.3 Cryosectioning

The cryostat (Leica, USA) was set to - 30 °C, and samples were quickly removed from the -70 °C and mounted onto the stubs within the cryostat using a drop of OCT. The sections were cut on the cryostat, and placed onto the slides which were kept at - 30 °C until use.

6.3.8.4 Safranin O staining of cryoembedded samples

Once all sections had been cut, the slides were left to incubate at room temperature for 10 minutes to melt the OCT. Following this sections were stained as per Section 2.2.6.2, and visualised on the light microscope.

6.3.8.5 Fluorescent peptide solution formulation

P_{11}-8 with a conjugated Fluorescein isothiocyanate (FITC) group was manufactured and purchased from CS-Bio. A working solution was made up a concentration of 10 mg.mL^{-1} in distilled water. When peptide was formulated for gel delivery to the scaffolds, the working solution was applied prior to delivery to a final concentration of 1 in 50. The FITC-tagged peptide was subsequently delivered as described previously in Section 6.3.8.

6.3.8.6 Fluorescent microscopy

Cryosectioned samples were mounted onto slides, and left at room temperature for 10 minutes before mounting with fluorescent mounting media. The samples were then visualised on a fluorescence microscope under the FITC (517 nm) channel.

6.4 Results

6.4.1 Initial cell seeding optimisation

Decellularised scaffolds seeded statically (Figure 6.5) appeared to have attached homogeneously over the articular cartilage surface, and stained positively as LIVE cells after 24 hours. Instead of penetration deep into the middle and deep zones of the cartilage, the cells had stacked on top of each other on top of the superficial layer. The scaffolds which were vacuum cycled post cell seeding, also showed a thick band of viable chondrocytes, indicating that the vacuum applied did not effect cell viability. However, the cells were not evenly distributed and were located towards the edge of the scaffold, and this method did not appear to improve cell penetration as hypothesised.

The injected samples demonstrated minimal LIVE staining, with the majority of cells uptaking the ethidium dye. From the H&E sections, the channels created by the 30G needle are visible, and chondrocytes can be seen lining this channel. In terms of penetration, cells were visible in the middle and deep zones, however, these cells were not viable.

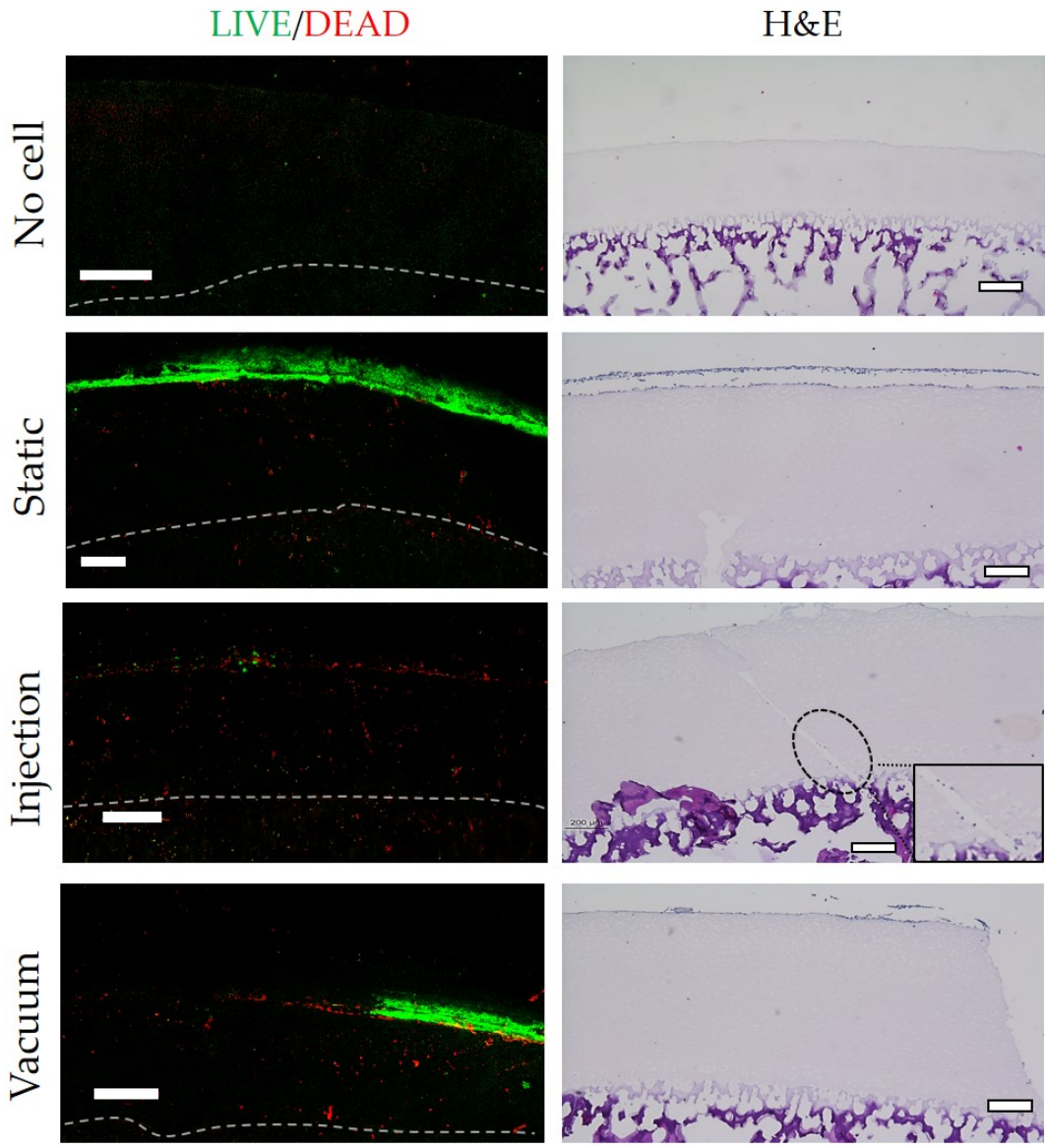

Figure 6.5: Decellularised osteochondral scaffolds seeded with C20A4 cells. Cells were delivered statically, injected or via vacuum seeding. These scaffolds were stained with A. LIVE/DEAD or B. H&E. White dotted line represents the boundary between articular cartilage and subchondral bone. Scale bars = 500 µm

6.4.2 Active cell seeding methods

Following the initial cell seeding attempt, it was clear that methods beyond static seeding would be required, and two strategies were investigated. The first of these was described as 'active seeding' whereby forces such as centrifugation and vacuum creation would be investigated. The second approach was described as 'matrix disruption' whereby the cartilage matrix was disrupted using either enzymatic digestion with collagenase or via lyophilisation overnight. The optimisation and results

from these attempts are detailed below, beginning with active seeding methods, followed by matrix disruption.

6.4.2.1 Vacuum

Following the failed vacuum attempt in (Figure 6.5), the ability of vacuum to improve recellularisation of scaffolds was investigated further. In this comparison the samples were pre-treated with channels to provide a greater porosity for cell penetration following application of a vacuum.

In the histology (Figure 6.6), the seeded cells can be observed on the surface of the cartilage in the statically seeded samples. However, in the samples with channels alone cells can be observed below the surface within the channels at Day 1 and 7. The same can be observed in the channels with vacuum at Day 7, but less prevalent at Day 1.

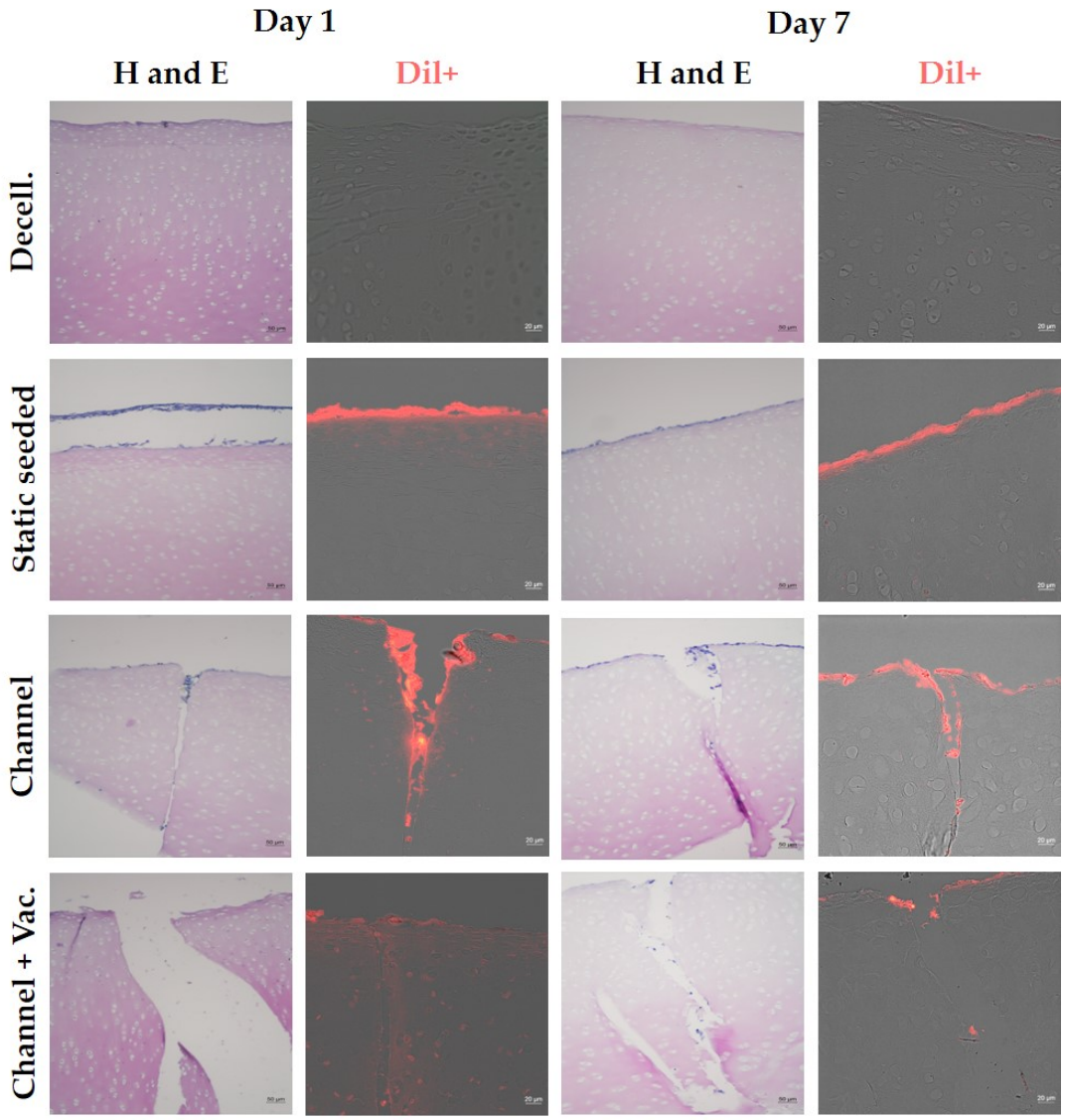

Figure 6.6: Decellularised cartilage seeded with chondrocytes, with channels and a combination of channels and vacuum. Scaffolds were untreated, seeded statically, seeded statically with channels and seeded with vacuum treatment with channels. Samples were seeded with Dil+ labelled chondrocytes, and cultured for 7-days with samples taken at Day 1 (n = 3) and Day 7 (n = 3). Sections were stained with H& E or imaged under fluorescence microscopy for Dil+ cells. H& E scale bars = 50 µm and Dil+ = 20 µm

Total DNA content was used as an approximation of relative cell delivery. Statically seeded samples had a significantly higher DNA content than the decellularised alone samples (Figure 6.7). The application of a vacuum caused an increase in DNA content compared with the channels alone, however, this difference was not significant. However, the channel alone samples were significantly lower than the statically seeded samples. The same trend observed at Day 1 was replicated at Day 7, and there were no significant differences between the time points.

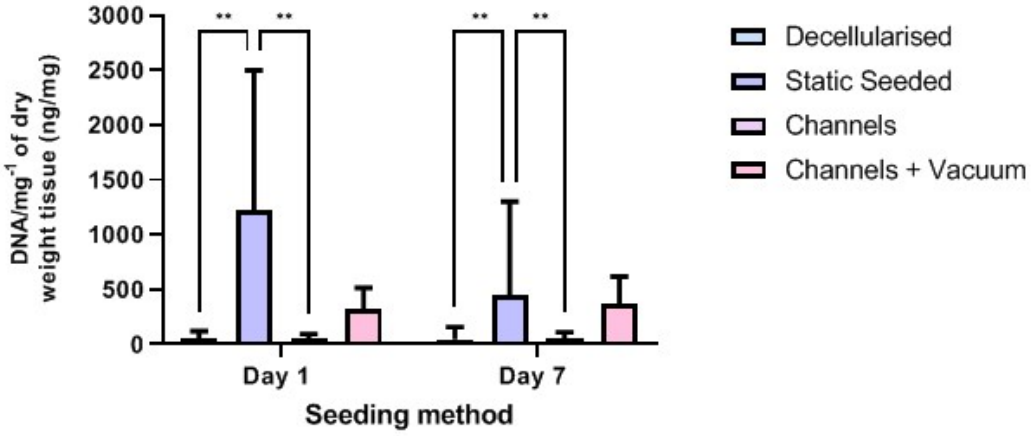

Figure 6.7: DNA content in decellularised cartilage seeded with chondrocytes, with channels and a combination of channels and vacuum. A decellularised alone sample was used as the negative control (n =3 per timepoint). Samples size for all groups = 3. Errors bars = 95% C.I. 1-way ANOVA performed, with a post-hoc Tukey's test. ** = $p < 0.005$.

Overall, it appeared that although application of a vacuum showed a trend of improved cell penetration, it was difficult to discern any significant improvement over treatment with channels alone.

6.4.2.2 Centrifugation

The effectiveness of centrifugal force alongside channels was also assessed against static and channel alone controls. The histology in Figure 6.8 demonstrates that where channels were present the chondrocytes occupied the length of the channel, at a relatively low cell density. Qualitatively, there appeared to be no difference in cell density between the samples with channels with and without centrifugation. Furthermore, between Day 1 and Day 7 there was no discernible difference.

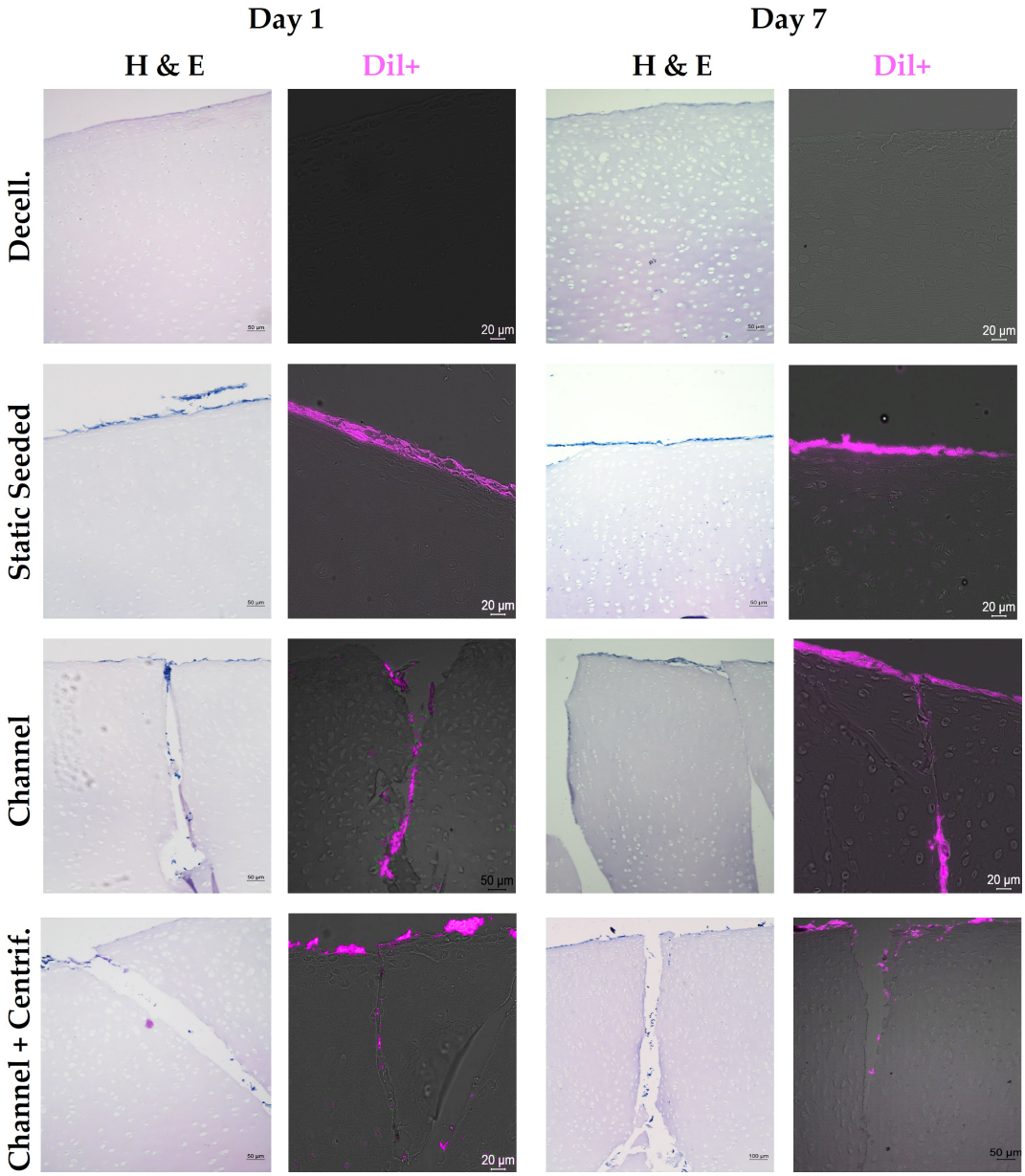

Figure 6.8: Decellularised cartilage seeded with chondrocytes, with channels and a combination of channels and centrifugation. Untreated decellularised scaffolds were used as a negative control. H& E scale bars = 50 µm and Dil+ = 20 µm.

The quantitative data from the total DNA assay demonstrated the same trend however, with no significant differences between Day 1 and Day 7 measurements, as well as no differences between the three seeded scaffold groups. However, at Day 1 there was a significantly higher total DNA content in the static and centrifuged samples versus the decellularised control (Figure 6.9). Although there was no significant difference there appeared to be a reduction in DNA at Day 7 versus Day 1 in both the statically seeded and centrifuged samples, likely a result of cell removal during

media changes.

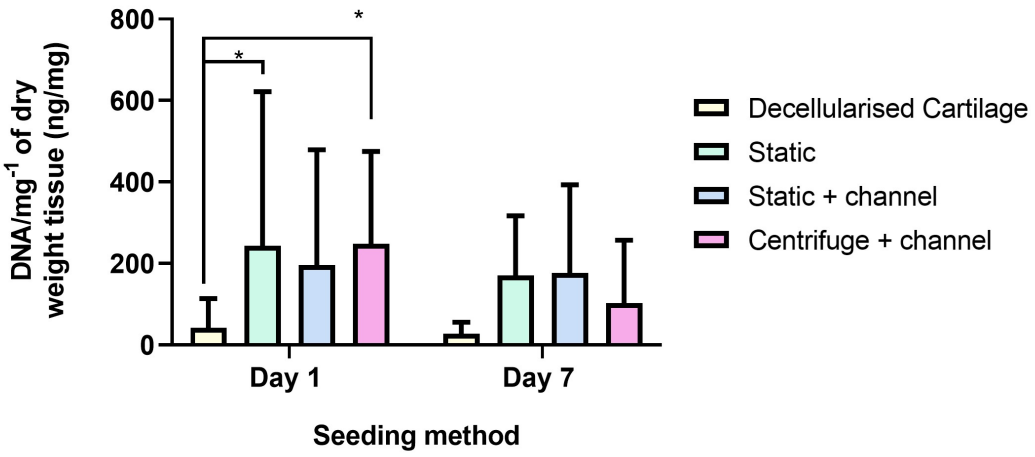

Figure 6.9: DNA content of decellularised cartilage seeded with chondrocytes (n = 3), with channels (n = 3) and a combination of channels and centrifugation (n = 3). Untreated decellularised scaffolds were used as a negative control. Errors bars = 95% C.I. 1-way ANOVA performed, with a post-hoc Tukey's test. ** = $p < 0.05$.

Furthermore, from the viability data (Figure 6.10) there appeared to be no significant difference in the metabolic activity of chondrocytes seeded on any of the three scaffold groups. However, once the viability was normalised to the DNA content (Figure 6.11), the viability was higher for the centrifuge samples at Day 7, however, this increase was not significant as a result of variable data.

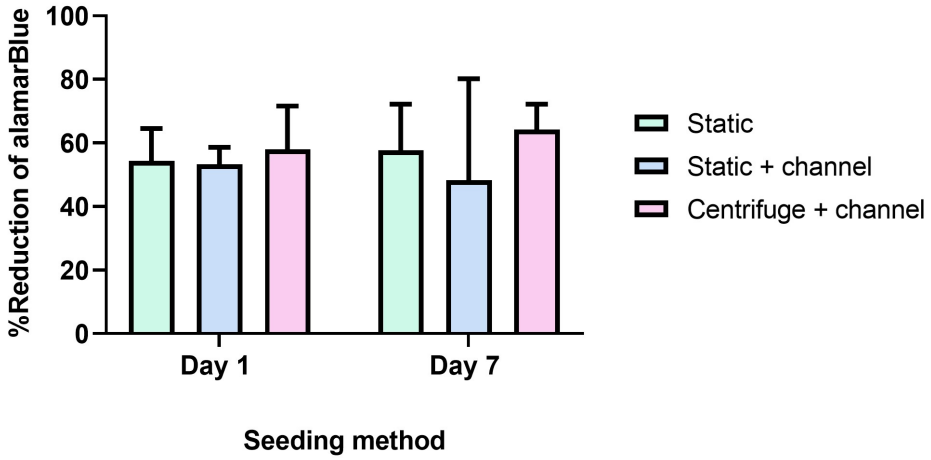

Figure 6.10: Metabolic activity of chondrocytes seeded onto decellularised cartilage with channels and a combination of channels and centrifugation. Percentage reduction calculations were subject to an Arc-Sin transformation for statistical analysis. Error bars = 95% C.I. 2-way ANOVA performed, with a post-hoc Tukey's test.

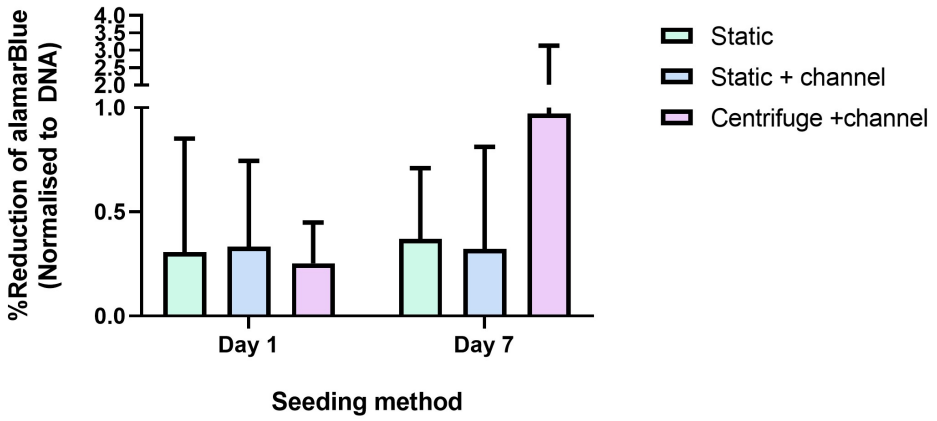

Figure 6.11: DNA content in decellularised cartilage seeded with chondrocytes, with channels and a combination of channels and centrifugation. Percentage reduction calculations were subject to an Arc-Sin transformation for statistical analysis. Error bars = 95% C.I. 2-way ANOVA performed, with a post-hoc Tukey's test.

6.4.3 Matrix disruption

As mentioned previously, the second approach that was investigated for the improvement of cell seeding was 'matrix disruption'. Enzymatic disruption with a several collagenase concentrations was optimised and investigated, alongside varying degrees of lyophilisation.

6.4.3.1 Low concentration collagenase treatment

In order to improve cell penetration into the cartilage ECM, collagenase (62.5 and 31.25 units.mL^{-1}) was applied to the matrix to digest the collagen fibrils. The collagenase digested samples do not appear to show any surface fibrillation (Figure 6.12A), or disruption to the collagen matrix at these concentrations. In terms of penetration into the scaffolds, it appeared initially from the the LIVE/DEAD images that in both Day 1 and Day 16, both collagenase treatments allowed for cell penetration into the regions digested by the enzyme. However, this cell penetration was not seen in the H& E images. It was suspected that these masses were artefacts from the sectioning process prior to LIVE/DEAD staining and imaging. Both the LIVE/DEAD and H& E images show good cell attachment to the superficial zone of the cartilage at both day 1 and 16.

There appeared to be a significant reduction in cell viability at Day 1 for scaffolds treated with both collagenase concentration. No significant difference in cell viability was observed between the lower and higher collagenase concentration. By day 16 however, significant increases in viability were seen compared with the day 1 viability measurements for both collagenase digested samples, indicating a recovery of the initial reduced values.

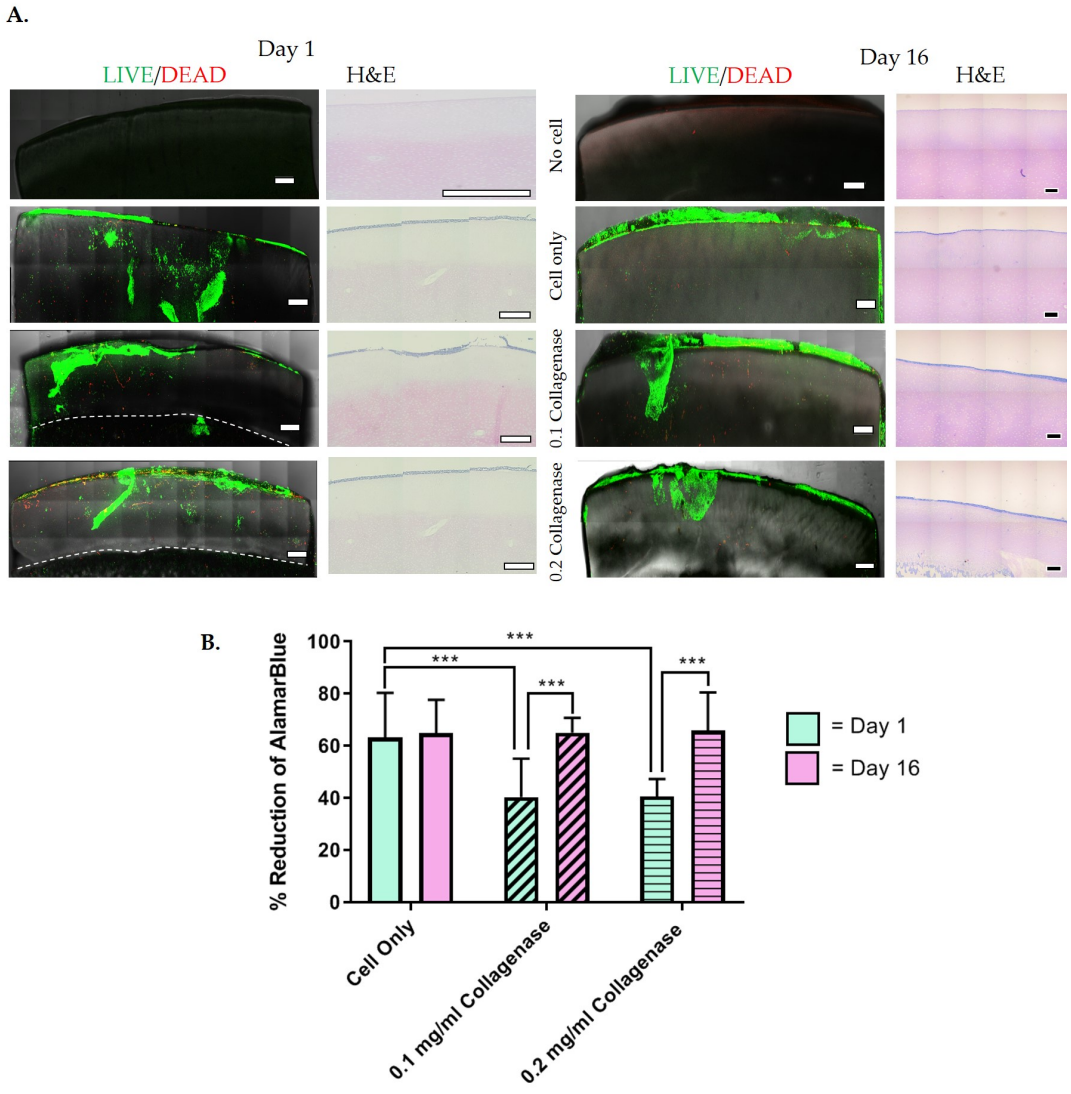

Figure 6.12: Decellularised osteochondral scaffolds seeded with C20A4 cells. Cells were delivered statically onto scaffolds treated with 0, 0.1 and 0.2 mg.mL^{-1} collagenase solution for 30 minutes. Scaffolds were left to culture for 1 and 16 days. A) These scaffolds were stained with LIVE/DEAD and H&E. White dotted line represents the boundary between articular cartilage and subchondral bone. White scale bars = 500 µm and black scale bars = 200 µm. B) Chondrocyte viability post-recellularisation was also determined by % reduction of AlamarBlue of C20A4 chondrocytes, seeded onto decellularised osteochondral matrices (n=3). Percentage reduction calculations were subject to an Arc-Sin transformation for statistical analysis. Two-way anova with Tukey's multiple comparisons test was performed on the transformed data (***=p<0.001).

6.4.3.2 Higher concentration collagenase treatment

Upon treatment with a higher collagenase concentration, all staining methods show a disruption to the superficial zone collagen structure after 90 minutes static and agitation treatment (Figure 6.13). The Sirius Red stain viewed under both TL and PL shows an ablation of the superficial zone staining, which is reflected in the H and E staining. Interestingly, the collagenase treatment also causes a removal of the GAGs from the matrix by 135 minutes as seen in the Saf O/Fast Green staining. When comparing the agitated and static collagenase treatment there does not appear any significant difference in amount or depth of matrix degradation.

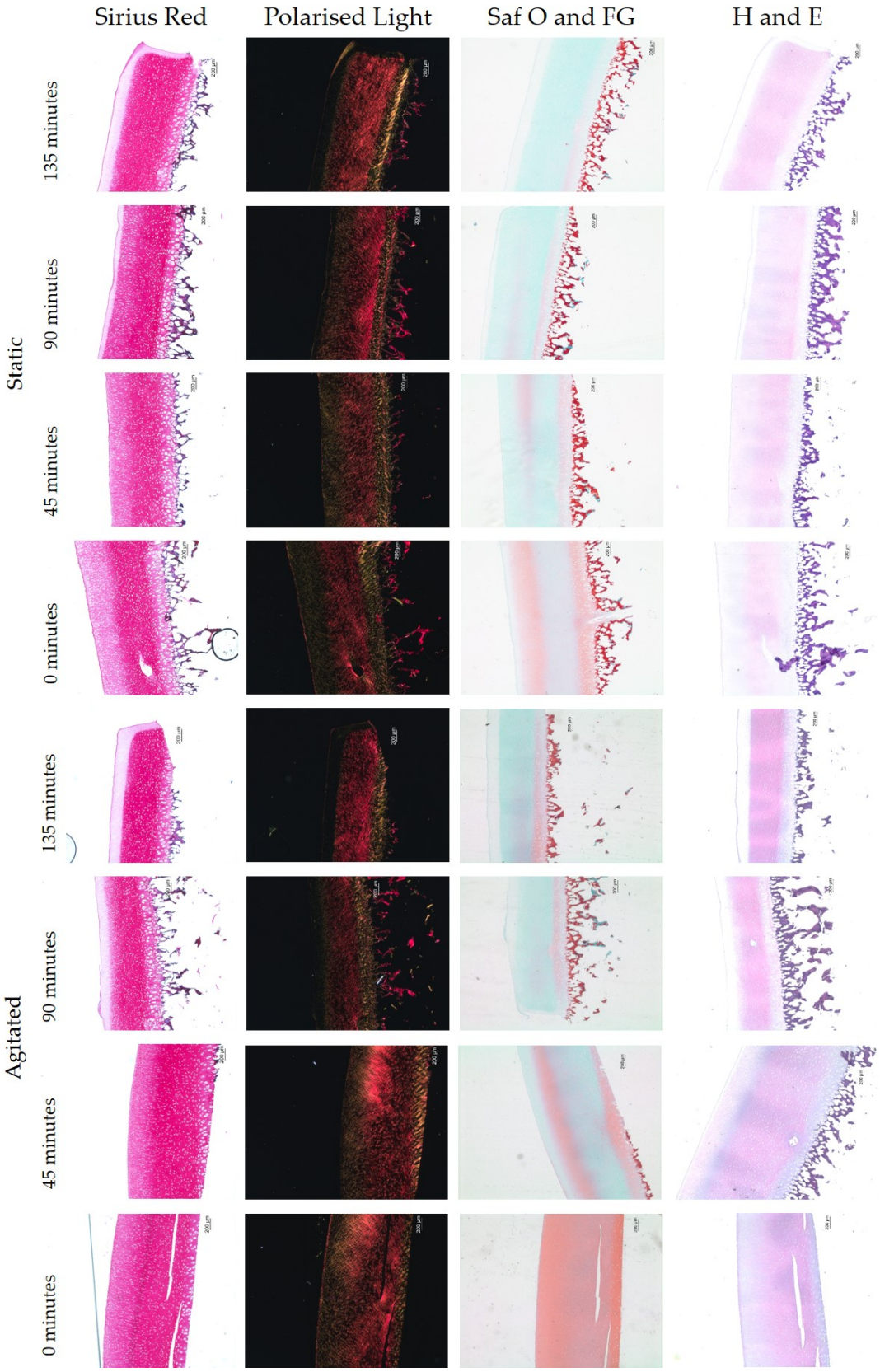

Figure 6.13: Histological assessment of decellularised osteochondral scaffolds treated with 1 mg.mL^{-1} collagenase Scaffolds were treated for 0, 45, 90 and 135 minute intervals with and without agitation. Scale bars = 200 µm

Following the initial optimisation, conditions of 1mg.mL^{-1} collagenase for 90 minutes without agitation were used to pre-treat scaffolds prior to cell seeding. At Day 1, the statically seeded samples resemble previously seen results, with the formation of a thin band of cells on top of the superficial layer (Figure 6.14). This treatment showed an increase over the decellularised sample in terms of the total DNA content (87 ng.mg^{-1} versus 456 ng.mg^{-1}) (Figure 6.15). However, this difference was not statistically significant. Despite the presence of cell remnants within the decellularised control samples, the DNA results indicated a decellularised sample. The collagenase treated samples at Day 1, appeared to have a larger band of cells on the surface of the tissue, and an increased density of cell nuclei within the superficial and middle zones of the cartilage from the H and E and Dil + images in Figure 6.14. This observation is supported by a greater DNA content of 1164 ng.mg^{-1} of tissue. Despite the disruption to the collagen matrix, the collagenase treatment appeared to have no effect on the metabolic activity of the seeded chondrocyte compared with the statically seeded samples (Figure 6.16).

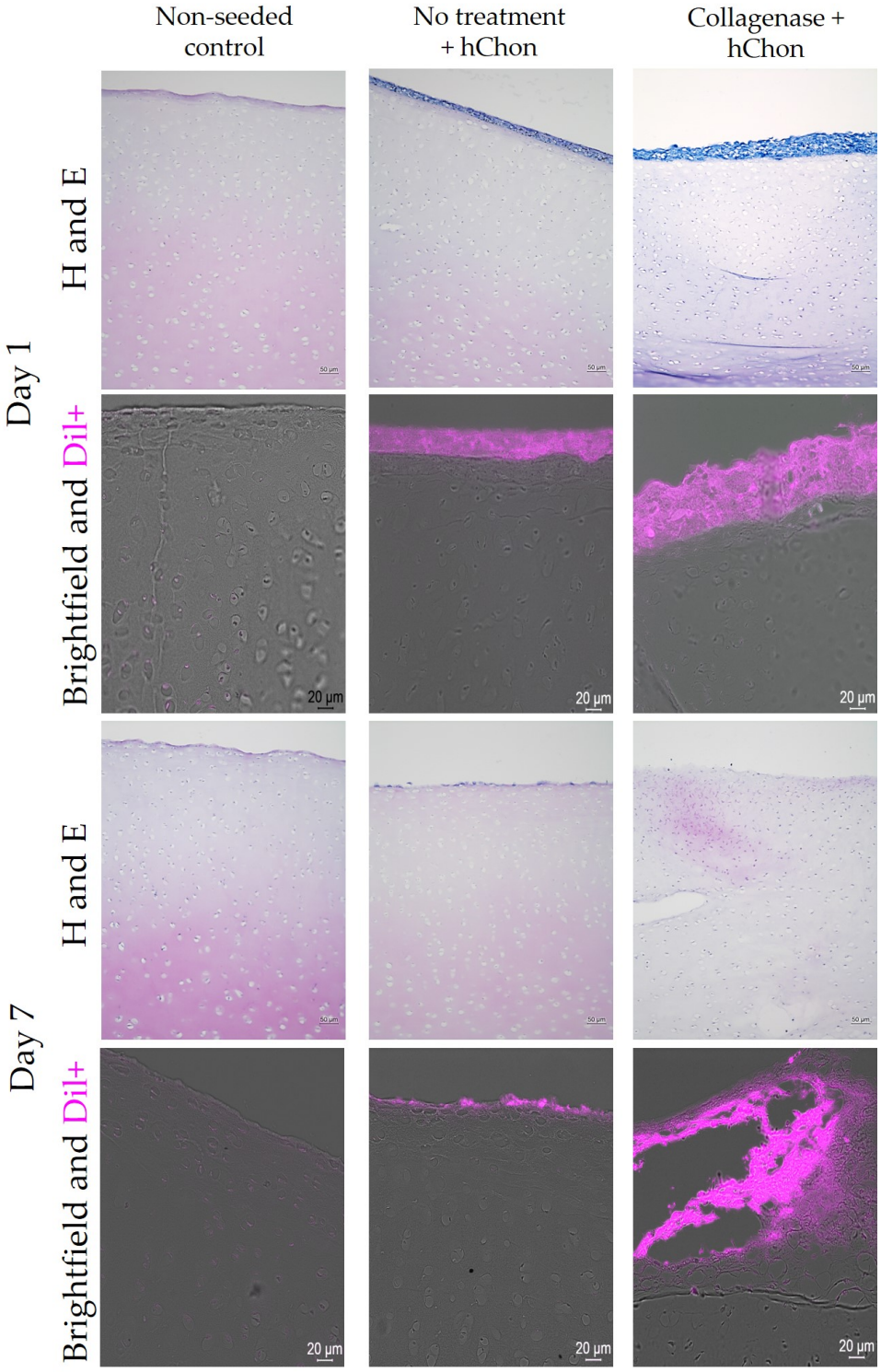

Figure 6.14: Distribution of chondrocytes within decellularised matrices with and without collagenase treatment at Day 1 and Day 7. Sections were either stained with H and E, or visualised under fluorescence for Dil+ chondrocytes. Scale bars = 50 µm (H and E) and 20 µm (Dil+)

By Day 7, in both static and collagenase treated samples the prominent cell layer on the superficial zone at Day 1 (Figure 6.14) was no longer visible. In the statically

seeded sample, there are several cells on top of the superficial zone, but still no penetration into the deeper zones of cartilage. However, in the H & E images of the collagenase treated samples, there appeared to be a drastic increase in the cell content, especially in the superficial layer. The Dil + images illustrated the same observation, however, the collagenase treated sample was more distorted, possibly an artefact of the histology process. The DNA content of the collagenase treated samples at Day 7 (Figure 6.15), reflected this qualitative data showing significantly higher DNA content compared to decellularised and untreated controls. The mean total DNA content of the collagenase treated samples was 1926.8 ng.mg^{-1}, which surpass values observed previously in native cartilage samples (Figure 4.7).

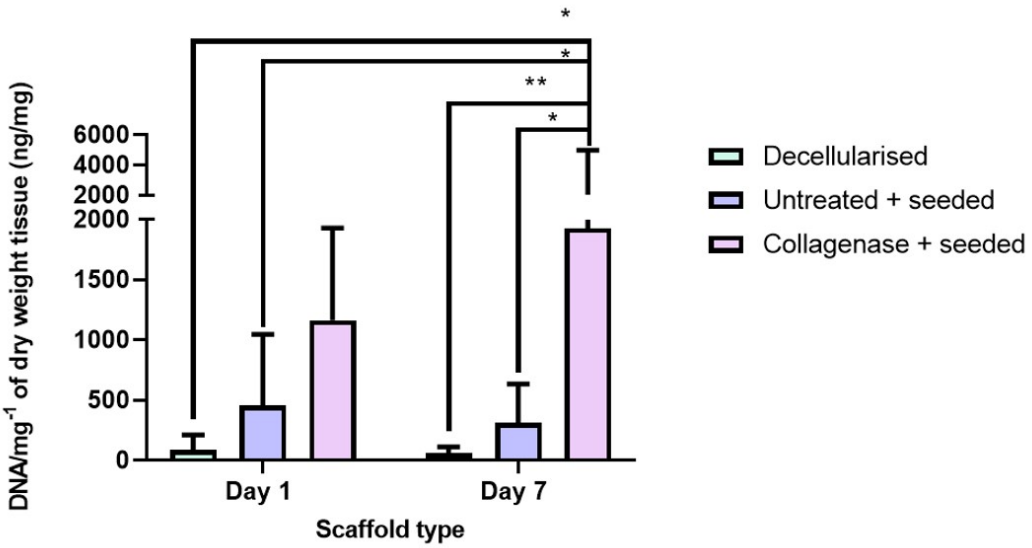

Figure 6.15: Total DNA content of decellularised (n =3), statically seeded (n = 3) and collagenase treated + seeded (n = 3) at Day 1 and Day 7. Error bars = 95% C.I. 2-way ANOVA performed with post-hoc Tukey's multiple comparisons test. * = p <0.05, ** = p <0.005.

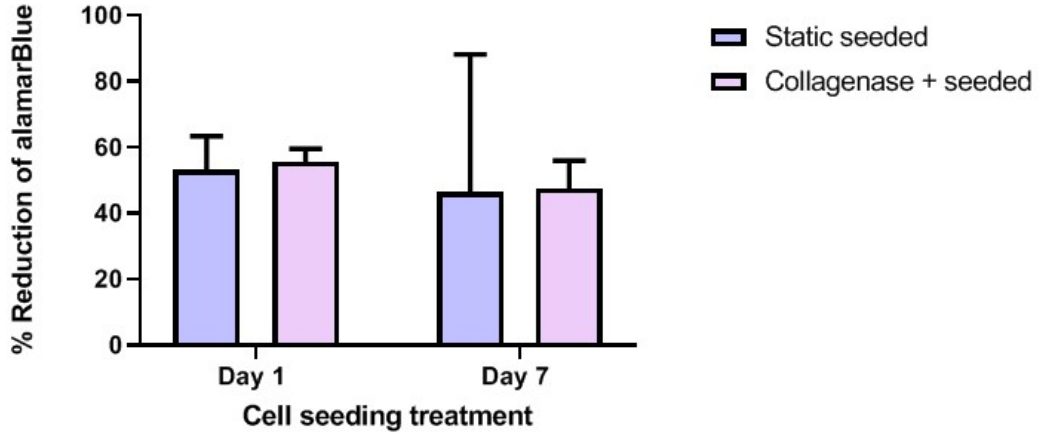

Figure 6.16: Metabolic activity of chondrocytes seeded on decellularised matrices with (n = 3) and without (n = 3) collagenase treatment. 2-way ANOVA performed on Arc-Sin transformed data, followed by Sidak's post-hoc multiple comparisons test.

6.4.3.3 Lyophilisation

6.4.3.4 Initial optimisation

Scaffold lyophilisation was another method which was investigated, for the possibility of increasing cell penetration and distribution throughout all layers of the cartilage. The hypothesis was that lyophilisation would disrupt the collagen fibrils allowing for an increase in porosity, as well as increasing the hydration potential in the scaffold and hence it's ability to soak up cell suspension.

Firstly, a gradient of lyophilised scaffolds was generated through tracking weight loss over time (Figure 6.19A). It was determined from interpolation that scaffolds were completely lyophilised after 147 minutes. Macroscopically, after complete lyophilisation the cartilage had compacted and in some areas had contracted on top of the subchondral bone (Figure 6.17).

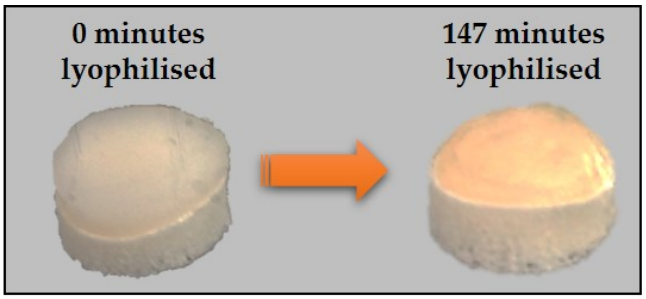

Figure 6.17: Macroscopic comparison of untreated and lyophilised decellularised scaffolds.

6.4.3.5 Histological examination of lyophilised decellularised cartilage compared with native and decellularised tissues

Following lyophilisation, scaffolds were first examined histologically to determine the consequence on the extracellular matrix structure following rehydration. Below in Figure 6.18 the Sirius red staining under polarised light indicates a maintenance of the native collagen alignment in both native, decellularised and lyophilised samples. Specifically, the bright birefringence in the superficial zone was maintained across all samples. It appears from the decellularised and lyophilised samples that there was a slight reduction in collagen density in the middle zone compared with the superficial and deep zones. As the lyophilised and decellularised samples were matched, it is likely that this was a result of the decellularisation rather than lyophilisation. The Safranin O and Fast Green samples showed a high GAG concentration in the native sample, which was drastically reduced in decellularisation as reported previously in Figure 4.9. The GAG staining pattern in the lyophilised sample appeared to stay relatively similar to the decellularised sample, possibly exhibiting slightly increased GAG loss. Finally the H&E demonstrated a removal of cells between the native and decellularised samples, and a lack of disruption to the gross architecture of the cartilage.

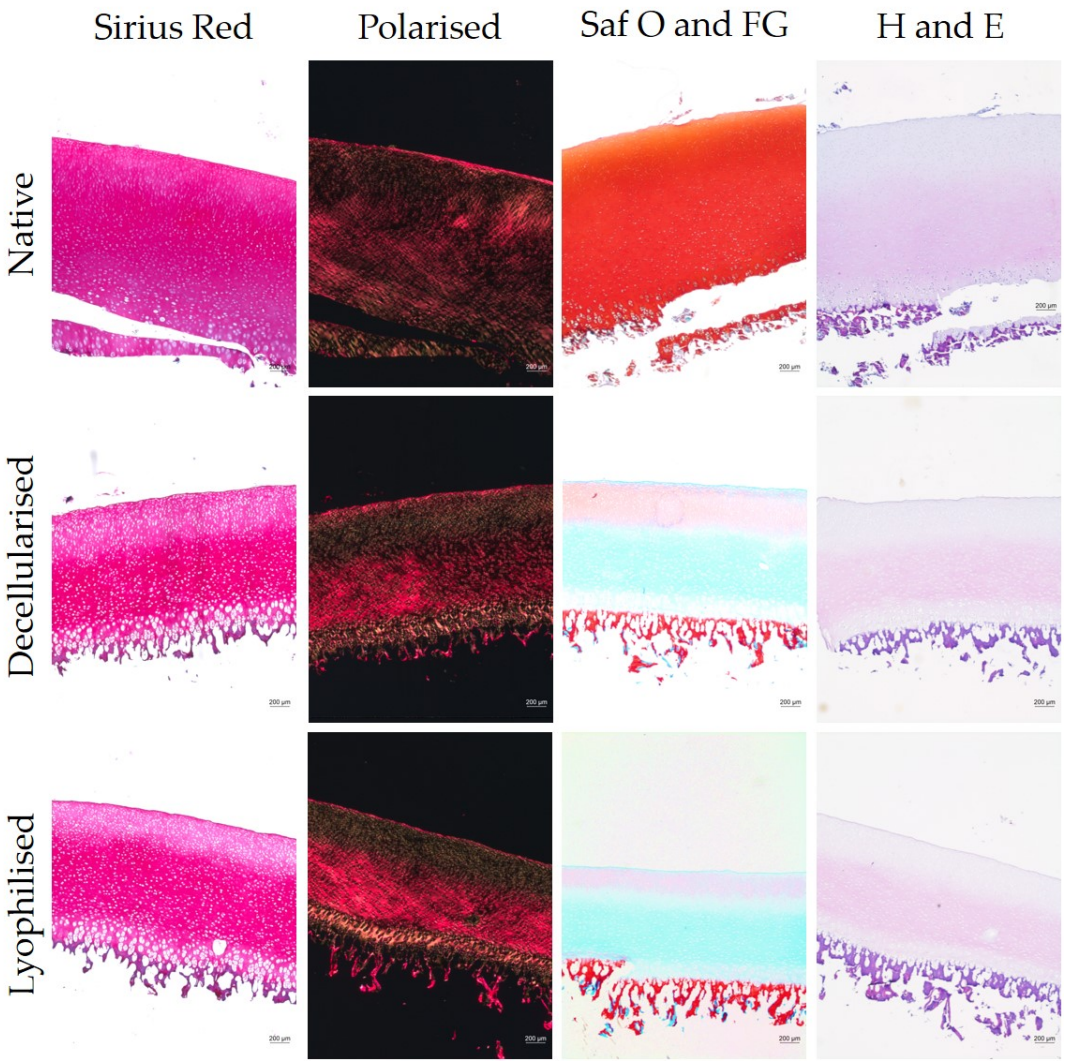

Figure 6.18: Histological comparison of native, decellularised and lyophilised decellularised cartilage. From left to right, paraffin wax embedded samples were stained with sirius red and observed with transmitted and polarised light, as well as safranin O and fast green and haematoxylin and eosin staining. Scale bar = 200 µm.

6.4.3.6 Initial seeding of variably lyophilised scaffolds

Following lyophilisation, the scaffolds were seeded with C20A4 cells. It was observed that the higher the degree of lyophilisation the faster the cell suspension was taken up. Notably by 2 hours of incubation with the initial cell suspension, the 75% and 100% scaffolds had a 'dry' superficial layer compared to the lower lyophilised samples which still maintained a cell suspension droplet on their surface. Interestingly, on rehydration with media, it was observed that the lyophilised scaffold recovered their pre-lyophilisation macroscopic appearance.

The observation that the 75% and 100% groups had dried out after only 2 out of 3 hours of cell attachment, showed significant reductions in viability compared to 0, 25 and 50% lyophilised scaffolds (Figure 6.19B). This pattern was observed in the LIVE/DEAD staining as well (Figure 6.19C). The 0% and 50% samples had a homogenous green band of viable cells on the superficial layer, with minimal penetration. However, the 75% and 100% groups show little to no viable cells, accompanied by a low concentration of red non-viable cells. This result may indicate problems with attachment due to lower total cells (viable or non-viable) observed in the 75% and 100% groups. Furthermore, it appears that the viability of any cells that had attached was compromised by the dry nature of the scaffold.

The LIVE/DEAD images for the 75% and 100% samples appear to show the presence of cells in the middle and deep layers of the cartilage, however, further characterisation would be necessary to determine this.

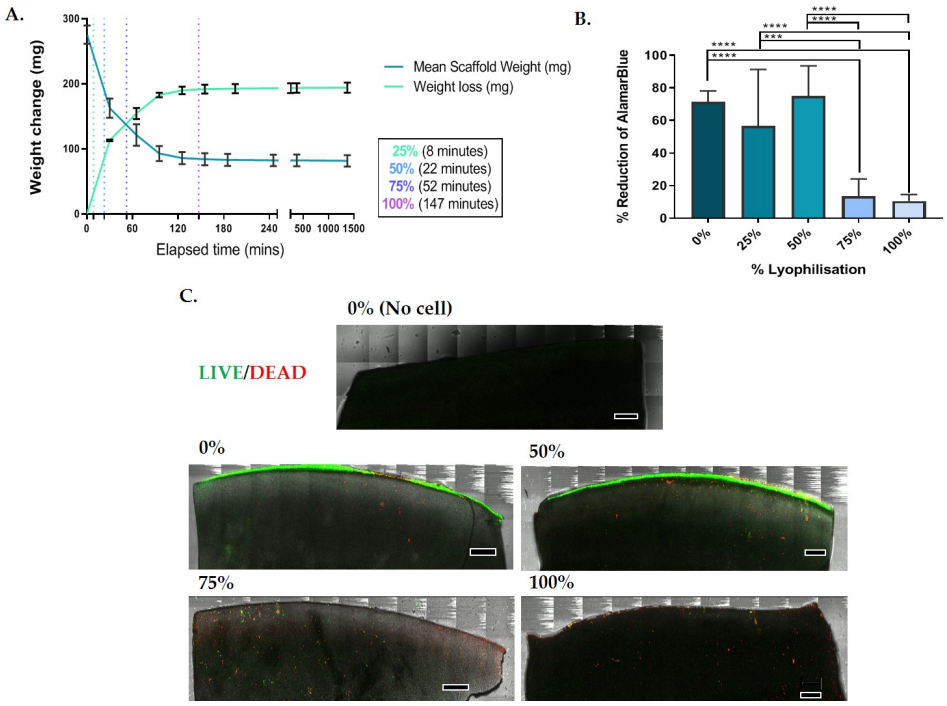

Figure 6.19: Effect of the degree of lyophilisation on seeding of decellularised osteochondral scaffolds. A) Weight loss (mg) of decellularised scaffolds over time. Dotted lines represent 25, 50, 75 and 100% water loss intervals determined from interpolations from a linear regression (hyperbola fit). Error bars ± 95% confidence limits. B) Viability of C20A4 cells seeded on scaffolds (n=3) subjected to a range of lyophilisation states (0, 25, 50, 75 and 100% lyophilised), measured through % reduction of alamarBlue and C) LIVE/DEAD staining. Error bars ± 95% confidence limits. One-way ANOVA performed ($p<0.0001$), followed by Tukey's multiple comparisons test. *** = $p<0.0005$ and **** = $p<0.0001$. Scale bar = 500 µm.

6.4.3.7 Higher media volume with 100% lyophilised scaffolds

Whilst viability was maintained in the 25% and 50% lyophilised samples, there was no beneficial effect on cell penetration. Therefore, it was decided to continue with focus on improving viability with the 100% lyophilised samples, to see if the greater degree of lyophilisation may provide an increased capacity for absorption of cell suspension or an increased collagen fibre disruption, to improve repopulation. The hypothesis for the lower viability is that the scaffolds dried out due to the increased capacity of the lyophilised scaffolds to uptake fluid. As approximately 200 mg of wet weight was removed from the scaffolds in Figure 6.19A, the initial volume for cell suspension was increased from 50 µL to 200 µL. However, in reality this was not possible without the fluid spilling off the cartilage surface, so only 100 µL was able to be delivered to the scaffolds, meaning only 50% of the intended cell concentration was applied (0.5×10^6).

The increased media volume appeared to improve the discrepancy in viability, as no significant difference was observed between the cell only and lyophilised groups (Figure 6.20A). The LIVE/DEAD images support this finding, showing a viable layer of cells in the superficial zone, as well as an appearance of viable cells in the middle, deep and bone layers of the cells. The H&E shows that in the untreated group the cells appeared to reside on the top of the scaffold, however, this thick layer was not visible in the lyophilised group. This may indicate that the cells have been absorbed into the scaffold, given that these scaffolds are giving similar viability measurements to the untreated scaffolds. However, this was difficult to determine as there was not clear evidence of cells from the H&E images.

In terms of disruption to the ECM, it was evident from the LIVE/DEAD image that lyophilisation had disrupted the cartilage bone interface. For the cartilage portion, no obvious damage was observable, this may be explained by the fact that the scaffolds had rehydrated by the point that histology was performed. Cells were observed in the chondrons and lower subchondral bone portions, it is currently inconclusive whether these cells were remnants from an unsuccessful decellularisation, or successfully seeded C20A4 chondrocytes.

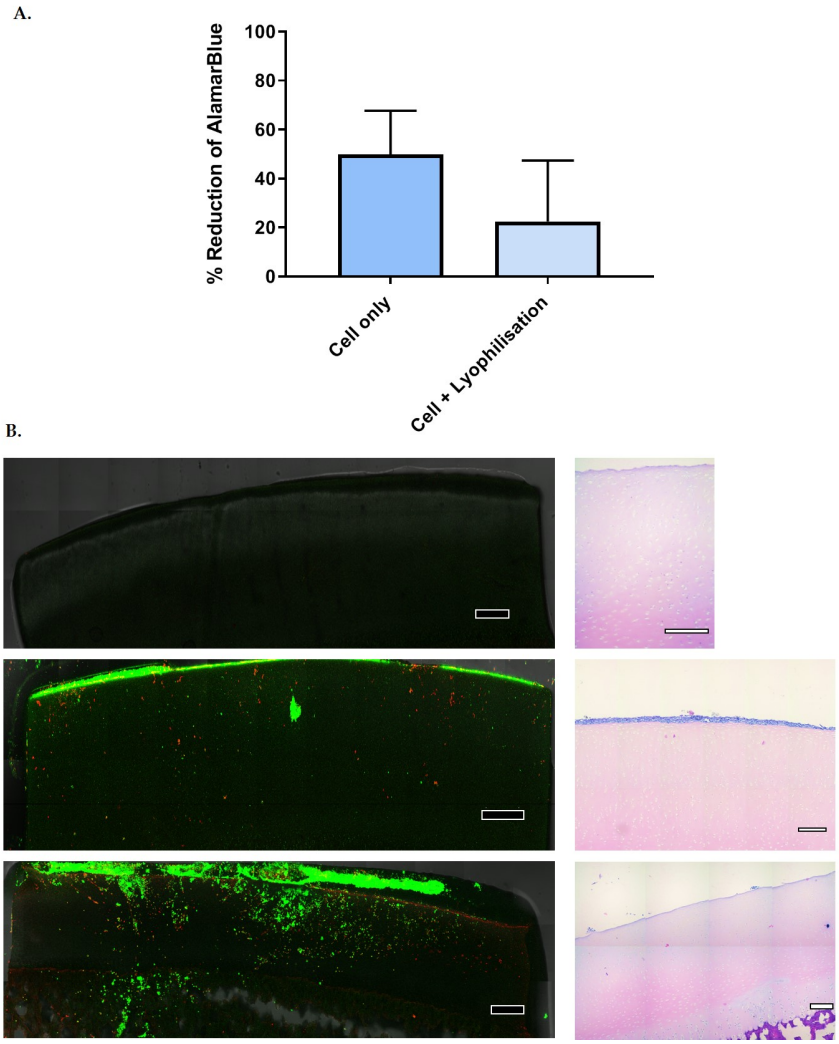

Figure 6.20: Viability of chondrocytes seeded onto 100% lyophilised scaffolds in a larger initial seeding volume. A) Comparison of cell viability between cell only and 100% lyophilised scaffolds (n = 3) seeded with 0.5 x 10^6 cells. Error bars ± 95% confidence limits. One-way ANOVA performed, followed by Tukey's multiple comparisons test. B) Viability and penetration of chondrocytes seeded onto decellularised scaffolds, measured through LIVE/DEAD staining. Top = no cell control, middle = cell only control, and bottom is a 100% lyophilised scaffold seeded with chondrocytes. Scale bar = 500 µm.

6.4.3.8 Lyophilised with labelled chondrocytes

Due to promising but inconclusive results regarding cell penetration seen in Figure 6.20, the cell seeding was repeated but labelled chondrocytes were used, and the samples were immediately fixed rather than live imaged, in order to minimise cell smearing. Furthermore, the process was improved to deliver 1 x 10^6 cells in 200µL by using a seeding ring with a 8 mm inner diameter. This was sealed with 1% agarose in the well, to avoid cell suspension leaking out of the seeding ring. The

rationale behind this was to increase exposure of the lyophilised scaffold to the cell suspension, without losses due to spillages.

From the Dil+ images in Figure 6.21, in the static cell seeding cells at Day 1 and Day 7 were located only on the superficial surfaces. However, in the scaffolds that were lyophilised and rehydrated in cell suspension, cells were observed on the surface and below in the middle/deep zones. This same observation was made in the H & E results (Figure 6.22).

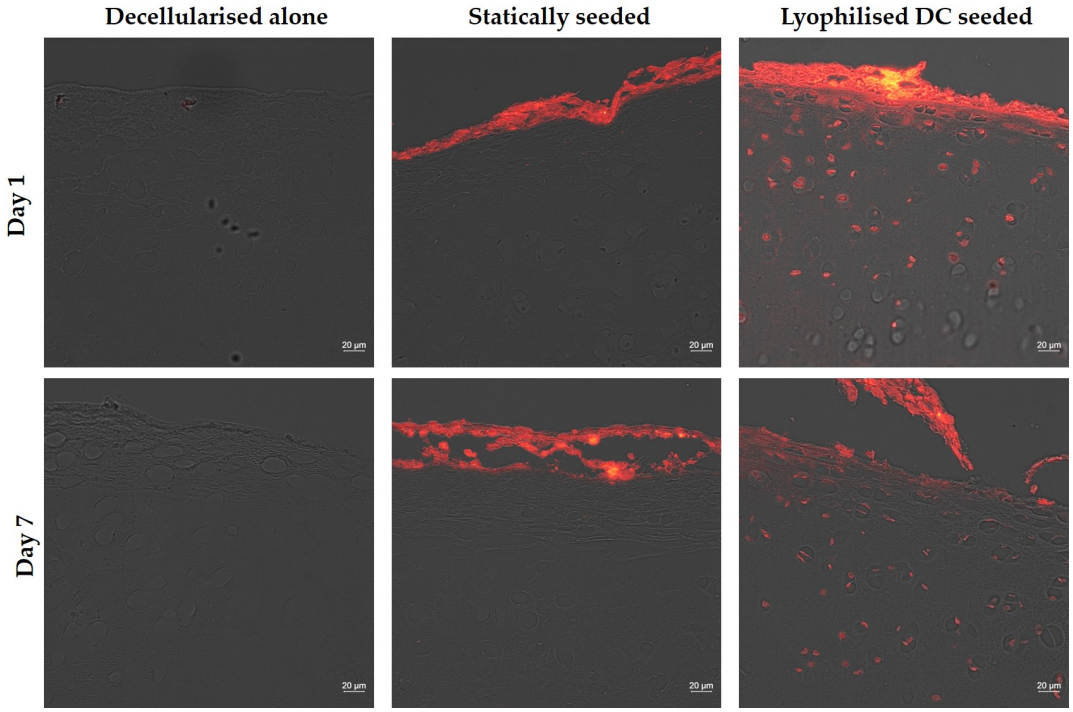

Figure 6.21: Dil+ labelled chondrocytes seeded onto decellularised matrices. Seeding onto lyophilised decellularised scaffolds (n=3) was compared with untreated decellularised scaffolds (n=3) and unseeded controls (n=3). The images presented are plugs from the same initial sheet. Images were taken under brightfield, and under a fluorescence filter for Dil+ cells (orange). Scale bars = 20 µm.

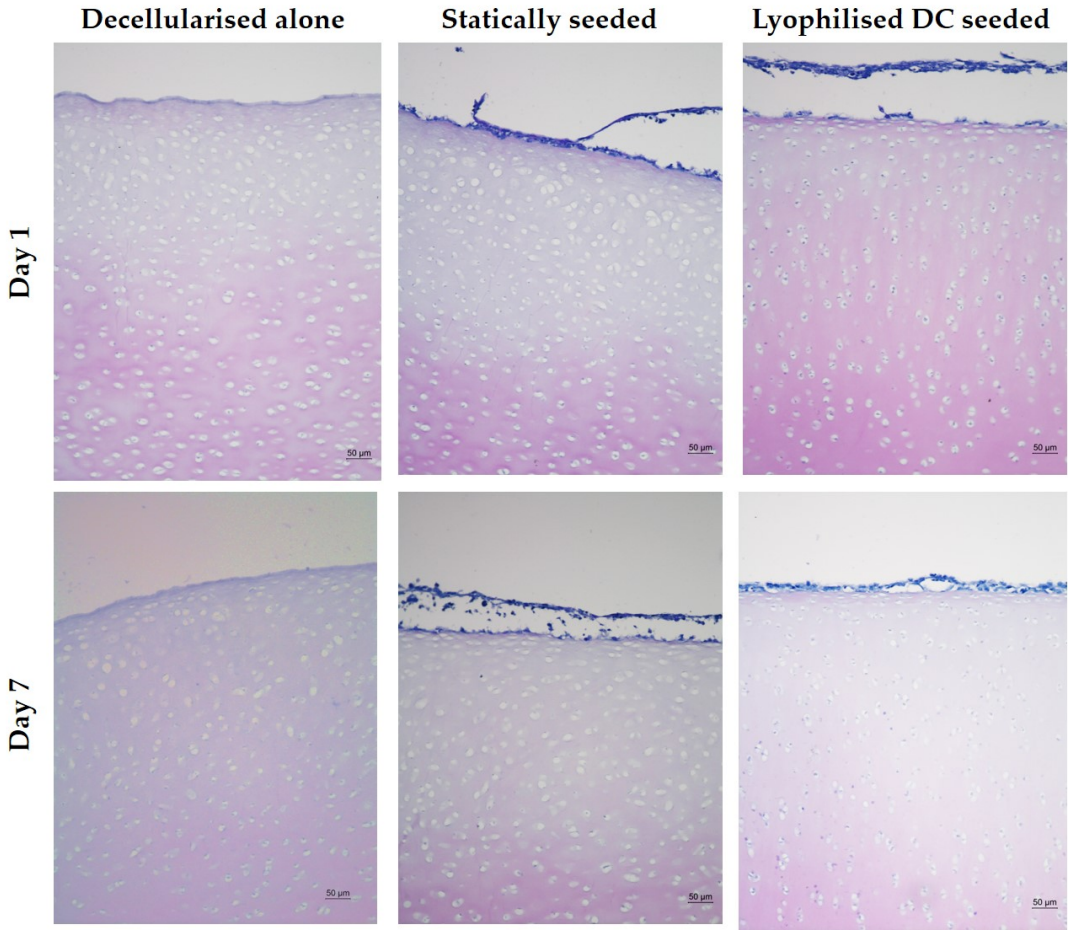

Figure 6.22: H & E staining of chondrocytes seeded onto decellularised matrices. Seeding onto lyophilised decellularised scaffolds (n=3) was compared with untreated decellularised scaffolds (n=3) and unseeded controls (n=3). The images presented are plugs from the same initial sheet. Images were taken under brightfield. Scale bars = 20 µm.

Both the H & E and Dil+ images showed that chondrocytes have occupied the chondrons of the cartilage when they penetrate the cartilage. The distribution appeared fairly homogenous, however, there was still a great concentration of cells on the surface.

The total DNA content (Figure 6.23) showed that both seeded groups (static and lyophilised) had significantly higher DNA content compared with the decellularised controls at Day 1 and Day 7. The statically seeded cells had a significantly higher DNA content compared to the lyophilised scaffolds at Day 1 and 7. However, both sets of seeded scaffolds had DNA content of $\approx$ 750 ng.mg^{-1} + at Day 1, which approaches previously observed levels for native controls (Figure 4.7). At Day 7 there was a reduction in the DNA content for the lyophilised scaffolds to $\approx$ 450 ng.mg^{-1},

this difference was not significant however.

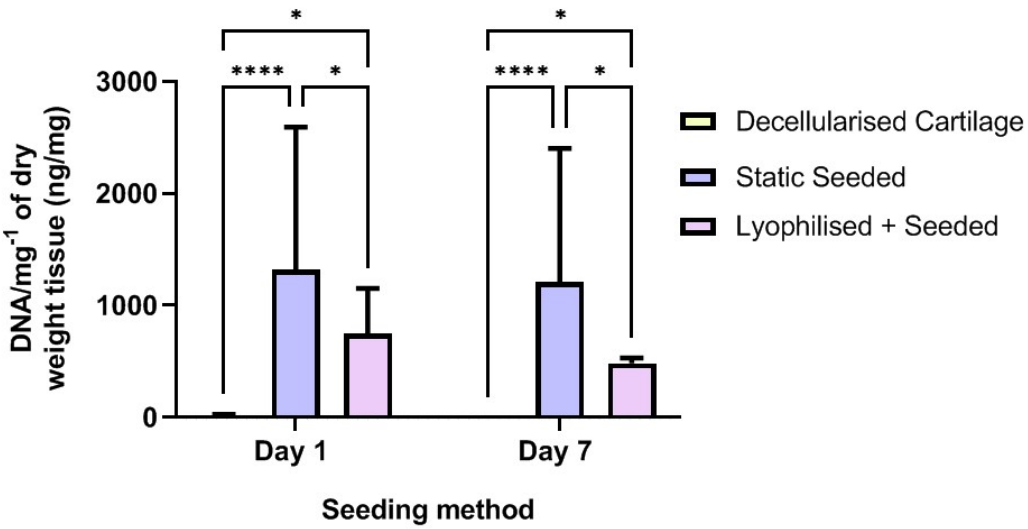

Figure 6.23: Total DNA content of decellularised (n =3), statically seeded (n = 3) and lyophilised + seeded (n = 3) at Day 1 and Day 7. Error bars = 95% C.I. 2-way ANOVA performed with post-hoc Tukey's multiple comparisons test. * = p <0.05, **** = p <0.0001.

6.4.4 Restoring the GAG content and biomechanical properties of decellularised cartilage

Another potential drawback of decellularised scaffolds is the reduced stiffness in compression, likely a result of the reduced GAG content (Figure 4.23). A hypothesis is that by restoring the GAG content, the compressive properties will be restored. Following on from the apparent success with the cell seeding using the lyophilised method (Figure 6.21), the same method was investigated in the delivery of P_{11}-8/CS to decellularised scaffolds.

6.4.4.1 Fixation of P_{11}-8 with NBF or EDC fixative

Histology and biochemical assays were chosen as the principal methods of determining GAG delivery to the matrices. In order to ensure quick peptide fixation within the matrix, EDC was investigated as an alternative fixation method to 48 hours in NBF.

When compared with NBF fixed samples, it is clear from the Safranin O staining that EDC showed a much improved fixation of the P_{11}-8/CS (Figure 6.24). This was

shown by the much higher intensity of the Safranin O staining. When comparing the different time points, it appeared as if the 180 minutes was required to give complete fixation, as compared to all previous time points, this sample had the greatest concentration of hydrogel remaining post-processing.

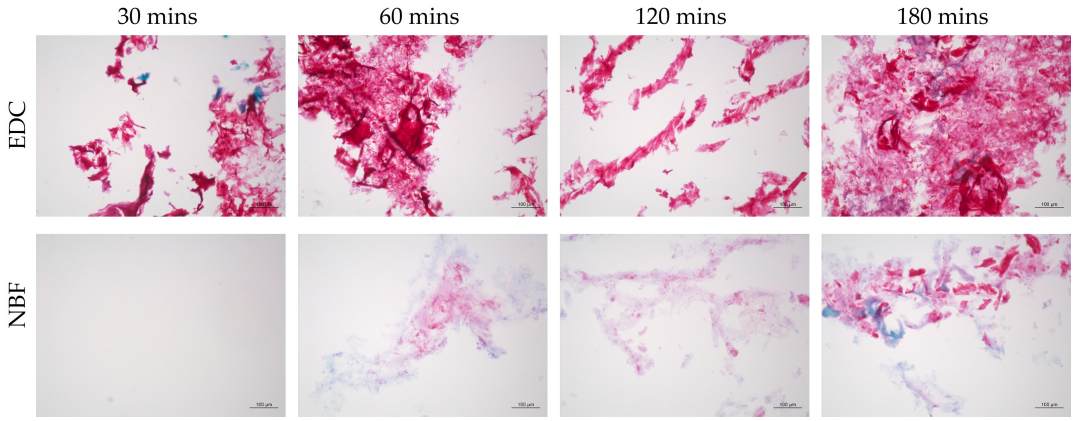

Figure 6.24: Fixation of P_{11}-8/CS hydrogels. Hydrogels were fixed with EDC or 10% NBF for 30, 60, 120 and 180 minutes, cryosectioned and stained with Safranin O and FG. Scale bars = 100 µm

6.4.4.2 Restoration of GAG content

Despite previous work being conducted with 20 mg.mL^{-1} gels in the encapsulation studies, pilot experiments demonstrated that these gels assembled too quickly or were too viscous to soak into the lyophilised matrices. Therefore, for the gel delivery experiments 10 mg.mL^{-1} gels were used.

Firstly, from the histology (Figure 6.25) it appeared as if peptide had been delivered indicated by the red safranin O staining. The peptide appeared to accumulate in the deep zone/subchondral bone layer, as well as in the upper middle zone. Similarly to the cell seeding it appeared as if the peptide accumulated in the chondrons, alongside greater accumulations in the extracellular matrix region.

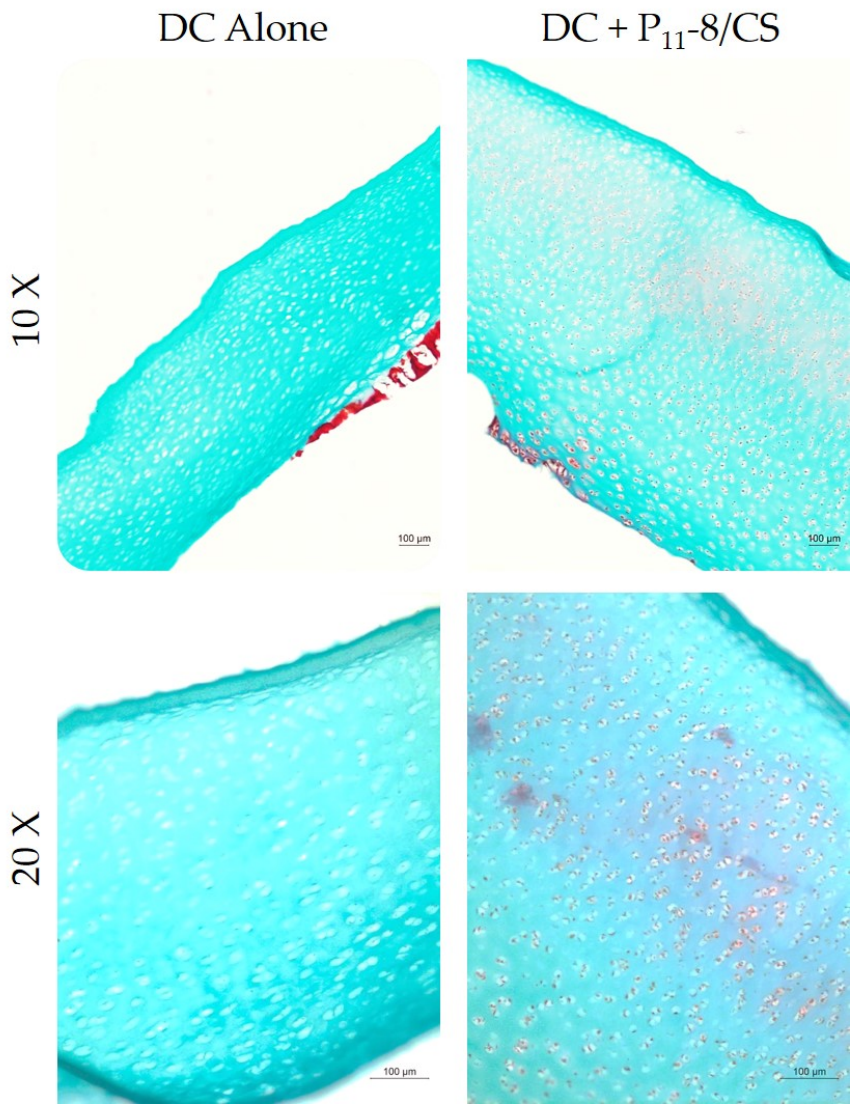

Figure 6.25: P_{11}-8/CS delivery to decellularised matrices. Samples fixed in EDC following indentation testing, cryosectioned and stained with Safranin O and Fast Green. Scale bars = 100 µm

6.4.4.3 Fluorescent peptide

Whilst the Safranin O indicates the presence of the CS component, it does not demonstrate the distribution of the P_{11}-8. Therefore, in order to determine exact location of the P_{11}-8, a FITC tagged peptide was delivered to the DC samples, using the same method as defined previously. The fluorescent images displayed in Figure 6.26, demonstrate a lack of fluorescence in the DC-Alone samples. However, in the DC-GAG samples there were two staining patterns observed. FITC signal was detected throughout the cartilage, demonstrated by the fluorescent signal in the treated sample. There appeared to be a stronger signal in the superficial zone, however, this

may be an artefact of the sectioning process. In other samples, distinct concentrated aggregations of P_{11}-8 were seen. As with the Safranin O staining (Figure 6.25), fluorescence was detected within the chondrons.

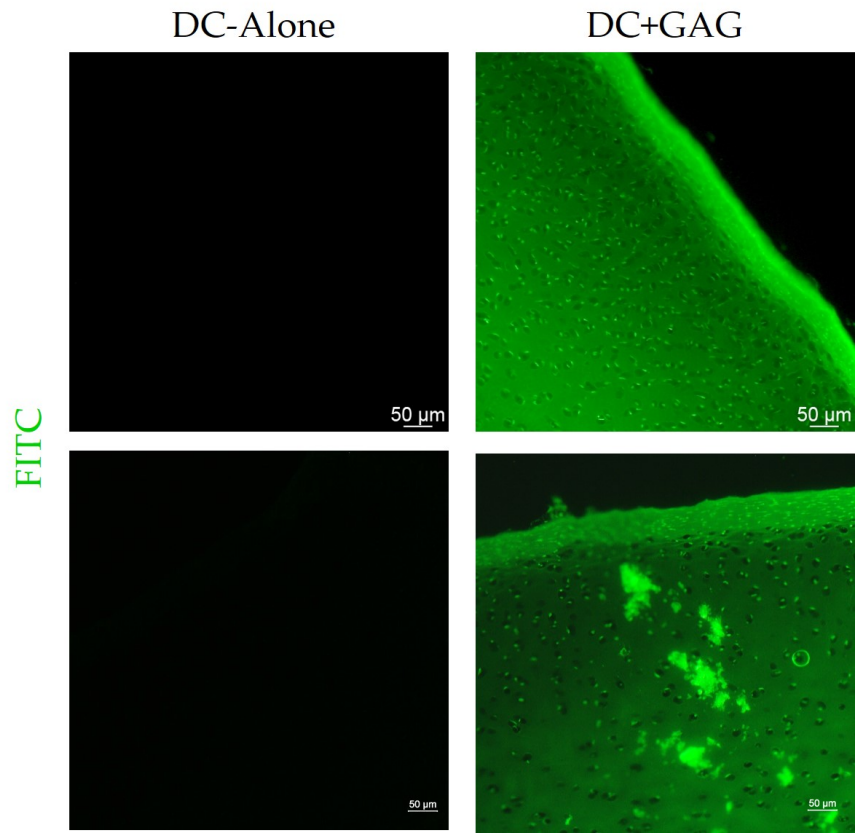

Figure 6.26: FITC tagged P_{11}-8/CS delivery to decellularised cartilage. Decellularised samples alone (n = 3) and FITC-GAG delivery samples (n = 3) were frozen immediately in OCT, cryosectioned, and imaged using a fluorescent microscope (512 nm). Scale bars = 50 µm

In agreement with the histology, the GAG assay showed an increase in GAG content compared with the decellularised cartilage (Figure 6.27) however this difference was not significant.

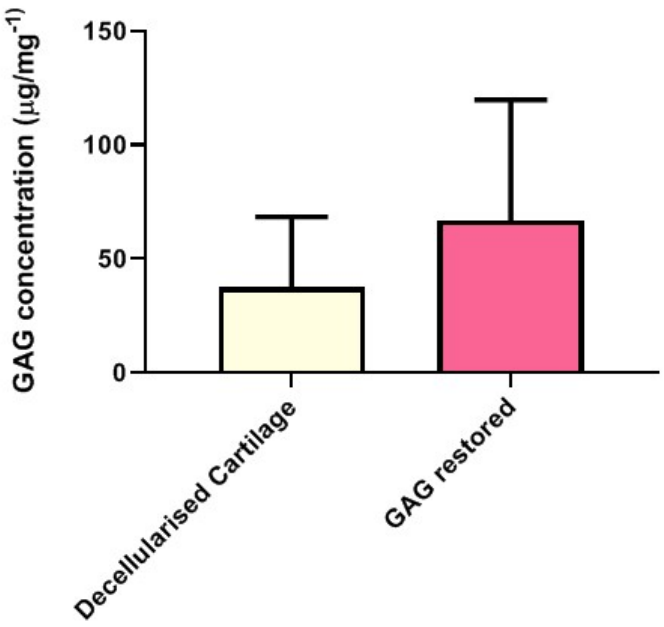

Figure 6.27: GAG concentration in decellularised scaffolds alone (n = 3) versus GAG-'restored' samples (n = 3). Error bars = 95% C.I. Unpaired t-test performed.

6.4.4.4 Restoration of percentage deformation

Despite the minimal effect on the overall GAG content, when measuring the mechanical properties prior to the GAG assay there was a reduction in the percentage deformation in samples with delivered GAG (Figure 6.28). This difference was not significant (p = 0.0538), however, in each samples from the same initial samples (GAG and Lyo-DC) there was a reduction in percentage deformation with GAG restored samples compared with the untreated control.

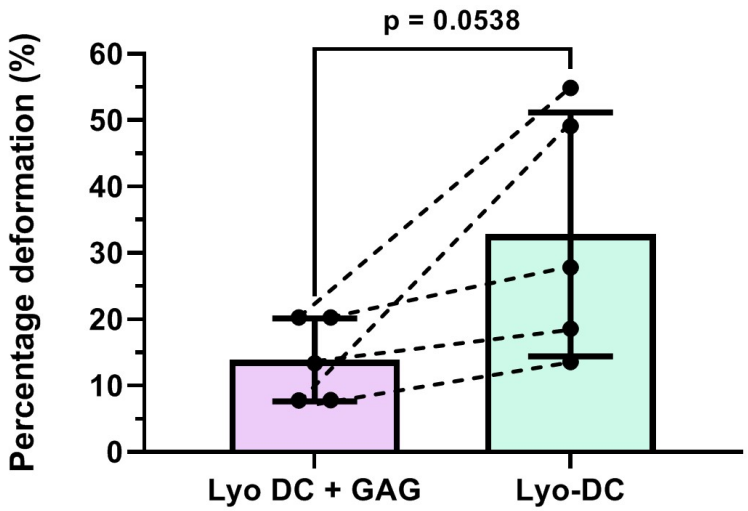

Figure 6.28: Percentage deformation of decellularised (Lyo-DC) and GAG delivery samples. Samples from each group (n = 5) were subject to indentation, and total deformation was normalised to cartilage thickness. Points on bar chart represent individual data points and dotted lines connect samples from the same decellularised sheet. Error bars = +/- 95% C.I

6.5 Discussion

6.5.1 Recellularising decellularised osteochondral scaffolds

6.5.1.1 Channels with active seeding methods

These data provide indications that in order to fully recellularise decellularised cartilage, some disruption of the ECM structure is required.

This conclusion was reached after early optimisation showed that static and vacuum seeding did not achieve cell penetration below the superficial zone (Figure 6.5). Despite this, the observed cell attachment across the superficial layer was accompanied by the cell viability at the 24 hour timepoint in the static and vacuum groups. The theory for vacuum seeding was based on research by (Griffon *et al.*, 2011; Tan *et al.*, 2012), however, in this instance it appears as if the vacuum has caused the cells to adhere towards one edge of the scaffold. This is accompanied by an absence of increased cell penetration. This is likely due to the low porosity of cartilage meaning

that upon release of the vacuum the cell suspension has moved towards areas of less resistance, causing asymmetric cell seeding. In the 'injection' group (Figure 6.5), there was a distinct lack of adhered viable cells. This may be due to the use of a 30 G needle, which may cause shear stress to the delivered cells. However, it has been shown that cell delivery with 30 G needles does not have a significant effect on viability, and that low flow rates (20 µL/min) have a much greater effect (Amer *et al.*, 2015). In this experiment, the flow rate was not controlled for. Where the injection was delivered, an ablation in the cartilage structure was made, in which L929 were visible in the H & E image in Figure 6.5B.

Vacuum seeding was investigated further, however, with channels to allow for greater 'porosity' in the cartilage surface. The histology and cell tracker images demonstrate that where channels were present cells occupied throughout the depth at both Day 1 and Day 7. The same was observed with the channel + vacuum samples. It should be mentioned that the channels were difficult to locate whilst serial sectioning, therefore not all channels were visualised. In both the channel alone and channel + vacuum groups there is limited evidence of lateral migration of cells out of the channel area. The DNA assay showed an increase in total DNA content when the vacuum was used Figure 6.7, however this difference was not statistically significant. The static seeded samples showed a DNA content of around 1000 ng.mg^{-1}, however these data were extremely variable. Taken together the histological and DNA quantification data appear to demonstrate no added benefit of adding the extra processing step of vacuum.

A similar investigation was conducted into the use of centrifugation to 'force' cells into created channels. Cells occupied the channels with and without centrifugation according to the histology and cell tracker images in Figure 6.8. The DNA assay showed limited differences between groups, however, at Day 1 the centrifuged and statically seeded samples were significantly higher than the decellularised samples Figure 6.9. However, again there was no discernible improvement in terms of DNA content against the static control or channel controls alone. Similarly to the vacuum data, it appears that any improvement (cell penetration) can be achieved through use of channels alone without the requirement for further seeding methodologies.

Several groups researching recellularisation of decellularised cartilage have also investigated the use of channels to improve recellularisation. (Bautista *et al.*, 2016) utilised channels created with a 30 G needle, alongside both vacuum and centrifugation. The histological results appear similar, with the majority of cells occupying the surface, accompanied by cell infiltration along the channels. Channels were also investigated by (Luo *et al.*, 2017), who observed repopulation of the channels, as well as deposition of GAGs and collagen. Both authors observed no lateral migration of cells from the channels into the ECM, and both can be described as a partial recellularisaton of the cartilage. One potential concern with the channels, would be a compromise of the mechanical properties of cartilage. Only one study reports any data of this kind, showing no significant difference between the compressive modulus of their decellularised cartilage with and without channels (Luo *et al.*, 2017). However, the tribological effects of this are yet to be determined.

6.5.1.2 Collagenase digestion

Following on from this, more subtle methods of matrix disruption were investigated. Firstly, the enzymatic degradation of cartilage at low concentration was investigated over a 16 day timecourse. Firstly, this experiment showed further evidence of extended cell viability of L929s on the decellularised scaffold (Figure 6.12). Initially, it appears from the LIVE/DEAD staining that cells have migrated below the surface into the cartilage ECM. However, this pattern was not reflected in the H & E staining, indicating that the cell masses below the surface were likely an artefact of the sectioning and LIVE/DEAD process. This may be explained by the fact that the scaffolds were bisectioned with a scalpel immediately post-culture without any fixation.

Collagenase treatment caused a significant reduction ($p < 0.001$) of viability at both concentrations compared with the cell only control (Figure 6.12B). However, this reduction was corrected by day 16 at both concentrations, to the same level as the control.

One observation from the H & E in Figure 6.12A was the similarity in cartilage ECM structure between the collagenase treated scaffolds and compared the undigested

controls. Therefore, it was decided to increase the collagenase concentration, and investigate the effect of incubation time and culture method on cartilage digestion. The H & E staining in Figure 6.13 shows that with the higher concentration of collagenase, by 90 minutes there was an ablation of staining in the superficial zone in both treatment groups. The data showed a removal of collagen from the superficial zone, as well as a reduction in total GAGs throughout the cartilage. This may indicate a disruption to the GAG-collagen mesh in the cartilage middle zone, or the removal of collagen causing an increased permeability and susceptibility for GAG removal (Sophia Fox *et al.*, 2009).

Upon recellularisation it appeared that the disruption to the superficial zone allowed for improved cell seeding. The effect appeared to be a much improved cell attachment at Day 1, followed by migration into the cartilage matrix by Day 7 (Figure 6.14), importantly without any effect on viability (Figure 6.16). Indications of improved cell attachment and migration were confirmed by the DNA content. At Day 1 there was a DNA content of above 1000 ng.mg^{-1} which increased to $\approx$ 2000 ng.mg^{-1} by Day 7. These levels meet and surpass previously measured levels for native cartilage (Figure 4.7). Interestingly, by Day 7 the thick band of cells on the superficial layer at Day 1 in the collagenase treated samples, has disappeared, and the cells appear to have migrated into the matrix. This result closely matches results observed by (Seol *et al.*, 2014), who observed a higher migration of chondrocytes into bovine articular cartilage treated with collagenase.

Whilst collagenase treatment improved cell seeding, the effect on the macro-structure of cartilage was evident. During sample processing for histology, collagenase treated cartilage had the appearance of a translucent hydrogel. The superficial zone of articular cartilage especially has been shown to play a pivotal role in the tissues dynamic compressive properties. Confined and unconfined compression testing of osteochondral plugs with a removed superficial zone demonstrated reduced dynamic moduli across a range of strains (10-30%) compared with a fully intact plug (Gannon *et al.*, 2015). The authors hypothesise that it is the collagen content and arranged Benninghoff structure found in intact skeletally mature cartilage which contributes to the ability of the superficial zone to resist deformation, therefore providing fluid

support. This was based on the observation that plugs with the removed superficial zone had a higher permeability (Gannon *et al.*, 2015). Whilst the superficial zone was still present in our study, the macroscopic data (Figure 6.14) demonstrated substantial collagen network disruption within the superficial layer, therefore, it would be reasonable to assume a similar impact on the dynamic compressive biomechanical properties if a similar testing regime was used with these scaffolds. Interestingly, in the referenced study, there was no effect on the equilibrium biomechanical properties upon removal of the superficial layer (H_A and Young's modulus) in immature tissue. In skeletally mature tissue, these properties were higher than the intact plugs, due to the higher GAG content and compressive resistance in the deeper zones. Due to mode of application of the collagenase in our study, it is unlikely that the damage is restricted to just the superficial zone. Furthermore, the histological data shows an increase in GAG removal, therefore it is unlikely that the static properties would remain or improve in the decellularised scaffolds investigated in this study.

As one of the key features of decellularised scaffolds is the structural similarity to the native tissue, disrupting the tissue integrity with enzymatic digestion may impact the experience of load by the cells, ultimately impacting cell viability and phenotype (Statham *et al.*, 2022). Therefore, lyophilisation of the cartilage, followed by rehydration with cell suspension was investigated.

6.5.1.3 Lyophilised scaffolds

Fully dehydrated osteochondral plugs were obtained after 147 minutes (Figure 6.19), and it was found that using 50 µL of cell suspension, degree of lyophilisation was related to cell viability. This was likely a result of the cell culture media rehydrating the cartilage, therefore it cannot serve it's role as a nutrient source to the suspended cells. As a result, cell suspension volume was increased to 200 µL (Figure 6.20) which overcame the previous viability issues. Both the LIVE/DEAD images and histologically it appears as if viable cells had penetrated below the superficial zone in the lyophilised treatment scaffolds. However, due to previous concerns about cell artefacts as a result of the sectioning of unfixed tissue, the experiment was repeated with cell tracker labelled cells that were fixed with NBF following cell delivery and

culture.

The results of this experiment (Figures 6.21 and 6.22) demonstrated that labelled chondrocytes seeded onto lyophilised scaffolds penetrated into the cartilage ECM and occupied the decellularised chondrons. At the time of writing, the author is not aware of any other literature using lyophilisation to aid the recellularisation of decellularised cartilage. However, it has been used in the recellularisation of poly (ethylene glycol) fumarate hydrogels with MSCs (Lim *et al.*, 2013).

As discussed previously, most groups investigating recellularisation of decellularised cartilage have had to rely on creation of channels to aid recellularisation (Bautista *et al.*, 2016; Luo *et al.*, 2017). The DNA content of the lyophilised group was significantly higher than the decellularised cartilage, but lower than the statically seeded samples. The cause of this is uncertain, there is possibility that in lyophilised samples cell suspension may be drawn into the bone region as well as the cartilage. However, the DNA content was still approaching levels seen in native cartilage, therefore, it is possible to simply increase the initial seeding density to account for this loss. It must be said that there is no consensus of DNA content or cell density in scaffolds for cartilage tissue engineering. In this study 1 million cells were delivered per scaffold (5 million cells/ml), however, cartilage tissue engineering studies have used up to 100 million cells/ml, which were seeded onto a silk scaffold (Talukdar *et al.*, 2011). The authors noted significant changes in biochemical composition and biomechanical properties over a range of 20 - 100 million cells/ml. Therefore, further investigation into optimal seeding densities for these scaffolds is warranted.

One potential drawback of this method is the effect of lyophilisation on the compressive properties of cartilage. Whilst not directly compared in this work, when lyophilised scaffolds were investigated in a later study (Figure 6.28) the average percentage deformation was >30% compared with <20% for untreated decellularised scaffolds in Figure 4.21. Lyophilisation has been shown to affect mechanical properties of decellularised arterial scaffolds (Sheridan *et al.*, 2013). The authors found that the conditions of freeze drying were also shown to drastically affect the mechanical properties.

In this study, as mentioned previously, the scaffold group referred to as 'lyophilised',

is placed into the freeze drier at ambient temperature rather than in a frozen state. The rationale behind this was to preserve cartilage structure, rather than increasing pore size. It is unknown whether the inclusion of a freezing step prior to drying would improve recellularisation, and what effect this would have on the mechanical properties.

6.5.2 P_{11}-8/CS delivery to decellularised cartilage

The success observed with the cell seeding of the lyophilised grafts in Figure 6.21, led to investigation of the ability of P_{11}-8/CS to restore the GAG content of decellularised hydrogels. Initial optimisation experiments demonstrated that EDC was suitable for the fixation of P_{11}-8/CS, for cryosectioning and Safranin O staining (Figure 6.24). The aim was to fix peptide quickly, to prevent peptide disassembly prior to fixation. This was clear when compared with the NBF fixed samples, which after 3 hours showed minimal Safranin O staining. EDC works best at lower temperatures as well, which further helps to prevents peptide disassembly.

Several techniques were attempted in optimising the delivery to the P_{11}-8/CS to the lyophilsied matrices. It was decided that preventing assembly with sonication for at least 15 minutes would enable the lyophilised cartilage to rehydrate with P_{11}-8/CS, whilst keeping along similar timings to previous peptide protocols. However, with 20 mg.mL^{-1} gels the peptide assembled on the surface of the cartilage, in spite of sonication. Therefore, the decision was made to reduce the P_{11}-8/CS concentration to 10 mg.mL^{-1}, to allow for a longer period prior to peptide assembly.

The Safranin O staining appeared to show a degree of GAG restoration within the deeper zones of the cartilage. The staining appeared to be present in the chondrons from the subchondral transition point, up to the superficial zone. There also appeared to be concentrated zones of peptide accumulation spanning the cartilage ECM region (Figure 6.25). However, it must be noted that there were variable amounts of GAG removal from decellularised samples, therefore it was difficult to be certain from these results alone that the staining was a direct result of peptide delivery or inconsistent decellularisation. Attempts were made to mitigate this by using plugs from the same decellularised 'sheet' for comparison.

FITC-conjugated P_{11}-8 was purchased from CS-Bio in order to track peptide delivery specifically. Two samples are shown in Figure 6.26, which demonstrated two of the observed staining patterns. In the decellularised alone there was no autofluorescence at the exposure used, however, samples seeded with FITC-doped peptide showed bright fluorescence under the FITC filter. Staining in the bottom right panel (DC + GAG - Figure 6.26) matched that observed in the 20 x Safranin O stained histology sample (Figure 6.25). As well as a general fluorescence through the tissue, fluorescent signal intensity appeared higher in the superficial zone and the chondrons (as observed with the recellularisation attempts in Figure 6.21). There is a possibility that the intense staining was an artefact from folding of the cartilage edge over the tissue, as intensity in the cartilage edges has been seen in previous cryosectioned samples (Figure 6.25). However, there is no signal in the control, so it is more likely that any this was an amplification of the GAG delivery rather than a false positive.

This method was taken forward to determine the effect of GAG delivery on percentage deformation. Lyophilised cartilage samples with and without GAG delivery were subject to indentation testing, followed by a GAG assay. It was hypothesised that delivery of P_{11}-8/CS to the cartilage would increase cartilage GAG concentration, which would be accompanied by a decrease in percentage deformation.

The GAG assay demonstrated a non-significant increase in GAG concentration in treated samples, however, these samples had already been subject to a 15 minute PBS equilibration, followed by a 1 hour indentation. Therefore, it is hard to determine the initial GAG delivery from this data alone, and the lack of a significant increase may be due to poor P_{11}-8/CS retention in the scaffolds rather than a low delivery (Figure 6.27). The effect on the percentage deformation was a reduction in percentage deformation from > 30% to <15% (Figure 6.28). Despite a decrease in deformation in all GAG-treated samples from the same sheet, the small sample size (n = 5) and the large inherent variation in the starting material properties meant that the reduction was not significant ($p = 0.0538$). Future experiments with increased sample sizes would be useful in determining whether this is a viable method of restoring native biomechanical properties.

Previous research using P11-X family of peptides along with CS in the treatment

of musculoskeletal tissue, has shown restoration of native biomechnical properties (Miles *et al.*, 2016). In this instance stiffness of their intervertebral disc model increases in the pathological state, and treatment with P_{11}-12/CS reduced the stiffness back to the native state. However, in this same study it was shown that P_{11}-8/CS (1:2) had an increased modulus when testing alone versus P_{11}-12/CS (1:2), therefore it is difficult to compare with our study. It could be hypothesised that augmentation of tissues with GAGs, will restore the mechanical properties towards native function. Whether this is through an increased or decreased stiffness may be tissue specific, depending on the function of GAG within said tissue.

An element of the study by (Miles *et al.*, 2016) that was not recorded in our study was P_{11}-8/CS retention post-delivery, which was observed to be 92% in their study. Due to influence CS may have on the final material properties, retention within the matrices is an important variable to determine.

Whilst this work provides exciting indications for a minimally destructive method of delivering P_{11}-8/CS to decellularised cartilage, there are several potential limitations of this study. Whilst not directly comparable, it appears that lyophilisation increases the percentage deformation of the scaffolds, therefore, the marginal improvement shown in Figure 6.28 may only be restoring the biomechanical properties of the untreated decellularised scaffold, rather than conferring further improvement. To control for this, larger studies should follow on from this with greater sample sizes, and groups comparing these separate variables. Furthermore, due to the large percentage deformation observed in the Lyo-DC samples, the assumptions for use of the biphasic model were invalid. This restricted the derivation of material properties from this data, to percentage deformation alone.

Unpublished work from our laboratory has shown effective delivery of P_{11}-8/CS using injections to both cartilage and meniscus. In this work, injection was avoided due to potential damage to both the scaffold and reconstituted cells. However, future work should investigate the potential of the injection of a P_{11}-8/CS + cells suspension, for restoration of cellular content as well as biomechanical properties.

6.6 Conclusions

The aim of this work was to investigate the possibility of enhancing decellularised osteochondral scaffolds with chondrocytes and with P_{11}-8/CS separately. Firstly, this data has shown that it is possible to culture chondrocytes on decellularised scaffolds, whilst maintaining viability, for up to 16 days in vitro. Furthermore, the data has shown that with static seeding and vacuum/centrifugation it is not possible to improve cell penetration into decellularised cartilage. However, by permeabilisation the matrix with channels, enzymatic digestion and lyophilisation it is possible to disrupt the matrix enough to allow cell penetration. The preferred method from this investigation was lyophilisation, due to the extent of recellularisation, as well as the minimal damage observed via histological methods. Future work should investigate long-term culture with chondrocytes, to determine whether the matrix fosters an environment for chondrocytes to deposit neo-matrix components (Collagen II, GAGs), resulting in tissue maturation.

Secondly, using decellularised scaffolds treated by the lyophilised method, P_{11}-8/Cs delivery was investigated with the potential to augment the mechanical properties of the scaffolds. Data has shown it is possible to deliver GAGs, and reduce percentage deformation. The differences in this instance were not significant, therefore further optimisation is warranted before progressing further with this method.

Chapter 7

Assessment of recellularised osteochondral matrices under loading in a viable knee joint simulation model

7.1 Introduction

A protocol has been developed to recellularise decellularised OC scaffolds in Chapter 6. Data has shown that it is possible to keep cells within these scaffolds viable for a period up to 7-days, with the potential for longer with the inclusion of extended time points. A limitation of these studies is the fact that they were conducted in static culture plates, which is of limited relevance to the dynamic *in-situ* environment. As well as viability, it is also important to understand cell response to mechanical loading in 3D with regards to gene expression and ECM deposition. Furthermore, how the repopulated scaffolds respond biomechanically to such loading *in-situ*, could potentially provide important information for later *in-vivo* studies. The current culture set-up is limited in enabling further understanding surrounding these factors.

Ex-vivo culture of porcine osteochondral tissue has been developed and used as a tool to assess osteochondral allograft implantations (Elson *et al.*, 2015). The authors demonstrated that it was possible to maintain viability of porcine osteochondral

plugs for up to 20 days. Such *ex-vivo* culture models allow for investigation of viability, gene expression and scaffold ECM integrity in a 3D environment. Previous work from the Institute of Medical and Biological Engineering (University of Leeds) has developed the osteochondral allograft work (Elson *et al.*, 2015) towards the creation of a whole-joint organ culture model (Fox *et al.*, 2016). This "living knee joint simulation model" is composed of a porcine femoral condyle and tibial plateau within a single-station simulator capable of axial loading. The model has been used to investigate several conditions including: effect of loading (static and dynamic) on gene expression, viability and GAG content overtime, as well as the effect of anti-inflammatory treatment on similar parameters.

This chapter details a proof of concept study, investigating the feasibility of using this living knee joint model for *ex-vivo* studies into the performance/function of recellularised scaffolds detailed in Chapter 6. Previous studies have only investigated intact condyles, therefore this study aims to firstly investigate the process of creating a defect in the femoral condyles and implanting recellularised scaffolds under sterile conditions. Furthermore, studies will aim to demonstrate maintenance of viability of repopulated cells in the organ culture model under dynamic loading over a course of 7-days. The incorporation of loading is important to determine protection of chondrocytes by the scaffolds, as well as mechanical integrity of the scaffolds. Although outside the remit of this study, the importance of loading in chondrocyte biosynthesis and cartilage graft maturation would be of great interest (Statham *et al.*, 2022).

If successful this study will not only provide a platform for further development of the recellularised scaffolds, but serve as a stand-alone model for evaluating cartilage tissue engineering scaffolds *in-situ*.

7.2 Aims and Objectives

7.2.1 Aims

The work in this chapter aimed to:

- Investigate the feasibility of using the living knee joint simulation model as a means of evaluating the performance of recellularised osteochondral grafts implanted into defects in the model.
- Evaluate the process of creating defects in the model and implanting recellularised scaffolds
- Investigate the resultant cell behaviour in both the recellularised scaffolds and host-tissue

7.2.2 Objectives

- Obtain fresh porcine legs, and attempt to replicate natural living knee joint model set up, following protocol developed by Natalie Fox (Fox *et al.*, 2016).
- Create defect in medial and lateral condyles, using osteochondral allograft transfer system, whilst maintaining sterility
- Recellularise decellularised osteochondral scaffolds for use in controls and for implantation into defect
- Culture scaffolds within bioreactor over 7-day process under cyclic compression
- Extract scaffolds and analyse using histological methods to assess cell viability in donor tissue and recellularised scaffolds, as well as cell retention and/or migration between the two tissues

7.3 Materials and Methods

7.3.1 Tissue procurement

Fresh porcine legs were obtained from a local abattoir (J Penny, Leeds, UK) within 4 hours of sacrifice. Under aseptic conditions, the tibial plateau and femoral condyles were obtained. Underlying cancellous bone was reamed using a dremell to a thickness of 4-5 mm, and the bone was washed with DPBS using a Waterpik to remove

bone marrow. Following this the tissues were subject to an overnight wash at 4 °C in 500 mL Hank's balanced salt solution (Sigma Aldich, USA) with heparin (12.5 $IU.mL^{-1}$), Penicillin (200 $U.mL^{-1}$), Streptomycin (200 $U.mL^{-1}$), gentamycin (50 $\mu g.mL^{-1}$), amphotericin B (2.5 $\mu g.mL^{-1}$) (All additives Merck Life Science, UK).

The following day, the osteochondral tissue to be cultured was transferred in a defined culture medium of: Dulbecco's modified Eagle's medium (DMEM, Gibco, Life technologies, UK) supplemented with glutamine (2 mM), sodium pyruvate (1 mM), penicillin (100 $U.mL^{-1}$), streptomycin (100 $\mu g.mL^{-1}$), gentamycin (50 $\mu g.mL^{-1}$), amphotericin B (2.5 $\mu g.mL^{-1}$), ITS (insulin, transferrin and selenous acid premix (BD Biosciences, UK)) (0.1% (v/v), ascorbic acid (50 $\mu g.mL^{-1}$) (Merck Life Science UK Ltd, UK), dexamethasone (0.1 µM) (Merck Life Science UK Ltd, UK) and Hepes (25 mM) (Lonza, UK).

7.3.2 Seeded plug preparation

Osteochondral porcine tissue was dissected, shaped, and decellularised as described previously in Section 4.3.1. 9 mm plugs were taken using a biopsy punch, and the scaffolds were subsequently lyophilised overnight. On the day before rig set up, 1 million cells were seeded onto lyophilised scaffolds (n = 5), and left overnight to attach as described in 6.3.4.2. The controls in this study were unseeded scaffolds, which had been through the lyophilisation process, but were rehydrated in media alone.

7.3.3 Plug implantation and rig set up

The following day, the femoral condyles were removed from the antibiotic wash inside an Class II safety cabinet, wrapped in sterile gause and foil, then gripped in a vice. Following this, a 9 mm guided drill (Arthrex, OATS) was used to create an implantation site (Figure 7.1) in a region of the medial and lateral condyles which had been pre-determined as contact sites based on alignment studies performed previously. Following the initial drilling, a 9 mm slot drill was used to create a flat-bottomed defect, the depth of which was measured to $\approx$ 5 mm depth. If any

cartilage/bone was loose in the defect, this was removed with sterile forceps and scalpel blade.

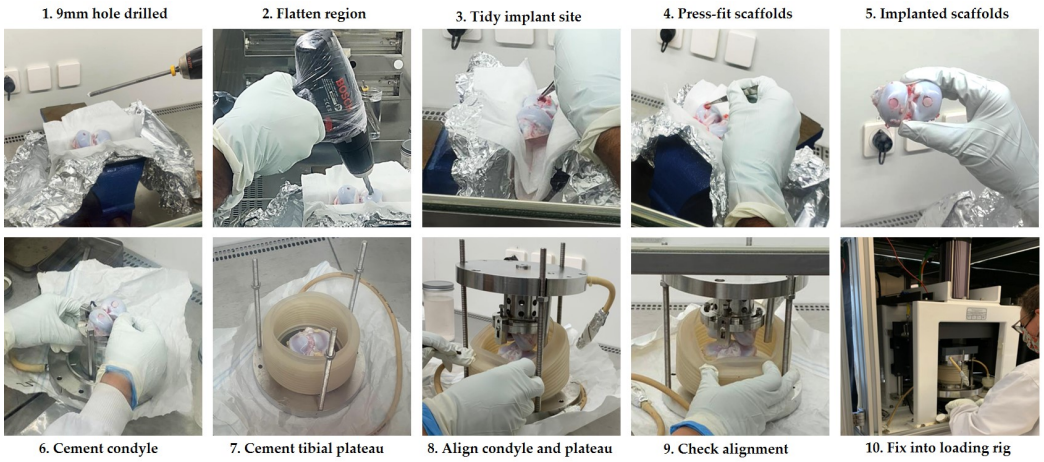

Figure 7.1: Natural knee loading rig set up. Procedure of drilling hole, implanting scaffold and cementing knee joints into the rig. Visualisation of method described in Section 7.3.3)

Once the defect site was clear, the seeded scaffolds were removed from culture and press-fit into the defect on the medial side, and the non-seeded scaffold was press-fit into the lateral condyle. Following this, both the femoral condyle and tibial plateau were attached to plates that formed the loading rig with poly(methyl methacrylate) (PMMA) bone cement, which was left for 14 minutes to set. The condyle and plateau were aligned and contact adjusted before final assembly (Figure 7.2). The condyles were encased within a sterile silicone gaiter, which was filled with the culture medium defined previously. The rig assembly was tightened, and inserted into the custom manufactured loading rig. Once assembled, the culture medium was sparged with 10% CO_2 in balanced air and maintained at 37°C for 7-days, with medium exchanged on day 4.

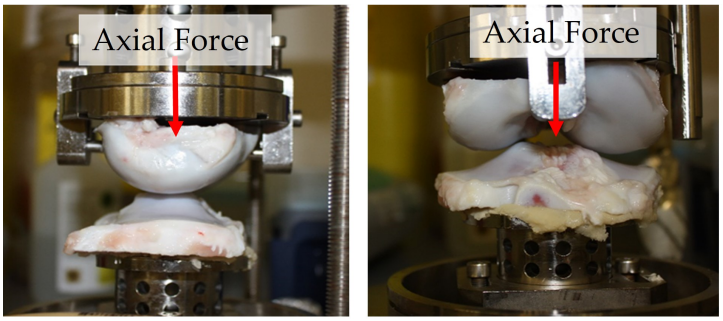

Anteroposterior Frontal

Figure 7.2: Condyles aligned on the simulator loading plates. Anteroposterior and frontal view of the femoral condyles and tibial plateau loaded onto the loading plate. Red arrow demonstrates direction of axial force. Figures adapted from images supplied by Natalie Fox, University of Leeds

7.3.4 Single station whole joint loading rig parameters

The natural knee loading rig was an electromechanically operated single station simulator (Simulation Solutions, UK) with a linear motor to control the Axial Force (AF) load axis. Once in the rig, the loaded organ culture was run on a 24 hour cycle (n = 1), which was a standard cycle defined through previous testing by Natalie Fox (unpublished data). The loading profile consisted of: 1 hour loading at a load of 10-400N at 1Hz, 4 hours rest (contact surfaces separated), 1 hour loading (as previous) and 18 hours of rest (as previous) (Figure 7.3). This cycle was repeated for the 7-days of culture. A spring system was used to move the opposing condyles apart during the compression cycle, to allow media to circulate the loaded condyles.

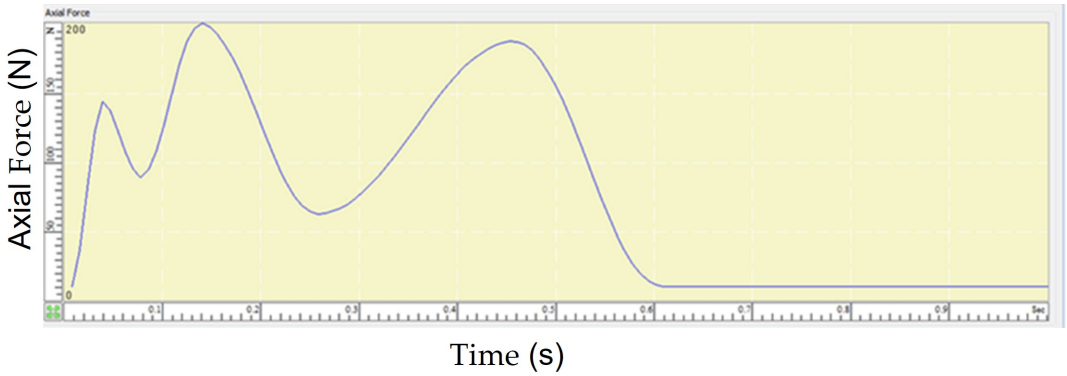

Figure 7.3: Simulator loading profile. Loading profile (N) versus time (S) at a frequency of 1 Hz

7.3.5 Downstream analysis

Following 7-days of culture, the media was removed using a MasterFlex pump, and the rig was disassembled and the condyles were removed. A hacksaw was used to remove a cuboid section from the area surrounding the plug implant site. The cuboids were bisectioned, half was used for LIVE/DEAD staining as described previously, whilst the other half was processed for paraffin wax embedding and ultimately H & E staining.

7.4 Results

7.4.1 Implantation

Following the culture period, the rig was dismantled and as shown in Figure 7.4A & B, the scaffolds were still fixed in the femoral condyle, indicating success of the interference fit. The fit was looser than desired, as shown in Figure 7.4B, there is a clear gap between the scaffold and the condyle. Following dissection, the tissue was bisected demonstrating the fit of the scaffolds within the tissue (Figure 7.4B). One edge showed alignment with the cartilage (green arrow), subchondral zone and bone. However, the opposite side (red arrow) is slightly looser and out of line.

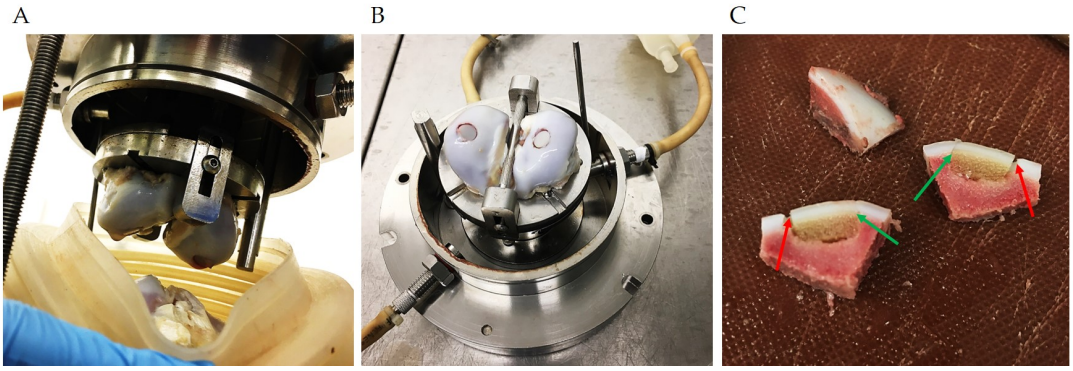

Figure 7.4: Decellularised scaffold implantation into porcine femoral condyle post-culture. A) Femoral condyle with decellularised scaffolds intact following 7-day culture. B) Arial view of the implanted scaffolds. C) Cross-sectional view of decellularised scaffolds implanted in the condyle. Red arrows indicated areas of worse fit, and green arrows indicate a good fit. The two labelled scaffolds are halves of the same plug.

7.4.2 Live/Dead Viability Assessment

Under both conditions the *ex-vivo* tissue surrounding the scaffolds retained viability up to Day 7 (Figure 7.5). In the non-seeded scaffolds there was an absence of live or dead cells in the scaffold.

In the seeded scaffolds, a faint band of cells are visible on the surface of the scaffolds under the calcein channel (green) (Figure 7.5), indicating live cells present after 7-days of dynamic culture. These are more visible from the increased digital zoom image in (Figure 7.6). There was also a signal under the dead channel, however, it later transpired that the Dil+ cell tracker fluoresced under the same channel. Therefore, it was not possible to distinguish between Dil+ labelled cells, and dead cells.

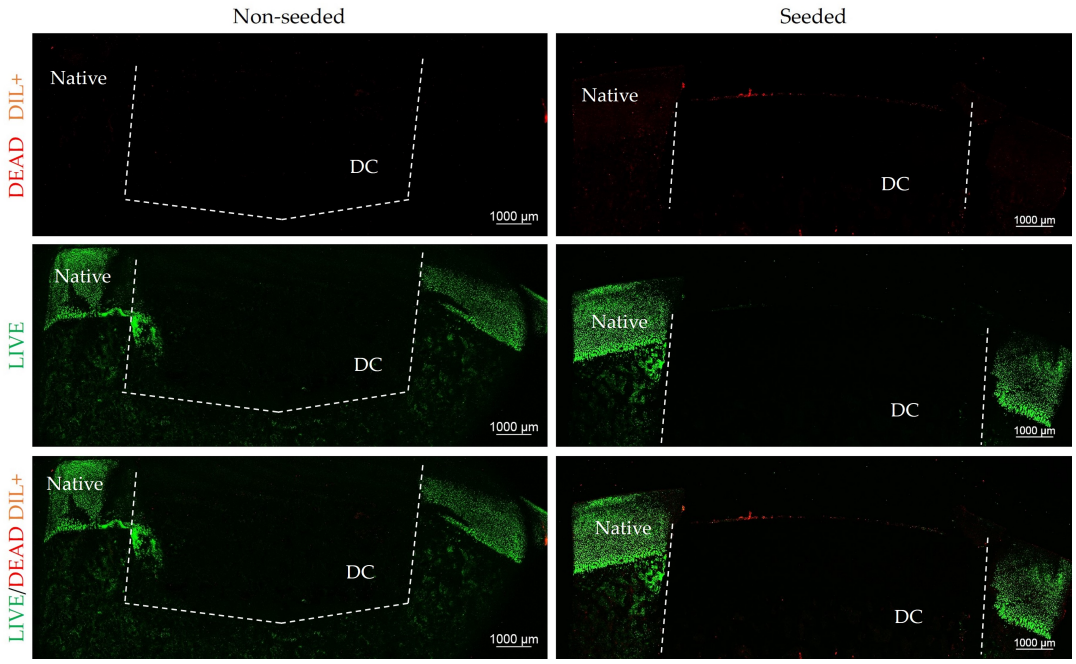

Figure 7.5: Live/Dead viability assessment of recellularised scaffolds implanted into the whole joint rig at Day 7. Seeded (right) and non-seeded (left) scaffolds were implanted into the femoral condyle (scaffolds indicated by dashed lines and labelled 'DC' and host tissue labelled 'native'). The Dead/Dil + (top), LIVE (middle) and Live/Dead/Dil+ (bottom) channels are separated. Scale bar = 1000 µm.

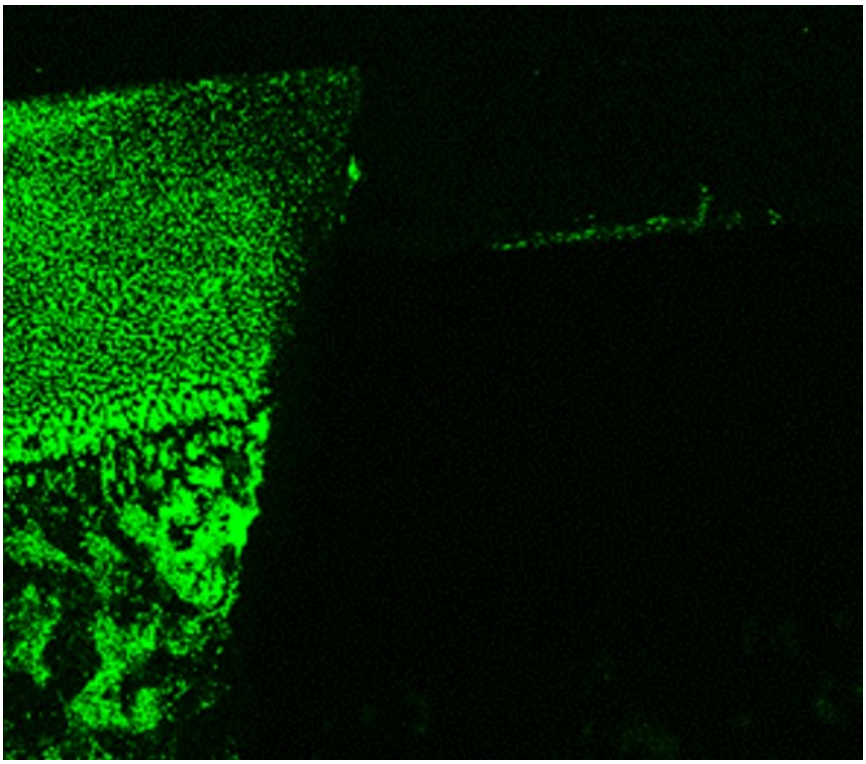

Figure 7.6: Enlarged section of seeded scaffold from whole joint rig at Day 7.

The non-seeded control in Figure 7.7 displayed a lack of fluorescence under the Live channel, and what appears to be autofluorescence under the Dead/Dil+ channel. Whereas the seeded sample contained viable cells across the superficial zone. There is an overlap of this staining with cells that fluoresce under the Dead/Dil+ channel.

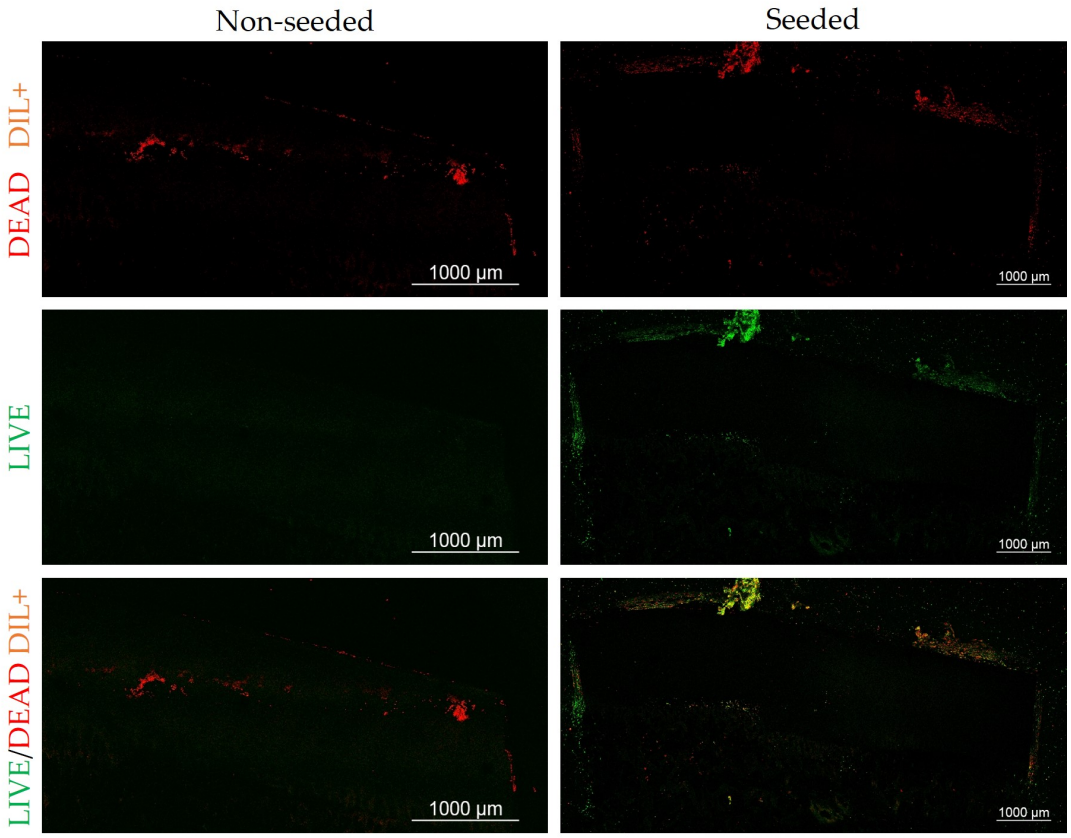

Figure 7.7: Live/Dead assessment of recellularised culture plate controls. Seeded (right) and non-seeded scaffolds (left) were cultured in a well-plate for 7-days. The Dead/Dil + (top), LIVE (middle) and Live/Dead/Dil+ (bottom) channels are separated. Scale bar = 1000 µm.

The presence of cell tracker labelled cells on the apical surface of the seeded scaffold (Figure 7.8) confirms that the live cells on the surface of the seeded decellularised scaffold in Figure 7.5 are cell tracker labelled chondrocytes. Dil+ fluorescence was absent from the unseeded scaffolds as expected. The Dil+ cells were also seen on the lateral scaffold edge, whilst none were observed below the surface.

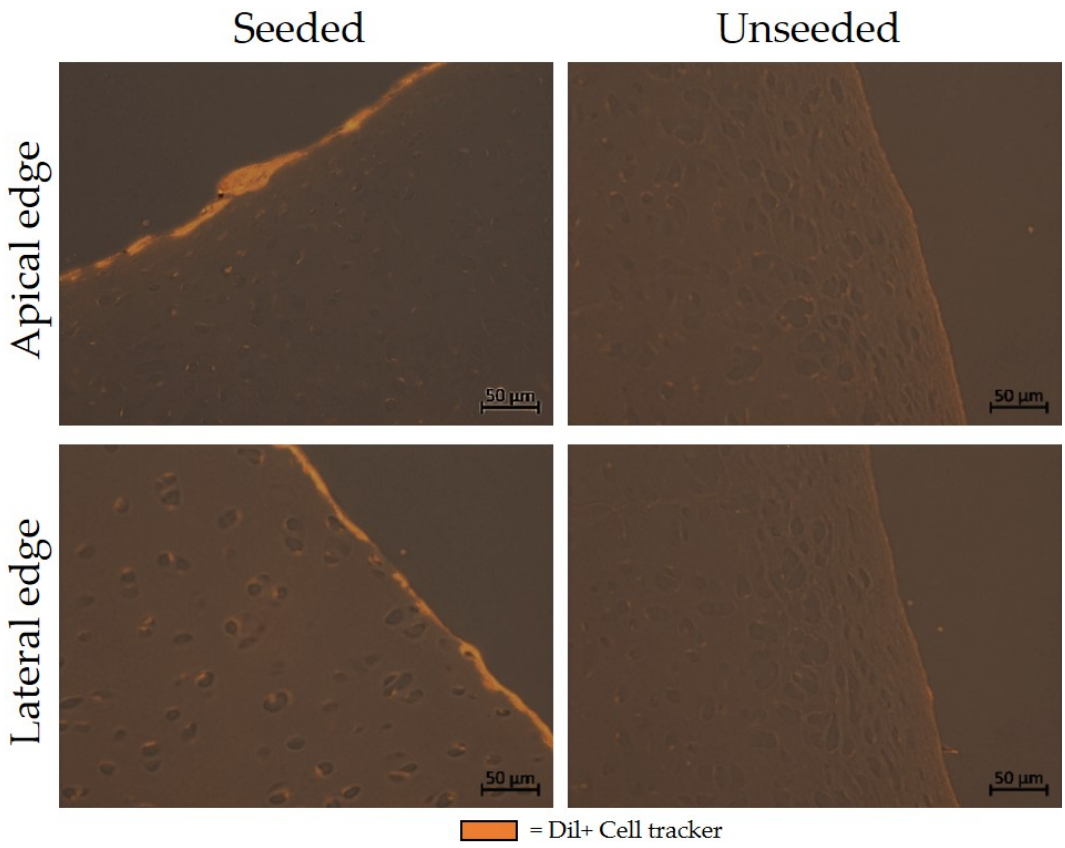

Figure 7.8: Presence of chondrocytes on decellularised scaffolds after 7-days in culture. Apical and lateral sections of scaffolds implanted in the *ex-vivo* living knee joint model were visualised using fluorescence microscopy. Orange staining represent Dil+ labelled chondrocytes. Scale bar = 50 µm.

The *in-situ* images in Figure 7.9 confirm the identity of the cells on the surface of the seeded scaffolds. It appears that no migration of chondrocytes from the scaffolds into the host tissue had occurred. However, in both seeded and unseeded scaffolds there were DAPI positive cells which were not Dil+ indicating that the cells were from the host tissue or residual cells from the decellularisation process.

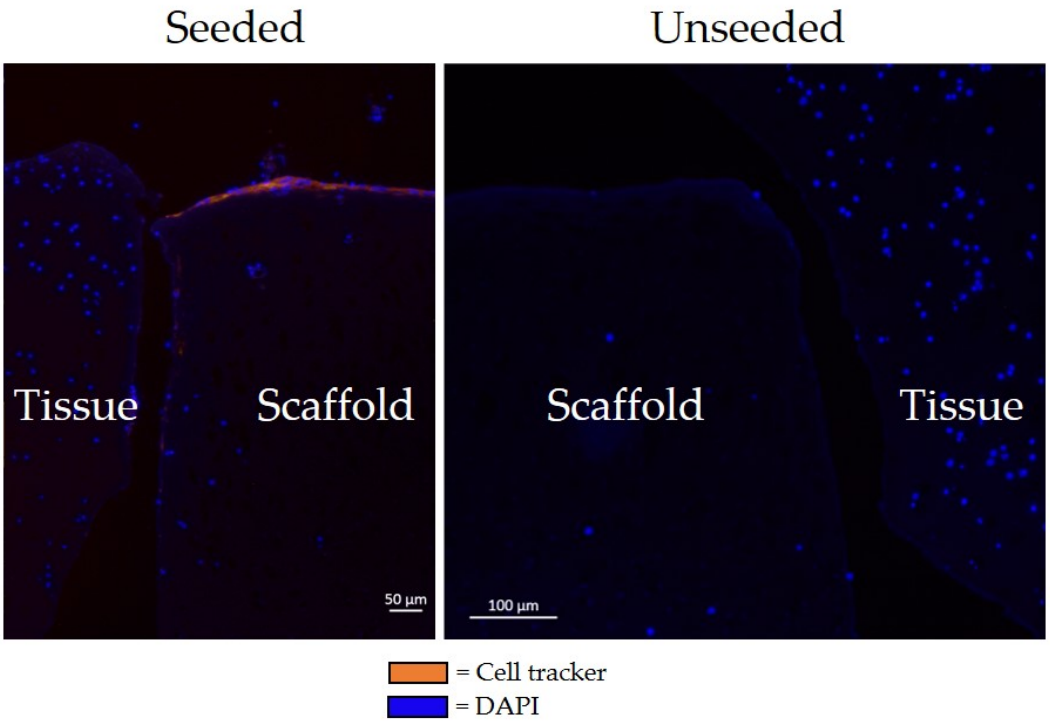

Figure 7.9: DAPI and Cell tracker staining of recellularised scaffolds implanted in the *ex-vivo* living knee joint model. Seeded (left) and non-seeded scaffold (right) sections were visualised using fluorescence microscopy. Cell tracker labelled porcine chondrocytes were visualised under the orange channel, whilst all other unlabelled cells were visualised under the DAPI channel. Scale bar = 50 and 100 µm.

7.5 Discussion

As described previously, mechanical loading is essential for healthy cartilage development and homeostasis. The effect of mechanical stimuli on the biosynthetic response of cells is known as mechanotransduction and has been employed in functional cartilage tissue engineering to generate mature constructs for implantation. Over time cartilage constructs that have received mechanical stimulation have improved functional properties (Bian *et al.*, 2010; Schätti *et al.*, 2011; Finlay *et al.*, 2016). One method of recreating such mechanical cues, is through the use of bioreactors capable of application of compressive force. This work in this chapter described a feasibility study into the incorporation of a repopulated decellularised matrix into an *ex-vivo* living knee joint simulation model.

This study showed successful creation of an osteochondral defect model for scaffold evaluation. Decellularised scaffolds were recellularised and implanted into the

condyles, and remained fixed in the condyle for the duration of study. Furthermore, live cells were observed in the host tissue as well as on the scaffold following 7-days of dynamic compression. Whilst this investigation was successful as a proof-of-concept study, many challenges and learnings were highlighted through the process, which will be discussed below, with an aim to be implemented in future studies.

The first challenge in this proof of concept study, was the creation of a defect of appropriate dimensions for the implantation of the 9 mm decellularised scaffold. The defect was created using the Arthrex drilling kit, within a class II safety cabinet. The site of implantation was chosen based on what was predicted to be the contact surface on the femoral condyle. The contact surface was predicted based on previously dissected condyles from prior experiments, which used transfer of Microset replication material (101FF, Microset Products Ltd, UK) onto the femoral condyle from the tibial plateau. However, due to the unique geometry of condyles from different donors, the lack of articulation and the requirement to maintain sterility, ensuring that the implantation site was also a contact area was fairly subjective. In this study it appeared that the scaffolds were at the contact point (Figure 7.4A), however, for accurate studies in the future judging the effect of biomechanical loading on deposition and/or gene expression, a more reliable alignment method should be incorporated. One solution may be using sterile surgical pens to mark the site to drill the defect. However, some research has indicated that the dyes within the pen can have a negative impact on chondrocyte viability (Getgood *et al.*, 2011). However, if the marker is being used to mark the area to create a defect and remove the cartilage, this may not have an influence on viability in this model due to the low residence time. Conversely, Indian ink injections through a 28/30G needle have been used to label cartilage, whilst maintaining sterility and cytocompatibility (Pfeifer *et al.*, 2012)

Once the site was chosen, the Athrex drill design allowed accurate drill placement at the desired site of implantation. The defect was drilled to a depth of 5 mm. The depth of which was monitored using 5 mm depth markings. Once this was achieved, the base of the graft was flattened using a 8 mm slot drill. As shown in Figure 7.4C, the depth of the defects was appropriate for the depth of the scaffold,

as in most instances the cartilage surfaces were aligned. However, in the process of bottoming out the implantation sites with the slot drill, the implantation sites were marginally wider due to the slot drill geometry, which caused the drill to slip. Unlike the Arthrex kit which was tapered and had a guide for accurate drilling, the slot drill bit was both flat and was three-fluted, therefore had a reduced contact area and guiding into the defect. Likely, this drill bit is better for removing bulk material, rather than finishing a defect.

As can be shown by the red arrows in Figure 7.4C, there was a dilation of the implantation site, resulting in the presence of a gap between the graft and the host tissue. Using a very similar model, (Bowland *et al.*, 2020) demonstrated that where osteochondral pins were implanted into dilated defects, a much lower force was required to cause graft subsistence to 1.25 mm below flush. Such surface incongruity has been shown to be a burden on rehabilitation, graft repair and integration and joint biomechanics (Wu *et al.*, 2002; Nosewicz *et al.*, 2014; Cowie *et al.*, 2021). Despite this, the grafts remained within the implantation site for the test duration, which was previously unknown and is promising to take this approach forward. To improve for the next run, the arthrex guided drill should be used to drill the majority of the defect depth, whilst more gentle methods of bottoming the defect should be investigated. For example the use of autoclavable grinding point sets, could allow for more control when bottoming the defect.

Accurate defect creation is an area of interest for both pre-clinical and tissue engineering applications alike. Researchers have managed to achieve deviation of 0.05 mm in defect depth (0.5 mm set point) and diameter (6 mm set point), using a purposefully designed "crown mill" to create an initial circular groove in a porcine femoral condyle, which defines the defect site. They subsequently use a "front mill" to remove the tissue within the newly created groove (Schwarz *et al.*, 2015). Importantly for the use of this tool in *in-vivo* applications, sterility was maintained. Furthermore, a custom built and automated defect creation mill (ArtCut) was developed by researchers to create defects in *ex-vivo* osteochondral models (Schwab

et al., 2021). The software controlled drilling allowed for high-throughput and reproducible defect creation. Importantly, due to a sterilisation step that occurs pre-drilling, sterility was maintained in the process. The aforementioned examples from the literature potential process improvement means, that would be necessary for the further development of this model as a reproducible pre-clinical assessment tool.

Alongside the method development, this study also achieved analytical method development. The principal output method of this study was histological outcomes (LIVE/DEAD, DAPI and cell tracker staining). One oversight in the development of the protocol was the overlap in emission spectra of both ethidium and the Dil+ cell tracker, which is shown below in Figure 7.10. The result of this, was that it was difficult to understand the extent of chondrocyte cell death on the surface of the decellularised scaffold in both the negative control (Figure 7.7) and the scaffold implanted in the living knee joint (Figure 7.5). This issue can easily be resolved by using a cell tracker with a peak emission at a different wavelength, as shown above with Cell Tracker Blue (Thermo Fisher Scientific, USA) (Figure 7.10).

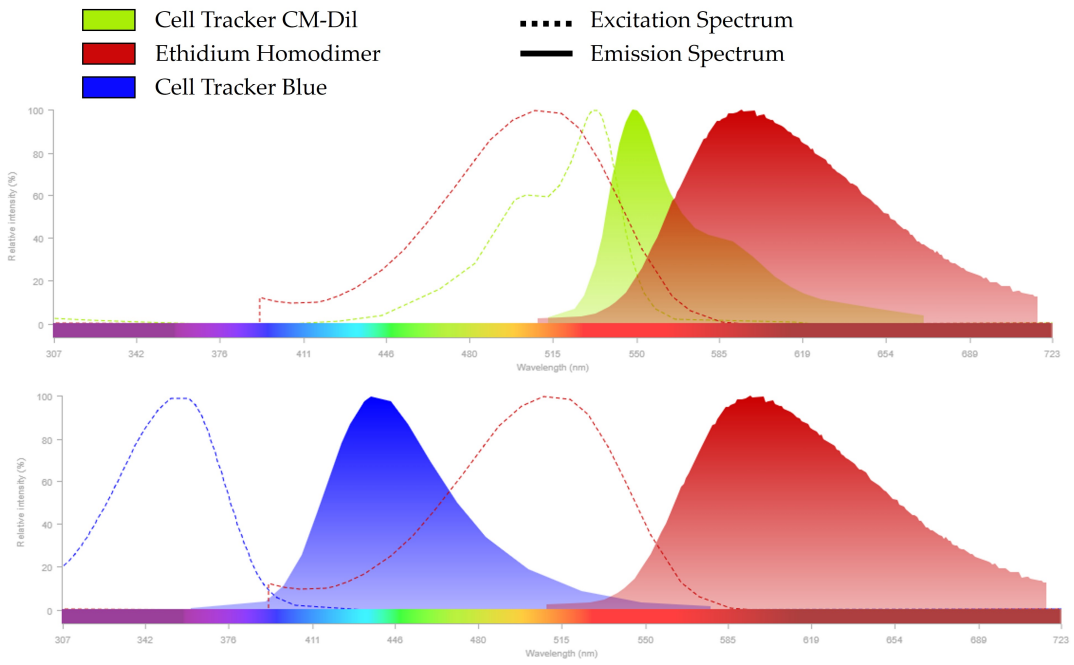

Figure 7.10: Excitation and emission spectra for Dil+ and Ethidium homodimer

The LIVE/DEAD data in Figure 7.5, confirms that by Day 7 the bulk of the host tissue had retained viability, in spite of the damage caused by defect creation. Cell death was confined to the site of defect creation, more readily visible in the seeded sample.

Furthermore, it appears from these figures that there was a population of live cells present on the scaffold surface (Figure 7.5). Which has promising indications for progression of this model for further use. Having said this, it appears that there was a lower cell density on the surface of the scaffold when compared with the culture plate control in Figure 7.7. This could possibly be the result of impact of the opposing condyles, causing the cells to detach from the cartilage surface. From the data in Figure 6.21, it was expected that cells would be visible below the superficial layer of the cartilage. However, from the data in Figure 7.5, cells (live or dead) were absent from these zones. On closer inspection of the histology sections in Figure 7.8, a positive signal was observed within the chondrons in the seeded samples which was absent in the unseeded samples. Despite this, the recellularised cell density was greatly reduced when compared with the signal from the native host cartilage (Figure 7.5).

7.6 Conclusion

Taken together, this study serves as an important proof of concept study into the development of this *ex-vivo* living knee joint simulation model to include a defect. If refined as suggested in this discussion, the model could provide a wealth of information into the use of recellularised osteochondral grafts for cartilage repair. In the literature, systems do exist to mechanically stimulate cells/cell-scaffold composites to create cartilage, through mimicking load and motion within articulating joints (Schätti *et al.*, 2011). This model, albeit using synthetic material, is capable of imparting both compression and shear onto scaffolds. Although our test configuration is currently confined to loading through the vertical axis, with the correct equipment there is no reason why this model would be unsuitable for more complex joint movements. Whilst such bioreactors can provide valuable information to the user, the potential benefit of the *ex-vivo* osteochondral culture model, is the simulation of the *in-situ* environment without the need the associated cost and ethical concerns surrounding *in-vivo* animal models. Through implantation into the condyles it is likely that the graft will be imposed to more physiologically relevant and complex

biomechanical stimuli. As well as a model for mechanical stimulation and cell response, it also can serve as a model to investigate more clinically driven research questions such as the consequence of implantation techniques, which would not be possible in other bioreactors.

Future work into this model should aim to address the issues highlighted in this chapter, with a focus on the implantation technique. Following on from this, analytics development should aim towards gene expression studies in the repopulated scaffold subject to loading within the rig. As well as analytical development, a potential limitation of this model is the fact it is only possible to run one sample at a time. At the present time of model creation, one replicate is sufficient. However, in the case of successful model development, potential for increasing the throughput of the model should be highlighted as a "nice-to-have".

Chapter 8

General Discussion

8.1 Summary of thesis aims and key findings

The aim of this research was to investigate the development of decellularised porcine osteochondral (OC) scaffolds as matrices to support chondrocyte implantation for the repair of large, shallow cartilage lesions. First of all, the cost-effectiveness of the intervention versus M-ACI was assessed, concluding that in order to be cost-effective the key drivers are clinical success akin to osteochondral allograft implantation. Following this, the efficacy of decellularisation for scaffolds of dimensions (2 cm (l) x 2 cm (w) x 5 mm (h)) appropriate to treat large shallow lesions was assessed. The decellularised scaffolds exhibited identical cytocompatibility, histological cell removal and reduction in DNA as seen with production of smaller OC plugs (8 mm (d) x 10 mm (h)). Biomechanical evaluation, and finite element modelling of OC decellularised scaffolds predicted an equilibrium elastic modulus of 0.1 MPa, which was significantly lower than the native cartilage.

Following the successful decellularisation, attempts were made to enhance the scaffolds through both recellularisation and GAG restoration with GAG doped self-assembling peptides (P_{11}-8/CS). Due to the dense ECM structure of cartilage, static seeding methods demonstrated no penetration of chondrocytes into the cartilage. Therefore, both physical and enzymatic cartilage disruption methods were investigated alongside dynamic seeding methods. Overnight lyophilisation of scaffolds demonstrated the most promising results across the pre-defined success criteria of cell penetration depth and homogeneity as well as DNA content post-recellularisation.

This method was also applied to the GAG restoration using P11-8/CS hydrogels. When rehydrated with monomeric peptide/CS solution, a trend for a reduction in percentage deformation was observed in restored cartilage.

The P_{11}-8/CS system was also assessed as a matrix for cell implantation. The process was adapted to resuspend the monomeric P_{11}/CS in cell culture media. This had no significant effect over the storage modulus, and showed similarity to acellular preparation methods investigated previously. Cell viability within P_{11}-8/CS was demonstrated with both L-929 (fibroblast) and C20A4 (chondrocyte) cell lines, as well as with primary porcine chondrocytes. Furthermore, an increased expression of chondrogenic markers (ACAN/ColII/COMP) was detected in chondrocytes encapsulated in self-assembling peptides versus monolayer controls.

Finally, a pilot proof of concept study was performed investigating the recellularised scaffolds developed previously, using an in-house *ex-vivo* living knee joint simulation model capable of dynamic compression. Scaffolds remained *in-situ* throughout the 7-day culture period, and viability was maintained in areas surrounding graft implantation as well as cells on the surface of the graft. Findings of this study, have identified process improvements to be implicated for later development.

This thesis investigated the interaction of three key elements (chondrocytes, decellularised osteochondral scaffolds, P_{11}-8/CS) which have been used in a variety of combinations. The results show the potential use of certain elements separately, and indicate the benefit of use together in one device. The Figure below describes this interactions between the elements, alongside the benefits of the approach (Figure 8.1).

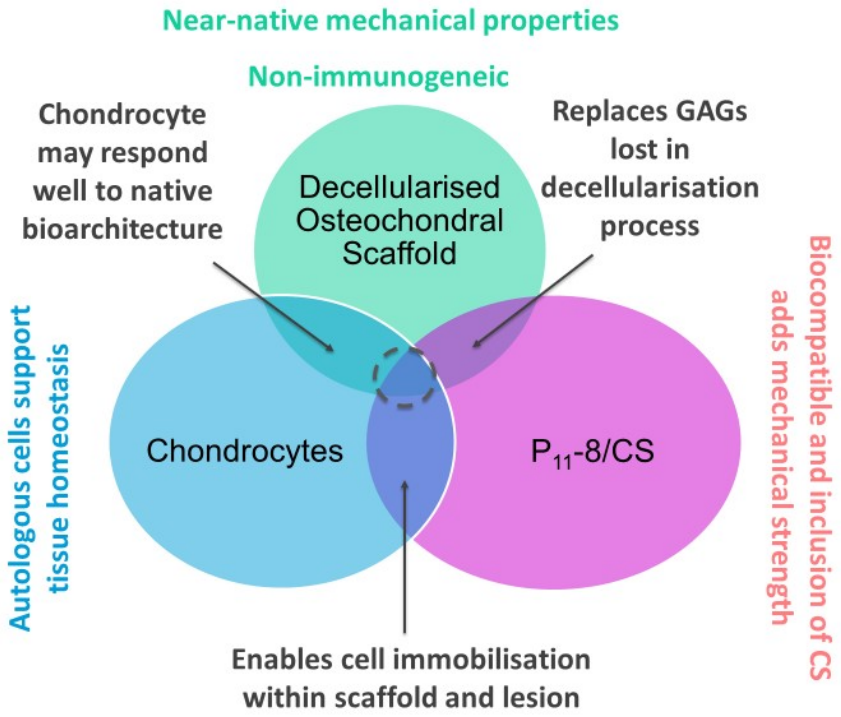

Figure 8.1: Graphic depicting the three interacting elements investigated in this thesis

8.2 Decellularised cartilage scaffolds as matrices for cell implantation

8.2.1 Clinical need for Decellularised cartilage

The underlying hypothesis for the use of repopulated decellularised osteochondral scaffolds in the treatment of large shallow cartilage lesions is multifaceted.

Firstly, the maintenance of near-native extracellular matrix structure in terms of collagen alignment (Figure 4.12) and retention of native ECM molecules such as Collagen II (Figure 4.11), VI (Figure 4.13) and reduced GAG (Figure 4.10), may provide both a structural and biomechanical advantage over other cell-seeded scaffold approaches. Despite the significant reduction in predicted equilibrium modulus, a modulus of approximately 0.1 MPa for decellularised cartilage is much improved in comparison with popular soft biomaterials, such as agarose, which are frequently seen in the kPa range (approx. 0.02 MPa) (Yang *et al.*, 2020). Furthermore, the properties seen in this study are pre-recellularisation/maturation, and in the literature

significant improvements in scaffolds biomechanical properties (83% of native cartilage stiffness) have been observed with ECM derived scaffolds after longer term culture (Kang *et al.*, 2014).

Secondly, both the biomechanical and biomolecular properties of scaffolds have been shown to play an important role in chondrocyte homeostasis and matrix deposition (Statham *et al.*, 2022). Therefore, the aforementioned retention of key components of articular cartilage may have an important chondroinductive effect as seen in the literature (Sutherland *et al.*, 2015).

Thirdly, the ability to completely decellularise porcine derived tissue of larger dimensions (4cm^2 diameter) has promising indications for cartilage repair from both a clinical and translational perspective. In larger lesions, the likelihood of capacity for spontaneous repair is much lower, such defects are termed critical cartilage defects. In these cases, scaffolds and/or cells are required to stimulate regeneration and restore cartilage surface congruity. In the case of large shallow cartilage lesions, the ability to implant decellularised scaffolds of dimensions at least up to 4cm^2, may facilitate an immediate recovery of biomechanical strength in the joint. Furthermore, cell removal and DNA reduction below the 50 ng.mg^{-1} threshold (Crapo *et al.*, 2011) from porcine tissue opens the door to xenogeneic supply of organs, reducing demand on healthy donor tissue. The use of porcine tissue from the meat industry provides a substantial cost reduction compared with osteochondral allografting (£6,661 vs £15,560 inc. implantation) (Figure 3.5) (Mistry *et al.*, 2019).

8.2.2 Decellularised cartilage development

In order to generate scaffold dimensions discussed above, significant changes were made to the production process. In place of shaping the scaffold to the previously developed "mushroom" structure, an "OC sheet" process was developed (depicted below in Figure 8.2), of dimensions suitable for the treatment of large cartilage lesions. The quality assessment data (DNA assay (Figure 4.7) and cytocompatibility assay (Figure 4.17)), demonstrated that the decellularisation process was still appropriate for the new dimensions. The benefit of such an approach, is the ability to treat

large defect with a single scaffold, overcoming the issue of fibrosis, frequently observed in mosaicplasty (Erol and Karakoyun, 2016). Scaffolds of these dimensions may also be used as "templates" for use in conjunction with 3-D scanning technology, for production of bespoke shaped scaffolds for enhanced fit (Li *et al.*, 2017). Acquisition of the defect "template" could inform designs to be used with laser-cutting technology to shape the scaffold accurately according to the 3D geometry of the defect.

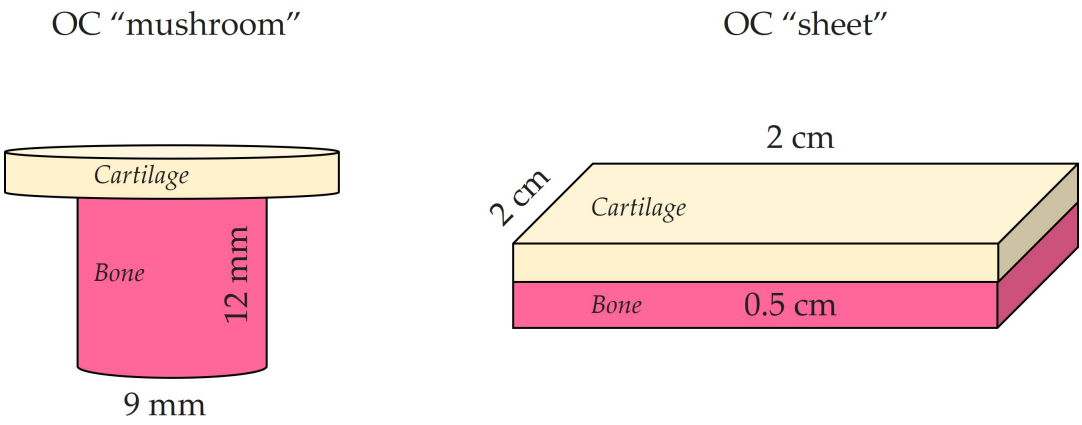

Figure 8.2: Previous and updated osteochondral scaffold dimensions. Graphical representation showing previous "mushroom" (left) shaping process versus the newly developed "OC sheet" (right) shape and dimensions.

Several studies have investigated decellularisation of cartilage (Fermor *et al.*, 2015a; Bautista *et al.*, 2016; Luo *et al.*, 2017), however, to the authors knowledge this is one of the largest, alongside (Kheir *et al.*, 2011), which have been successfully decellularised under the 50 ng.mg^{-1} threshold. Furthermore, of these studies fewer still are attempting decellularisation with OC tissue, of which the largest dimensions attempted are 12 mm (diameter) by 10 mm (height) (Neunaber *et al.*, 2022). Whilst the benefits of this approach have been discussed previously, implantation of larger grafts may pose a risk for repopulation with endogenous cells alone, which has been cited as a reason for graft failure in previous decellularised cartilage implantation clinical studies (Farr *et al.*, 2016).

The new dimensions also facilitate a much simpler manufacturing process, compared to the previously utilised "mushroom" shape, which required the use of an allograft transfer system and a sterilisable hammer to remove the OC plug from

the centre of the "mushroom". Whilst this an important consideration for the future development of the process, it also highlights an existing criticism of decellularised tissues compared with synthetically fabricated biomaterials. Such materials have the benefit of reproducibility of manufacture (O'brien, 2011), and can be fabricated to approach the complex biomechanical properties of cartilage (Means *et al.*, 2019). To be cost-effective, a scaffold must be able to be manufactured reproducibly in large batches (Partap *et al.*, 2010). Furthermore, to be suitable for implantation into patients, the process must be GMP compliant, and also follow the requirements set for the manufacturing process of human cell-based products by the European Medicines Agency (EMEA) (EMEA/CHMP/410869/2006). The tissue shaping and plug removal are process steps with the most open manipulation. Both new processes certainly improve reliability, and drastically reduce failure rates. However, the tissue shaping process would require contact with sterile gloves, which may increase the risk of contamination if breaches in aseptic technique occur. Adaptations could be made to the decellularised OC production process to become GMP compliant. These would include measures such as transitioning to the use of GMP-grade decellularisation reagents, terminal sterilisation (Hennessy *et al.*, 2017), tissue processing in an ISO 5 clean room (Tírico *et al.*, 2016) or closed system. Such changes of course come at an additional cost in terms of monetary (eg. Figure 3.1) and time, where it is estimated that GMP operations require twice as much time as non-GMP (consultation with industry expert). Current unpublished work from our group, has detailed the development an automated decellularisation system (ADS) based on the University of Leeds process. For porcine bone decellularisation, this system has yielded decellularised bone plugs, produced with automated solution changes, agitation, temperature control with a closed system. Adaptation of our process into this system would be a great first step towards GMP-compliance, alongside reducing open manipulation steps in tissue shaping.

As well as assessing success of decellularisation, further biological characterisation of the decellularised scaffolds was performed, to assess the content following decellularisation. The loss of CS/GAGs from cartilage following decellularisation has been well reported in the literature from this group (Kheir *et al.*, 2011; Fermor *et al.*,

2015a). The preserved collagen II content and structure is important for the biomechanical function of these scaffolds (Figure 4.12), and may provide structural cues for appropriate tissue regeneration and maturation (Luo *et al.*, 2017). Collagen VI was also retained pericellularly in the decellularised tissue, the benefit of this may be in both maintenance of the biochemical niche surrounding the chondrocyte, as well as in the appropriate load transmission via the PCM (Statham *et al.*, 2022).

The effect of decellularisation on the bulk biomechanical properties of the scaffolds was assessed using creep deformation. These results confirmed previous findings that the reduced GAG content causes a significant increase in the percentage deformation observed in decellularised scaffolds compared with the native cartilage tissue (Figure 4.21). Finite element modelling predicted the equilibrium elastic modulus of the decellularised cartilage to be 0.065 MPa compared with 0.235 MPa for the native tissue, which is similar to values seen in the literature for decellularised osteochondral grafts (Neunaber *et al.*, 2022).

Herein, introduces one of the key remaining challenges surrounding the use of decellularised tissues for the repair of articular cartilage. Inappropriate scaffold mechanical properties could lead to further surgical complications and/or inappropriate load transmission to the engrafted/repopulated cells. The properties of the native cartilage tissue have been used as a benchmark to aim for, however, limited work has currently been done to establish a threshold for appropriate biomechanical properties for tissue engineered cartilage materials. As it is difficult to compare between mechanical testing set-ups, a hydrogel/MACI control should have been included in this study to benchmark against the lower end of mechanical properties. However, it has been reported that hydrogels are typically one order of magnitude lower than native cartilage (Tatman *et al.*, 2015), whereas in this instance the decellularised grafts are within the same order.

A finite element study has investigated the effect of osteochondral graft mechanical properties of contact stress in recipient and donor tissue, as well as the effect on peak compressive strain and Von Mises stress. The analysis concluded that there was no significant effect on the graft, even with a 33% lower modulus than the native tissue (D'Lima *et al.*, 2009). They later discuss the practice of extracting osteochondral

grafts from non-load bearing locations and that their study supports the continued practice of this. In our study the mean equilibrium elastic modulus of the decellularised grafts was 30% of that of native cartilage (n = 6). Future work should investigate the potential effect of this reduced modulus *in-situ* through physiologically relevant models, to truly understand the implications for both graft failure and/or high local strains in the scaffold. Studies linking inconsistent aggrecan content in cartilage constructs to scaffold "buckling" have indicated cell death as a result of high local strains (Middendorf *et al.*, 2020). Therefore, appropriate scaffolds for tissue engineering should aim for consistent ECM content and structure.

Whilst in this instance the decellularised moduli fall short of the native moduli, an advantage which these scaffolds have over other interventions, is the overall retention of articular cartilage fibre alignment, porosity, structure and zonal arrangement (Figure 4.12). As mentioned previously, the hypothesis is that the retention of these biochemical and biomechanical cues, will serve as a optimal platform for cell repopulation and further scaffold maturation. This has been exemplified in several studies, which have shown decellularised cartilage is chondroinductive (Sutherland *et al.*, 2015) and when repopulated with chondrocyte can instruct deposition of cartilage matrix with a zone dependent structure and micromechanical properties (Luo *et al.*, 2017). Furthermore, as a starting material for cell repopulation decellularised cartilage derived matrices can achieve restoration of the Young's modulus and compressive moduli of native cartilage (Kang *et al.*, 2014; Li *et al.*, 2019).

8.3 Recellularisation of decellularised matrices

This hypothesis formed the basis for the recellularisation work presented in this thesis. *In-vitro* recellularisation of decellularised tissues has been applied for lots of soft-tissue types, for example heart, lung and liver tissue (Reviewed in: (Hillebrandt *et al.*, 2019)). However, as a result of its function dependent structure, cartilage has inherent differences to these tissue types such as low porosity and lack of pore interconnectivity which make repopulation of the tissue a more difficult task. This was validated by the initial cell seeding results depicted in Figure 6.5, which demonstrate

that after 24 hours, the C20A4 cells remain on the surface of the cartilage.

This result was expected, and the results from injection and vacuum seeding methods (Solchaga *et al.*, 2006) showed no improvement. Back pressure in the syringe meant any delivered cells were non-viable, and vacuum seeding was inconsistent, with preferential repopulation of the bone compartment. The method could be investigated further for the seeding of cartilage/bone only grafts, however, for osteochondral plugs it was inappropriate. Furthermore, both methods had a large amount of open processing steps that would likely to difficult to repeat in a clinical setting or sterile manufacture facility. Although the seeding did not penetrate below the superficial zone, there were several important findings from this study. Most importantly the cells attached to the cartilage, retained viability upon seeding and maintained a relatively homogenous seeding pattern over the surface of the cartilage.

Following this initial proof of concept, a number of other techniques were attempted to improve the quality of cell seeding. Prior to this, a three part criteria for successful seeding was defined. This was based on depth of cell penetration, homogeneity of seeding throughout the scaffold, and number of cells delivered. Depth and homogeneity of seeding were assessed using histological methods. The cells were labelled with a CM-Dil (Thermofisher, UK) cell tracker, which was chosen due to it's ability to be used with formalin fixation and paraffin wax embedding. This removed the burden away from 3-D live cell imaging, allowing for higher throughput of conditions. Viability was assessed using alamarBlue reagent which is a resazurin derived assay, sensitive for metabolic activity, through reduction of the compound via the electron transport chain.

Although delivery of cells via injection was ruled out, the creation of micro-channels in cartilage was investigated alongside further seeding methods. The combination of microchannels and either centrifugation or vacuum, demonstrated no significant improvement over static seeding methods in terms of DNA content (Figures 6.9 and 6.7). Cells were observed deeper in the cartilage in both channel groups with and without additional active seeding (centrifuge/vacuum). Cells were observed attached to the channels with limited lateral migration into the tissue ECM. This result

is in line with work investigating a similar approach, which also saw limited lateral migration of cells out of the artificially created channels (Bautista *et al.*, 2016; Luo *et al.*, 2017).

Overall, it was determined that the method was too variable for subsequent study, and was not effective enough in terms of improved seeding efficiency to compensate for the damage created to the tissue. Some of the complications resulting from channel creation, have been overcome through the use of higher precision technologies such as CO_2 lasers (Nürnberger *et al.*, 2021). Using this laser, a decellularised construct was created with 150 µm channels engraved across the basal surface of a decellularised scaffold. The channels were a cone shape with the widest point at the base of the cartilage scaffold. The purpose of this was to direct tissue regeneration in a vertical direction, in order to align with the fibre alignment of the native tissue. *In-vitro* and *In-vivo* implantation studies demonstrated ECM deposition and integration of the neo-tissue with the scaffold. The *In-vivo* defect model also demonstrated bone marrow invasion of the scaffold, resulting in integration between the host-tissue, scaffold and neotissue (Nürnberger *et al.*, 2021).

This study shows that despite the possible damage to the cartilage integrity, the processing of decellularised cartilage into grafts, can be an effective solution to improve integration. In this project, where creation of channels is necessary for the application, we hypothesise that preservation of the cartilage surface integrity is more important than the cell repopulation of deeper cartilage zones.

In order to overcome the limited permeability of cartilage (either through the articular surface or cut surfaces/channels) researchers have investigated collagenase treatment to partially degrade the cartilage, thereby increasing permeability. Application of collagenase has been shown to allow improved migration of chondrocytes out of host tissue (Seol *et al.*, 2014) as well as improved integration of grafts into the host tissue (Janssen *et al.*, 2006). This technique was optimised (Figure 6.12) and applied for improving the permeability of cartilage for recellularisation initially with the C20A4 cell line. Optimisation data saw an ablation of the upper superficial zone after 90 minutes, with agitation resulting in deeper digestion of the collagen fibrils. Interestingly after 45 minutes of treatment, no damage was visible in the sirius red

staining under brightfield or polarised light. However, there seemed to be a reduction in GAG content and a paler eosin (ECM) stain in the same region after 45 minutes indicating potentially lighter disruption to the collagen structure, allowing GAG to be released from the matrix. The disruption observed following 90 minutes of treatment was substantial and may be a hindrance for correct cartilage function. Further work should investigate the region between 45 minutes and 90 minutes, to target permeabilisation over ablation.

In spite of this, recellularisation studies were successful with apparent cell engraftment into the matrix by Day 7, with DNA content approaching that of native tissue. There was clear evidence macroscopically and histologically of disruption to the cartilage following treatment with collagenase, the biomechanical effect of this was not assessed.

In Figure 6.14, some cells can be observed in the non-seeded control. This highlights, an uncertainty arising from this data as well as all other recellularisation studies, whether the cells visible in the treated conditions are repopulated cells or remnant cells from the decellularisation process (< 5% of original cells). Despite this H & E image, it still appears as if the cell density is higher in the collagenase treated conditions, and the DNA data certainly reinforces this. The purpose of including the CM-Dil+ cell tracker was to mitigate for the presence of residual cells/cell artefacts, however, it appears under this channel there is low level autofluorescence from remnant material. In this instance, the use of several analytical methods (qualitative and quantitative), mitigates this possible area of uncertainty. At Day 7, the DNA content approaches 2000 ng.mg^{-1}, without the presence of a thick cell layer on the surface, indicating increased DNA/cell content within the tissue itself.

Lyophilisation of cartilage to improve recellularisation was the more innovative approach used to address the low permeability of cartilage to cells. One of the first findings was that upon rehydration of lyophilised cartilage, the native structure remains histologically intact and undisrupted despite dehydration (Figure 6.18). Following optimisation of the seeding process, cell seeding experiments were carried out. H & E staining appears to show cell staining in both the superficial and middle zones of the lyophilised scaffolds (Figure 6.21). To confirm their identity, the sections

were imaged with fluorescence microscopy for the presence of Dil+ labelled cells. In these images, the background was accounted for by using the unseeded scaffold as a reference to adjust the exposure, and as a result the images are a lot clearer, demonstrating that the cells below the surface may indeed be the original C20A4 seeded cells.

Taking all of this data together, the collagenase and lyophilised treatment were chosen as the most successful. Benefits of the collagenase treatment were the vastly improved cell attachment and cell content compared with both the static and unseeded controls. However, the disruption to the superficial zone collagen fibre structure is vast, and likely to compromise the functional properties of the scaffold which is one of the key expected benefits of the technology. Future work should investigate milder collagenase treatment, with minimal collagen disruption the aim. Biomolecular assays and immunofluorescence antibodies can be used to assess the denatured collagen content following enzymatic degradation. Following this, the relationship between collagen degradation and biomechanical function should be explored.

The same investigations would need to be performed for the lyophilised tissue, as the impact of the cycling between hydrated and rehydrated states has yet to be investigated. It is likely that there will be some impact on these due to the temporary disruption of the collagen fibres structure once dehydrated. However, when comparing the Sirius red staining between the collagenase and lyophilised treatments, the preservation of collagen in the lyophilised samples was clear to see. From the cell tracker labelled images it appears as if the seeded cells have repopulated the chondrons within the middle/deep zones. Whilst the DNA content was lower in these samples compared with collagenase, this is something which could be amended and accounted for by further optimisation of the cell seeding densities.

From a GMP perspective the collagenase treatment also adds an extra adventitious agent which requires extra documentation, testing and processing to remove. Whereas, the lyophilised technique does not require any additional reagents. Another benefit of the lyophilised approach, is that it facilitates a much simpler seeding process, in that the scaffold is rehydrated in a cell suspension. The hypothetical clinical use for this scaffold (depicted in Figure 8.3), would be that the scaffold is supplied and

stored in its lyophilised form. This would then be used alongside external autologous chondrocyte implantation, where the scaffold would then be rehydrated with cell suspension and incubated for 3 hours prior to implantation.

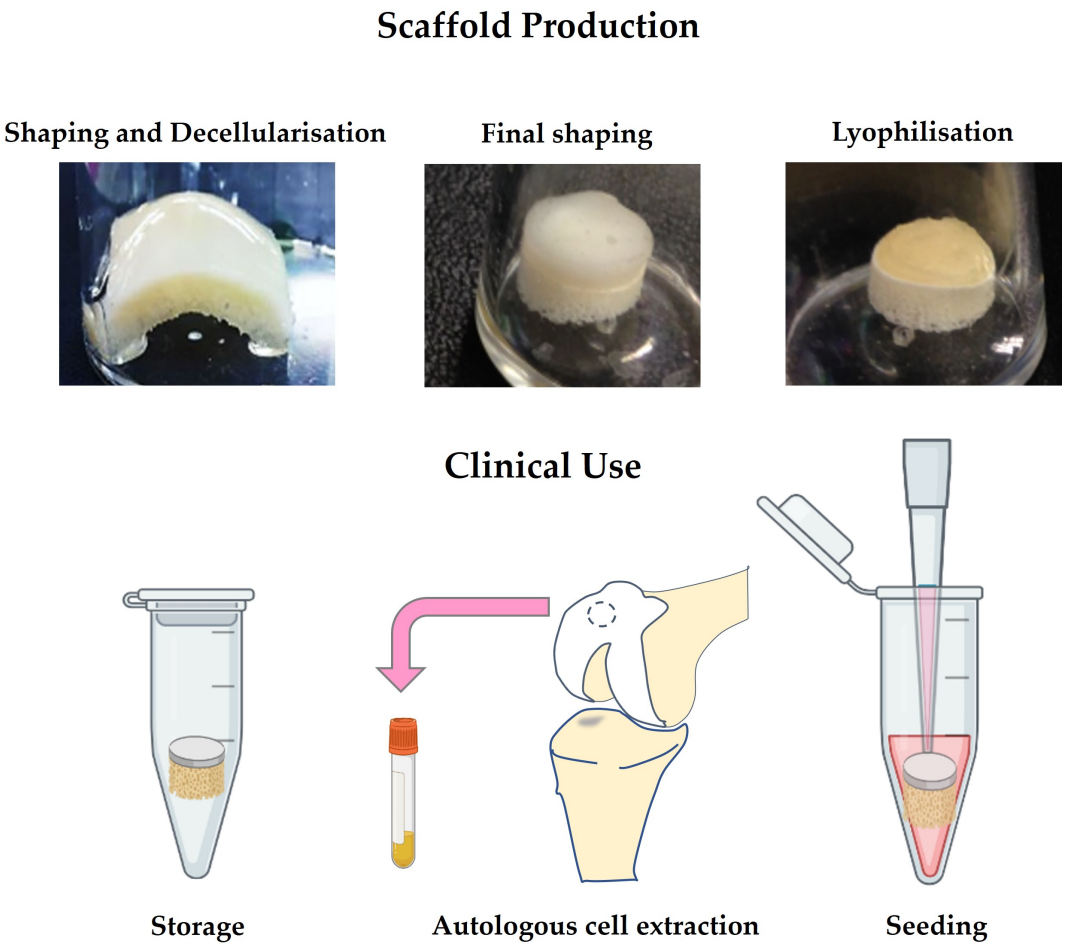

Figure 8.3: Graphical representation of the proposed clinical usage strategy for repopulated lyophilised decellularised scaffolds

The choice of cells for these recellularisation studies were C20A4 chondrocyte cell line, due to the ability to achieve high cell numbers quicker than primary chondrocytes. These cell are immortalised and likely have a different cell phenotype compared with primary chondrocytes, as well as being more robust in terms of cell viability. Results from the proof of concept viable knee joint simulator (Figure 7.7) have shown that primary chondrocytes seeded after 7-days remained viable on the surface of repopulated lyophilised scaffolds. Future work, should investigate the viability of seeded primary chondrocytes under the same conditions, as this cannot

be assumed from these studies alone. However, chondrocytes in the host tissue remained viable, therefore if the seeded cells are located within the tissue, a similar finding could be hypothesised.

Gene expression also becomes an important factor when using primary chondrocytes. For deposition of appropriate repair material, the chondrogenic phenotype must be maintained. Whilst not defined as such in a distinct panel of genes, chondrogenic express higher levels of Collagen II (COL2A1), Aggrecan (ACAN), cartilage oligomeric protein (COMP), and have been used as markers of chondrogenesis (Suchorska *et al.*, 2017). Collagen I is also used as a indicator of differentiation towards a more fibroblastic phenotype (Darling and Athanasiou, 2005). Previous research has indicated that decellularised cartilage can act as a substrate for chondrogenesis (Sutherland *et al.*, 2015). Therefore, future work should look at establishing the same phenotype retention with the decellularised cartilage developed in this work.

As well as gene expression, matrix deposition is also of interest from two perspectives. The first of these is to more accurately model the *In-vivo* environment, to see if the scaffold demonstrates an ability support deposition of hyaline cartilage like neotissue. Secondly, as alluded to previously, if the repopulated scaffolds demonstrate significant levels of GAG deposition, a defined pre-culture/maturation period prior to implantation could be implicated. This may serve to address some of the existing concerns of low GAG content as well as increase de-formability of decellularised tissue.

With the current length of study (7-days) it is unlikely to see vast improvements in either GAG deposition or improvements in the modulus of the constructs. Studies have seen significant increases in GAG deposition after 14-day period (Owida *et al.*, 2018). Improvements in moduli may require both longer (8-weeks) and more complex culture conditions such as compressive loading, which have demonstrated significantly higher improvements in modulus than static, non-loaded cultures (Finlay *et al.*, 2016). On the other hand, after similar period (8-weeks) following *in-vivo* implantation into a rabbit defect model, decellularised tissue has shown 83% recovery of the native tissue modulus (Kang *et al.*, 2014). Here represents two approaches which could be utilised, either pre-maturation of the scaffold prior to implantation,

or reliance on tissue maturation following implantation. The authors believe the latter would be preferable from a translational perspective, due to reduction in open processing steps, additional equipment and resource usage (e.g. time/cost) in the production.

Another aspect of long-term culture with primary chondrocytes which has not been investigated in the work is the capacity of primary chondrocytes to migrate through the scaffold over time. Several models for chondrocyte migration through cartilage exist. The two with the most traction appear to be cell process extension and protease mediated migration. Chondrocytes have been shown to migrate through hydrogels (Gosiewska *et al.*, 2001) and even 3D pre-clinical models have observed chondrocyte migration out of explants over time (Lyman *et al.*, 2000). Biomechanical loading of repopulated scaffolds has shown the potential for improved repopulation compared to unloaded scaffolds (Nachtsheim *et al.*, 2019). In this study, the effects of time and loading on migration of chondrocytes has not been explored. The use of pre-clinical, organotypic bioreactors would give further insight into the ability of such remodelling to occur with these scaffolds *in-situ*.

8.3.1 Assessment of recellularised scaffolds in a viable porcine knee joint simulation model

Once a method of repopulation was chosen, a proof of concept osteochondral defect model was attempted. This work built upon a "living knee joint" simulation capable of uniaxial cyclic compression, by creating defects in the articular surface. The defects were filled with two decellularised scaffolds, one of which was unseeded and the other was repopulated. The aims of this study were to assess 1) feasibility of both creating the model 2) maintenance of sterility and 3) viability of cells repopulated on the scaffold and surrounding the defect. From a feasibility perspective, the defect model was straightforward to produce and despite a looser fit than desired, both scaffolds remained in the defect for the entirety of the culture period (Figure 7.4). Furthermore, despite the several open processing steps within the safety cabinet, sterility was maintained throughout the culture. As discussed previously, despite

encouraging indications of feasibility of this model to evaluate osteochondral defects and scaffold implantation, there were several conditions which would require further optimisation. One process which needs further optimisation is the accurate matching of defect diameter and depth with that of the decellularised graft. Ideally, grafts should be press-fit into the defect, with both a congruous surface with the host tissue and contact made with the bottom of the defect. Furthermore, more work should be performed into ensuring the contact surfaces are opposite to each other, and are aligned to contact during the cyclic compression cycle.

Despite this, it was encouraging to see that after 7-days culture, Dil+ cells were present on the surface of the graft (Figure 7.9) and that it is a possibility that some of these cells are viable following the culture period (Figure 7.6). This indicates that the adhesion of the chondrocytes to the matrix is adequate to withstand compression *In-situ*. However, when comparing against the seeding of C20A4 cells onto these scaffolds, the cell number does seem substantially lower post-culture in the whole joint rig, which likely indicates cell removal due to contact with the opposing surface. This removal of articular chondrocytes was expected, which is the basis behind seeding cells into the middle and deeper zones if possible. Seeded chondrocytes were observed in the chondrons of the explant apical section(Figure 7.8), however, in the lateral section autofluorescence from the PCM makes it difficult to discern positive cells.

To the authors knowledge, this is the first example of a cartilage defect model within a whole viable knee joint. Studies have used cartilage defect models which use cartilage sheets (Jiang *et al.*, 2020), or OC plugs as a culture system to test biomaterials such as chondrogide (Melle *et al.*, 2012). However, none of these studies use mechanical stimulation. A negative of our approach, is that biomechanical regimes are based on compression only, when *in-vivo* loading is much more complicated. Bespoke bioreactors have been developed which are capable of both dynamic compression and shear, which demonstrate improved chondrogenic gene expression than either loading modality alone (Schätti *et al.*, 2011). This technology has been further developed to load an osteochondral organ culture model, consisting of an osteochondral

plug with a drilled defect. This set-up was used to test chondrocyte-seeded fibrin-polyurethane constructs, and demonstrated improvements in chondrogenic gene expression versus static culture controls (Vainieri *et al.*, 2018). The use of smaller scale set-ups also can improve the throughput of the testing methodology. The key advantage of our approach over this, is the physiologically relevant contact, scale and truly *in-situ* load transmission.

In conclusion, the further development of this natural living knee joint bioreactor has demonstrated positive potential as a model for the evaluation of osteochondral grafts *in-situ*. This allows determination and potential optimisation of several parameters surrounding graft fixation, gene expression in response to mechanical loading, cell migration and viability, without the requirement of costly animal studies. Of course, such *in-vivo* models will be required further down-the-line for translational purposes, however, this set up can allow a greater informed strategy leading into this work. Furthermore, due to the incorporation of the single station simulator a variety of loading configurations can be investigated to further develop biomechanical and mechanobiological studies in relation to cartilage regeneration. However, considerations should be noted surrounding the low-throughput nature of the set up (n=1).

8.4 Development of self-assembling peptides as matrices for GAG and cell delivery

As demonstrated in Figure 8.1, as well as decellularised scaffolds, P_{11}-8/CS hydrogels were investigated as matrices for the implantation of autologous chondrocytes. This work was a progression of work into the P_{11}-X family developed in the School of Chemistry at the University of Leeds (Aggeli *et al.*, 1997). Studies have investigated the use of members of the P_{11}-X family (including P_{11}-8) as matrices for cell implantation (Maude *et al.*, 2011) previously, as well as GAG doped hydrogels for restoration of biomechanical properties to GAG depleted tissues (Miles *et al.*, 2016; Warren, 2017; Barco *et al.*, 2018). The aim of this work was to attempt to combine the

two capabilities above into one device (P_{11}-8/CS and chondrocytes) for the restoration and regeneration of early-stage cartilage lesions. Furthermore, once optimised the aim was to deliver the hydrogel, initially without cells, to decellularised tissues in an attempt to recover native biomechanical properties pre-implantation through restoration of GAG content.

8.4.1 P_{11}-8/CS process adaptation and resultant material properties

The most up to date process, prior to this study, for the production of P_{11}-8/CS hydrogels involved the use of sodium acetate (pH = 4) to monomerise the peptide prior to lyophilisation. Initial studies (Figure 5.12), demonstrated poor viability of seeded cells into these matrices, likely due to residual acid associated with the peptide, therefore, the first step was to adapt the production process to produce reproducible gels akin in rheological properties to the acellular types, which are capable of supporting cell growth. Therefore, both the sodium acetate addition, and lyophilisation step were removed, and the peptide powder was directly resuspended in DMEM+.

Following several iterations, a suitable preparation method of gel preparation was decided on (Section 5.2), and referred to as Iteration 2. This used vortexing, sonication to overcome initial complications associated with early gelation. Viability comparisons of this iteration demonstrated that cell viability was maintained when compared with collagen hydrogels (Figure 5.13) over a 14-day timecourse. Aside from at Day 7, the metabolic activity was significantly lower in P_{11}-8/CS than in the collagen hydrogels for L929 cells. However, with C20A4 chondrocytes, there was no significant difference in metabolic activity at Day 1 or Day 14. As the more physiologically relevant cell type, these results are encouraging (Figure 5.14).

The material properties of the hydrogels were also important from a cell support perspective (Statham *et al.*, 2022) as well as by conferring an ability to restore biomechanical strength of GAG depleted cartilage (Barco *et al.*, 2018). Therefore, a rheological study was carried out, investigating both solvent type and length of equilibration time on G′/G″. Following a 24 hour equilibration, P_{11}-8/CS hydrogels had an elastic modulus of 30 kPa, which compared well to other examples of chondroitin sulphate containing hydrogels (7-33 kPa) (Wang *et al.*, 2016). In the cited study, hydrogels of

this range of moduli better supported neocartilage formation *in-vivo*, over weaker (1 kPa) hydrogels which failed mechanically *in-situ*.

The control for this study was the previous gel formulation developed by (Warren, 2017), which was prepared in 130 mM NaCl solution to impart a pH trigger and stable self-assembly. As both the solvent and it's components are likely to effect self-assembly, there was a suspicion that resuspending the gels in supplemented DMEM (5% FBS, 2% P/S, 1% LG) would effect self-assembly and therefore the rheological properties of the gels. As shown in Figure 5.8 the G' and G" were not significantly different between hydrogels resuspended in salt solution or supplemented DMEM. The more significant effect, was equilibration time, with 24 hour equilibration showing significantly higher G' compared with 3 hour equilibration. The implication of these results is interesting from both a translation and clinical perspective. Mobilisation of the knee joint post ACI tends to occur at 12-24 hours post-surgery (Ebert *et al.*, 2021), which may offer a window of knee immobilisation which would allow the gel to equilibrate *in-situ*. Future work should aim for better resolution of the gelation kinetics of this gel preparation, between the two timepoints (3 and 24 hours), to determine if, and at what point the G' peaks over this equilibration period.

To recap, the term "equilibration time" refers to the time in which the gels are left undisturbed prior to medium addition. The reasoning behind the 3 hour equilibration, was to preserve cell viability by introducing media supplementation early as possible without disrupting gelation. However, in a brief comparison (data not shown), it was determined that cell viability was comparable following 3 and 24 hour equilibration. This is demonstrated in the viability results shown in Figure 5.15, which demonstrates viable chondrocytes in gels which were left to equilibrate for 24 hours at 37°C. The maintained viability in these gels, was most likely due to the DMEM+ in the gel mixture, which is sufficient to support/maintain cell viability for at least 24 hours prior to medium addition.

Another key discussion point for this work is the omission of cells from these hydrogels during rheological testing, due to biosafety regulations with the equipment used. It is unknown how exactly the presence of cells within the system would alter these properties. One hypothesis is that the chondrocytes over time would remodel

and/or degrade the hydrogel (Feng *et al.*, 2014), which may result in a reduction in gel modulus. However, scaffold remodelling may also result in improvements to the gel modulus through ECM deposition (Kisiday *et al.*, 2002). Future work should investigate how the repopulated gels respond to prolonged culture in terms of ECM deposition and material properties.

The primary objective of this work was to have a gel compatible of encapsulating primary chondrocytes, therefore, time was not available to delve deeper in material development and optimisation of gel material properties. However, work by (Warren *et al.*, 2021) has demonstrated how processing steps such as vortexing can change P_{11}-X family rheological properties by two orders of magnitude. Furthermore, alterations of the peptide:GAG ratio can result in increases in diameter of the peptide fibrils, resulting in a more robust gel. There is an interaction between both these parameters, relating to both fibre thickness and increased interconnectivity, that confers an ability to tune peptide rheological properties. As this work was conducted on P_{11}-12, future work should investigate process optimisations to see if further improvements to gel stiffness can be achieved, with the P_{11}-8/CS system.

Despite the promising results demonstrated here, what is yet to be investigated is the stability of these hydrogels within cartilage and under dynamic compression at physiologically relevant loads as would be expected during daily activities. Using the living knee joint bioreactor, P_{11}-8/CS stability and/or retention should be investigated.

8.4.2 Ability of the hydrogels to support viability and phenotypic stability of primary chondrocytes

After initial PoC (Figure 5.13) with L929 cells, a repeat was performed with the C20A4 chondrocytes, as mentioned previously. The similarity in the ability of both the collagen hydrogel model and P_{11}-8/CS gels to support chondrocyte viability and proliferation is certainly promising. Although not directly measured here, the gene expression data utilising primary chondrocytes indicates viability through increases in gene expression over the time course (Figure 5.17) . However, future work

should still investigate repeating the previous viability assays on encapsulated primary chondrocytes.

Whilst viability of cells is extremely important in initial development of a biomaterial for tissue engineering, in cartilage tissue engineering maintenance of the chondrogenic phenotype is imperative for appropriate tissue repair. As mentioned previously, qPCR was used to probe chondrogenesis, as extracting viable cells for identification by flow cytometry (Wang *et al.*, 2001) was not achievable, due to their integration in the scaffold. Whilst qPCR analysis is a relatively routine technique to probe such changes, in this project due to the encapsulation of the cells in P_{11}-8/CS, this work ended up being a significant piece of method development. Using physical agitation, and tituration alongside a Trizol extraction method (Section 5.3.3.3), cDNA yields were achieved which satisfied both concentration and purity thresholds for qPCR analysis.

Once optimised with C20A4 cells, it was immediately evident that the chondrogenic gene expression from the cell line was minimal, as reported in the literature (Finger *et al.*, 2004). This resulted in the move to primary chondrocytes extracted from porcine cartilage. As a result of the requirement for expansion to meet the cell requirements for the study, the chondrocytes had dedifferentiated as a result of passaging and extended 2D culture. However, using a redifferentiation protocol adapted from the literature (Huey *et al.*, 2013), which detailed a 6-day differentiation process on chondrocyte aggregates in the presence of TGF-*beta*. The fold-change of markers associated with chondrogenesis (Aggrecan, Collagen II, COMP) were substantially upregulated, whilst markers of dedifferentiation remained unchanged (Collagen I).

The gene expression study used the redifferentiated chondrocytes as the starting material for both the monolayer control and the chondrocytes encapsulated in the P_{11}-8/CS system. The aim of this study was to show that cells encapsulated in P_{11}-8/CS did not dedifferentiate upon encapsulation, rather than to demonstrate P_{11}-8/CS as a chondrogenic material. Therefore, a monolayer was determined to be an appropriate control. The data shows a drop in both COL2A1 and ACAN expression in the monolayer, with a fold-change below 1 in both instances. For both these gene's in the P_{11}-8/CS samples, there was a drop at Day 7 below Day 0 values, followed

by a recovery back to either redifferentiated levels of expression (ACAN) or a 6-fold increase in expression (COL2A1) by Day 21. COMP expression also had a >10-fold change in expression by Day 21. For all gene associated with chondrogenesis, by Day 14 the P_{11}-8/CS samples had a significantly higher fold-change in gene expression compared with the monolayer samples. There was also an increase in COL1A2 expression in both monolayer and P_{11}-8/CS samples, but there was no significant difference between the two (>6-fold change by Day 21). Although, COL1A2 expression can be indicative of a hypertrophic phenotype, it's increased expression with time is often seen in cartilage tissue engineering studies (Cambria *et al.*, 2020; Ge *et al.*, 2021). Studies have found that such collagen I expression can be suppressed by mechanostimulation (Ge *et al.*, 2021). Calculating the ratio of Collagen II:Collagen I gene expression can give further insight into the differentiation status of the cells. As shown in Figure 5.18 from Day 7, Collagen II signalling dominates Collagen I, indicating an overall healthy chondrogenic phenotype.

Comparison of the results observed here with other gene expression studies is difficult, due to variation in condition, cell type and RT-qPCR methodologies. As mentioned previously, the following study should include further controls to assess the level of chondrogenic gene expression compared with other interventions. A study comparing gene expression in MACI interventions (Albrecht *et al.*, 2011), used a cartilage biopsy as a baseline to assess gene expression against. Interestingly, all interventions tested (CaReS ®, followed by Novocart ®3D, Hyalograft ®C and MACI ®) showed lower gene expression compared with the cartilage biopsy. The authors cite long-culture periods pre-seeding as a potential reason behind this, therefore, the inclusion of our redifferentiation step may be beneficial in achieving physiologically relevant gene expression. Furthermore, the authors also cite higher cell densities as a driving factor of chondrogenic phenotype retention. Including cell seeding density, there are still many parameters to explore regarding P_{11}-8/CS preparation to optimise for optimal gene expression.

Overall, this data demonstrated suitability of P_{11}-8/CS as a scaffold for chondrocyte encapsulation. Following this gene expression data, work should focus on ECM deposition and the relationship of any deposition into the development of the P_{11}-8/CS

material properties. Development of this platform should investigate application in restoration of early-stage cartilage lesions where GAG depletion has occurred.

8.4.3 P_{11}-8/CS delivery to decellularised scaffolds

The other potential use of this platform is in conjunction with decellularised scaffolds (Figure 8.1). As described extensively, the loss of GAGs from decellularised scaffolds has an impact on the biomechanical properties of these scaffolds. Therefore, we hypothesised that delivery of P_{11}-8/CS to these scaffolds, may restore the native GAG content as well as the biomechanical properties. It is important to note that due to constraints, delivery of P_{11}-8/CS to decellularised scaffolds alongside chondrocytes was not investigated.

The Safranin O staining (Figure 6.25) and FITC tagged peptide (Figure 6.26) images appeared to demonstrate successful delivery of GAG to the cartilage. From the FITC images, it appears that peptide delivery was ubiquitous throughout the cartilage, with some areas of more dense aggregates of peptide. The Safranin O staining also demonstrated similar aggregates of CS, however, what was also evident from these images was the localisation of peptide to the chondrons, which was similar to cell seeding results. However, GAG delivery appeared throughout all cartilage zones.

Treatment with P_{11}-8/CS appeared to reduce the percentage deformation of the scaffolds, although it was marginally not significant ($p = 0.0538$). This was likely due to the amount of GAG delivered. Using the same treatment, when a GAG assay was performed on "GAG-restored" scaffolds, there was no significant increase in the GAG content, despite the promising histological outcomes.

Previous work by Warren, (2017) who delivered P_{11}-8/CS to GAG depleted osteochondral samples, saw similar improvements in percentage deformation. The GAG depleted sample exhibited approximately 30% deformation, whereas samples treated with P_{11}-8/CS injections showed 15% deformation (Warren, 2017). Work with a similar experimental set up saw P_{11}-8/CS restored cartilage with values very similar to the recovery seen in our samples, however the variability between repeats was much higher in our samples.

Several conclusions may be made from this study. Firstly, the mean percentage deformation observed in the Lyo-DC scaffolds alone was approximately 30-35%. Which is approximately 10% higher than the values obtained for untreated decellularised scaffolds (20%) with the same testing set up. Therefore, following lyophilisation and GAG delivery, these data may only represent a 5% recovery (15%) in percentage deformation from the decellularised cartilage samples. How this improvement in percentage deformation affects the equilibrium modulus is unknown, as the presence of the peptide in the cartilage invalidates the model. However, 5% closer to the native value (5%-7%) is likely still an important improvement.

Another observation from this data, is that the greater recovery is seen in scaffolds with the higher initial percentage deformation post-lyophilisation. This may indicate a non-linear relationship between GAG restoration. Other studies have observed R^2 values of 0.6-0.8 (Treppo *et al.*, 2000; Pfeiffer *et al.*, 2008), for the correlation between GAG content and moduli in both natural and tissue engineered cartilage. This is expected, given the known contribution of other components such a collagen, water and other ECM molecules to the biomechanical function of cartilage. Given the variability in both the recovery, and initial starting biomechanical properties of decellularised cartilage, future work should investigate non-invasive screening methods to aim to enrich scaffolds with preferred mechanical properties. Studies have reported correlations of 0.8 relating the equilibrium modulus of cartilage with quantitative MRI images (Nieminen *et al.*, 2004; Nykänen *et al.*, 2019). Such screening, could allow for either selection of scaffolds with higher moduli or for stratification of scaffolds to treat patients with variable biomechanical requirements.

8.5 Future work

Throughout this thesis, during the discussion chapters, suggestions on experimental improvements have been made as well as suggestions for future work to progress the development of these devices. This chapter will aim to summarise the more

higher priority suggestions with an aim towards continued progression of these devices on the path towards clinical adoption.

8.5.1 Continued *In-vitro* characterisation

Whilst movement towards *in-vivo* studies is certainly important for translation, in order to get to that stage, further *In-vitro* evidence must be gathered.

(i) *Further characterisation of decellularised scaffold-cell interaction*

To this point we have demonstrated viability of C20A4 chondrocytes on the surface of statically seeded decellularised cartilage up to Day 16 - with no significant change to the metabolic activity from Day 1 (Figure 6.12). With the active seeded methods however, viability (inferred via metabolic activity) has only been detected up to Day 7. Therefore, future work should focus on extending these studies up to 21-days, which is considered long-term culture (Divieto and Sassi, 2015). For these studies, if there is availability of primary healthy human articular chondrocytes (hAC), the priority should be to use this cell type, as the most clinically relevant cell type. This work should investigate whether the current recellularisation process is also appropriate for use with primary cell types. Progression beyond this, should further investigate viability of this construct (decellularised osteochondral scaffolds with hACs) under cyclic compression using the viable knee joint simulation model described in Chapter 7. The combination of this viability data should give sufficient viability data to progress to *in-vivo* studies.

Due to the many interactions of seeding methods investigated in Chapter 6, much of the recellularisation work has not been subject to extensive optimisation. Currently, 1 x 10^6/mL C20A4 cells are delivered to each scaffold (equivalent of 5 x 10^6/mL), which has shown successful repopulation and maintenance of viability. However, the effect of varying the cell density on cell seeding efficiency and viability has not yet been investigated. Studies investigating repopulation of M-ACI scaffolds have used densities from 0.5 - 50 x 10^6

cells/mL, with reports of ceiling effects above 10 x 10^6 cells/mL (Olderøy *et al.*, 2014; Cao *et al.*, 2020).

As well as viability and penetration of cells, gene expression and extracellular matrix deposition should be investigated. Generating a data set similar to the data shown in Figure 5.17 for P_{11}-8/CS, should be prioritised for the decellularised scaffolds in conjunction with healthy primary chondrocytes. Furthermore, if osteoarthritic chondrocytes are available, it would be interesting to assess the ability of these matrices to restore the cells chondrogenic potential, as has been demonstrated for materials in the literature (Cao *et al.*, 2020). In terms of extracellular matrix deposition, 16-weeks of extended culture alongside mechanical loading has shown significant ECM deposition as well as recovery of compressive modului equivalent to native cartilage in PET scaffolds (Finlay *et al.*, 2016). Future study design, should investigate similar culture length with and without biomechanical loading (using natural knee joint bioreactor), with chondrogenic gene expression, cartilage ECM deposition and recovery of biomechanical properties as readouts.

(ii) *Optimisation of parameters in preparation of cell seeded P_{11}-8/CS hydrogels*

Similarly to the decellularised scaffolds, for the P_{11}-8/CS gels, previous viability and gene expression studies should be repeated with human articular chondrocytes to demonstrate clinical relevance. Alongside these measures, development of rheological properties and ECM molecule deposition over time should be assessed.

As well as adaptation to use with hACs, several parameters have potential for further optimisation, including:

(a) Cell seeding density

(b) P_{11}-8 and CS concentration and ratio between components

(c) Solvent composition

(d) Length of vortexing during gel preparation

With the relative ease of production, and potential for higher-throughput screening, a design of experiment (DoE) approach could be used to optimise the

above parameters for the outputs: metabolic activity, collagen II/ACAN expression and storage modulus determined by rheology. The DoE approach uses design spaces, to assess several factors, ranges and responses in one experiment to generate significant data sets.

Finally, as discussed above, the solvent media composition should be investigated. Currently, the media is supplemented with FBS, P/S and L-G within DMEM. Removal of FBS and P/S should be prioritised for translational purposes, especially with FBS due to safety concerns. If removal of any component has drastic effects over the gel performance or cell encapsulation, GMP alternative should be sought after.

(iii) *Delivery of P_{11}-8/CS hydrogels and decellularised OC scaffolds*

As one of the major limitations of the decellularised scaffolds is the reduction in GAGs and therefore the increased percentage deformation, the delivery of P_{11}-8/CS to the scaffolds warrants further investigation. The current data shows that a trend in reduced percentage deformation ($p = 0.056$) versus decellularised scaffolds alone (pre-treated with lyophilisation and rehydrated). One approach would further pursue delivery to lyophilised cartilage, however, the self-assembly could be prevented by a lower pH environment allowing full penetration of the P_{11}-8/CS into the cartilage. Upon penetration into the cartilage it has been shown that the physiological environment can trigger self-assembly. If the pH trigger was successful in maintaining the monomeric state of the P_{11}-8/CS, a higher concentration of P_{11}-8/CS could be used (20 $mg.mL^{-1}$) which would double the delivery of CS, and may have a significant effect in improving the biomechanical properties of cartilage.

Given the hypothetical benefits of both recellularisation and GAG delivery to decellularised scaffolds, the combination of all three components (cells, scaffold and P_{11}-8/CS) may yield a scaffold with optimised properties. Such an approach would address many of the existing concerns (integrations and biomechanical properties) with decellularised scaffolds.

(iv) *Development of the defect model*

Given the increasing desire to minimise the use of animal models, the further development of the natural living knee joint defect model could be very impactful. For the purpose of the devices developed in this thesis, it can test a variety of factors including:

(a) Graft fixation

(b) P_{11}-8/CS stability within cartilage under cyclic compression

(c) Mechanobiological response of chondrocytes within decellularised cartilage

(d) Integration/regeneration studies of repopulated materials *in-situ*

However, in order to achieve this several adjustments need to be made to the model set up including:

(a) Alignment of contact surfaces

(b) Appropriate method of defect creation under sterile conditions

As discussed in Chapter 7, alignment of the contact surfaces could be performed by aligning the condyles in the test configurations, and marking the contact area with a sterile marker or an injection of sterile indian ink (Pfeifer *et al.*, 2012). Following the identification of the defect site, precise and accurate drilling of a defect site should be prioritised, by development of a custom mill/drill with limiters on both depth (5 mm) and lateral migration - to permit a press fit implantation of the decellularised scaffold into the scaffold. Collaboration or consultation with surgical teams could yield drilling techniques and practices to ensure accurate defect creation.

(v) *Further investigation of the biomechanical and tribological decellularised porcine osteochondral tissue*

Much of the focus for biomechanical evaluation of decellularised porcine osteochondral in this study and in the literature has focussed on the compressive properties of articular cartilage, as a result of it's load bearing function. What is yet to be directly investigated is the effect of the cartilage permeabilisation

methods (collagenase digestion and lyophilisation) on the elastic equilibrium modulus of the tissue.

Alongside the biomechanical properties of cartilage under compression, the biotribological properties of cartilage are essential in it's correct function as a tissue. Using a pin-on-plate set up, it is possible to determine the friction coefficient for cartilage (Kanca *et al.*, 2018). Therefore, future work should focus on the assess the effect of decellularisation on the tribological properties of decellularised porcine cartilage.

8.5.2 Industrialisation

As well as the incremental optimisations and suggestions for subsequent development of decellularised cartilage and P_{11}-8/CS as devices for cell implantation, it is also important to ensure that the devices are being developed in a manner to meet both translational and regulatory requirements. The following areas for future investigation will cover process improvements and *in-vivo* assessment.

(i) *Decellularisation process length*

The current process for decellularisation is 8-weeks including time for quality assessment and characterisation. On examining the process, there are many 24 hour washes, and 72 hour washes due to working hour restrictions. As discussed previously, research in our group has developed an automated decellularisation system (ADS). This device allows for decellularisation changes at any time, reducing the requirement for users to perform manual changes outside work hours. This has the potential to significantly reduce the length of the decellularisation process. Work on the ADS from the iMBE group (Cowell *et al*. 2022 (unpublished data)) has shown that the 24/72 hour washes can be shortened to 3 hours with no significant changes to the decellularisation quality. This reduced the process length from 42-days to 13-days. Therefore, process development is suggested for future investigation, with a focus on the effect of reducing length of wash on quality of decellularisation of osteochondral sheets. The impact of this work would be significant, in terms of reduction

of both labour costs, use of laboratory resource, and potential scaffold production capacity per year. This scenario can be used in the cost-effectiveness study presented in Chapter 3, to re-evaluate the ICER with a shorter process and assumedly lower cost. The move towards automation is essential for scale-up of this technology.

(ii) *In-vivo assessment of recellularised porcine osteochondral grafts*

Subject to positive results in the further *In-vitro* testing, *In-vivo* work should follow. Historically M-ACI studies have worked with rabbit (Willers *et al.*, 2005), sheep (Jones *et al.*, 2008) and equine (Frisbie *et al.*, 2008) models for pharmacodynamic, biodistribution and local tolerance studies which have contributed to the European Medicines Agency (EMA) assessment report for MACI (European Medicines Agency, 2013) (N.B. MACI has since been withdrawn and is no longer authorised). The aforementioned models were used as they are recognised osteochondral defect models.

Decellularised osteochondral scaffolds have been implanted in ovine femoral condyle defect models (Fermor, 2018) at the University of Leeds, which have shown graft failure by 26-weeks. In order to demonstrate improved effectiveness of a cell-seeded approach, the study should investigate a large animal osteochondral defect model. The defect should have an implanted porcine derived decellularised matrix with autologous (porcine, ovine, equine etc.) derived articular chondrocytes seeded onto the scaffolds.

8.5.3 Conclusion

To conclude, this work describes the development of both decellularised osteochondral scaffolds and self-assembling peptides as devices to support regeneration of articular cartilage through use in conjunction with chondrocytes. Key milestones were achieved for the decellularised scaffolds, firstly in the cost-effectiveness study which demonstrated the cost-effectiveness of decellularised osteochondral scaffolds for chondrocyte implantation over MACI. Secondly in the development of two methods of seeding chondrocytes onto and into the scaffolds. As well as this, PoC studies

were performed into improving the scaffolds biomechanical properties through delivery of P_{11}-8/CS and development of a osteochondral defect bioreactor model to test these interventions in the future. Future work should focus on long-term culture studies, alongside biomechanical loading accompanied by gene expression/ECM deposition studies. Furthermore, key translational concerns still remain, in terms of the feasibility of reproducible and scalable manufacture of the scaffolds.

Secondly, the P_{11}-8/CS system was progressed to encapsulate cells for the first time. The effect of the process adaptation was negligible on the rheological properties, and the TEM images showed similar fibre connectivity. Furthermore, the primary porcine chondrocytes retained expression of key chondrogenic genes (Collagen II, COMP, Aggrecan), during extended culture. These data show potential for P_{11}-8/CS alone to act as a cell delivery vehicle for early stage cartilage lesions, to restore GAG content and regenerate damaged tissue. As above, biomechanical property evolution over time should be investigated, as well as a further optimisation of preparation conditions and the resultant biomechanical properties.

Taken separately, both research streams have potential for use as separate devices for cartilage lesions at different stages of progression (early-stage and large shallow cartilage lesions). However, use in combination could yield scaffolds with both enhanced regenerative potential with improved biomechanical properties. Successful translation of such a device could yield a future therapy which could more effectively repair articular cartilage lesions, potentially prolonging the function of the natural knee and delaying the requirement for prosthetic intervention.

Chapter 9

Appendix

9.1 Equipment

Table 9.1: Equipment A list of general equipment used and the suppliers.

Equipment	Model	Supplier
Automatic cell counter	Countess II (Brightfield)	Invitrogen
Autoclave	MVA C40 Benchtop	Priorclave
Automatic Pipettes	Gilson P2-1000	Anachem Ltd
Balances	GX-2000	A&D
Bench top centrifuge	5415R	Eppendorf
Centrifuge	Harrier 15/80	Sanyo Biomedical Europe
Class II safety cabinet	Heraeus 85	Kendro
CO_2 Incubator	MCO-20AIC	Sanyo Biomedical Europe
Confocal Laser Scanning Microscope	LSM88 Inverted	Zeiss
Cryostat	CM3050S	Leica
Dental flosser	Waterpik Ultra Water Flosser WP-120	Waterpik
Digital microscope camera	AXIOCAM MRc5	Zeiss
Dissection equipment	Various	Fine Scientific Tools Ltd
Dremel drill	8200	Dremel
Forceps		Samco
Freeze drier	ModulyoD-230	Thermo Savant
Freezer (-20˚C)	Electrolux 3000	Jencons PLC
Freezer (-80˚C)	Various	Sanyo Biomedical
Fridge	Electrolux ER8817C	Jencons PLC
Fume hood	N/A	Whiteley fume extraction solutions
Hand drill	-	Bosch
Heated forceps	Speci-leps	Bios Europe
Histology moulds (32 x 23 x 14 mm)	3803085E	LeiceBiosystems
Histology water bath	MH8515	Barnstead Electrothermal
Histology hot plate	E18.1	Raymond A Lamb
Indentation rig	Custom	University of Leeds
Liquid nitrogen dewar	BIO65	Jencons Plc
Linear variable differential transducer	RPD D5-200 H	Electrosence
Magnetic stirrer	-	Fisher Scientific
MasterFlex Drive		VWR
Microbalance, 7 figure digital	ABJ220-4NM	KERN
Microscope, upright light	AXIO Imager.M2	Zeiss
Microtome semi-automatic	RM2255	Leica Biosystems
Nanodrop spectrophotometer	ND-1000	Labtech International
Osteochondral allograft transfer system	OATS	Arthrex
Orbital incubator	S150	Stuart

Equipment	Model	Supplier
Oscillating hand saw	AFM14 FEIN AkkuMultimaster	Fein
Piezoelectric force transducer	Part No. 060-1896-02	Electrosense
Pipette boy	Acu	Integra biosciences
Pestle and mortar	-	Victor
Plate Shaker	IKA KS130 basic	Jencons PLC
pH meter	3510 pH meter	Jenway
qPCR machine	Mx3000P	Stratagene
Rheometer	Pro Rheometer	Malvern Kinexus
Scalpel handle size 3	12464070	Fisher Scientific
Scalpel handle size 4	12348019	Fisher Scientific
Single station simulator	-	Simulation solutions
Simulator accessories	Custom	University of Leeds
Slide holders	E102	Raymond A Lamb
Sonication bath	U300H	Ultrawave
Stainless steel indenter	-	University of Leeds
Stainless steel slip gauges	-	University of Leeds
Spectrophotometer	Multiskan	Thermo Fisher Scientific
Sterilisation oven	HAS/200/SS	GenLab
Transmission electron microscope	1400	JEO
Tissue processor	TP1020	Leica
Vacuum pump		
Vernier callipers	-	-
Vortexer	Topmix FB15024	Fisher scientific
Water bath	Grant JB Nova	Wolf Laboratories
Water purifier	Option 7	ELGA
Wax dispenser	E66	Raymond A Lamb
Wax oven	GPWAX-SO-HYD	Jim Engineering Ltd

9.2 Consumables

Table 9.2: Consumables A list of general consumables used and the suppliers.

Consumables	Model	Supplier
3M Steri-Strip Skin Closure	-	Medisave
Autoclave bags	Plain closure bags	Westfield Medical
Bijou tube 5 ml	-	Scientific Laboratory Supplies Ltd
Biopsy Punch	8 mm	Stiefel
Cell culture flasks	T75, T175	Thermo Fisher Scientific Ltd
Cell counting chamber slide	Countess (disposable)	Invitrogen
Cell strainer	70 µL	Greiner Bio-One
Centrifuge tubes	50 mL	Corning
Coverslips	(22 x 64 mm)	Scientific Laboratory Supplies Ltd
Cryovials	Cryolife	Nunc International Corporation
DNAeasy Blood & Tissue	-	Qiagen
Filter paper	-	Scientific Laboratory Supplies Ltd
Histology cassettes	EMB-130-020R	Thermo Fisher Scientific Ltd
Histology cover slips (50 x 70 mm)	3800198G	Leica Biosystems
Histology slides (superfrost plus 25 x 75 mm)	10149870	Fisher Scientific
Imaging quality well plate	96-well, Lumox	Starstedt
Microtome blades (Feather N35)	3808311E	Leica Biosystems
Microtubes	1.5 mL and 2 mL	Eppendorf
Optical bottom petri dish	-	Starstedt
OptiplateTM	96-well	PerkinElmerTM
Parafilm		Bemis
PCR Plate	96-well, non-skirted	Thermo Fisher Scientific
PCR Tubes & Caps	0.2 mL (8-strip)	Thermo Fisher Scientific
PCR Caps (MicroAmp)	8-strip, Flat, Optical	Thermo Fisher Scientific
Pipette tips	10, 20, 200, 1000 µL	Star Labs
Plastic syringes	1, 2, 5, 10, 20, 50 mL	Scientific Laboratory Supplies Ltd
RNA Clean-Up Kit	-	New England Biolabs
Scalpel blade	Size 10, 22	Fisher Scientific
Serological pipettes	5, 10, 25, 50 mL	Sigma Aldrich
Sterile containers	50, 150 and 250 mL	Scientific Laboratory Supplies Ltd
Sterile filters	20 and 70 µm	
Sterile gauze	Non woven	Medisave
Sterile Loop	-	Fisher Scientific
Stripettes	1, 2, 5, 10, 25 mL	Sigma-Aldrich Ltd
Syringe (hypodermic) 25 G Tissue Culture Flask	- T25, T75, T175	Terumo Tissue Culture Flask
Universals	25 ml	Scientific Laboratory Supplies Ltd
Well plates (flat-bottomed)	6, 12, 24, 48, 96-well plates	Nunc International Corporation

9.3 Chemicals and Reagents

Table 9.3: Chemicals and Reagents A list of general chemical and reagents used and the suppliers.

Chemical/Reagent	Supplier
1, 9 dimethylene blue	Sigma-Aldrich
Absolute ethanol	Thermo Fisher Scientific
Acetic Acid	Thermo Fisher Scientific
Acetone	VWR International
Aprotinin (10000 KIU/mL)	Nordic Pharma
AlamarBlue	Biorad
Amphotericin B	Merck Life Science
Anchored oligo $(dT)_{20}$ primer	Jena Biosciences
Ascorbic acid	Merck Life Science
ATPLite-M assay	Perkin-Elmer
Benzonase nuclease hc, purity > 90%	Merck Chemicals
Bovine Serum Albumin	Sigma-Aldrich
Calcium Chloride	VWR International
Calf thymus DNA	Sigma Aldrich
Chloroform	Sigma
Chondroitin Sulphate	Sigma Aldrich
Chondroitin Sulphate Antibody (C-8035)	Sigma Aldrich
Citric acid	VWR International
CO2 in air 5% (v/v)	British Oxygen Company
Collagen II (MAB1330)	Millipore
Collagen VI antibody (ab6588)	Abcam
Collagenase	Sigma Aldrich
Cyanoacrylate contact adhesive	Scotch Super Glue Liquid
DABCO	Sigma Aldrich
DAB+ Substrate Chroogen System	DA
DAKO Anti-mouse HRP	DAKO
DAPI (4', 6-diamidino-2-phenylindoledihydrochloride)	Sigma Aldrich
Dexamethasone	Merck Life Science
Dimethyl sulfoxide (DMSO)	Sigma Aldrich
DNase	Sigma Alrich
DNase/RNase free water	5 Prime
DNeasy blood and tissue reagents	Qiagen
DPBS without Ca^{2+}/Mg^{2+}	Sigma Aldrich
DPX mountant	Atom Scientific
Dulbecco's modified eagle medium (DMEM)	Sigma Aldrich
EDC (1-ethyl-3-(3-dimethylaminopropyl)carbodiimide hydrochloride)	Sigma Aldrich
EDTA (disodium ethylenediaminetetraacetic acid)	Thermo Fisher Scientific
Eosin	VWR International
Ethanol	Thermo Fisher Scientific
Fast green	Sigma

Chemical/Reagent	Supplier
Fibroblast growth factor-2	Peprotech
Fluorescence mounting medium	Dako
Fetal bovine serum (FBS)	Sera Labs
Gentamycin	Sigma Aldrich
Giemsa stain	VWR International
Glasgow's minimal essential medium (GMEM)	Sigma Aldrich
Haematoxylin (Mayer's)	Atom Scientific
Haematoxylin (Weigert's)	Atom Scientific
Hank's balanced salt solution (HBSS)	Siga
Heparin	Merck Life Science
Hepes	Lonza
Hydrochloric Acid (6 M)	Thermo Fisher Scientific
Hydrogen Peroxide	Sigma Aldrich
IgG1	DAKO
Insulin, transferrin and selenous acid premix	BD Biosciences
Isopropanol	Thermo Fisher Scientific
L-glutamine (200 mM)	Sigma Aldrich
LIVE/DEAD™ Viability/Cytotoxicity kit	Thermo Fisher Scientific (Invitrogen)
Lard	Tesco
Magnesium chloride hexahydrate	Thermo Fisher Scientific
Neutral Buffered Formalin (10% v/v)	Thermo Fisher Scientific
Omniscript reverse transcription kit	Qiagen
Optimal Cutting Temperature Fluid	Tissue Tek
Miller's Stain	Raymond A Lamb
MES (2-(N-morpholino)ethanesulfonic acid)	Sigma Aldrich
Monosodium citrate	Sigma Aldrich
NHS (N-Hydroxysuccinimide)	Thermo Fisher Scientific
Nuclease free water	VWR International
Oxalic acid (dihydrate)	VWRI
P_{11}-8	CS-Bio
P_{11}-8-FITC	CS-Bio
Papain	Sigma Aldrich
Paraffin Wax	Raymond A Lamb
Picric acid	Sigma Aldrich
Penicillin (5000 U/mL) / streptomycin (5 mg/mL)	Sigma Aldrich
Peracetic acid (32%)	Sigma Aldrich
Potassium permanganate	Thermo Fisher Scientific
Proteinase K (>600 mAU/mL)	Qiagen
RAFT™ Reagent Kit for 3D culture	Lonza Bioscience
Random Hexamer primer	Thermo Fisher

Chemical/Reagent	Supplier
Rat tail type I collagen (> 2mg/mL in 0.6% acetic acid (v/v))	First Link UK
RNAlater	Sigma
RNase inhibitor (40U/μL)	Fisher Scientific (Invitrogen)
RNase OUT	G Biosciences
Safranin O	Acros
Scott's tap water	Atom Scientific
Sirius red	VWR Internation
Sodium chloride	Thermo Fisher Scientific
Sodium dodecyl sulphate	Sigma Aldrich
Sodium hydroxide	Thermo Fisher Scientific
Sodium pyruvate	Merck Life Sciences
Streptomycin	Merck Life Sciences
Transforming growth factor-beta	Peprotech
Thioglycollate medium USP	Sigma Aldrich
Trigene	Scientific Laboratory Supplies
Trizma base	Sigma Aldrich
TRIzol™	Fisher Scientific
Trypsin-EDTA solution (0.5 %; w/v)	Sigma Aldrich
Tryptone soya broth	Sigma Aldrich
Tryptose phosphate broth (TPB)	Sigma Aldrich
Turbo DNase	Thermo Fisher
UltraPure™ 10% (w/v) sodium dodecyl sulphate solution	Invitrogen Life Technologies
Virkon	Scientific Laboratory Supplies
Vybrant™ CM-Dil Cell-Labelling Solution	Thermo Fisher Scientific
Xylene	Atom Scientific

Bibliography

Abdelgaied, A *et al.* (2015). "Comparison of the biomechanical tensile and compressive properties of decellularised and natural porcine meniscus". In: *Journal of biomechanics* 48.8, pp. 1389–1396.

Adkisson, H. D. *et al.* (2010a). "Immune evasion by neocartilage-derived chondrocytes: Implications for biologic repair of joint articular cartilage". In: *Stem Cell Research* 4.1, pp. 57–68. ISSN: 1873-5061. DOI: https://doi.org/10.1016/j.scr.2009.09.004. URL: http://www.sciencedirect.com/science/article/pii/S1873506109000920.

Adkisson, H. Davis th *et al.* (2010b). "The potential of human allogeneic juvenile chondrocytes for restoration of articular cartilage". In: *The American journal of sports medicine* 38.7, pp. 1324–1333. ISSN: 1552-3365 0363-5465. DOI: 10.1177/0363546510361950. URL: https://www.ncbi.nlm.nih.gov/pubmed/20423988https://www.ncbi.nlm.nih.gov/pmc/PMC3774103/.

Aggeli, Amalia *et al.* (2003). "Self-Assembling Peptide Polyelectrolyte β-Sheet Complexes Form Nematic Hydrogels". In: *Angewandte Chemie International Edition* 42.45, pp. 5603–5606.

Aggeli, b) A *et al.* (1997). "Responsive gels formed by the spontaneous self-assembly of peptides into polymeric β-sheet tapes". In: *Nature* 386.6622, pp. 259–262.

Akiyama, H. *et al.* (2002). "The transcription factor Sox9 has essential roles in successive steps of the chondrocyte differentiation pathway and is required for expression of Sox5 and Sox6". In: *Genes Dev* 16.21, pp. 2813–28. ISSN: 0890-9369 (Print) 0890-9369. DOI: 10.1101/gad.1017802.

Akizuki, S. *et al.* (1986). "Tensile properties of human knee joint cartilage: I. Influence of ionic conditions, weight bearing, and fibrillation on the tensile modulus". In: *J*

Orthop Res 4.4, pp. 379–92. ISSN: 0736-0266 (Print) 0736-0266. DOI: 10.1002/jor.1100040401.

Akmal, M *et al.* (2005). "The effects of hyaluronic acid on articular chondrocytes". In: *The Journal of bone and joint surgery. British volume* 87.8, pp. 1143–1149.

Albrecht, C *et al.* (2011). "Gene expression and cell differentiation in matrix-associated chondrocyte transplantation grafts: a comparative study". In: *Osteoarthritis and cartilage* 19.10, pp. 1219–1227.

Alvarez, J. *et al.* (2000). "Different bone growth rates are associated with changes in the expression pattern of types II and X collagens and collagenase 3 in proximal growth plates of the rat tibia". In: *J Bone Miner Res* 15.1, pp. 82–94. ISSN: 0884-0431 (Print) 0884-0431. DOI: 10.1359/jbmr.2000.15.1.82.

Amer, Mahetab H, Lisa J White, and Kevin M Shakesheff (2015). "The effect of injection using narrow-bore needles on mammalian cells: administration and formulation considerations for cell therapies". In: *Journal of Pharmacy and Pharmacology* 67.5, pp. 640–650.

Andrade, Renato *et al.* (2016). "Knee donor-site morbidity after mosaicplasty–a systematic review". In: *Journal of experimental orthopaedics* 3.1, p. 31.

Archer, Charles W. and Philippa Francis-West (2003). "The chondrocyte". In: *The International Journal of Biochemistry & Cell Biology* 35.4, pp. 401–404. ISSN: 1357-2725. DOI: https://doi.org/10.1016/S1357-2725(02)00301-1. URL: http://www.sciencedirect.com/science/article/pii/S1357272502003011.

Aref-Eshghi, Erfan *et al.* (2015). "Overexpression of MMP13 in human osteoarthritic cartilage is associated with the SMAD-independent TGF-β signalling pathway". In: *Arthritis research & therapy* 17.1, p. 264.

Armoiry, Xavier *et al.* (2019). "Autologous chondrocyte implantation with Chondrosphere for treating articular cartilage defects in the knee: An Evidence Review Group perspective of a NICE Single Technology Appraisal". In: *PharmacoEconomics*, pp. 1–8.

Armstrong, C. G. and V. C. Mow (1982). "Variations in the intrinsic mechanical properties of human articular cartilage with age, degeneration, and water content". In: *J Bone Joint Surg Am* 64.1, pp. 88–94. ISSN: 0021-9355 (Print) 0021-9355.

Arzi, Boaz *et al.* (2015). "Cartilage immunoprivilege depends on donor source and lesion location". In: *Acta biomaterialia* 23, pp. 72–81.

Ashraf, S. *et al.* (2016). "Regulation of senescence associated signaling mechanisms in chondrocytes for cartilage tissue regeneration". In: *Osteoarthritis and Cartilage* 24.2, pp. 196–205. ISSN: 1063-4584. DOI: https://doi.org/10.1016/j.joca.2015.07.008. URL: http://www.sciencedirect.com/science/article/pii/S1063458415012388.

Ashwell, M. S. *et al.* (2013). "Changes in chondrocyte gene expression following in vitro impaction of porcine articular cartilage in an impact injury model". In: *J Orthop Res* 31.3, pp. 385–91. ISSN: 0736-0266. DOI: 10.1002/jor.22239.

Atala, Anthony (2007). "Engineering tissues, organs and cells". In: *Journal of Tissue Engineering and Regenerative Medicine* 1.2, pp. 83–96. ISSN: 1932-7005. DOI: 10.1002/term.18. URL: https://doi.org/10.1002/term.18.

Ateshian, Gerard A (2009). "The role of interstitial fluid pressurization in articular cartilage lubrication". In: *Journal of biomechanics* 42.9, pp. 1163–1176.

Ateshian, Gerard A and Huiqun Wang (1995). "A theoretical solution for the frictionless rolling contact of cylindrical biphasic articular cartilage layers". In: *Journal of biomechanics* 28.11, pp. 1341–1355.

Athanasiou, Kyriacos A *et al.* (1991). "Interspecies comparisons of in situ intrinsic mechanical properties of distal femoral cartilage". In: *Journal of orthopaedic research* 9.3, pp. 330–340.

Awad, H. A. *et al.* (2004). "Chondrogenic differentiation of adipose-derived adult stem cells in agarose, alginate, and gelatin scaffolds". In: *Biomaterials* 25.16, pp. 3211–22. ISSN: 0142-9612 (Print) 0142-9612. DOI: 10.1016/j.biomaterials.2003.10.045.

Barco, A *et al.* (2018). "On the design and efficacy assessment of self-assembling peptide-based hydrogel-glycosaminoglycan mixtures for potential repair of early stage cartilage degeneration". In: *Journal of Peptide Science* 24.8-9, e3114.

Barco, Andreas. (2017). "Self-assembling peptides for cartilage regeneration". PhD thesis.

Bartha, Lajos *et al.* (2006). "Autologous osteochondral mosaicplasty grafting". In: *Journal of Orthopaedic & Sports Physical Therapy* 36.10, pp. 739–750.

Basad, Erhan *et al.* (2010). "Matrix-induced autologous chondrocyte implantation versus microfracture in the treatment of cartilage defects of the knee: a 2-year randomised study". In: *Knee Surgery, Sports Traumatology, Arthroscopy* 18.4, pp. 519–527. DOI: 10.1007/s00167-009-1028-1. URL: https://doi.org/10.1007/s00167-009-1028-1.

Bauer, Mats and RW Jackson (1988). "Chondral lesions of the femoral condyles: a system of arthroscopic classification". In: *Arthroscopy: The Journal of Arthroscopic & Related Surgery* 4.2, pp. 97–102.

Bautista, Catherine A. *et al.* (2016). "Effects of Chondroitinase ABC-Mediated Proteoglycan Digestion on Decellularization and Recellularization of Articular Cartilage". In: *PLOS ONE* 11.7, e0158976. DOI: 10.1371/journal.pone.0158976. URL: https://doi.org/10.1371/journal.pone.0158976.

Bayliss, Lee E *et al.* (2017). "The effect of patient age at intervention on risk of implant revision after total replacement of the hip or knee: a population-based cohort study". In: *The Lancet* 389.10077, pp. 1424–1430.

Beck, Emily C *et al.* (2016). "Approaching the compressive modulus of articular cartilage with a decellularized cartilage-based hydrogel". In: *Acta biomaterialia* 38, pp. 94–105.

Bell, Carol J *et al.* (2006). "Self-assembling peptides as injectable lubricants for osteoarthritis". In: *Journal of Biomedical Materials Research Part A: An Official Journal of The Society for Biomaterials, The Japanese Society for Biomaterials, and The Australian Society for Biomaterials and the Korean Society for Biomaterials* 78.2, pp. 236–246.

Bhosale, A. M. and J. B. Richardson (2008). "Articular cartilage: structure, injuries and review of management". In: *Br Med Bull* 87, pp. 77–95. ISSN: 0007-1420. DOI: 10.1093/bmb/ldn025.

Bi, Weimin *et al.* (2001). "Haploinsufficiency of Sox9 results in defective cartilage primordia and premature skeletal mineralization". In: *Proceedings of the National Academy of Sciences* 98.12, pp. 6698–6703.

Bian, Liming *et al.* (2010). "Dynamic mechanical loading enhances functional properties of tissue-engineered cartilage using mature canine chondrocytes". In: *Tissue Engineering Part A* 16.5, pp. 1781–1790.

Biant, Leela C *et al.* (2014). "Long-term results of autologous chondrocyte implantation in the knee for chronic chondral and osteochondral defects". In: *The American journal of sports medicine* 42.9, pp. 2178–2183.

Biological evaluation of medical devices – Part 5: Tests for in vitro cytotoxicity (June 2009). Standard. Geneva, CH: International Organization for Standardization.

Blaney Davidson, E. N. *et al.* (2009). "Increase in ALK1/ALK5 ratio as a cause for elevated MMP-13 expression in osteoarthritis in humans and mice". In: *J Immunol* 182.12, pp. 7937–45. ISSN: 0022-1767. DOI: 10.4049/jimmunol.0803991.

Blom, A. B. *et al.* (2007). "Crucial role of macrophages in matrix metalloproteinase-mediated cartilage destruction during experimental osteoarthritis: involvement of matrix metalloproteinase 3". In: *Arthritis Rheum* 56.1, pp. 147–57. ISSN: 0004-3591 (Print) 0004-3591. DOI: 10.1002/art.22337.

Bolano, Luis and Joseph A Kopta (1991). "The immunology of bone and cartilage transplantation". In: *Orthopedics* 14.9, pp. 987–996.

Bonaventure, J *et al.* (1994). "Reexpression of cartilage-specific genes by dedifferentiated human articular chondrocytes cultured in alginate beads". In: *Experimental cell research* 212.1, pp. 97–104.

Bondeson, Jan *et al.* (2010). "The role of synovial macrophages and macrophage-produced mediators in driving inflammatory and destructive responses in osteoarthritis". In: *Arthritis & Rheumatism* 62.3, pp. 647–657.

Bonnet, C. S. and D. A. Walsh (2005). "Osteoarthritis, angiogenesis and inflammation". In: *Rheumatology (Oxford)* 44.1, pp. 7–16. ISSN: 1462-0324 (Print) 1462-0324. DOI: 10.1093/rheumatology/keh344.

Bosnakovski, Darko *et al.* (2006). "Chondrogenic differentiation of bovine bone marrow mesenchymal stem cells (MSCs) in different hydrogels: influence of collagen type II extracellular matrix on MSC chondrogenesis". In: *Biotechnology and bioengineering* 93.6, pp. 1152–1163.

Bowland, Philippa *et al.* (2020). "Biomechanical assessment of the stability of osteochondral grafts implanted in porcine and bovine femoral condyles". In: *Proceedings of the Institution of Mechanical Engineers, Part H: Journal of Engineering in Medicine* 234.2, pp. 163–170.

Brittberg, Mats and Carl S Winalski (2003). "Evaluation of cartilage injuries and repair". In: *JBJS* 85, pp. 58–69.

Brittberg, Mats *et al.* (1994). "Treatment of Deep Cartilage Defects in the Knee with Autologous Chondrocyte Transplantation". In: *New England Journal of Medicine* 331.14, pp. 889–895. ISSN: 0028-4793. DOI: 10.1056/NEJM199410063311401. URL: https://doi.org/10.1056/NEJM199410063311401.

Brittberg, Mats *et al.* (2018). "Matrix-Applied Characterized Autologous Cultured Chondrocytes Versus Microfracture: Five-Year Follow-up of a Prospective Randomized Trial". In: *The American Journal of Sports Medicine* 46.6, pp. 1343–1351. ISSN: 0363-5465. DOI: 10.1177/0363546518756976. URL: https://doi.org/10.1177/0363546518756976.

Brown, T. D. *et al.* (2006). "Posttraumatic osteoarthritis: a first estimate of incidence, prevalence, and burden of disease". In: *J Orthop Trauma* 20.10, pp. 739–44. ISSN: 0890-5339 (Print) 0890-5339. DOI: 10.1097/01.bot.0000246468.80635.ef.

Buchta, C. *et al.* (2005). "Biochemical characterization of autologous fibrin sealants produced by CryoSeal and Vivostat in comparison to the homologous fibrin sealant product Tissucol/Tisseel". In: *Biomaterials* 26.31, pp. 6233–41. ISSN: 0142-9612 (Print) 0142-9612. DOI: 10.1016/j.biomaterials.2005.04.014.

Buckwalter, JA and HJ Mankin (1998). "Articular cartilage: tissue design and chondrocyte-matrix interactions." In: *Instructional course lectures* 47, pp. 477–486.

Buckwalter, Joseph A (1992). "Mechanical injuries of articular cartilage". In: *The Iowa orthopaedic journal* 12, p. 50.

Buckwalter, Joseph A *et al.* (2013). "The roles of mechanical stresses in the pathogenesis of osteoarthritis: implications for treatment of joint injuries". In: *Cartilage* 4.4, pp. 286–294.

Burks, Robert T. *et al.* (2006). "The Use of a Single Osteochondral Autograft Plug in the Treatment of a Large Osteochondral Lesion in the Femoral Condyle: An Experimental Study in Sheep". In: *The American Journal of Sports Medicine* 34.2, pp. 247–255. ISSN: 0363-5465. DOI: 10.1177/0363546505279914. URL: https://doi.org/10.1177/0363546505279914.

Buschmann, Michael D *et al.* (1992). "Chondrocytes in agarose culture synthesize a mechanically functional extracellular matrix". In: *Journal of orthopaedic research* 10.6, pp. 745–758.

Butler, D. L., S. A. Goldstein, and F. Guilak (2000). "Functional tissue engineering: the role of biomechanics". In: *J Biomech Eng* 122.6, pp. 570–5. ISSN: 0148-0731 (Print) 0148-0731.

Caligaris, Matteo and Gerard A Ateshian (2008). "Effects of sustained interstitial fluid pressurization under migrating contact area, and boundary lubrication by synovial fluid, on cartilage friction". In: *Osteoarthritis and Cartilage* 16.10, pp. 1220–1227.

Cambria, Elena *et al.* (2020). "Cell-laden agarose-collagen composite hydrogels for mechanotransduction studies". In: *Frontiers in bioengineering and biotechnology* 8, p. 346.

Cao, Chenxi *et al.* (2020). "Effects of cell phenotype and seeding density on the chondrogenic capacity of human osteoarthritic chondrocytes in type I collagen scaffolds". In: *Journal of Orthopaedic Surgery and Research* 15.1, pp. 1–11.

Caplan, A. I. *et al.* (1997). "Principles of cartilage repair and regeneration". In: *Clin Orthop Relat Res* 342, pp. 254–69. ISSN: 0009-921X (Print) 0009-921x.

Caron, Marjolein MJ *et al.* (2012). "Redifferentiation of dedifferentiated human articular chondrocytes: comparison of 2D and 3D cultures". In: *Osteoarthritis and cartilage* 20.10, pp. 1170–1178.

Carrick, Lisa M *et al.* (2007). "Effect of ionic strength on the self-assembly, morphology and gelation of pH responsive β-sheet tape-forming peptides". In: *Tetrahedron* 63.31, pp. 7457–7467.

Chen, Feng *et al.* (2016). "An injectable enzymatically crosslinked carboxymethylated pullulan/chondroitin sulfate hydrogel for cartilage tissue engineering". In: *Scientific reports* 6.1, pp. 1–12.

Chen, Hongmei *et al.* (2009). "Drilling and microfracture lead to different bone structure and necrosis during bone-marrow stimulation for cartilage repair". In: *Journal of Orthopaedic Research* 27.11, pp. 1432–1438. DOI: doi:10.1002/jor.20905. URL: https://onlinelibrary.wiley.com/doi/abs/10.1002/jor.20905.

Chevalier, Xavier (1993). "Fibronectin, cartilage, and osteoarthritis". In: *Seminars in arthritis and rheumatism*. Vol. 22. 5. Elsevier, pp. 307–318.

Chevalier, Xavier, Florent Eymard, and Pascal Richette (2013). "Biologic agents in osteoarthritis: hopes and disappointments". In: *Nature reviews Rheumatology* 9.7, p. 400.

Chircov, Cristina, Alexandru Mihai Grumezescu, and Ludovic Everard Bejenaru (2018). "Hyaluronic acid-based scaffolds for tissue engineering". In: *Rom J Morphol Embryol* 59.1, pp. 71–76.

Chu, C. R. *et al.* (1997). "Osteochondral repair using perichondrial cells. A 1-year study in rabbits". In: *Clin Orthop Relat Res* 340, pp. 220–9. ISSN: 0009-921X (Print) 0009-921x.

Chubinskaya, Susan *et al.* (2008). "Effects induced by BMPS in cultures of human articular chondrocytes: comparative studies". In: *Growth Factors* 26.5, pp. 275–283.

Clar, C *et al.* (2005). "Clinical and cost-effectiveness of autologous chondrocyte implantation for cartilage defects in knee joints: systematic review and economic evaluation." In: *Health Technology Assessment (Winchester, England)* 9.47, pp. iii–iv.

Cowie, Raelene M *et al.* (2021). "An experimental simulation model to assess wear of the porcine patellofemoral joint". In: *Plos one* 16.4, e0250077.

Crapo, Peter M, Thomas W Gilbert, and Stephen F Badylak (2011). "An overview of tissue and whole organ decellularization processes". In: *Biomaterials* 32.12, pp. 3233–3243.

Crawford, D. C., T. M. DeBerardino, and 3rd Williams R. J. (2012). "NeoCart, an autologous cartilage tissue implant, compared with microfracture for treatment of distal femoral cartilage lesions: an FDA phase-II prospective, randomized clinical trial after two years". In: *J Bone Joint Surg Am* 94.11, pp. 979–89. ISSN: 0021-9355. DOI: 10.2106/jbjs.K.00533.

Czitrom, A. A. *et al.* (1986). "Bone and cartilage allotransplantation. A review of 14 years of research and clinical studies". In: *Clinical orthopaedics and related research* 208, pp. 141–145. ISSN: 0009-921X. URL: http://europepmc.org/abstract/MED/3522021.

Dare, D. and S. Rodeo (2014). "Mechanisms of post-traumatic osteoarthritis after ACL injury". In: *Curr Rheumatol Rep* 16.10, p. 448. ISSN: 1523-3774. DOI: 10.1007/s11926-014-0448-1.

Darling, Eric M and Kyriacos A Athanasiou (2005). "Rapid phenotypic changes in passaged articular chondrocyte subpopulations". In: *Journal of orthopaedic research* 23.2, pp. 425–432.

David-Raoudi, Maha *et al.* (2009). "Chondroitin sulfate increases hyaluronan production by human synoviocytes through differential regulation of hyaluronan synthases: role of p38 and Akt". In: *Arthritis & Rheumatism: Official Journal of the American College of Rheumatology* 60.3, pp. 760–770.

Davies, RPW *et al.* (2006). "Self-assembling β-sheet tape forming peptides". In: *Supramolecular Chemistry* 18.5, pp. 435–443.

Degen, Ryan M. *et al.* (2016). "Acute Delamination of Commercially Available Decellularized Osteochondral Allograft Plugs: A Report of Two Cases". In: *Cartilage* 7.4, pp. 316–321. ISSN: 1947-6035 1947-6043. DOI: 10.1177/1947603515626973. URL: https://www.ncbi.nlm.nih.gov/pubmed/27688840https://www.ncbi.nlm.nih.gov/pmc/PMC5029564/.

Denbeigh, Janet M *et al.* (2021). "Modernizing storage conditions for fresh osteochondral allografts by optimizing viability at physiologic temperatures and conditions". In: *Cartilage* 13.1_suppl, 280S–292S.

Derrett, Sarah *et al.* (2005). "Cost and health status analysis after autologous chondrocyte implantation and mosaicplasty: a retrospective comparison". In: *International journal of technology assessment in health care* 21.3, pp. 359–367.

Desrochers, Jane, Matthias W Amrein, and John R Matyas (2013). "Microscale surface friction of articular cartilage in early osteoarthritis". In: *Journal of the mechanical behavior of biomedical materials* 25, pp. 11–22.

Divieto, Carla and Maria Paola Sassi (2015). "A first approach to evaluate the cell dose in highly porous scaffolds by using a nondestructive metabolic method". In: *Future science OA* 1.4.

Dong, Hengjin and Martin Buxton (2006). "Early assessment of the likely cost-effectiveness of a new technology: a Markov model with probabilistic sensitivity analysis of

computer-assisted total knee replacement". In: *International Journal of Technology Assessment in Health Care* 22.2, p. 191.

Donnan, F. G. (1924). "The Theory of Membrane Equilibria". In: *Chemical Reviews* 1.1, pp. 73–90. ISSN: 0009-2665. DOI: 10.1021/cr60001a003. URL: https://pubs.acs.org/doi/abs/10.1021/cr60001a003.

Donohue, J MICHAEL *et al.* (1983). "The effects of indirect blunt trauma on adult canine articular cartilage." In: *JBJS* 65.7, pp. 948–957.

Dopirak, Ryan, James L Bond, and Stephen J Snyder (2007). "Arthroscopic total rotator cuff replacement with an acellular human dermal allograft matrix." In: *International Journal of Shoulder Surgery* 1.1.

Duarte Campos, D. F. *et al.* (2012). "Supporting Biomaterials for Articular Cartilage Repair". In: *Cartilage* 3.3, pp. 205–21. ISSN: 1947-6035 (Print) 1947-6035. DOI: 10.1177/1947603512444722.

Dugard, M. N. *et al.* (2017). "Development of a Tool to Predict Outcome of Autologous Chondrocyte Implantation". In: *Cartilage* 8.2, pp. 119–130. ISSN: 1947-6035 (Print) 1947-6035. DOI: 10.1177/1947603516650002.

D'Lima, Darryl D, Peter C Chen, and Clifford W Colwell Jr (2009). "Osteochondral grafting: effect of graft alignment, material properties, and articular geometry". In: *The open orthopaedics journal* 3, p. 61.

Ebert, J. R. *et al.* (2011). "Clinical and magnetic resonance imaging-based outcomes to 5 years after matrix-induced autologous chondrocyte implantation to address articular cartilage defects in the knee". In: *Am J Sports Med* 39.4, pp. 753–63. ISSN: 0363-5465. DOI: 10.1177/0363546510390476.

Ebert, Jay R *et al.* (2021). "An accelerated 6-week return to full weight bearing after matrix-induced autologous chondrocyte implantation results in good clinical outcomes to 5 years post-surgery". In: *Knee Surgery, Sports Traumatology, Arthroscopy* 29.11, pp. 3825–3833.

Edwards, Peter K, Timothy Ackland, and Jay R Ebert (2014). "Clinical rehabilitation guidelines for matrix-induced autologous chondrocyte implantation on the tibiofemoral joint". In: *journal of orthopaedic & sports physical therapy* 44.2, pp. 102–119.

Edwards, Peter K, Timothy R Ackland, and Jay R Ebert (2013). "Accelerated weight-bearing rehabilitation after matrix-induced autologous chondrocyte implantation in the tibiofemoral joint: early clinical and radiological outcomes". In: *The American journal of sports medicine* 41.10, pp. 2314–2324.

Ekenstedt, K. J. *et al.* (2006). "Effects of chronic growth hormone and insulin-like growth factor 1 deficiency on osteoarthritis severity in rat knee joints". In: *Arthritis Rheum* 54.12, pp. 3850–8. ISSN: 0004-3591 (Print) 0004-3591. DOI: 10.1002/art.22254.

Elder, Steven *et al.* (2017). "Evaluation of genipin for stabilization of decellularized porcine cartilage". In: *Journal of Orthopaedic Research* 35.9, pp. 1949–1957.

Elhadad, Amir A *et al.* (2022). "A multidisciplinary perspective on the latest trends in artificial cartilage fabrication to mimic real tissue". In: *Applied Materials Today* 29, p. 101603.

Elson, KM *et al.* (2015). "Non-destructive monitoring of viability in an ex vivo organ culture model of osteochondral tissue". In: *eCells and Materials Journal* 29, pp. 356–369.

Englund, M., A. Guermazi, and L. S. Lohmander (2009). "The meniscus in knee osteoarthritis". In: *Rheum Dis Clin North Am* 35.3, pp. 579–90. ISSN: 0889-857x. DOI: 10.1016/j.rdc.2009.08.004.

Erol, Mehmet Fatih and Ozgur Karakoyun (2016). "A new point of view for mosaicplasty in the treatment of focal cartilage defects of knee joint: honeycomb pattern". In: *Springerplus* 5.1, pp. 1–6.

European Medicines Agency (2013). *Assessment report - MACI*. https://www.ema.europa.eu/en/documents/assessment-report/maci-epar-public-assessment-report_en.pdf.

Familiari, Filippo *et al.* (2018). "Clinical outcomes and failure rates of osteochondral allograft transplantation in the knee: a systematic review". In: *The American journal of sports medicine* 46.14, pp. 3541–3549.

Fan, Zhiyong *et al.* (2006). "Role of mitogen-activated protein kinases and NFκB on IL-1β-induced effects on collagen type II, MMP-1 and 13 mRNA expression in normal articular human chondrocytes". In: *Rheumatology international* 26.10, pp. 900–903.

Farr, Jack *et al.* (2016). "High Failure Rate of a Decellularized Osteochondral Allograft for the Treatment of Cartilage Lesions". In: *The American Journal of Sports Medicine* 44.8, pp. 2015–2022. ISSN: 0363-5465. DOI: 10.1177/0363546516645086. URL: https://doi.org/10.1177/0363546516645086.

Fellows, Christopher R *et al.* (2016). "Adipose, bone marrow and synovial joint-derived mesenchymal stem cells for cartilage repair". In: *Frontiers in genetics* 7, p. 213.

Feng, Qian *et al.* (2014). "Cell-mediated degradation regulates human mesenchymal stem cell chondrogenesis and hypertrophy in MMP-sensitive hyaluronic acid hydrogels". In: *PLoS One* 9.6, e99587.

Fermor, B. *et al.* (2002). "Induction of cyclooxygenase-2 by mechanical stress through a nitric oxide-regulated pathway". In: *Osteoarthritis and Cartilage* 10.10, pp. 792–798. ISSN: 1063-4584. DOI: https://doi.org/10.1053/joca.2002.0832. URL: http://www.sciencedirect.com/science/article/pii/S1063458402908320.

Fermor, H (2018). "EARLY INTERVENTION THERAPIES FOR CARTILAGE LESION REPAIR". In: *Orthopaedic Proceedings*. Vol. 100. SUPP_16. The British Editorial Society of Bone & Joint Surgery, pp. 112–112.

Fermor, Hazel L (2013). "Engineering of Natural Cartilage Substitution Biomaterials". PhD thesis.

Fermor, Hazel L. *et al.* (2015a). "Development and characterisation of a decellularised bovine osteochondral biomaterial for cartilage repair". In: *Journal of materials science. Materials in medicine* 26.5, pp. 186–186. ISSN: 1573-4838 0957-4530. DOI: 10.1007/s10856-015-5517-0. URL: https://www.ncbi.nlm.nih.gov/pubmed/25893393https://www.ncbi.nlm.nih.gov/pmc/PMC4412724/.

Fermor, HL *et al.* (2015b). "Biological, biochemical and biomechanical characterisation of articular cartilage from the porcine, bovine and ovine hip and knee". In: *Bio-medical materials and engineering* 25.4, pp. 381–395.

Fernandes, J. C., J. Martel-Pelletier, and J. P. Pelletier (2002). "The role of cytokines in osteoarthritis pathophysiology". In: *Biorheology* 39.1-2, pp. 237–46. ISSN: 0006-355X (Print) 0006-355x.

Filardo, Giuseppe *et al.* (2011). "Arthroscopic second-generation autologous chondrocyte implantation: a prospective 7-year follow-up study". In: *The American journal of sports medicine* 39.10, pp. 2153–2160.

Finger, Florian *et al.* (2004). "Phenotypic characterization of human chondrocyte cell line C-20/A4: a comparison between monolayer and alginate suspension culture". In: *Cells Tissues Organs* 178.2, pp. 65–77.

Finlay, Scott *et al.* (2016). "In vitro engineering of high modulus cartilage-like constructs". In: *Tissue Engineering Part C: Methods* 22.4, pp. 382–397.

Finnson, K. W. *et al.* (2010). "Endoglin differentially regulates TGF-beta-induced Smad2/3 and Smad1/5 signalling and its expression correlates with extracellular matrix production and cellular differentiation state in human chondrocytes". In: *Osteoarthritis Cartilage* 18.11, pp. 1518–27. ISSN: 1063-4584. DOI: 10.1016/j.joca.2010.09.002.

Finnson, K. W. *et al.* (2012). "TGF-b signaling in cartilage homeostasis and osteoarthritis". In: *Front Biosci (Schol Ed)* 4, pp. 251–68. ISSN: 1945-0516.

Fitzgerald, Jonathan B. *et al.* (2008). "Shear- and Compression-induced Chondrocyte Transcription Requires MAPK Activation in Cartilage Explants". In: *Journal of Biological Chemistry* 283.11, pp. 6735–6743. DOI: 10.1074/jbc.M708670200. URL: http://www.jbc.org/content/283/11/6735.abstract.

Flahiff, C. M. *et al.* (2002). "Osmotic loading to determine the intrinsic material properties of guinea pig knee cartilage". In: *J Biomech* 35.9, pp. 1285–90. ISSN: 0021-9290 (Print) 0021-9290.

Font-Rodriguez, David E, Giles R Scuderi, and John N Insall (1997). "Survivorship of cemented total knee arthroplasty." In: *Clinical orthopaedics and related research* 345, pp. 79–86.

Forster, H and J Fisher (1996). "The influence of loading time and lubricant on the friction of articular cartilage". In: *Proceedings of the Institution of Mechanical Engineers, Part H: Journal of Engineering in Medicine* 210.2, pp. 109–119.

Fortier, L. A. *et al.* (2002). "Insulin-like growth factor-I enhances cell-based repair of articular cartilage". In: *J Bone Joint Surg Br* 84.2, pp. 276–88. ISSN: 0301-620X (Print) 0301-620x.

Fox, Natalie *et al.* (2016). "Development of an Ex-Vivo Organ Culture Model of the Femoral-Tibial Joint". In: *Orthopaedic Research Society 2015 Annual Meeting*. Leeds.

Freed, L. E. and G. Vunjak-Novakovic (1995). "Cultivation of cell-polymer tissue constructs in simulated microgravity". In: *Biotechnol Bioeng* 46.4, pp. 306–13. ISSN: 0006-3592 (Print) 0006-3592. DOI: 10.1002/bit.260460403.

French, Margaret M *et al.* (2002). "Chondrogenic activity of the heparan sulfate proteoglycan perlecan maps to the N-terminal domain I". In: *Journal of Bone and Mineral Research* 17.1, pp. 48–55.

Frenkel, S. R. and P. E. Di Cesare (2004). "Scaffolds for articular cartilage repair". In: *Ann Biomed Eng* 32.1, pp. 26–34. ISSN: 0090-6964 (Print) 0090-6964.

Frisbie, DD *et al.* (2008). "Evaluation of autologous chondrocyte transplantation via a collagen membrane in equine articular defects–results at 12 and 18 months". In: *Osteoarthritis and Cartilage* 16.6, pp. 667–679.

Fukui, N. *et al.* (2008). "Zonal gene expression of chondrocytes in osteoarthritic cartilage". In: *Arthritis Rheum* 58.12, pp. 3843–53. ISSN: 0004-3591 (Print) 0004-3591. DOI: 10.1002/art.24036.

Fukumoto, T. *et al.* (2003). "Combined effects of insulin-like growth factor-1 and transforming growth factor-beta1 on periosteal mesenchymal cells during chondrogenesis in vitro". In: *Osteoarthritis Cartilage* 11.1, pp. 55–64. ISSN: 1063-4584 (Print) 1063-4584.

Gannon, Alanna R *et al.* (2015). "The changing role of the superficial region in determining the dynamic compressive properties of articular cartilage during postnatal development". In: *Osteoarthritis and Cartilage* 23.6, pp. 975–984.

Ge, Yuxiang *et al.* (2021). "Effects of mechanical compression on chondrogenesis of human synovium-derived mesenchymal stem cells in agarose hydrogel". In: *Frontiers in bioengineering and biotechnology* 9.

Gerlier, Laetitia *et al.* (2010). "The cost utility of autologous chondrocytes implantation using ChondroCelect® in symptomatic knee cartilage lesions in Belgium". In: *Pharmacoeconomics* 28.12, pp. 1129–1146.

Getgood, A. *et al.* (2009). "Articular cartilage tissue engineering: today's research, tomorrow's practice?" In: *J Bone Joint Surg Br* 91.5, pp. 565–76. ISSN: 0301-620x. DOI: 10.1302/0301-620x.91b5.21832.

Getgood, Alan *et al.* (2011). "Reduced chondrocyte viability is associated with the use of surgical marker pen ink". In: *The American Journal of Sports Medicine* 39.6, pp. 1270–1274.

Ghosh, P. and T. K. Taylor (1987). "The knee joint meniscus. A fibrocartilage of some distinction". In: *Clin Orthop Relat Res* 224, pp. 52–63. ISSN: 0009-921X (Print) 0009-921x.

Gilbert, Sophie and Emma Blain (2018). "Cartilage mechanobiology: How chondrocytes respond to mechanical load". In: pp. 99–126. ISBN: 9780128129524. DOI: 10.1016/B978-0-12-812952-4.00004-0.

Gilbert, Thomas W, John M Freund, and Stephen F Badylak (2009). "Quantification of DNA in biologic scaffold materials". In: *Journal of Surgical Research* 152.1, pp. 135–139.

Gilpin, Anna and Yong Yang (2017). "Decellularization Strategies for Regenerative Medicine: From Processing Techniques to Applications". In: *BioMed Research International* 2017, p. 13. DOI: 10.1155/2017/9831534. URL: https://doi.org/10.1155/2017/9831534.

Glenn, J. D. and K. A. Whartenby (2014). "Mesenchymal stem cells: Emerging mechanisms of immunomodulation and therapy". In: *World J Stem Cells* 6.5, pp. 526–39. ISSN: 1948-0210 (Print) 1948-0210. DOI: 10.4252/wjsc.v6.i5.526.

Goldring, Mary B (2012). "Chondrogenesis, chondrocyte differentiation, and articular cartilage metabolism in health and osteoarthritis". In: *Therapeutic advances in musculoskeletal disease* 4.4, pp. 269–285.

Goldring, Mary B. and Kenneth B. Marcu (2009). "Cartilage homeostasis in health and rheumatic diseases". In: *Arthritis research & therapy* 11.3, pp. 224–224. ISSN: 1478-6362 1478-6354. DOI: 10.1186/ar2592. URL: https://www.ncbi.nlm.nih.gov/pubmed/19519926https://www.ncbi.nlm.nih.gov/pmc/PMC2714092/.

Goldring, Mary B., Kaneyuki Tsuchimochi, and Kosei Ijiri (2005). "The control of chondrogenesis". In: *Journal of Cellular Biochemistry* 97.1, pp. 33–44. ISSN: 0730-2312. DOI: 10.1002/jcb.20652. URL: https://doi.org/10.1002/jcb.20652.

Goldshmid, Revital and Dror Seliktar (2017). "Hydrogel modulus affects proliferation rate and pluripotency of human mesenchymal stem cells grown in three-dimensional culture". In: *ACS Biomaterials Science & Engineering* 3.12, pp. 3433–3446.

Gomoll, Andreas H. (2013). "Osteochondral Allograft Transplantation Using the Chondrofix Implant". In: *Operative Techniques in Sports Medicine* 21.2, pp. 90–94. ISSN: 1060-1872. DOI: https://doi.org/10.1053/j.otsm.2013.03.002. URL: http://www.sciencedirect.com/science/article/pii/S1060187213000257.

Gopu, S, A Abdelgaied, and LM Jennings (2017). "Prediction of Mechanical Properties of Porcine's Articular Cartilage using Computational Methods". In: *MECH5825M Professional Project*.

Gosiewska, Anna *et al.* (2001). "Development of a three-dimensional transmigration assay for testing cell–polymer interactions for tissue engineering applications". In: *Tissue Engineering* 7.3, pp. 267–277.

Grenier, Stephanie, Madhu M Bhargava, and Peter A Torzilli (2014). "An in vitro model for the pathological degradation of articular cartilage in osteoarthritis". In: *Journal of biomechanics* 47.3, pp. 645–652.

Griffin, Darvin J. *et al.* (2015). "Mechanical characterization of matrix-induced autologous chondrocyte implantation (MACI®) grafts in an equine model at 53 weeks". In: *Journal of Biomechanics* 48.10, pp. 1944–1949. ISSN: 0021-9290. DOI: https://doi.org/10.1016/j.jbiomech.2015.04.010. URL: http://www.sciencedirect.com/science/article/pii/S0021929015002262.

Griffon, Dominique J *et al.* (2011). "A comparative study of seeding techniques and three-dimensional matrices for mesenchymal cell attachment". In: *Journal of tissue engineering and regenerative medicine* 5.3, pp. 169–179.

Gudas, Rimtautas *et al.* (2009). "A prospective, randomized clinical study of osteochondral autologous transplantation versus microfracture for the treatment of osteochondritis dissecans in the knee joint in children". In: *Journal of Pediatric Orthopaedics* 29.7, pp. 741–748.

Gudas, Rimtautas *et al.* (2012). "Ten-Year Follow-up of a Prospective, Randomized Clinical Study of Mosaic Osteochondral Autologous Transplantation Versus Microfracture for the Treatment of Osteochondral Defects in the Knee Joint of Athletes". In: *The American Journal of Sports Medicine* 40.11, pp. 2499–2508. ISSN: 0363-5465. DOI: 10.1177/0363546512458763. URL: https://doi.org/10.1177/0363546512458763.

Gudas, Rimtautas *et al.* (2013). "Comparison of Osteochondral Autologous Transplantation, Microfracture, or Debridement Techniques in Articular Cartilage Lesions Associated With Anterior Cruciate Ligament Injury: A Prospective Study With a 3-Year Follow-up". In: *Arthroscopy: The Journal of Arthroscopic & Related Surgery* 29.1, pp. 89–97. ISSN: 0749-8063. DOI: https://doi.org/10.1016/j.arthro.2012.06.009. URL: http://www.sciencedirect.com/science/article/pii/S0749806312015186.

Guilak, F. *et al.* (1994). "The effects of matrix compression on proteoglycan metabolism in articular cartilage explants". In: *Osteoarthritis Cartilage* 2.2, pp. 91–101. ISSN: 1063-4584 (Print) 1063-4584.

Guilak, F. *et al.* (1999). "The deformation behavior and mechanical properties of chondrocytes in articular cartilage". In: *Osteoarthritis Cartilage* 7.1, pp. 59–70. ISSN: 1063-4584 (Print) 1063-4584. DOI: 10.1053/joca.1998.0162.

Guilak, Farshid *et al.* (2006). "The pericellular matrix as a transducer of biomechanical and biochemical signals in articular cartilage". In: *Annals of the New York Academy of Sciences* 1068.1, pp. 498–512.

Guo, Hongqiang and Peter A. Torzilli (2016). "Shape of chondrocytes within articular cartilage affects the solid but not the fluid microenvironment under unconfined compression". In: *Acta biomaterialia* 29, pp. 170–179. ISSN: 1742-7061 1878-7568. DOI: 10.1016/j.actbio.2015.10.035. URL: http://www.ncbi.nlm.nih.gov/pmc/articles/PMC4681666/.

Haapala, Jussi *et al.* (1999). "Remobilization does not fully restore immobilization induced articular cartilage atrophy." In: *Clinical orthopaedics and related research* 362, pp. 218–229.

Haddo, Omar *et al.* (2004). "The use of chondrogide membrane in autologous chondrocyte implantation". In: *The Knee* 11.1, pp. 51–55.

Hambly, Karen *et al.* (2006). "Autologous chondrocyte implantation postoperative care and rehabilitation: science and practice". In: *The American journal of sports medicine* 34.6, pp. 1020–1038.

Haslauer, C. M. *et al.* (2013). "Loss of extracellular matrix from articular cartilage is mediated by the synovium and ligament after anterior cruciate ligament injury". In: *Osteoarthritis Cartilage* 21.12, pp. 1950–7. ISSN: 1063-4584. DOI: 10.1016/j.joca.2013.09.003.

Hattori, Takako *et al.* (2010). "SOX9 is a major negative regulator of cartilage vascularization, bone marrow formation and endochondral ossification". In: *Development* 137.6, pp. 901–911.

He, Z. *et al.* (2016). "Strain-induced mechanotransduction through primary cilia, extracellular ATP, purinergic calcium signaling, and ERK1/2 transactivates CITED2 and downregulates MMP-1 and MMP-13 gene expression in chondrocytes". In: *Osteoarthritis Cartilage* 24.5, pp. 892–901. ISSN: 1063-4584. DOI: 10.1016/j.joca.2015.11.015.

Hennessy, Ryan S *et al.* (2017). "Supercritical carbon dioxide–based sterilization of decellularized heart valves". In: *Basic to Translational Science* 2.1, pp. 71–84.

Hillebrandt, Karl H *et al.* (2019). "Strategies based on organ decellularization and recellularization". In: *Transplant International* 32.6, pp. 571–585.

Hongisto, Vesa *et al.* (2013). "High-throughput 3D screening reveals differences in drug sensitivities between culture models of JIMT1 breast cancer cells". In: *PloS one* 8.10, e77232.

Horner, A *et al.* (1999). "Immunolocalisation of vascular endothelial growth factor (VEGF) in human neonatal growth plate cartilage". In: *The Journal of Anatomy* 194.4, pp. 519–524.

Horton, Melissa T *et al.* (2013). "Revision osteochondral allograft transplantations: do they work?" In: *The American journal of sports medicine* 41.11, pp. 2507–2511.

Hsu, Shan-hui *et al.* (2006). "Evaluation of biodegradable polyesters modified by type II collagen and Arg-Gly-Asp as tissue engineering scaffolding materials for cartilage regeneration". In: *Artificial organs* 30.1, pp. 42–55.

Huang, Brian J, Jerry C Hu, and Kyriacos A Athanasiou (2016). "Effects of passage number and post-expansion aggregate culture on tissue engineered, self-assembled neocartilage". In: *Acta biomaterialia* 43, pp. 150–159.

Huey, Daniel J, Jerry C Hu, and Kyriacos A Athanasiou (2013). "Chondrogenically tuned expansion enhances the cartilaginous matrix-forming capabilities of primary, adult, leporine chondrocytes". In: *Cell transplantation* 22.2, pp. 331–340.

Hunter, David J, Jason J McDougall, and Francis J Keefe (2008). "The symptoms of osteoarthritis and the genesis of pain". In: *Rheumatic Disease Clinics of North America* 34.3, pp. 623–643.

Hunziker, E. B. *et al.* (2015). "An educational review of cartilage repair: precepts & practice – myths & misconceptions – progress & prospects". In: *Osteoarthritis and Cartilage* 23.3, pp. 334–350. ISSN: 1063-4584. DOI: https://doi.org/10.1016/j.joca.2014.12.011. URL: http://www.sciencedirect.com/science/article/pii/S1063458414013831.

Hwang, Nathaniel S *et al.* (2007). "Response of zonal chondrocytes to extracellular matrix-hydrogels". In: *FEBS letters* 581.22, pp. 4172–4178.

Irianto, Jerome *et al.* (2014). "Depletion of chondrocyte primary cilia reduces the compressive modulus of articular cartilage". In: *Journal of Biomechanics* 47.2, pp. 579–582. ISSN: 0021-9290. DOI: https://doi.org/10.1016/j.jbiomech.2013.11.040. URL: http://www.sciencedirect.com/science/article/pii/S0021929013005940.

Jamburidze, Akaki *et al.* (2017). "High-frequency linear rheology of hydrogels probed by ultrasound-driven microbubble dynamics". In: *Soft Matter* 13.21, pp. 3946–3953.

Janssen, Luuk M *et al.* (2006). "Short-duration enzymatic treatment promotes integration of a cartilage graft in a defect". In: *Annals of Otology, Rhinology & Laryngology* 115.6, pp. 461–468.

Jay, Gregory D. and Kimberly A. Waller (2014). "The biology of Lubricin: Near frictionless joint motion". In: *Matrix Biology* 39, pp. 17–24. ISSN: 0945-053X. DOI: https://doi.org/10.1016/j.matbio.2014.08.008. URL: http://www.sciencedirect.com/science/article/pii/S0945053X14001619.

Jenniskens, Y. M. *et al.* (2006). "Biochemical and functional modulation of the cartilage collagen network by IGF1, TGFB2 and FGF2". In: *Osteoarthritis and Cartilage* 14.11, pp. 1136–1146. ISSN: 1063-4584. DOI: https://doi.org/10.1016/j.joca.

2006.04.002. URL: http://www.sciencedirect.com/science/article/pii/S106345840600104X.

Jensen, C. G. *et al.* (2004). "Ultrastructural, tomographic and confocal imaging of the chondrocyte primary cilium in situ". In: *Cell Biol Int* 28.2, pp. 101–10. ISSN: 1065-6995 (Print) 1065-6995. DOI: 10.1016/j.cellbi.2003.11.007.

Jha, Amit K. *et al.* (2009). "Perlecan domain I-conjugated, hyaluronic acid-based hydrogel particles for enhanced chondrogenic differentiation via BMP-2 release". In: *Biomaterials* 30.36, pp. 6964–6975. ISSN: 0142-9612. DOI: https://doi.org/10.1016/j.biomaterials.2009.09.009. URL: http://www.sciencedirect.com/science/article/pii/S0142961209009259.

Jiang, Ching-Chuan *et al.* (2020). "Collagenase treatment of cartilaginous matrix promotes fusion of adjacent cartilage". In: *Regenerative therapy* 15, pp. 97–102.

Jiang, Xianfang *et al.* (2018). "Therapy for cartilage defects: functional ectopic cartilage constructed by cartilage-simulating collagen, chondroitin sulfate and hyaluronic acid (CCH) hybrid hydrogel with allogeneic chondrocytes". In: *Biomaterials science* 6.6, pp. 1616–1626.

Jin, M. *et al.* (2001). "Tissue shear deformation stimulates proteoglycan and protein biosynthesis in bovine cartilage explants". In: *Arch Biochem Biophys* 395.1, pp. 41–8. ISSN: 0003-9861 (Print) 0003-9861. DOI: 10.1006/abbi.2001.2543.

Johnson, Christine C. *et al.* (2017). "High Short-Term Failure Rate Associated With Decellularized Osteochondral Allograft for Treatment of Knee Cartilage Lesions". In: *Arthroscopy: The Journal of Arthroscopic & Related Surgery* 33.12, pp. 2219–2227. ISSN: 0749-8063. DOI: https://doi.org/10.1016/j.arthro.2017.07.018. URL: http://www.sciencedirect.com/science/article/pii/S0749806317307594.

Johnson, Simon M *et al.* (2020). "Clinical outcomes and ultrasonographic viability of GraftJacket® augmented rotator cuff repair: a prospective follow-up study with mean follow-up of forty-one months". In: *Journal of Clinical Orthopaedics and Trauma* 11, S372–S377.

Jones, CW *et al.* (2008). "Matrix-induced autologous chondrocyte implantation in sheep: objective assessments including confocal arthroscopy". In: *Journal of Orthopaedic Research* 26.3, pp. 292–303.

Jung, Youngmee *et al.* (2008). "Cartilage regeneration with highly-elastic three-dimensional scaffolds prepared from biodegradable poly (l-lactide-co-caprolactone)". In: *Biomaterials* 29.35, pp. 4630–4636.

Juran, Cassandra M, M Franklin Dolwick, and Peter S McFetridge (2015). "Engineered microporosity: enhancing the early regenerative potential of decellularized temporomandibular joint discs". In: *Tissue Engineering Part A* 21.3-4, pp. 829–839.

Kamekura, S. *et al.* (2006). "Contribution of runt-related transcription factor 2 to the pathogenesis of osteoarthritis in mice after induction of knee joint instability". In: *Arthritis Rheum* 54.8, pp. 2462–70. ISSN: 0004-3591 (Print) 0004-3591. DOI: 10.1002/art.22041.

Kanbe, K. *et al.* (2007). "Pericellular matrilins regulate activation of chondrocytes by cyclic load-induced matrix deformation". In: *J Bone Miner Res* 22.2, pp. 318–28. ISSN: 0884-0431 (Print) 0884-0431. DOI: 10.1359/jbmr.061104.

Kanca, Yusuf *et al.* (2018). "Tribological properties of PVA/PVP blend hydrogels against articular cartilage". In: *Journal of the mechanical behavior of biomedical materials* 78, pp. 36–45.

Kang, Hongjun *et al.* (2014). "In vivo cartilage repair using adipose-derived stem cell-loaded decellularized cartilage ECM scaffolds". In: *Journal of tissue engineering and regenerative medicine* 8.6, pp. 442–453.

Karim, Asima, Anish K Amin, and Andrew C Hall (2018). "The clustering and morphology of chondrocytes in normal and mildly degenerate human femoral head cartilage studied by confocal laser scanning microscopy". In: *Journal of anatomy* 232.4, pp. 686–698.

Kawabe, N. and M. Yoshinao (1991). "The repair of full-thickness articular cartilage defects. Immune responses to reparative tissue formed by allogeneic growth plate chondrocyte implants". In: *Clin Orthop Relat Res* 268, pp. 279–93. ISSN: 0009-921X (Print) 0009-921x.

Kawakami, Yasuhiko, Joaquín Rodriguez-León, and Juan Carlos Izpisúa Belmonte (2006). "The role of TGFBs and Sox9 during limb chondrogenesis". In: *Current Opinion in Cell Biology* 18.6, pp. 723–729. ISSN: 0955-0674. DOI: https://doi.org/10.1016/j.ceb.2006.10.007. URL: http://www.sciencedirect.com/science/article/pii/S0955067406001608.

Kayal, Celine, Rebecca J Shipley, and James B Phillips (2019). "Physical and mechanical properties of RAFT-stabilised collagen gels for tissue engineering applications". In: *Journal of the mechanical behavior of biomedical materials* 99, pp. 216–224.

Kelley, Timothy F. *et al.* (2002). "Chondrocyte Repopulation of Allograft Cartilage: A Preliminary Investigation and Strategy for Developing Cartilage Matrices for Reconstruction". In: *Otolaryngology–Head and Neck Surgery* 127.4, pp. 265–270. ISSN: 0194-5998. DOI: 10.1067/mhn.2002.128344. URL: https://doi.org/10.1067/mhn.2002.128344.

Kheir, Ehab *et al.* (2011). "Development and characterization of an acellular porcine cartilage bone matrix for use in tissue engineering". In: *Journal of biomedical materials research Part A* 99.2, pp. 283–294.

Kirkham, J *et al.* (2007). "Self-assembling peptide scaffolds promote enamel remineralization". In: *Journal of dental research* 86.5, pp. 426–430.

Kirsch, T. and K. von der Mark (1992). "Remodelling of collagen types I, II and X and calcification of human fetal cartilage". In: *Bone Miner* 18.2, pp. 107–17. ISSN: 0169-6009 (Print) 0169-6009.

Kisiday, J *et al.* (2002). "Self-assembling peptide hydrogel fosters chondrocyte extracellular matrix production and cell division: implications for cartilage tissue repair". In: *Proceedings of the National Academy of Sciences* 99.15, pp. 9996–10001.

Kisiday, John D *et al.* (2009). "Dynamic compression stimulates proteoglycan synthesis by mesenchymal stem cells in the absence of chondrogenic cytokines". In: *Tissue Engineering Part A* 15.10, pp. 2817–2824.

Klatt, Andreas R *et al.* (2006). "TAK1 downregulation reduces IL-1β induced expression of MMP13, MMP1 and TNF-alpha". In: *Biomedicine & pharmacotherapy* 60.2, pp. 55–61.

Kleemann, RU *et al.* (2005). "Altered cartilage mechanics and histology in knee osteoarthritis: relation to clinical assessment (ICRS Grade)". In: *Osteoarthritis and Cartilage* 13.11, pp. 958–963.

Knutsen, G. *et al.* (2004). "Autologous chondrocyte implantation compared with microfracture in the knee. A randomized trial". In: *J Bone Joint Surg Am* 86-a.3, pp. 455–64. ISSN: 0021-9355 (Print) 0021-9355.

Knutsen, G. *et al.* (2007). "A randomized trial comparing autologous chondrocyte implantation with microfracture. Findings at five years". In: *J Bone Joint Surg Am* 89.10, pp. 2105–12. ISSN: 0021-9355 (Print) 0021-9355. DOI: 10.2106/jbjs.G.00003.

Komorowski, Matthieu and Jesse Raffa (2016). "Markov models and cost effectiveness analysis: applications in medical research". In: *Secondary analysis of electronic health records*, pp. 351–367.

Kon, E. *et al.* (2013). "Matrix assisted autologous chondrocyte transplantation for cartilage treatment: A systematic review". In: *Bone & joint research* 2.2, pp. 18–25. ISSN: 2046-3758. DOI: 10.1302/2046-3758.22.2000092. URL: https://www.ncbi.nlm.nih.gov/pubmed/23610698https://www.ncbi.nlm.nih.gov/pmc/PMC3626217/.

Korhonen, Rami K and Simo Saarakkala (2011). "Biomechanics and modeling of skeletal soft tissues". In: *Theoretical biomechanics*, pp. 113–132.

Kosinska, Marta Krystyna *et al.* (2015). "Articular joint lubricants during osteoarthritis and rheumatoid arthritis display altered levels and molecular species". In: *PloS one* 10.5, e0125192.

Kraan, P. M. van der *et al.* (2009). "TGF-beta signaling in chondrocyte terminal differentiation and osteoarthritis: modulation and integration of signaling pathways through receptor-Smads". In: *Osteoarthritis Cartilage* 17.12, pp. 1539–45. ISSN: 1063-4584. DOI: 10.1016/j.joca.2009.06.008.

Kraan, Peter M. van der, Esmeralda N. Blaney Davidson, and Wim B. van den Berg (2010). "A role for age-related changes in TGFbeta signaling in aberrant chondrocyte differentiation and osteoarthritis". In: *Arthritis research & therapy* 12.1, pp. 201–201. ISSN: 1478-6362 1478-6354. DOI: 10.1186/ar2896. URL: https://www.ncbi.nlm.nih.gov/pubmed/20156325https://www.ncbi.nlm.nih.gov/pmc/PMC2875624/.

Kraan, PM Van der and WB Van den Berg (2012). "Chondrocyte hypertrophy and osteoarthritis: role in initiation and progression of cartilage degeneration?" In: *Osteoarthritis and cartilage* 20.3, pp. 223–232.

Kreuz, PC *et al.* (2006). "Results after microfracture of full-thickness chondral defects in different compartments in the knee". In: *Osteoarthritis and cartilage* 14.11, pp. 1119–1125.

Kumar, Manishekhar *et al.* (2016). "Native honeybee silk membrane: a potential matrix for tissue engineering and regenerative medicine". In: *RSC Advances* 6.59, pp. 54394–54403.

Kumar, P. *et al.* (2001). "Role of uppermost superficial surface layer of articular cartilage in the lubrication mechanism of joints". In: *J Anat* 199.Pt 3, pp. 241–50. ISSN: 0021-8782 (Print) 0021-8782 (Linking).

Kvist, Alexander J. *et al.* (2008). "The major basement membrane components localize to the chondrocyte pericellular matrix — A cartilage basement membrane equivalent?" In: *Matrix Biology* 27.1, pp. 22–33. ISSN: 0945-053X. DOI: https://doi.org/10.1016/j.matbio.2007.07.007. URL: http://www.sciencedirect.com/science/article/pii/S0945053X07001072.

Kwan, A. P. *et al.* (1991). "Macromolecular organization of chicken type X collagen in vitro". In: *J Cell Biol* 114.3, pp. 597–604. ISSN: 0021-9525 (Print) 0021-9525.

Kyle, Stuart *et al.* (2012). "Rational Molecular Design of Complementary Self-Assembling Peptide Hydrogels". In: *Advanced healthcare materials* 1.5, pp. 640–645.

Laasanen, MS *et al.* (2003). "Biomechanical properties of knee articular cartilage". In: *Biorheology* 40.1, 2, 3, pp. 133–140.

Lai, W. M., J. S. Hou, and V. C. Mow (1991). "A Triphasic Theory for the Swelling and Deformation Behaviors of Articular Cartilage". In: *Journal of Biomechanical Engineering* 113.3, pp. 245–258. ISSN: 0148-0731. DOI: 10.1115/1.2894880. URL: http://dx.doi.org/10.1115/1.2894880.

Lai, Yongjie *et al.* (2014). "ADAMTS-7 forms a positive feedback loop with TNF-α in the pathogenesis of osteoarthritis". In: *Annals of the rheumatic diseases* 73.8, pp. 1575–1584.

Langer, F *et al.* (1978). "The immunogenicity of allograft knee joint transplants." In: *Clinical orthopaedics and related research* 132, pp. 155–162.

Langer, R. and J. P. Vacanti (1993). "Tissue engineering". In: *Science* 260.5110, p. 920. DOI: 10.1126/science.8493529. URL: http://science.sciencemag.org/content/260/5110/920.abstract.

LaPrade, R. F. and J. C. Botker (2004). "Donor-site morbidity after osteochondral autograft transfer procedures". In: *Arthroscopy* 20.7, e69–73. ISSN: 0749-8063. DOI: 10.1016/j.arthro.2004.06.022.

Larson, Christopher M *et al.* (2002). "Retention of the native chondrocyte pericellular matrix results in significantly improved matrix production". In: *Matrix biology* 21.4, pp. 349–359.

Leddy, Holly A., Susan E. Christensen, and Farshid Guilak (2008). "Microscale Diffusion Properties of the Cartilage Pericellular Matrix Measured Using 3D Scanning Microphotolysis". In: *Journal of Biomechanical Engineering* 130.6, pp. 061002–061002–8. ISSN: 0148-0731. DOI: 10.1115/1.2979876. URL: http://dx.doi.org/10.1115/1.2979876.

Lee, C. R. *et al.* (2000). "Effects of harvest and selected cartilage repair procedures on the physical and biochemical properties of articular cartilage in the canine knee". In: *Journal of Orthopaedic Research* 18.5, pp. 790–799. ISSN: 0736-0266. DOI: 10.1002/jor.1100180517. URL: https://doi.org/10.1002/jor.1100180517.

Lee, J. *et al.* (2016). "CD24 enrichment protects while its loss increases susceptibility of juvenile chondrocytes towards inflammation". In: *Arthritis Res Ther* 18.1, p. 292. ISSN: 1478-6354. DOI: 10.1186/s13075-016-1183-y.

Lee, Jennifer K *et al.* (2017a). "Tension stimulation drives tissue formation in scaffold-free systems". In: *Nature materials* 16.8, pp. 864–873.

Lee, Jieun *et al.* (2017b). "Human iPSC-derived chondrocytes mimic juvenile chondrocyte function for the dual advantage of increased proliferation and resistance to IL-1B". In: *Stem cell research & therapy* 8.1, pp. 244–244. ISSN: 1757-6512. DOI: 10.1186/s13287-017-0696-x. URL: https://www.ncbi.nlm.nih.gov/pubmed/29096706https://www.ncbi.nlm.nih.gov/pmc/PMC5667438/.

Lee, Whasil *et al.* (2014). "Synergy between Piezo1 and Piezo2 channels confers high-strain mechanosensitivity to articular cartilage". In: *Proceedings of the National Academy of Sciences of the United States of America* 111.47, E5114–E5122. ISSN: 1091-6490 0027-8424. DOI: 10.1073/pnas.1414298111. URL: https://www.ncbi.nlm.nih.gov/pubmed/25385580https://www.ncbi.nlm.nih.gov/pmc/PMC4250098/.

Levy, Yadin D *et al.* (2013). "Do fresh osteochondral allografts successfully treat femoral condyle lesions?" In: *Clinical Orthopaedics and Related Research®* 471.1, pp. 231–237.

Li, Lan *et al.* (2017). "In situ repair of bone and cartilage defects using 3D scanning and 3D printing". In: *Scientific reports* 7.1, pp. 1–12.

Li, Tao *et al.* (2018). "Self-crosslinking and injectable chondroitin sulfate/pullulan hydrogel for cartilage tissue engineering". In: *Applied Materials Today* 10, pp. 173–183.

Li, Xiaomeng *et al.* (2016). "3D culture of chondrocytes in gelatin hydrogels with different stiffness". In: *Polymers* 8.8, p. 269.

Li, Yaqiang *et al.* (2019). "Decellularized cartilage matrix scaffolds with laser-machined micropores for cartilage regeneration and articular cartilage repair". In: *Materials Science and Engineering: C* 105, p. 110139.

Liacini, Abdelhamid *et al.* (2003). "Induction of matrix metalloproteinase-13 gene expression by TNF-α is mediated by MAP kinases, AP-1, and NF-κB transcription factors in articular chondrocytes". In: *Experimental cell research* 288.1, pp. 208–217.

Lieberthal, Jason, Nisha Sambamurthy, and Carla R Scanzello (2015). "Inflammation in joint injury and post-traumatic osteoarthritis". In: *Osteoarthritis and cartilage* 23.11, pp. 1825–1834.

Lim, Chin Tat *et al.* (2013). "Repair of osteochondral defects with rehydrated freeze-dried oligo [poly (ethylene glycol) fumarate] hydrogels seeded with bone marrow mesenchymal stem cells in a porcine model". In: *Tissue Engineering Part A* 19.15-16, pp. 1852–1861.

Lim, Hong-Chul *et al.* (2012). "Current treatments of isolated articular cartilage lesions of the knee achieve similar outcomes". In: *Clinical orthopaedics and related research* 470.8, pp. 2261–2267. ISSN: 1528-1132 0009-921X. DOI: 10.1007/s11999-012-2304-9. URL: https://www.ncbi.nlm.nih.gov/pubmed/22422593https://www.ncbi.nlm.nih.gov/pmc/PMC3392395/.

Liu, Mei *et al.* (2017). "Injectable hydrogels for cartilage and bone tissue engineering". In: *Bone research* 5, p. 17014.

Loeser, Richard F (1993). "Integrin-mediated attachment of articular chondrocytes to extracellular matrix proteins". In: *Arthritis & Rheumatism: Official Journal of the American College of Rheumatology* 36.8, pp. 1103–1110.

Lovati, Arianna B, Marta Bottagisio, and Matteo Moretti (2016). "Decellularized and engineered tendons as biological substitutes: a critical review". In: *Stem cells international* 2016.

Lu, X. L. and V. C. Mow (2008). "Biomechanics of articular cartilage and determination of material properties". In: *Med Sci Sports Exerc* 40.2, pp. 193–9. ISSN: 0195-9131 (Print) 0195-9131 (Linking). DOI: 10.1249/mss.0b013e31815cb1fc.

Lu, X. L. *et al.* (2007). "The generalized triphasic correspondence principle for simultaneous determination of the mechanical properties and proteoglycan content of articular cartilage by indentation". In: *J Biomech* 40.11, pp. 2434–41. ISSN: 0021-9290 (Print) 0021-9290. DOI: 10.1016/j.jbiomech.2006.11.015.

Luo, Lu *et al.* (2016). "Decellularization of porcine articular cartilage explants and their subsequent repopulation with human chondroprogenitor cells". In: *Journal of the mechanical behavior of biomedical materials* 55, pp. 21–31.

Luo, Lu *et al.* (2017). "Engineering tissues that mimic the zonal nature of articular cartilage using decellularized cartilage explants seeded with adult stem cells". In: *ACS Biomaterials Science & Engineering* 3.9, pp. 1933–1943.

Lyman, R, SS Kelley, and G Lee (2000). "Chondrocyte process extension and migration response to partial thickness cartilage injuries in human explants". In: *Proc Orthopaedic Res Soc* 46, p. 0929.

Mahomed, M. N., R. J. Beaver, and A. E. Gross (1992). "The long-term success of fresh, small fragment osteochondral allografts used for intraarticular post-traumatic defects in the knee joint". In: *Orthopedics* 15.10, pp. 1191–9. ISSN: 0147-7447 (Print) 0147-7447.

Mahomed, Nizar N *et al.* (2005). "Epidemiology of total knee replacement in the United States Medicare population". In: *JBJS* 87.6, pp. 1222–1228.

Maldonado, Maricela and Jin Nam (2013). "The role of changes in extracellular matrix of cartilage in the presence of inflammation on the pathology of osteoarthritis". In: *BioMed research international* 2013.

Manferdini, Cristina *et al.* (2022). "RGD-Functionalized Hydrogel Supports the Chondrogenic Commitment of Adipose Mesenchymal Stromal Cells". In: *Gels* 8.6, p. 382.

Mansour, Joseph M (2003). "Biomechanics of cartilage". In: *Kinesiology: the mechanics and pathomechanics of human movement* 2, pp. 66–79.

Marlovits, S. *et al.* (2006). "Cartilage repair: generations of autologous chondrocyte transplantation". In: *Eur J Radiol* 57.1, pp. 24–31. ISSN: 0720-048X (Print) 0720-048x. DOI: 10.1016/j.ejrad.2005.08.009.

Martin, I. *et al.* (2000). "Modulation of the mechanical properties of tissue engineered cartilage". In: *Biorheology* 37.1-2, pp. 141–7. ISSN: 0006-355X (Print) 0006-355x.

Masouros, S. D., A. M. J. Bull, and A. A. Amis (2010). "(i) Biomechanics of the knee joint". In: *Orthopaedics and Trauma* 24.2, pp. 84–91. ISSN: 1877-1327. DOI: https://doi.org/10.1016/j.mporth.2010.03.005. URL: http://www.sciencedirect.com/science/article/pii/S1877132710000308.

Mauck, R. L., X. Yuan, and R. S. Tuan (2006). "Chondrogenic differentiation and functional maturation of bovine mesenchymal stem cells in long-term agarose culture". In: *Osteoarthritis Cartilage* 14.2, pp. 179–89. ISSN: 1063-4584 (Print) 1063-4584. DOI: 10.1016/j.joca.2005.09.002.

Mauck, R. L. *et al.* (2000). "Functional tissue engineering of articular cartilage through dynamic loading of chondrocyte-seeded agarose gels". In: *J Biomech Eng* 122.3, pp. 252–60. ISSN: 0148-0731 (Print) 0148-0731.

Maude, Steven *et al.* (2011). "De novo designed positively charged tape-forming peptides: Self-assembly and gelation in physiological solutions and their evaluation as 3D matrices for cell growth". In: 7, pp. 8085–8099. DOI: 10.1039/C0SM00974A.

McCullen, S. D. *et al.* (2012). "Anisotropic fibrous scaffolds for articular cartilage regeneration". In: *Tissue Eng Part A* 18.19-20, pp. 2073–83. ISSN: 1937-3341. DOI: 10.1089/ten.TEA.2011.0606.

McNulty, A. L. *et al.* (2013). "Synovial fluid concentrations and relative potency of interleukin-1 alpha and beta in cartilage and meniscus degradation". In: *J Orthop Res* 31.7, pp. 1039–45. ISSN: 0736-0266. DOI: 10.1002/jor.22334.

Means, A Kristen *et al.* (2019). "Double network hydrogels that mimic the modulus, strength, and lubricity of cartilage". In: *Biomacromolecules* 20.5, pp. 2034–2042.

Meinert, Christoph *et al.* (2017). "A novel bioreactor system for biaxial mechanical loading enhances the properties of tissue-engineered human cartilage". In: *Scientific reports* 7.1, pp. 1–14.

Melle, Marloes L De Vries-van *et al.* (2012). "An osteochondral culture model to study mechanisms involved in articular cartilage repair". In: *Tissue Engineering Part C: Methods* 18.1, pp. 45–53.

Meyers, M. H., W. Akeson, and F. R. Convery (1989). "Resurfacing of the knee with fresh osteochondral allograft". In: *The Journal of bone and joint surgery. American*

volume 71.5, pp. 704–713. ISSN: 0021-9355. URL: http://europepmc.org/abstract/MED/2659599http://www.ejbjs.org/cgi/content/abstract/71/5/704.

Middendorf, Jill M *et al.* (2020). "Heterogeneous matrix deposition in human tissue engineered cartilage changes the local shear modulus and resistance to local construct buckling". In: *Journal of Biomechanics* 105, p. 109760.

Miles, DE *et al.* (2016). "Peptide: glycosaminoglycan hybrid hydrogels as an injectable intervention for spinal disc degeneration". In: *Journal of Materials Chemistry B* 4.19, pp. 3225–3231.

Millward-Sadler, S. J. *et al.* (1999). "Integrin-regulated Secretion of Interleukin 4: A Novel Pathway of Mechanotransduction in Human Articular Chondrocytes". In: *The Journal of Cell Biology* 145.1, p. 183. DOI: 10.1083/jcb.145.1.183. URL: http://jcb.rupress.org/content/145/1/183.abstract.

Mistry, Hema *et al.* (2017). "Autologous chondrocyte implantation in the knee: systematic review and economic evaluation". In.

Mistry, Hema *et al.* (2019). "The cost-effectiveness of osteochondral allograft transplantation in the knee". In: *Knee Surgery, Sports Traumatology, Arthroscopy* 27.6, pp. 1739–1753.

Mithoefer, Kai *et al.* (2012). "Current concepts for rehabilitation and return to sport after knee articular cartilage repair in the athlete". In: *journal of orthopaedic & sports physical therapy* 42.3, pp. 254–273.

Mlynarik, V. and S. Trattnig (2000). "Physicochemical properties of normal articular cartilage and its MR appearance". In: *Invest Radiol* 35.10, pp. 589–94. ISSN: 0020-9996 (Print) 0020-9996.

Mobasheri, Ali and Mark Batt (2016). "An update on the pathophysiology of osteoarthritis". In: *Annals of physical and rehabilitation medicine* 59.5-6, pp. 333–339.

Montalbano, G *et al.* (2018). "Synthesis of bioinspired collagen/alginate/fibrin based hydrogels for soft tissue engineering". In: *Materials Science and Engineering: C* 91, pp. 236–246.

Moore, Amanda N and Jeffrey D Hartgerink (2017). "Self-assembling multidomain peptide nanofibers for delivery of bioactive molecules and tissue regeneration". In: *Accounts of chemical research* 50.4, pp. 714–722.

Morrison, J. B. (1968). "Bioengineering analysis of force actions transmitted by the knee joint". In: *Bio-Med. Engng.* 3, pp. 164–170. URL: https://ci.nii.ac.jp/naid/10029607782/en/.

Moutos, Franklin T, Lisa E Freed, and Farshid Guilak (2007). "A biomimetic three-dimensional woven composite scaffold for functional tissue engineering of cartilage". In: *Nature materials* 6.2, p. 162.

Mow, V. C., A. Ratcliffe, and A. R. Poole (1992). "Cartilage and diarthrodial joints as paradigms for hierarchical materials and structures". In: *Biomaterials* 13.2, pp. 67–97. ISSN: 0142-9612 (Print) 0142-9612 (Linking).

Mow, Van C and X Edward Guo (2002). "Mechano-electrochemical properties of articular cartilage: their inhomogeneities and anisotropies". In: *Annual review of biomedical engineering* 4.1, pp. 175–209.

Mow, Van C *et al.* (1989). "Biphasic indentation of articular cartilage—II. A numerical algorithm and an experimental study". In: *Journal of biomechanics* 22.8-9, pp. 853–861.

Mueller-Rath, Ralf *et al.* (2010). "Condensed cellular seeded collagen gel as an improved biomaterial for tissue engineering of articular cartilage". In: *Bio-medical materials and engineering* 20.6, pp. 317–328.

Nachtsheim, Julia *et al.* (2019). "Chondrocyte colonisation of a tissue-engineered cartilage substitute under a mechanical stimulus". In: *Medical Engineering & Physics* 74, pp. 58–64.

Nam, J. *et al.* (2009). "Biomechanical thresholds regulate inflammation through the NF-kappaB pathway: experiments and modeling". In: *PLoS One* 4.4, e5262. ISSN: 1932-6203. DOI: 10.1371/journal.pone.0005262.

Nargang, Tobias M *et al.* (2014). "Liquid polystyrene: a room-temperature photocurable soft lithography compatible pour-and-cure-type polystyrene". In: *Lab on a chip* 14.15, pp. 2698–2708.

Navarro, M. *et al.* (2017). "3 - Arthrology". In: *Morphological Mouse Phenotyping*. Ed. by Jesús Ruberte, Ana Carretero, and Marc Navarro. Academic Press, pp. 55–62. ISBN: 978-0-12-812805-3. DOI: https://doi.org/10.1016/B978-0-12-812972-2.50003-9. URL: http://www.sciencedirect.com/science/article/pii/B9780128129722500039.

Nawaz, Syed Z *et al.* (2014). "Autologous chondrocyte implantation in the knee: mid-term to long-term results". In: *JBJS* 96.10, pp. 824–830.

Negoro, Takaharu *et al.* (2018). "Trends in clinical trials for articular cartilage repair by cell therapy". In: *NPJ Regenerative medicine* 3.1, pp. 1–10.

Nehrer, S., M. Spector, and T. Minas (1999). "Histologic analysis of tissue after failed cartilage repair procedures". In: *Clin Orthop Relat Res* 365, pp. 149–62. ISSN: 0009-921X (Print) 0009-921x.

Neunaber, Claudia *et al.* (2022). "Towards the development of osteochondral allografts with reduced immunogenicity". In: *Journal of the Mechanical Behavior of Biomedical Materials* 133, p. 105359.

NICE (2017). "Autologous chondrocyte implantation for treating symptomatic articular cartilage defects of the knee". In: *Technology appraisal guidance*.

Nicodemus, Garret D. and Stephanie J. Bryant (2008). "Cell encapsulation in biodegradable hydrogels for tissue engineering applications". In: *Tissue engineering. Part B, Reviews* 14.2, pp. 149–165. ISSN: 1937-3376 1937-3368. DOI: 10.1089/ten.teb.2007.0332. URL: https://www.ncbi.nlm.nih.gov/pubmed/18498217https://www.ncbi.nlm.nih.gov/pmc/PMC2962861/.

Nieminen, Miika T *et al.* (2004). "Prediction of biomechanical properties of articular cartilage with quantitative magnetic resonance imaging". In: *Journal of biomechanics* 37.3, pp. 321–328.

Nosewicz, Tomasz L *et al.* (2014). "Influence of basal support and early loading on bone cartilage healing in press-fitted osteochondral autografts". In: *Knee Surgery, Sports Traumatology, Arthroscopy* 22.6, pp. 1445–1451.

Nurminskaya, Maria and Thomas F Linsenmayer (1996). "Identification and characterization of up-regulated genes during chondrocyte hypertrophy". In: *Developmental dynamics: an official publication of the American Association of Anatomists* 206.3, pp. 260–271.

Nürnberger, S *et al.* (2021). "Repopulation of decellularised articular cartilage by laser-based matrix engraving". In: *EBioMedicine* 64, p. 103196.

Nykänen, Olli *et al.* (2019). "T2* and quantitative susceptibility mapping in an equine model of post-traumatic osteoarthritis: assessment of mechanical and structural

properties of articular cartilage". In: *Osteoarthritis and Cartilage* 27.10, pp. 1481–1490.

O'Brien, Bernie J *et al.* (2002). "Is there a kink in consumers' threshold value for cost-effectiveness in health care?" In: *Health economics* 11.2, pp. 175–180.

O'brien, Fergal J (2011). "Biomaterials & scaffolds for tissue engineering". In: *Materials today* 14.3, pp. 88–95.

Ogura, Takahiro *et al.* (2019). "Survival analysis of revision autologous chondrocyte implantation for failed ACI". In: *The American journal of sports medicine* 47.13, pp. 3212–3220.

O'hEireamhoin, Sven *et al.* (2012). "Recapitulating aspects of the oxygen and substrate environment of the damaged joint milieu for stem cell-based cartilage tissue engineering". In: *Tissue Engineering Part C: Methods* 19.2, pp. 117–127.

Olderøy, Magnus Ø *et al.* (2014). "Biochemical and structural characterization of neocartilage formed by mesenchymal stem cells in alginate hydrogels". In: *PloS one* 9.3, e91662.

ONS, Office for National Statistics (2017). "Overview of the UK population: July 2017". In: *Overview of the UK population*.

Owida, HA *et al.* (2018). "Induction of zonal-specific cellular morphology and matrix synthesis for biomimetic cartilage regeneration using hybrid scaffolds". In: *Journal of The Royal Society Interface* 15.143, p. 20180310.

O'Conor, Christopher J. *et al.* (2014). "TRPV4-mediated mechanotransduction regulates the metabolic response of chondrocytes to dynamic loading". In: *Proceedings of the National Academy of Sciences* 111.4, p. 1316. DOI: 10.1073/pnas.1319569111. URL: http://www.pnas.org/content/111/4/1316.abstract.

Pacifici, M., E. Koyama, and M. Iwamoto (2005). "Mechanisms of synovial joint and articular cartilage formation: recent advances, but many lingering mysteries". In: *Birth Defects Res C Embryo Today* 75.3, pp. 237–48. ISSN: 1542-975X (Print) 1542-975X (Linking). DOI: 10.1002/bdrc.20050.

Pan, Qiuhui *et al.* (2009). "Bone Morphogenetic Protein-2 induces chromatin remodeling and modification at the proximal promoter of Sox9 gene". In: *Biochemical and Biophysical Research Communications* 379.2, pp. 356–361. ISSN: 0006-291X. DOI:

https://doi.org/10.1016/j.bbrc.2008.12.062. URL: http://www.sciencedirect.com/science/article/pii/S0006291X08024637.

Park, I. K. and C. S. Cho (2010). "Stem Cell-assisted Approaches for Cartilage Tissue Engineering". In: *Int J Stem Cells* 3.2, pp. 96–102. ISSN: 2005-3606 (Print) 2005-3606.

Park, Seonghun *et al.* (2003). "Cartilage interstitial fluid load support in unconfined compression". In: *Journal of biomechanics* 36.12, pp. 1785–1796.

Park, Yong-Beom *et al.* (2017). "Cartilage regeneration in osteoarthritic patients by a composite of allogeneic umbilical cord blood-derived mesenchymal stem cells and hyaluronate hydrogel: Results from a clinical trial for safety and proof-of-concept with 7 years of extended follow-up". In: *Stem cells translational medicine* 6.2, pp. 613–621.

Partap, Sonia, Frank Lyons, and Fergal J O'Brien (2010). "Scaffolds & surfaces". In: *Basic Engineering for Medics and Biologists*. IOS Press, pp. 187–201.

Pawaskar, Sainath Shrikant, John Fisher, and Zhongmin Jin (2010). "Robust and general method for determining surface fluid flow boundary conditions in articular cartilage contact mechanics modeling". In: *Journal of biomechanical engineering* 132.3.

Pearle, Andrew D, Russell F Warren, and Scott A Rodeo (2005). "Basic science of articular cartilage and osteoarthritis". In: *Clinics in sports medicine* 24.1, pp. 1–12.

Pelttari, K., E. Steck, and W. Richter (2008). "The use of mesenchymal stem cells for chondrogenesis". In: *Injury* 39 Suppl 1, S58–65. ISSN: 0020-1383 (Print) 0020-1383. DOI: 10.1016/j.injury.2008.01.038.

Pesesse, L., C. Sanchez, and Y. Henrotin (2011). "Osteochondral plate angiogenesis: a new treatment target in osteoarthritis". In: *Joint Bone Spine* 78.2, pp. 144–9. ISSN: 1297-319x. DOI: 10.1016/j.jbspin.2010.07.001.

Peterson, L. *et al.* (2000). "Two- to 9-year outcome after autologous chondrocyte transplantation of the knee". In: *Clin Orthop Relat Res* 374, pp. 212–34. ISSN: 0009-921X (Print) 0009-921x.

Peterson, Lars *et al.* (2003). "Treatment of osteochondritis dissecans of the knee with autologous chondrocyte transplantation: results at two to ten years". In: *JBJS* 85, pp. 17–24.

Pfeifer, Christian *et al.* (2012). "Cartilage labelling for mechanical testing in T-peel configuration". In: *International orthopaedics* 36.7, pp. 1493–1499.

Pfeiffer, E *et al.* (2008). "The effects of glycosaminoglycan content on the compressive modulus of cartilage engineered in type II collagen scaffolds". In: *Osteoarthritis and Cartilage* 16.10, pp. 1237–1244.

Poole, C. Anthony, Michael H. Flint, and Brent W. Beaumont (1987). "Chondrons in cartilage: Ultrastructural analysis of the pericellular microenvironment in adult human articular cartilages". In: *Journal of Orthopaedic Research* 5.4, pp. 509–522. ISSN: 0736-0266. DOI: 10.1002/jor.1100050406. URL: https://doi.org/10.1002/jor.1100050406.

Poole, C Anthony, Zi-Jun Zhang, and Jacqueline M Ross (2001). "The differential distribution of acetylated and detyrosinated alpha-tubulin in the microtubular cytoskeleton and primary cilia of hyaline cartilage chondrocytes". In: *The Journal of Anatomy* 199.4, pp. 393–405. ISSN: 1553-0795.

Prieto-Alhambra, Daniel *et al.* (2014). "Incidence and risk factors for clinically diagnosed knee, hip and hand osteoarthritis: influences of age, gender and osteoarthritis affecting other joints". In: *Annals of the rheumatic diseases* 73.9, pp. 1659–1664.

Quintero, Maritza *et al.* (2008). "Granulocyte-macrophage colony stimulating factor is anabolic and interleukin-1B is catabolic for rat articular chondrocytes". In: *Cytokine* 44.3, pp. 366–372. ISSN: 1043-4666. DOI: https://doi.org/10.1016/j.cyto.2008.10.003. URL: http://www.sciencedirect.com/science/article/pii/S1043466608007588.

Rauch, Frank and Eckhard Schoenau (2001). "The developing bone: slave or master of its cells and molecules?" In: *Pediatric research* 50.3, p. 309.

Reinold, Michael M *et al.* (2006). "Current concepts in the rehabilitation following articular cartilage repair procedures in the knee". In: *Journal of Orthopaedic & Sports Physical Therapy* 36.10, pp. 774–794.

Robertsson, Otto *et al.* (2000). "Patient satisfaction after knee arthroplasty: a report on 27,372 knees operated on between 1981 and 1995 in Sweden". In: *Acta Orthopaedica Scandinavica* 71.3, pp. 262–267.

Rose, Brandon J and David L Kooyman (2016). "A tale of two joints: the role of matrix metalloproteases in cartilage biology". In: *Disease Markers* 2016.

Ross, Sarah and Caroline S. Hill (2008). "How the Smads regulate transcription". In: *The International Journal of Biochemistry & Cell Biology* 40.3, pp. 383–408. ISSN: 1357-2725. DOI: https://doi.org/10.1016/j.biocel.2007.09.006. URL: http://www.sciencedirect.com/science/article/pii/S1357272507003160.

Saarakkala, S *et al.* (2010). "Depth-wise progression of osteoarthritis in human articular cartilage: investigation of composition, structure and biomechanics". In: *Osteoarthritis and Cartilage* 18.1, pp. 73–81.

Sah, R. L. *et al.* (1994). "Differential Effects of bFGF and IGF-I on Matrix Metabolism in Calf and Adult Bovine Cartilage Explants". In: *Archives of Biochemistry and Biophysics* 308.1, pp. 137–147. ISSN: 0003-9861. DOI: https://doi.org/10.1006/abbi.1994.1020. URL: http://www.sciencedirect.com/science/article/pii/S0003986184710204.

Saha, Asit K and Sean S Kohles (2012). "A cell-matrix model of anabolic and catabolic dynamics during cartilage biomolecule regulation". In: *International Journal of Computers in Healthcare* 1.3, p. 214.

Sanchez, C. *et al.* (2005). "Osteoblasts from the sclerotic subchondral bone downregulate aggrecan but upregulate metalloproteinases expression by chondrocytes. This effect is mimicked by interleukin-6, -1beta and oncostatin M pre-treated non-sclerotic osteoblasts". In: *Osteoarthritis Cartilage* 13.11, pp. 979–87. ISSN: 1063-4584 (Print) 1063-4584. DOI: 10.1016/j.joca.2005.03.008.

Sanchez-Adams, Johannah *et al.* (2014). "The mechanobiology of articular cartilage: bearing the burden of osteoarthritis". In: *Current rheumatology reports* 16.10, p. 451.

Saris, Daniel BF *et al.* (2009). "Characterized chondrocyte implantation results in better structural repair when treating symptomatic cartilage defects of the knee in a randomized controlled trial versus microfracture". In: *The American journal of sports medicine* 36.2, pp. 235–246.

Scanzello, Carla R, Anna Plaas, and Mary K Crow (2008). "Innate immune system activation in osteoarthritis: is osteoarthritis a chronic wound?" In: *Current opinion in rheumatology* 20.5, pp. 565–572.

Scharstuhl, Alwin *et al.* (2002). "Inhibition of endogenous TGF-β during experimental osteoarthritis prevents osteophyte formation and impairs cartilage repair". In: *The Journal of Immunology* 169.1, pp. 507–514.

Schätti, O *et al.* (2011). "A combination of shear and dynamic compression leads to mechanically induced chondrogenesis of human mesenchymal stem cells". In: *Eur Cell Mater* 22.214-225, b97.

Schipani, Rossana *et al.* (2020). "Reinforcing interpenetrating network hydrogels with 3D printed polymer networks to engineer cartilage mimetic composites". In: *Biofabrication* 12.3, p. 035011.

Schwab, Andrea *et al.* (2021). "Ex vivo osteochondral test system with control over cartilage defect depth–A pilot study to investigate the effect of oxygen tension and chondrocyte based treatments in chondral and full thickness defects in an organ model". In: *Osteoarthritis and Cartilage Open* 3.2, p. 100173.

Schwarz, Markus L *et al.* (2015). "Instruments for reproducible setting of defects in cartilage and harvesting of osteochondral plugs for standardisation of preclinical tests for articular cartilage regeneration". In: *Journal of orthopaedic surgery and research* 10.1, pp. 1–11.

Schwarz, Silke *et al.* (2012). "Decellularized cartilage matrix as a novel biomatrix for cartilage tissue-engineering applications". In: *Tissue engineering Part A* 18.21-22, pp. 2195–2209. ISSN: 1937-3341.

Seireg, A. and R. J. Arvikar (1975). "The prediction of muscular load sharing and joint forces in the lower extremities during walking". In: *Journal of Biomechanics* 8.2, pp. 89–102. ISSN: 0021-9290. DOI: https://doi.org/10.1016/0021-9290(75)90089-5. URL: http://www.sciencedirect.com/science/article/pii/0021929075900895.

Seol, Dongrim *et al.* (2014). "Effect of short-term enzymatic treatment on cell migration and cartilage regeneration: in vitro organ culture of bovine articular cartilage". In: *Tissue engineering Part A* 20.13-14, pp. 1807–1814.

Setayeshmehr, Mohsen *et al.* (2021). "Bioprinting Via a Dual-Gel Bioink Based on Poly (Vinyl Alcohol) and Solubilized Extracellular Matrix towards Cartilage Engineering". In: *International journal of molecular sciences* 22.8, p. 3901.

Shakibaei, Mehdi *et al.* (2006). "Igf-I extends the chondrogenic potential of human articular chondrocytes in vitro: Molecular association between Sox9 and Erk1/2". In: *Biochemical Pharmacology* 72.11, pp. 1382–1395. ISSN: 0006-2952. DOI: https:

//doi.org/10.1016/j.bcp.2006.08.022. URL: http://www.sciencedirect.com/science/article/pii/S000629520600534X.

Sheridan, William S, Garry P Duffy, and Bruce P Murphy (2013). "Optimum parameters for freeze-drying decellularized arterial scaffolds". In: *Tissue Engineering Part C: Methods* 19.12, pp. 981–990.

Sherman, S. L. *et al.* (2014). "Fresh osteochondral allograft transplantation for the knee: current concepts". In: *J Am Acad Orthop Surg* 22.2, pp. 121–33. ISSN: 1067-151X (Print) 1067-151x. DOI: 10.5435/jaaos-22-02-121.

Silver, F. H., G. Bradica, and A. Tria (2002). "Elastic energy storage in human articular cartilage: estimation of the elastic modulus for type II collagen and changes associated with osteoarthritis". In: *Matrix Biol* 21.2, pp. 129–37. ISSN: 0945-053X (Print) 0945-053x.

Simsa, Robin *et al.* (2019). "Effect of fluid dynamics on decellularization efficacy and mechanical properties of blood vessels". In: *PloS one* 14.8.

Slaughter, Brandon V *et al.* (2009). "Hydrogels in regenerative medicine". In: *Advanced materials* 21.32-33, pp. 3307–3329.

Smeriglio, Piera *et al.* (2015). "Collagen VI enhances cartilage tissue generation by stimulating chondrocyte proliferation". In: *Tissue Engineering Part A* 21.3-4, pp. 840–849.

Smith, Graham D *et al.* (2005). "Arthroscopic assessment of cartilage repair: a validation study of 2 scoring systems". In: *Arthroscopy: The Journal of Arthroscopic & Related Surgery* 21.12, pp. 1462–1467.

Smith, R. L. *et al.* (1995). "Effects of fluid-induced shear on articular chondrocyte morphology and metabolism in vitro". In: *J Orthop Res* 13.6, pp. 824–31. ISSN: 0736-0266 (Print) 0736-0266. DOI: 10.1002/jor.1100130604.

Solchaga, Luis A *et al.* (2006). "A rapid seeding technique for the assembly of large cell/scaffold composite constructs". In: *Tissue engineering* 12.7, pp. 1851–1863.

Soltz, M. A. and G. A. Ateshian (1998). "Experimental verification and theoretical prediction of cartilage interstitial fluid pressurization at an impermeable contact interface in confined compression". In: *J Biomech* 31.10, pp. 927–34. ISSN: 0021-9290 (Print) 0021-9290.

Somoza, Rodrigo A. *et al.* (2014). "Chondrogenic differentiation of mesenchymal stem cells: challenges and unfulfilled expectations". In: *Tissue engineering. Part B, Reviews* 20.6, pp. 596–608. ISSN: 1937-3376 1937-3368. DOI: 10.1089/ten.TEB.2013.0771. URL: https://www.ncbi.nlm.nih.gov/pubmed/24749845https://www.ncbi.nlm.nih.gov/pmc/PMC4241862/.

Sonnenberg, Frank A and J Robert Beck (1993). "Markov models in medical decision making: a practical guide". In: *Medical decision making* 13.4, pp. 322–338.

Sophia Fox, Alice J., Asheesh Bedi, and Scott A. Rodeo (2009). "The Basic Science of Articular Cartilage: Structure, Composition, and Function". In: *Sports Health* 1.6, pp. 461–468. ISSN: 1941-7381 1941-0921. DOI: 10.1177/1941738109350438. URL: http://www.ncbi.nlm.nih.gov/pmc/articles/PMC3445147/.

Statham, Patrick *et al.* (2022). "Reproducing the biomechanical environment of the chondrocyte for cartilage tissue engineering". In: *Tissue Engineering Part B: Reviews*.

Steadman, J. Richard *et al.* (1997). "Microfracture technique forfull-thickness chondral defects: Technique and clinical results". In: *Operative Techniques in Orthopaedics* 7.4, pp. 300–304. ISSN: 1048-6666. DOI: https://doi.org/10.1016/S1048-6666(97)80033-X. URL: http://www.sciencedirect.com/science/article/pii/S104866669780033X.

Steadman, J. Richard *et al.* (2003). "Outcomes of microfracture for traumatic chondral defects of the knee: Average 11-year follow-up". In: *Arthroscopy: The Journal of Arthroscopic & Related Surgery* 19.5, pp. 477–484. ISSN: 0749-8063. DOI: https://doi.org/10.1053/jars.2003.50112. URL: http://www.sciencedirect.com/science/article/pii/S0749806303001245.

Steck, Eric *et al.* (2005). "Induction of intervertebral disc–like cells from adult mesenchymal stem cells". In: *Stem cells* 23.3, pp. 403–411.

Strauss, Eric J. *et al.* (2005). "Biochemical and Biomechanical Properties of Lesion and Adjacent Articular Cartilage after Chondral Defect Repair in an Equine Model". In: *The American Journal of Sports Medicine* 33.11, pp. 1647–1653. ISSN: 0363-5465. DOI: 10.1177/0363546505275487. URL: https://doi.org/10.1177/0363546505275487.

Suchorska, Wiktoria Maria *et al.* (2017). "Gene expression profile in human induced pluripotent stem cells: Chondrogenic differentiation in vitro, part A". In: *Molecular Medicine Reports* 15.5, pp. 2387–2401.

Sutherland, Amanda J *et al.* (2015). "Decellularized cartilage may be a chondroinductive material for osteochondral tissue engineering". In: *PloS one* 10.5, e0121966.

Sward, P. *et al.* (2012). "Cartilage and bone markers and inflammatory cytokines are increased in synovial fluid in the acute phase of knee injury (hemarthrosis)–a cross-sectional analysis". In: *Osteoarthritis Cartilage* 20.11, pp. 1302–8. ISSN: 1063-4584. DOI: 10.1016/j.joca.2012.07.021.

Talukdar, Sarmistha *et al.* (2011). "Effect of initial cell seeding density on 3D-engineered silk fibroin scaffolds for articular cartilage tissue engineering". In: *Biomaterials* 32.34, pp. 8927–8937.

Tan, Lijun, Yijin Ren, and Roel Kuijer (2012). "A 1-min method for homogenous cell seeding in porous scaffolds". In: *Journal of biomaterials applications* 26.7, pp. 877–889.

Tang, Zhenyu *et al.* (2009). "Contributions of different intraarticular tissues to the acute phase elevation of synovial fluid MMP-2 following rat ACL rupture". In: *Journal of orthopaedic research* 27.2, pp. 243–248.

Tare, Rahul S *et al.* (2005). "Tissue engineering strategies for cartilage generation—micromass and three dimensional cultures using human chondrocytes and a continuous cell line". In: *Biochemical and biophysical research communications* 333.2, pp. 609–621.

Tatman, Philip David *et al.* (2015). "Multiscale biofabrication of articular cartilage: bioinspired and biomimetic approaches". In: *Tissue Engineering Part B: Reviews* 21.6, pp. 543–559.

Teixeira, José *et al.* (2018). "Extracellular acidification induces ROS-and mPTP-mediated death in HEK293 cells". In: *Redox biology* 15, pp. 394–404.

Thomas, Elaine, George Peat, and Peter Croft (2013). "Defining and mapping the person with osteoarthritis for population studies and public health". In: *Rheumatology* 53.2, pp. 338–345.

Tírico, Luís Eduardo Passarelli *et al.* (2016). "Development of a fresh osteochondral allograft program outside North America". In: *Cartilage* 7.3, pp. 222–228.

Toonstra, Jenny L. *et al.* (2016). "Patient Experiences of Recovery After Autologous Chondrocyte Implantation: A Qualitative Study". In: *Journal of athletic training* 51.12, pp. 1028–1036. ISSN: 1938-162X 1062-6050. DOI: 10.4085/1062-6050-51.12.12. URL: https://www.ncbi.nlm.nih.gov/pubmed/27835044https://www.ncbi.nlm.nih.gov/pmc/PMC5264558/.

Torzilli, P. A., M. Bhargava, and C. T. Chen (2011). "Mechanical Loading of Articular Cartilage Reduces IL-1-Induced Enzyme Expression". In: *Cartilage* 2.4, pp. 364–373. ISSN: 1947-6035 (Print) 1947-6035. DOI: 10.1177/1947603511407484.

Torzilli, PA *et al.* (1999). "Effect of impact load on articular cartilage: cell metabolism and viability, and matrix water content". In: *Journal of biomechanical engineering* 121.5, pp. 433–441.

Treppo, Steven *et al.* (2000). "Comparison of biomechanical and biochemical properties of cartilage from human knee and ankle pairs". In: *Journal of Orthopaedic Research* 18.5, pp. 739–748.

Tsuchiya, A. *et al.* (2005). "Expression of mouse HtrA1 serine protease in normal bone and cartilage and its upregulation in joint cartilage damaged by experimental arthritis". In: *Bone* 37.3, pp. 323–36. ISSN: 8756-3282 (Print) 1873-2763. DOI: 10.1016/j.bone.2005.03.015.

Ulstein, Svend *et al.* (2014). "Microfracture technique versus osteochondral autologous transplantation mosaicplasty in patients with articular chondral lesions of the knee: a prospective randomized trial with long-term follow-up". In: *Knee surgery, sports traumatology, arthroscopy : official journal of the ESSKA* 22.6, pp. 1207–1215. ISSN: 1433-7347 0942-2056. DOI: 10.1007/s00167-014-2843-6. URL: https://www.ncbi.nlm.nih.gov/pubmed/24441734https://www.ncbi.nlm.nih.gov/pmc/PMC4028546/.

Vainieri, Maria Letizia *et al.* (2018). "Mechanically stimulated osteochondral organ culture for evaluation of biomaterials in cartilage repair studies". In: *Acta Biomaterialia* 81, pp. 256–266.

Varghese, Shyni *et al.* (2008). "Chondroitin sulfate based niches for chondrogenic differentiation of mesenchymal stem cells". In: *Matrix Biology* 27.1, pp. 12–21.

Vega, Sebastián L, Mi Y Kwon, and Jason A Burdick (2017). "Recent advances in hydrogels for cartilage tissue engineering". In: *European cells & materials* 33, p. 59.

Verbruggen, Stefaan W *et al.* (2018). "Stresses and strains on the human fetal skeleton during development". In: *Journal of The Royal Society Interface* 15.138, p. 20170593.

Vincent, TL *et al.* (2007). "FGF-2 is bound to perlecan in the pericellular matrix of articular cartilage, where it acts as a chondrocyte mechanotransducer". In: *Osteoarthritis and cartilage* 15.7, pp. 752–763.

Von Der Mark, Klaus *et al.* (1977). "Relationship between cell shape and type of collagen synthesised as chondrocytes lose their cartilage phenotype in culture". In: *Nature* 267, p. 531. DOI: 10.1038/267531a0. URL: https://doi.org/10.1038/267531a0.

Vonk, Lucienne A *et al.* (2010). "Preservation of the chondrocyte's pericellular matrix improves cell-induced cartilage formation". In: *Journal of cellular biochemistry* 110.1, pp. 260–271.

Wang, Chong *et al.* (2020). "Cryogenic 3D printing of heterogeneous scaffolds with gradient mechanical strengths and spatial delivery of osteogenic peptide/TGF-β1 for osteochondral tissue regeneration". In: *Biofabrication* 12.2, p. 025030.

Wang, Lai *et al.* (2001). "Flow cytometric analysis of the human articular chondrocyte phenotype in vitro". In: *Osteoarthritis and Cartilage* 9.1, pp. 73–84.

Wang, Lina *et al.* (2013). "Decellularized musculofascial extracellular matrix for tissue engineering". In: *Biomaterials* 34.11, pp. 2641–2654.

Wang, Qi Guang, Alicia J El Haj, and Nicola J Kuiper (2008). "Glycosaminoglycans in the pericellular matrix of chondrons and chondrocytes". In: *Journal of anatomy* 213.3, pp. 266–273.

Wang, Qi Guang *et al.* (2010). "Molecular profiling of single cells in response to mechanical force: comparison of chondrocytes, chondrons and encapsulated chondrocytes". In: *Biomaterials* 31.7, pp. 1619–1625.

Wang, Tianyi, Janice H Lai, and Fan Yang (2016). "Effects of hydrogel stiffness and extracellular compositions on modulating cartilage regeneration by mixed populations of stem cells and chondrocytes in vivo". In: *Tissue Engineering Part A* 22.23-24, pp. 1348–1356.

Wang, Z. J. *et al.* (2014). "Repair of articular cartilage defects by tissue-engineered cartilage constructed with adipose-derived stem cells and acellular cartilaginous

matrix in rabbits". In: *Genet Mol Res* 13.2, pp. 4599–606. ISSN: 1676-5680. DOI: 10.4238/2014.June.18.2.

Wang, Zhifa *et al.* (2018). "Cartilaginous extracellular matrix derived from decellularized chondrocyte sheets for the reconstruction of osteochondral defects in rabbits". In: *Acta Biomaterialia* 81, pp. 129–145. ISSN: 1742-7061. DOI: https://doi.org/10.1016/j.actbio.2018.10.005. URL: http://www.sciencedirect.com/science/article/pii/S1742706118305956.

Wann, Angus K. T. *et al.* (2012). "Primary cilia mediate mechanotransduction through control of ATP-induced Ca2+ signaling in compressed chondrocytes". In: *The FASEB Journal* 26.4, pp. 1663–1671. ISSN: 0892-6638. DOI: 10.1096/fj.11-193649. URL: https://doi.org/10.1096/fj.11-193649.

Warren, James P *et al.* (2021). "Hydrodynamic Mixing Tunes the Stiffness of Proteoglycan-Mimicking Physical Hydrogels". In: *Advanced Healthcare Materials* 10.11, p. 2001998.

Warren, James Phillip. (2017). "Self-assembling peptide hydrogels for articular cartilage repair". PhD thesis.

Weightman, B. (1976). "Tensile fatigue of human articular cartilage". In: *Journal of Biomechanics* 9.4, pp. 193–200. ISSN: 0021-9290. DOI: https://doi.org/10.1016/0021-9290(76)90004-X. URL: http://www.sciencedirect.com/science/article/pii/002192907690004X.

Wiberg, C. *et al.* (2003). "Complexes of matrilin-1 and biglycan or decorin connect collagen VI microfibrils to both collagen II and aggrecan". In: *J Biol Chem* 278.39, pp. 37698–704. ISSN: 0021-9258 (Print) 0021-9258. DOI: 10.1074/jbc.M304638200.

Willers, Craig *et al.* (2005). "Autologous chondrocyte implantation with collagen bioscaffold for the treatment of osteochondral defects in rabbits". In: *Tissue engineering* 11.7-8, pp. 1065–1076.

Wong, C. *et al.* (2003). "Fibrin-based biomaterials to deliver human growth factors". In: *Thromb Haemost* 89.3, pp. 573–82. ISSN: 0340-6245 (Print) 0340-6245.

Wong, M., M. Siegrist, and X. Cao (1999). "Cyclic compression of articular cartilage explants is associated with progressive consolidation and altered expression pattern of extracellular matrix proteins". In: *Matrix Biol* 18.4, pp. 391–9. ISSN: 0945-053X (Print) 0945-053x.

Woodfield, Tim BF *et al.* (2004). "Design of porous scaffolds for cartilage tissue engineering using a three-dimensional fiber-deposition technique". In: *Biomaterials* 25.18, pp. 4149–4161.

Wright, M. *et al.* (1996). "Effects of intermittent pressure-induced strain on the electrophysiology of cultured human chondrocytes: evidence for the presence of stretch-activated membrane ion channels". In: *Clin Sci (Lond)* 90.1, pp. 61–71. ISSN: 0143-5221 (Print) 0143-5221.

Wright, M. O. *et al.* (1997). "Hyperpolarisation of cultured human chondrocytes following cyclical pressure-induced strain: Evidence of a role for α5B1 integrin as a chondrocyte mechanoreceptor". In: *Journal of Orthopaedic Research* 15.5, pp. 742–747. ISSN: 0736-0266. DOI: 10.1002/jor.1100150517. URL: https://doi.org/10.1002/jor.1100150517.

Wu, JZ, W Herzog, and EM Hasler (2002). "Inadequate placement of osteochondral plugs may induce abnormal stress-strain distributions in articular cartilage-finite element simulations". In: *Medical engineering & physics* 24.2, pp. 85–97.

Wysocka, Aleksandra *et al.* (2010). "Chondrocyte suspension in fibrin glue". In: *Cell and Tissue Banking* 11.2, pp. 209–215. ISSN: 1573-6814. DOI: 10.1007/s10561-009-9163-y. URL: https://doi.org/10.1007/s10561-009-9163-y.

Xu, L. *et al.* (2007). "Increased expression of the collagen receptor discoidin domain receptor 2 in articular cartilage as a key event in the pathogenesis of osteoarthritis". In: *Arthritis Rheum* 56.8, pp. 2663–73. ISSN: 0004-3591 (Print) 0004-3591. DOI: 10.1002/art.22761.

Xu, L. *et al.* (2014). "Induction of high temperature requirement A1, a serine protease, by TGF-beta1 in articular chondrocytes of mouse models of OA". In: *Histol Histopathol* 29.5, pp. 609–18. ISSN: 0213-3911. DOI: 10.14670/hh-29.10.609.

Xue, J. *et al.* (2018). "Repair of articular cartilage defects with acellular cartilage sheets in a swine model". In: *Biomed Mater* 13.2, p. 025016. ISSN: 1748-6041. DOI: 10.1088/1748-605X/aa99a4.

Yang, Qiang *et al.* (2008). "A cartilage ECM-derived 3-D porous acellular matrix scaffold for in vivo cartilage tissue engineering with PKH26-labeled chondrogenic bone marrow-derived mesenchymal stem cells". In: *Biomaterials* 29.15, pp. 2378–2387. ISSN: 0142-9612. DOI: https://doi.org/10.1016/j.biomaterials.

2008.01.037. URL: http://www.sciencedirect.com/science/article/pii/S0142961208000689.

Yang, X. *et al.* (2001). "TGF-beta/Smad3 signals repress chondrocyte hypertrophic differentiation and are required for maintaining articular cartilage". In: *J Cell Biol* 153.1, pp. 35–46. ISSN: 0021-9525 (Print) 0021-9525.

Yang, Yueh-Hsun Kevin, Courtney R Ogando, and Gilda A Barabino (2020). "In vitro evaluation of the influence of substrate mechanics on matrix-assisted human chondrocyte transplantation". In: *Journal of Functional Biomaterials* 11.1, p. 5.

Zhang, Lijie, Jerry Hu, and Kyriacos A Athanasiou (2009). "The role of tissue engineering in articular cartilage repair and regeneration". In: *Critical Reviews™ in Biomedical Engineering* 37.1-2.

Zhang, Man *et al.* (2007). "Congruence of imaging estimators and mechanical measurements of viscoelastic properties of soft tissues". In: *Ultrasound in medicine & biology* 33.10, pp. 1617–1631.

Zhang, Y. *et al.* (2011). "An essential role of discoidin domain receptor 2 (DDR2) in osteoblast differentiation and chondrocyte maturation via modulation of Runx2 activation". In: *J Bone Miner Res* 26.3, pp. 604–17. ISSN: 0884-0431. DOI: 10.1002/jbmr.225.

Zhang, Zijun (2014). "Chondrons and the Pericellular Matrix of Chondrocytes". In: *Tissue Engineering Part B: Reviews* 21.3, pp. 267–277. ISSN: 1937-3368. DOI: 10.1089/ten.teb.2014.0286. URL: https://doi.org/10.1089/ten.teb.2014.0286.